University of Alberta

"Cardiomyopathy mutations in cardiac troponin C: functional and structural consequences"

by

Olga Konstantinovna Baryshnikova ©

A thesis submitted to the Faculty of Graduate Studies and Research
in partial fulfillment of the requirements for the degree of

Doctor of Philosophy

Department of Biochemistry

Edmonton, Alberta
Fall 2008

Library and Archives Canada

Published Heritage Branch

395 Wellington Street
Ottawa ON K1A 0N4
Canada

Bibliothèque et Archives Canada

Direction du Patrimoine de l'édition

395, rue Wellington
Ottawa ON K1A 0N4
Canada

Your file Votre référence
ISBN: 978-0-494-46280-5
Our file Notre référence
ISBN: 978-0-494-46280-5

NOTICE:
The author has granted a non-exclusive license allowing Library and Archives Canada to reproduce, publish, archive, preserve, conserve, communicate to the public by telecommunication or on the Internet, loan, distribute and sell theses worldwide, for commercial or non-commercial purposes, in microform, paper, electronic and/or any other formats.

The author retains copyright ownership and moral rights in this thesis. Neither the thesis nor substantial extracts from it may be printed or otherwise reproduced without the author's permission.

AVIS:
L'auteur a accordé une licence non exclusive permettant à la Bibliothèque et Archives Canada de reproduire, publier, archiver, sauvegarder, conserver, transmettre au public par télécommunication ou par l'Internet, prêter, distribuer et vendre des thèses partout dans le monde, à des fins commerciales ou autres, sur support microforme, papier, électronique et/ou autres formats.

L'auteur conserve la propriété du droit d'auteur et des droits moraux qui protège cette thèse. Ni la thèse ni des extraits substantiels de celle-ci ne doivent être imprimés ou autrement reproduits sans son autorisation.

In compliance with the Canadian Privacy Act some supporting forms may have been removed from this thesis.

While these forms may be included in the document page count, their removal does not represent any loss of content from the thesis.

Conformément à la loi canadienne sur la protection de la vie privée, quelques formulaires secondaires ont été enlevés de cette thèse.

Bien que ces formulaires aient inclus dans la pagination, il n'y aura aucun contenu manquant.

Canada

моему отцу

ABSTRACT

Recent genetic analysis revealed a number of human mutations in cardiac troponin C (cTnC), which were linked to cardiomyopathy, the most common genetic disorder of the heart. This thesis explores structural and functional consequences of these mutations obtained using solution NMR spectroscopy. The L29Q and E59D/D75Y mutations did not affect the Ca^{2+} affinity of the N-domain of cTnC (cNTnC). Instead the affinity towards the switch region of cardiac troponin I (cTnI) was perturbed, especially in the presence of the cTnI N-terminus, responsible for the transferring of PKA signaling. PKA signal is transferred via modulating the affinity of cNTnC towards the switch region of cTnI, which was altered in the L29Q and E59D/D75Y mutants possibly resulting in the development of malfunctions. The other mutant studied, G159D, had a weaker affinity towards the anchoring region of cTnI, which likely results in a weaker anchoring of the entire troponin complex to the thin filament, thus leading to the heart dysfunction. Differences in chemical shifts and NOE connectivities support the notion of the weaker binding for the anchoring region of cTnI, however, the structure and dynamics of the G159D mutant remained unchanged. Since the N-terminus of cTnI plays an important role in the function of cNTnC and its mutants, the attempt has been made to determine individual pKa's for side chain carboxyl groups possibly involved in the formation of the complex using the modified pulse sequence HBHG(CBCG)CO. It was also determined in this work that the formation of the cNTnC•$cTnI_{1-29}$ complex is electrostatically driven. These results elaborate on the current model of Ca^{2+} regulated cardiac contraction and provide an insight on the nature of perturbed interactions in cardiomyopathy mutants of cTnC, which can be beneficial for the development of therapeutic strategies in cardiomyopathy.

A portion of this thesis (Appendices C and D) addresses structural and dynamic aspects of SDF-1α (a chemokine involved in cancer metastasis and HIV propagation) and the peptide agonists developed on the basis of SDF-1α. NMR solution structures of the peptide agonists, RSVM and ASLW, and the dimerization of SDF-1α studied by NMR relaxation methods are described.

ACKNOWLEDGMENTS

This document is a testament of scientific growth that I watched myself going through while being in Dr. Brian Sykes's lab. Comparing my graduate career to the ski hill, most of the time, the black diamonds I was taking barely matched my skills, and the expectations for easy pleasure were hardly ever met. However, finishing off my run and finding my legs intact is an exhilarating feeling, that gives me the courage to climb another chair lift and glimpse onto another mountain top. I would like to thank people who shared my run: Marion Benedict, who set me on this trip; Dr. Howard Young and Dr. Mark Glover, who held the hand on the pulse of my progress all the way down; Sue Smith and the secretaries, who helped me to navigate through mountains of paperwork; technicians, Angela Thiessen and Dave Corson, who taught me a few of the most important steps; Dr. Monica Li, who taught me how to write; computer specialists, Robert Boyko, Dr. Pascal Mercier, and Olivier Julien for not giving up on me; and many others, who lent me a hand or a piece of advice or a word of encouragement.

This has been also the time of personal growth, shared by the extended family of Brian's lab and our department. I would like to thank Drs. Brian Sykes, Monica Li, Leo Spyracopoulos, Howard Young, Mark Glover, Ross Edwards, and Andrew MacMillan for sharing their experiences and thoughts on philosophy and nature of science, life, politics, and music. I also thank my peers, who ended up with the same set of skis on the same hill, Ryan Hoffman, Xu Wang, Ian Robertson, Olivier Julien, and others, with whom we shared our days, questioned ourselves and the world around us, and at times admired the view.

The skier would have given up, was it not for the guardian angel, Dr. Sykes, who with paternal devotion followed me from the top to the bottom through the pits of despair, taught me all the strategies, and whose faith in the skier's ability has never failed. Apart from Brian's awe-inspiring expertise and love of NMR, his professional and personal qualities set an unsurpassable example to follow. For me, his love of science and love of people, scientific depth and creativity, his energy and wisdom have been (and always will be) inspirational.

Thank you all.

TABLE OF CONTENTS

	Page number
CHAPTER I	1
INTRODUCTION	
References	13
CHAPTER II	18
The effect of L29Q and E59D/D75Y cardiomyopathy mutations on the function of cNTnC	
Outline	18
Introduction	18
Results	19
Discussion	27
Conclusions	33
Materials and Methods	34
References	47
CHAPTER III	51
Consequences of the DCM mutation G159D on the structure and dynamics of cardiac troponin C and its interaction with troponin I	
Outline	51
Introduction	51
Results	53
Discussion	59
Materials and Methods	61
References	72
CHAPTER IV	76
Exploring the interaction between cNTnC and the N-terminus of cTnI	
Outline	76
Introduction	76

Results and Discussion 78
Conclusions 80
Materials and Methods 80
References 86

CHAPTER V 88
Towards the determination of the pKa's of side chain carboxyl groups involved in electrostatic interactions on the interface between cNTnC and the N-terminus of cTnI
Outline 88
Introduction 88
Results and Discussion 89
Conclusions 91
Materials and Methods 91
References 95

CHAPTER VI 97
Conclusions
References 102

APPENDIX A 103
The code for the HBHG(CBCG)CO pulse sequence

APPENDIX B 108
Buffer components as internal pH indicators for biomolecular NMR
Outline 108
Introduction 108
Results and Discussion 109
Conclusions 111
References 113

APPENDIX C 114
Structures of peptide agonists derived on the basis of SDF-1α reveal a

common motif possibly implicated in the binding to the CXCR4 receptor

Outline 114

Introduction 114

Results 116

Discussion 120

Materials and Methods 122

References 129

APPENDIX D 132

Dimerization of SDF-1α studied by NMR relaxation methods

Outline 132

Introduction 132

Results 134

Discussion 139

Materials and Methods 142

References 152

LIST OF TABLES

	Page number
Table I-1	8
Table II-1	23
Table II-2	25
Table II-3	26
Table II-4	31
Table III-1	55
Table III-2	57
Table III-3	63
Table B-1	110
Table C-1	117
Table C-2	118
Table C-3	119
Table C-4	124
Table C-5	125
Table D-1	135
Table D-2	137

LIST OF FIGURES

	Page number
Figure I-1	1
Figure I-2	2
Figure I-3	3
Figure I-4	10
Figure I-5	11
Figure II-1	37
Figure II-2	38
Figure II-3	39
Figure II-4	40
Figure II-5	41
Figure II-6	42
Figure II-7	45
Figure II-8	46
Figure III-1	64
Figure III-2	65
Figure III-3	66
Figure III-4	67
Figure III-5	68
Figure III-6	69
Figure III-7	70
Figure III-8	71
Figure IV-1	82
Figure IV-2	83
Figure IV-3	84
Figure IV-4	85
Figure V-1	92

Figure V-2 93
Figure V-3 94

Figure VI-1 100
Figure VI-2 101

Figure B-1 112

Figure C-1 126
Figure C-2 126
Figure C-3 127
Figure C-4 128

Figure D-1 144
Figure D-2 145
Figure D-3 146
Figure D-4 147
Figure D-5 147
Figure D-6 148
Figure D-7 149
Figure D-8 150
Figure D-9 151

LIST OF ABBREVIATIONS

AEDANS	5-((2-((iodoacetyl)amino)ethyl)amino)naphthalene-1-sulfonic acid
AIDS	acquired immunodeficiency syndrome
BAPTA	1,2-bis(o-aminophenoxy)ethane-N,N,N',N'-tetraacetic acid
cCTnC	the C-domain of cardiac troponin C
CD	circular dichroism
cNTnC	the N-domain of cardiac troponin C
CSD	chemical shift deviation
DCM	dilated cardiomyopathy
E59D/D75Y	the E59D/D75Y mutant of the N-domain of cardiac troponin C
FHC	familial hypertrophic cardiomyopathy
FID	Free induction decay
G159D	the G159D mutant of the C-domain of cardiac troponin C
HSQC	heteronuclear single quantum coherence
IAANS	2-(4'-(2"-iodoacetamido)phenyl)aminonaphthalene-6-sulfonic acid
INEPT	insensitive nuclei enhancement by polarization transfer
ITC	isothermal titration calorimetry
L29Q	the L29Q mutant of the N-domain of cardiac troponin C
MyBPC	myosin binding protein C
NCX	Na^+/Ca^{2+} exchanger
NMR	nuclear magnetic resonance
NOE	nuclear Overhauser effect
NOESY	Nuclear Overhauser Enhancement Spectroscopy
PENCE	Protein Engineering Network of Centres of Excellence
PKA	protein kinase A
PKC	protein kinase C
PKD	protein kinase D
PKG	protein kinase G
PLB	Phospholamban
RCM	restricted cardiomyopathy
RyR	ryanodine receptor
SDF-1α	stromal derived factor

SERCA	sarco/endoplasmic reticulum Ca^{2+}-ATPase
ssTnI (sTnI)	slow skeletal isoform of troponin I
Tn (cTn)	troponin complex (cardiac troponin complex)
TnC (cTnC)	troponin C (cardiac troponin C)
TnI (cTnI)	troponin I (cardiac troponin I)
TnT (cTnT)	troponin T (cardiac troponin T)
TOCSY	total correlation spectroscopy

CHAPTER I
INTRODUCTION

Cardiac muscle contraction: overall picture

The contractile unit in striated muscle consists of thick and thin filaments sliding along each other during contraction, as first proposed in 1954 (*1, 2*). The main proteins involved in this process are actin and tropomyosin, composing the thin filament, and myosin, composing the thick filament. The troponin complex was identified in 1963 as a 'protein factor' required to reproduce 'the natural actomyosin' from its parts (*3*). According to the current knowledge, a dozen of other proteins, such as titin, desmin, dystrophin, and nebulin are also important participants (*4, 5*). Muscle is organized as repeating dark (A-band) and light (I-band) zones, with the Z-discs located in the middle of the I-band (Fig. I-1). A sarcomere, the unit of contraction, has one dark A-band, the half of the light I-band at each end, and is limited by Z-disks.

Figure I-1. Sarcomere appearance in electron microscope, where the A-, I-, and Z-zones are indicated (taken from http://www.apsu.edu/thompsonj/Physiology/). M is mitochondria.

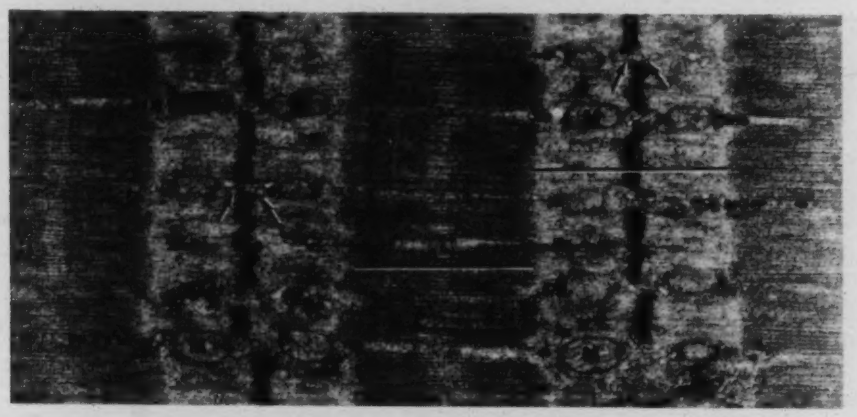

Thick filaments consist of myosin, which has a long rod-like domain connected to the head. Myosin heads bind to actin of the thin filament and hydrolyze ATP to promote the power stroke, leading to the pulling of actin ~10 nm toward the center of a sarcomere. According to the current understanding (*6*), at the beginning of the cycle, the myosin head is tightly bound to actin (Fig. I-2a), which dissociates from its actin site after binding ATP (Fig. I-2b). Upon hydrolysis of ATP, myosin undergoes a large conformational change, altering the angle between the myosin head and the thick

filament (Fig. I-2c). This allows myosin to bind weakly to another actin binding site (Fig. I-2d), which strengthens after the release of inorganic phosphate (Fig. I-2e), promoting the pulling of the thin filament (Fig. I-2f). Release of ADP results in a power stroke, upon completion of which, the myosin head is tightly bound to actin as at the beginning of the cycle (Fig. I-2a).

Figure I-2. Mechanism of force generation in muscle, with myosin heads interacting with actin of the thin filament (adopted from (*7*)). Different stages are shown as explained in the text.

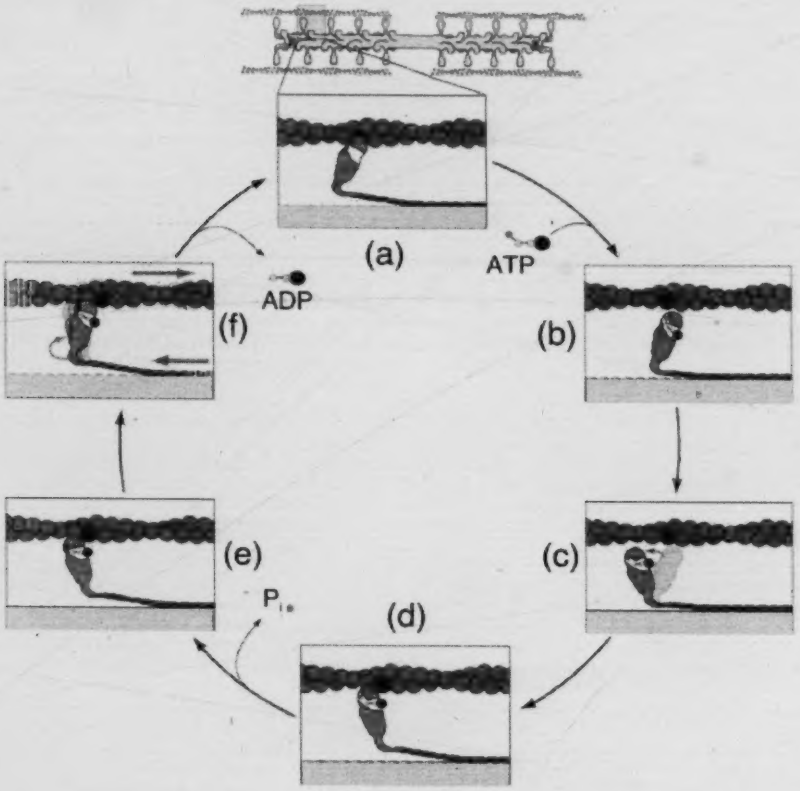

Myosin heads bind actin and perform the work in the open state of the thin filament. In the blocked state, myosin sites on actin are inhibited. The inhibition of actin is relieved upon Ca^{2+} stimulation, which is sensed by the cardiac troponin complex (cTn). cTn consists of troponin T (cTnT) that anchors cTn to the thin filament via tropomyosin; troponin I (cTnI) that inhibits the interaction between myosin and actin; and troponin C (cTnC) that binds Ca^{2+} and triggers the switch from the relaxed to the active state (Fig. I-

3). cTnC is a dumbbell shaped molecule with the structural C-domain (cCTnC) linked to the regulatory N-domain (cNTnC) through a stretch of 11 residues. The C-domain has a higher affinity for Ca^{2+} and stays saturated with Ca^{2+} or Mg^{2+} during the contracting-relaxing cycle. It is thought to be bound at all times to the anchoring region of cTnI (~ residues 34-71), which tethers cTnC to the thin filament. The N-domain has a lower affinity for Ca^{2+} and its Ca^{2+} binding site is occupied only when the concentration of Ca^{2+} is relatively high. This happens upon the release of Ca^{2+} from the sarcoplasmic reticulum after the stimulation. Upon Ca^{2+} binding, cNTnC binds to the switch region of cTnI (~ residues 147-163), which pulls the inhibitory region of cTnI (~ residues 128-147) away from its binding site on actin resulting in the movement of tropomyosin and the exposure of myosin binding sites on actin (Fig. I-3). This model of Ca^{2+} regulation was formulated based on numerous biochemical, biophysical, and physiological studies (*8-12*) including high resolution structures of cardiac (*13*) and skeletal troponin complexes (*14*). New reports have emerged that tackle other questions clarifying the position of the troponin complex on the actin fiber (*15*), the role of globular C-domain of cTnI (*16*), and the mechanism of signal transduction from troponin to tropomyosin (*16*), developing a more complete picture of muscle contraction.

Figure I-3. Model of Ca^{2+}-dependent regulation of cardiac muscle contraction. Figure adapted from (*11, 13*). cTnC is depicted in green, cTnT in white, cTnI in red, and actin and tropomyosin are in grey.

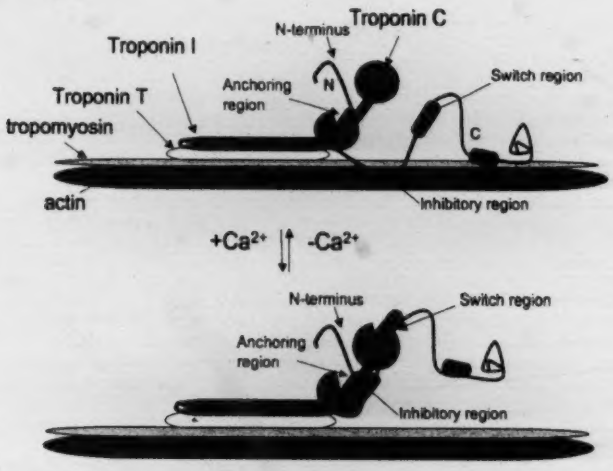

Ca^{2+} cycling in cardiomyocytes

The stimulation initiating cardiac contraction starts with the action potential generated by depolarizing of the sarcolemma by the voltage gated L-type Ca^{2+} channel (*17-20*). Ca^{2+} entry is sensed by the sarcoplasmic Ca^{2+} receptor, called ryanodine receptor (RyR). RyR mediates a process of Ca^{2+}-induced Ca^{2+} release from the sarcoplasm. Upon the release from the sarcoplasm, Ca^{2+} binds to cTnC of the thin filament promoting the contraction of muscle. Removal of Ca^{2+} from the cytosol is achieved by several mechanisms. The first mechanism is the sarcoplasmic uptake by the Ca^{2+} transporter (SERCA), which is regulated by phospholamban (PLB). The second mechanism of Ca^{2+} removal is the extrusion through the sarcolemmal Na^{+}/Ca^{2+} exchanger (NCX). During a Ca^{2+} cycle, the intracellular concentration of Ca^{2+} rises from 0.1 to > 1 μM, while the local concentration of Ca^{2+} in the proximity to a cluster of RyR's can reach > 100 μM (*20-22*). Ca^{2+} cycles are typically completed within ~ 400-600 ms (*21, 23*). Interestingly, different kinds of myocytes have different Ca^{2+} cycling patterns. For example, in ventrical myocytes local Ca^{2+} sparks give rise to a synchronized global Ca^{2+} signal due to the extensive network of T-tubules and sarcoplasmic invaginations delivering Ca^{2+} to the sarcomeres. In atrial myocytes, Ca^{2+} concentration sharply declines with the distance away from the sarcolemma due to the lack of inward spreading (*18*).

Regulation of Ca^{2+} regulated contraction by phosphorylation

In order to meet various needs of an organism, contractile machinery is fine tuned by the phosphorylation of its composing parts. The stimulation of β-adrenergic receptor by norepinephrine results in the generation of cAMP leading to the activation of downstream protein kinase A (PKA). Activated PKA phosphorylates several proteins central to the regulation of contractility. These proteins include the sarcolemmal Ca^{2+} channel, RyR, PLB, myosin binding protein C (MyBPC) and cTnI (*24, 25*). As a result of phosphorylation, the current through the sarcolemmal Ca^{2+} channel, the rate of Ca^{2+} reuptake by SERCA, and the rate of Ca^{2+} cycling are increased, attributed to the phosphorylation of the Ca^{2+} cycling machinery. The relaxation rate of the muscle is enhanced and the Ca^{2+} sensitivity of actomyosin ATPase is decreased, attributed to the phosphorylation of cTnI (*26*). The return to the baseline contractility is associated with the phosphorylation of PLB (*27*). The increase in cross-bridge cycling rate and the change in stretch-activation was shown to result from the phosphorylation of MyBPC (*28*). The overall consequence of β-adrenergic stimulation is the ~20% increase in power

output, due to the speeding up of the steps in Ca^{2+} and cross-bridge cycling (*29*). In spite of many efforts, the relative contribution of individual phosphorylated proteins to the increase in power output remains a matter of controversy.

The other mechanism for regulation of cardiac contraction is through the action of PKC, which phosphorylates cTnI and cTnT. At least 12 different PKC isoforms have been identified (*25*). The resultant contractility depends on many factors and has a wide range of effects on muscle function. Although the precise effects of PKC-dependent phosphorylation remain to be fully understood, there is an agreement that PKC phosphorylation of cTnI results in the decrease of Ca^{2+} activated tension and in sliding velocity. Other kinases, such as recently found PKG and PKD (*25, 30*), and their action on the sarcomeric proteins are beyond the scope of this introduction.

Phosphorylation of cTnI

PKA phosphorylates cTnI at residues Ser^{22} and Ser^{23} located in the cardiac specific N-terminus of cTnI (~ residues 1-29) adjacent to the anchoring region of cTnI (Fig. I-3). This results in the decrease of Ca^{2+} sensitivity of ATPase (*31-33*) and the increase of Ca^{2+} off-rates for the Tn complex (*34*). The N-terminus of cTnI has been cross-linked to cNTnC (*35*); however, this interaction has not been visualized in the crystal structures (*13*) or in NMR studies (*36-38*), except for the computational models (*39, 40*). Attempts have been made to obtain the binding constant using ITC (*35*) and fluorescent titrations (*37, 41, 42*); however, experiments were performed with long constructs of cTnI and therefore represent the complex function of several binding events. Available experimental data provides little insight on the molecular details of cNTnC binding to the N-terminus of cTnI, but suggests that the interaction of cNTnC with the N-terminus of cTnI (~ residues 1-29) affects the function of cNTnC and thus confer the signaling by PKA.

PKC phosphorylates cTnI at residues Ser^{43}, Ser^{45}, and Thr^{144}. First two residues are located at the anchoring region of cTnI (Fig. I-3), the affinity of which to cCTnC is expected to be altered by the presence of phosphorylation, but the binding was shown to be indistinguishable in NMR studies (*43*). The phosphorylation of Ser^{43} and Ser^{45} was attributed to the decrease in maximal Ca^{2+} activated tension (*44*). Thr^{144} is located at the inhibitory region of cTnI, and its phosphorylation was shown to decrease the affinity of cCTnC towards the $cTnI_{128-147}$ (*45*), which is in agreement with the increased inhibition of acto-myosin and the decrease in sliding velocity (*44*). PKC can also phosphorylate Ser^{22}

and Ser^{23}, suggesting the interdependence between PKA- and PKC- mediated effects and the complexity of the cTnI regulation by phosphorylation (*25*).

Mutations in sarcomeric proteins that cause cardiomyopathies: overview

Since the contractile machinery is composed of an array of proteins, with each of them playing a specific role, the number of vulnerable spots that can impair contractility is also significant. One of the leading genetic disorders of the heart, cardiomyopathy, can stem from mutations in proteins constructing the sarcomere, in proteins that align filaments inside myocytes (cytoskeletal proteins), and in the Ca^{2+} cycling machinery (*46-49*). Cardiomyopathies are divided into *dilated cardiomyopathy*, DCM, characterized by the enlarged ventricular chamber, weakened heart wall, and impaired systolic function; *hypertrophic cardiomyopathy*, FHC (an abbreviation for Familial Hypertrophic Cardiomyopathy), characterized by the thickened ventricular muscle, reduced volume of the ventricle, and impaired diastolic function (*48, 50*); and RCM, *restricted cardiomyopathy*, the least common type, characterized by the restrictive diastolic dysfunction. The prevalence of cardiomyopathy mutations in the general population is high (~0.2% for FHC for young adults 18 to 30 years of age (*51*)). Both, FHC and DCM, can result in sudden cardiac death especially in younger FHC patients (mean age, 45 ± 20 years) (*52*). At present, the following sarcomeric genes have been linked to cardiomyopathies: α-actin (*53*), α- and β-tropomyosin (*54*), troponin (*55, 56*), α- and β-myosin heavy chain (*57, 58*), regulatory and essential myosin light chains (*59*), and myosin binding protein C (*60*), with the total number of mutations exceeding 450 (*61*). Although unifying hypotheses are present, such as the inefficient utilization of ATP in FHC (*62*) or the reduced force development in DCM (*47, 63*), the majority of data suggests that cardiomyopathy is represented by a group of genetically distinct disorders that should be approached individually.

Cardiomyopathy mutations in cTn

Cardiomyopathy mutations were found in all three subunits of cTn (cTnC, cTnI, and cTnT) (*55, 56*), with the majority of mutations found in cTnI and cTnT (Table I-1). The structures and functions of cTnC and cTnI have been studied the most thoroughly, which allows for the assessment of a mutation in terms of specific molecular interactions, possibly perturbed by the mutation (Table I-1). In many cases, especially for cTnT, the

functions are overlapping. For example, a long stretch of cTnT is thought to interact with cTnC, actin, cTnI, and tropomyosin (*64-66*). In cTnI and cTnC, mutations are found throughout the sequence including all functional regions, and sometimes are in the regions, functions of which are unknown, suggesting the deficiencies in the current model of cardiac contraction. Physiological data, including motility assays, maximal force generated, and the Ca^{2+} sensitivity of force development and ATPase efficiency are available for a number of mutations (for reviews (*55, 56, 66, 67*)); however, the structural information pertaining to a particular perturbed interaction is scarce. Structural studies are complicated due to the location of many mutations in intrinsically unstructured regions; for example, the inhibitory region of cTnI, and the N- and C-termini of cTnI.

Often the linkage analysis is needed to establish the connection of a mutation with the development of the disease. For mutations in cTnC studied in this work, only one mutation, G159D, was subjected to the analysis of inheritance (*63*). Two other mutations, L29Q and E59D/D75Y, were found in single patients and suspected to cause cardiomyopathy, however the possibility of polymorphism remains (*68, 69*).

Biophysical techniques available for studying cardiomyopathies

To elucidate the mechanisms by which the mutations in sarcomeric proteins bring about the symptoms of cardiomyopathy, several biophysical techniques have proved to be useful. The study of motility was one of the first methods used to address this issue (*59*). In this type of assay, myosin is deposited onto a nitrocellulose platform and the translocation rate of fluorescently labeled actin filaments is recorded. In another method, the ATPase activity of myosin is measured in an assay performed on the mixture of F-actin, tropomyosin, myosin, and troponin complex (*70, 71*). After incubation with ATP the reaction is terminated and the released inorganic phosphate is measured. The efficiency of ATP hydrolysis is a measure of the myosin ATPase activity. Force development is another powerful technique available for probing the functional consequences of mutations in sarcomeric proteins (*72, 73*). In this assay, strips of cardiac muscle are mounted on a force transducer and immersed alternatively in relaxation (low Ca^{2+}) and contraction (high Ca^{2+}) solutions. The force generated during contraction is then measured. The advantage of this method is that soluble muscle proteins such as troponin can be stripped off the muscle and substituted by their recombinant analogues containing mutations or other modifications.

Table I-1. Cardiomyopathy mutations in human cTnT, cTnI, and cTnC, their location, and physiological consequences (*55, 56, 66, 67, 74*).

Gene	Mutation	Location	Binding partners of the particular region	Pheno-type
cTnT	A28V, S69F, F70L, P77L, I79N, E83K, D86A, R92W, R92L, R92Q, R94C, R94L, K97N, A104V, F110I, F110L, F110V, R130C	T1 domain	Tropomyosin	HCM
	DE160, E163K, E163R, S179F, DK210, E244D, K247E, N271I, K273E, R278C, R278P, R286C, R286H	T2 domain	cTnI, tropomyosin, cTnC, and actin	
	R141W	T1 domain	Tropomyosin	DCM
	A172S	T2 domain	cTnI, tropomyosin, cTnC, and actin	
cTnI	R21C	N-terminus	cNTnC	HCM
	P82S			
	Q130R, R141Q, R145G, R145Q	inhibitory region	cCTnC and actin	
	A157V, R162Q, R162P, R162W, S166F	switch region	cNTnC	
	DK177, K183E, DK183, R186Q, I195M, D196N, S199N, G203R, G203S, R204C, K206Q	C-domain	Actin	
	A2V	N-terminus	cNTnC	DCM
	L144Q, R145W	inhibitory region	cCTnC and actin	RCM
	A171T	switch region	cNTnC	
	K178E, D190G, R192H	C-domain	Actin	
cTnC	A8V, L29Q, C84Y	N-domain	the switch region and the N-terminus of cTnI	HCM
	E134D, D145E	C-domain	the anchoring and inhibitory regions of cTnI, and cTnT	
	E59D/D75Y	N-domain	the switch region and the N-terminus of cTnI	DCM
	G159D	C-domain	the anchoring and inhibitory regions of cTnI, and cTnT	

Structural techniques such as X-ray crystallography and NMR spectroscopy, when applicable, have proved to be very useful in tackling various aspects of protein biochemistry; however, in the quest for understanding cardiomyopathies, structural studies are lagging behind. In several reports, FHC and DCM mutations were mapped on the available structures of myosin (*75*) and cTn (*11, 63*). Studies of the mutations in MyBPC using 1D NMR spectroscopy were also reported (*76*). In our laboratory 2D NMR spectroscopy was used to elucidate the effects of FHC mutations of cTnI (R144G,

S149P, R162W) on the binding affinity of cTnI towards cTnC (*77*). However, no high-resolution structure of the sarcomeric protein with cardiomyopathy mutations is currently available and no atomic details of perturbed protein-protein interactions are known.

Methodology employed in present work

We have attempted to investigate the effect of cardiomyopathy mutations on the structure and function of cTnC using solution NMR spectroscopy. cTnC is a well behaved protein in NMR studies and the structure of cTnC has been detailed during years of research in Dr. Sykes' laboratory. We did expect that the cTnC mutants are also folded and well behaved proteins, so that their structures as well as other structural information could be obtained using NMR. In contrast, many mutations were found in cTnI, yet cTnI is a difficult target for traditional solution NMR due to its largely intrinsically disordered structure.

NMR is an extremely versatile technique that can provide a wealth of information about the system studied (*78*). Proteins (unlabeled or commonly labeled with ^{15}N and/or ^{13}C isotopes) are examined in solution at ~ mM concentrations, often together with their binding partners. The first very important parameter obtained by NMR is the chemical shift of individual nuclei (typically ^{1}H, ^{15}N, or ^{13}C), which is a parameter related to the chemical structure of the molecule and its chemical environment. NMR chemical shifts are measured relative to a reference compound and are field dependant. Differences in chemical shifts between the wild type protein and the mutant or the protein complex indicate the change in chemical environment and can be used to monitor changes during the titrations. They can be also mapped on the 3D structures, showing the surface affected by the mutation or complex formation. Another parameter is NOE (nuclear Overhauser effect), which is a change in the intensity of NMR signal due to through-space interactions between the nuclei. This parameter is used to obtain the constraints for structure calculations from 2D/3D NOESY NMR spectra. In relaxation experiments, NOE provides the information on flexibility of nuclei. Other parameters are T_1 and T_2 relaxation rates, describing the rate of decay for the NMR signal observed during pulsed NMR experiments. T_1 and T_2 depend on the tumbling rate of the molecule, exchange processes, and dynamic behavior of the nuclei. The line width of the NMR peak at the half height is related to T_2 ($\Delta\nu_{1/2} = 1/2\pi T_2$), so that the line broadening in NMR experiment (sharpness of the peaks) often indicative of the formation of complexes or chemical exchange processes (Fig. I-4) as explained further. Other parameters

obtained by NMR, such as dipolar couplings, spin-spin couplings, etc, are useful in many experiments, however, were not employed in this work.

Figure I-4. Differences in line broadening for the sample containing the same amount of protein, where the line is broadened due to the aggregation (a), and where the line is narrow, in agreement with the protein molecular weight (b). Traces were taken from {^{15}N, ^{1}H} HSQC experiments, with the frequency in Hz on the x-axis and the intensity in arbitrary units on the y-axis.

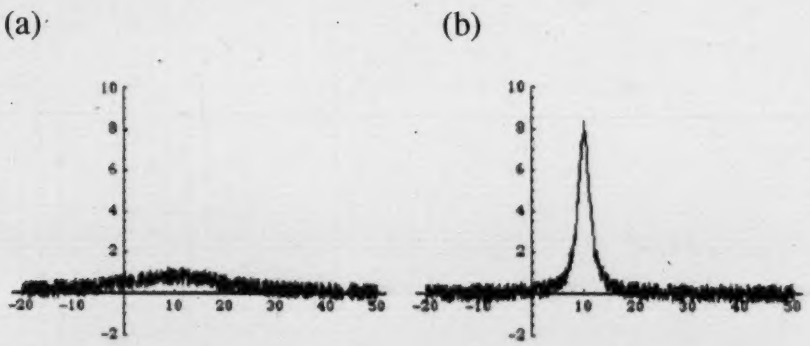

The dependence of T_2 on the molecular weight of a protein or its complex was often used in this work to indicate the increase in the molecular weight of protein species studied. When two predominant mechanisms for relaxation are dipole-dipole interaction between ^{15}N and ^{1}H nuclei and the chemical anisotropy of the ^{15}N nucleus, the relaxation parameters T_2, T_1, and NOE are given as following:

$$\frac{1}{T_1} = d^2[J(\omega_H - \omega_N) + 3J(\omega_N) + 6J(\omega_H + \omega_N)] + c^2 J(\omega_N),$$

$$\frac{1}{T_2} = \frac{d^2}{8}[4J(0) + J(\omega_H - \omega_N) + 3J(\omega_N) + 6J(\omega_H) + 6J(\omega_H + \omega_N)] + \frac{c^2}{6}[4J(0) + 3J(\omega_N)],$$

$$NOE = 1 + \frac{d^2}{4R_1}\frac{\gamma_H}{\gamma_N}[6J(\omega_H + \omega_N) - J(\omega_H - \omega_N)].$$

where $d = (\mu_o \hbar \gamma_H \gamma_N / 4\pi^2) r_{NH}^{-3}$, $c = \omega_N \Delta\sigma / \sqrt{3}$, μ_o is the permeability of free space, $\hbar$ is Planck's constant, γ_H and γ_N are magnetogyric ratios of the ^{15}N and ^{1}H nuclei, r_{NH} is the ^{15}N – ^{1}H bond length, $\Delta\sigma$ is the chemical shift anisotropy of the ^{15}N nucleus, and ω_N is the Larmor frequency of the ^{15}N nucleus (*79*). The spectral density function is described in Model Free approach as following:

$$J(\omega) = \frac{2}{5}\left(\frac{S^2\tau_m}{1+\omega^2{\tau_m}^2} + \frac{(1-S^2)\tau}{1+\omega^2\tau^2}\right),$$

where S^2 is the generalized order parameter, and $\frac{1}{\tau} = \left(\frac{1}{\tau_m} + \frac{1}{\tau_e}\right)$, with τ_e being the internal correlation time for molecular motions, and τ_m is the overall correlation time of a protein (*80*). The spectral density function for a typical protein depends on the frequency as shown in Figure I-V, where $J(0)$ (at zero) being an order of magnitude larger than $J(\omega_N)$ (at the frequency of ^{15}N), and similarly larger than $J(\omega_N + \omega_H)$, and $J(\omega_H - \omega_N)$. This will allow for the simplification of the equation for T_2, but not for T_1 and NOE.

$$\frac{1}{T_2} \approx \frac{d^2}{8}[4J(0)] + \frac{c^2}{6}[4J(0)]$$

Assuming negligible internal motions the spectral density will be denoted as following:

$$J(\omega) = \frac{2}{5}\frac{S^2\tau_m}{(1+\omega^2{\tau_m}^2)}.$$

At frequency zero, spectral density function $J(0)$ has a linear dependence on the overall correlation time. Thus the relaxation rate T_2 can be approximated to have a linear relationship with the overall correlation time as well, and consequently, with the molecular weight of the species.

Figure I-V. Spectral density function for backbone amide ^{15}N spins in *E.coli* ribonuclease. Figure is taken from (*79*), where the data shows the values of spectral density at several frequencies, including those acquired at different magnetic fields.

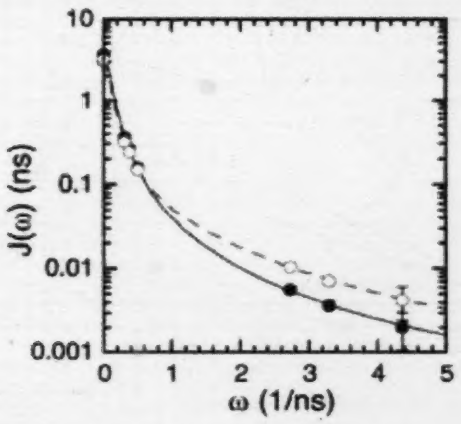

Objectives and organization of this thesis

The goal of this study was to address the structure and function of cardiomyopathy mutations in cTnC using solution state NMR spectroscopy. Chapter II describes the structural and functional aspects of the two mutants found in the N-domain of cTnC, L29Q and E59D/D75Y. We determined how these mutations affect the function of cNTnC and proposed the mechanism explaining the hypercontractility in L29Q and hypocontractility in E59D/D75Y. Chapter III presents the structure and function of the mutation found in the C-domain of cTnC, G159D. Based on the results obtained we have developed the hypothesis of the mechanism of G159D and the development of disease. Effects of the L29Q and E59D/D75Y mutations described in Chapter II were observed in the presence of the N-terminus of cTnI (~ residue 1-29), and the effect of the G159D mutation described in Chapter III was suggested to be mediated through the N-terminus of cTnI. The interaction between the N-terminus of cTnI and cNTnC as a function of ionic strength was explored in Chapter IV. Chapter V presents the pulse sequence, HBHG(CBCG)CO, developed to determine the individual side chain ionization constants for residues involved in the electrostatic interactions such as between cNTnC and the N-terminus of cTnI. Chapter VI concludes this thesis with the future outlook for the field of cardiac muscle contraction. The following additional material is gathered in the Appendices: the HBHG(CBCG)CO pulse sequence code (Appendix A); the method for pH determination of the NMR samples using buffer components (Appendix B); the NMR structures of peptide agonists developed on the base of SDF-1α (Appendix C); and the dimerization of SDF-1α studied by the NMR relaxation methods (Appendix D). The latter two projects were accomplished during the first three years of my PhD career in Dr. Sykes' laboratory and were a part of a collaborative PENCE project, discontinued due to the demise of our key collaborator Dr. Ian Clark-Lewis (UBC). In order to communicate a streamlined and focused discussion we decided to build our narrative around the cardiomyopathy mutations in cTnC leaving the story of SDF-1α in Appendices.

References

(1) Huxley, H., and Hanson, J. (1954) Changes in the cross-striations of muscle during contraction and stretch and their structural interpretation. *Nature 173*, 973-6.

(2) Huxley, A. F., and Niedergerke, R. (1954) Structural changes in muscle during contraction; interference microscopy of living muscle fibres. *Nature 173*, 971-3.

(3) Ebashi, S. (1963) Third Component Participating In The Superprecipitation Of 'Natural Actomyosin'. *Nature 200*, 1010.

(4) Geeves, M. A., and Holmes, K. C. (1999) Structural mechanism of muscle contraction. *Annu Rev Biochem 68*, 687-728.

(5) Clark, K. A., McElhinny, A. S., Beckerle, M. C., and Gregorio, C. C. (2002) Striated muscle cytoarchitecture: an intricate web of form and function. *Annu Rev Cell Dev Biol 18*, 637-706.

(6) Rayment, I., Holden, H. M., Whittaker, M., Yohn, C. B., Lorenz, M., Holmes, K. C., and Milligan, R. A. (1993) Structure of the actin-myosin complex and its implications for muscle contraction. *Science 261*, 58-65.

(7) Murphy, C. T., Rock, R. S., and Spudich, J. A. (2001) A myosin II mutation uncouples ATPase activity from motility and shortens step size. *Nat Cell Biol 3*, 311-5.

(8) Sykes, B. D. (2003) Pulling the calcium trigger. *Nat Struct Biol 10*, 588-9.

(9) Gordon, A. M., Homsher, E., and Regnier, M. (2000) Regulation of contraction in striated muscle. *Physiol Rev 80*, 853-924.

(10) Slupsky, C. M., and Sykes, B. D. (1996) *Muscle Proteins*, John Wiley & Sons, Chichester, UK.

(11) Li, M. X., Wang, X., and Sykes, B. D. (2004) Structural based insights into the role of troponin in cardiac muscle pathophysiology. *J Muscle Res Cell Motil 25*, 559-79.

(12) Solaro, R. J., and Rarick, H. M. (1998) Troponin and tropomyosin: proteins that switch on and tune in the activity of cardiac myofilaments. *Circ Res 83*, 471-80.

(13) Takeda, S., Yamashita, A., Maeda, K., and Maeda, Y. (2003) Structure of the core domain of human cardiac troponin in the Ca(2+)-saturated form. *Nature 424*, 35-41.

(14) Vinogradova, M. V., Stone, D. B., Malanina, G. G., Karatzaferi, C., Cooke, R., Mendelson, R. A., and Fletterick, R. J. (2005) Ca(2+)-regulated structural changes in troponin. *Proc Natl Acad Sci U S A 102*, 5038-43.

(15) Ferguson, R. E., Sun, Y. B., Mercier, P., Brack, A. S., Sykes, B. D., Corrie, J. E., Trentham, D. R., and Irving, M. (2003) In situ orientations of protein domains: troponin C in skeletal muscle fibers. *Mol Cell 11*, 865-74.

(16) Murakami, K., Yumoto, F., Ohki, S. Y., Yasunaga, T., Tanokura, M., and Wakabayashi, T. (2005) Structural basis for Ca2+-regulated muscle relaxation at interaction sites of troponin with actin and tropomyosin. *J Mol Biol 352*, 178-201.

(17) Woodcock, E. A., and Matkovich, S. J. (2005) Cardiomyocytes structure, function and associated pathologies. *Int J Biochem Cell Biol 37*, 1746-51.

(18) Bootman, M. D., Higazi, D. R., Coombes, S., and Roderick, H. L. (2006) Calcium signalling during excitation-contraction coupling in mammalian atrial myocytes. *J Cell Sci 119*, 3915-25.

(19) Bers, D. M. (2008) Calcium cycling and signaling in cardiac myocytes. *Annu Rev Physiol 70*, 23-49.

(20) Bers, D. M., and Guo, T. (2005) Calcium signaling in cardiac ventricular myocytes. *Ann N Y Acad Sci 1047*, 86-98.

(21) Cheng, H., Lederer, M. R., Lederer, W. J., and Cannell, M. B. (1996) Calcium sparks and [Ca2+]i waves in cardiac myocytes. *Am J Physiol 270*, C148-59.

(22) Takamatsu, T., and Wier, W. G. (1990) Calcium waves in mammalian heart: quantification of origin, magnitude, waveform, and velocity. *Faseb J 4*, 1519-25.

(23) Williams, D. A., Delbridge, L. M., Cody, S. H., Harris, P. J., and Morgan, T. O. (1992) Spontaneous and propagated calcium release in isolated cardiac myocytes viewed by confocal microscopy. *Am J Physiol 262*, C731-42.

(24) Metzger, J. M., and Westfall, M. V. (2004) Covalent and noncovalent modification of thin filament action: the essential role of troponin in cardiac muscle regulation. *Circ Res 94*, 146-58.

(25) Layland, J., Solaro, R. J., and Shah, A. M. (2005) Regulation of cardiac contractile function by troponin I phosphorylation. *Cardiovasc Res 66*, 12-21.

(26) Wolska, B. M., Arteaga, G. M., Pena, J. R., Nowak, G., Phillips, R. M., Sahai, S., de Tombe, P. P., Martin, A. F., Kranias, E. G., and Solaro, R. J. (2002) Expression of slow skeletal troponin I in hearts of phospholamban knockout mice alters the relaxant effect of beta-adrenergic stimulation. *Circ Res 90*, 882-8.

(27) Garvey, J. L., Kranias, E. G., and Solaro, R. J. (1988) Phosphorylation of C-protein, troponin I and phospholamban in isolated rabbit hearts. *Biochem J 249*, 709-14.

(28) Stelzer, J. E., Patel, J. R., Walker, J. W., and Moss, R. L. (2007) Differential roles of cardiac myosin-binding protein C and cardiac troponin I in the myofibrillar force responses to protein kinase A phosphorylation. *Circ Res 101*, 503-11.

(29) Herron, T. J., Korte, F. S., and McDonald, K. S. (2001) Power output is increased after phosphorylation of myofibrillar proteins in rat skinned cardiac myocytes. *Circ Res 89*, 1184-90.

(30) Avkiran, M., Rowland, A. J., Cuello, F., and Haworth, R. S. (2008) Protein kinase d in the cardiovascular system: emerging roles in health and disease. *Circ Res 102*, 157-63.

(31) Holroyde, M. J., Howe, E., and Solaro, R. J. (1979) Modification of Calcium requirements for activation of cardiac myofibrillar ATPase by cyclic AMP dependent phosphorylation. *Biochim. Biophys. Acta 586*, 63-69.

(32) Wattanapermpool, J., Guo, X., and Solaro, R. J. (1995) The unique amino-terminal peptide of cardiac troponin I regulates myofibrillar activity only when it is phosphorylated. *J Mol Cell Cardiol 27*, 1383-91.

(33) Zhang, R., Zhao, J., and Potter, J. D. (1995) Phosphorylation of both serine residues in cardiac troponin I is required to decrease the Ca2+ affinity of cardiac troponin C. *J Biol Chem 270*, 30773-80.

(34) Robertson, S. P., Johnson, J. D., Holroyde, M. J., Kranias, E. G., Potter, J. D., and Solaro, R. J. (1982) The effect of troponin I phosphorylation on the Ca2+-binding properties of the Ca2+-regulatory site of bovine cardiac troponin. *J Biol Chem 257*, 260-3.

(35) Ward, D. G., Brewer, S. M., Cornes, M. P., and Trayer, I. P. (2003) A cross-linking study of the N-terminal extension of human cardiac troponin I. *Biochemistry 42*, 10324-32.

(36) Finley, N., Abbott, M. B., Abusamhadneh, E., Gaponenko, V., Dong, W., Gasmi-Seabrook, G., Howarth, J. W., Rance, M., Solaro, R. J., Cheung, H. C., and Rosevear, P. R. (1999) NMR analysis of cardiac troponin C-troponin I complexes: effects of phosphorylation. *FEBS Lett 453*, 107-12.

(37) Abbott, M. B., Dong, W. J., Dvoretsky, A., DaGue, B., Caprioli, R. M., Cheung, H. C., and Rosevear, P. R. (2001) Modulation of cardiac troponin C-cardiac troponin I regulatory interactions by the amino-terminus of cardiac troponin I. *Biochemistry 40*, 5992-6001.

(38) Ward, D. G., Brewer, S. M., Gallon, C. E., Gao, Y., Levine, B. A., and Trayer, I. P. (2004) NMR and mutagenesis studies on the phosphorylation region of human cardiac troponin I. *Biochemistry 43*, 5772-81.

(39) Howarth, J. W., Meller, J., Solaro, R. J., Trewhella, J., and Rosevear, P. R. (2007) Phosphorylation-dependent conformational transition of the cardiac specific N-extension of troponin I in cardiac troponin. *J Mol Biol 373*, 706-22.

(40) Solaro, R. J., Rosevear, P., and Kobayashi, T. (2008) The unique functions of cardiac troponin I in the control of cardiac muscle contraction and relaxation. *Biochem Biophys Res Commun 369*, 82-7.

(41) Chandra, M., Dong, W. J., Pan, B. S., Cheung, H. C., and Solaro, R. J. (1997) Effects of protein kinase A phosphorylation on signaling between cardiac troponin I and the N-terminal domain of cardiac troponin C. *Biochemistry 36*, 13305-11.

(42) Dong, W. J., Chandra, M., Xing, J., She, M., Solaro, R. J., and Cheung, H. C. (1997) Phosphorylation-induced distance change in a cardiac muscle troponin I mutant. *Biochemistry 36*, 6754-61.

(43) Li, M. X., Wang, X., Lindhout, D. A., Buscemi, N., Van Eyk, J. E., and Sykes, B. D. (2003) Phosphorylation and mutation of human cardiac troponin I deferentially destabilize the interaction of the functional regions of troponin I with troponin C. *Biochemistry 42*, 14460-8.

(44) Burkart, E. M., Sumandea, M. P., Kobayashi, T., Nili, M., Martin, A. F., Homsher, E., and Solaro, R. J. (2003) Phosphorylation or glutamic acid substitution at protein kinase C sites on cardiac troponin I differentially depress myofilament tension and shortening velocity. *J Biol Chem 278*, 11265-72.

(45) Lindhout, D. A., Li, M. X., Schieve, D., and Sykes, B. D. (2002) Effects of T142 phosphorylation and mutation R145G on the interaction of the inhibitory region of human cardiac troponin I with the C-domain of human cardiac troponin C. *Biochemistry 41*, 7267-74.

(46) Redwood, C. S., Moolman-Smook, J. C., and Watkins, H. (1999) Properties of mutant contractile proteins that cause hypertrophic cardiomyopathy. *Cardiovasc Res 44*, 20-36.

(47) Morita, H., Seidman, J., and Seidman, C. E. (2005) Genetic causes of human heart failure. *J Clin Invest 115*, 518-26.

(48) Seidman, J. G., and Seidman, C. (2001) The genetic basis for cardiomyopathy: from mutation identification to mechanistic paradigms. *Cell 104*, 557-67.

(49) Karkkainen, S., and Peuhkurinen, K. (2007) Genetics of dilated cardiomyopathy. *Ann Med 39*, 91-107.

(50) Bruce, J. (2005) Getting to the heart of cardiomyopathies. *Nursing 35*, 44-7.

(51) Maron, B. J., Gardin, J. M., Flack, J. M., Gidding, S. S., Kurosaki, T. T., and Bild, D. E. (1995) Prevalence of hypertrophic cardiomyopathy in a general population of young adults. Echocardiographic analysis of 4111 subjects in the CARDIA Study. Coronary Artery Risk Development in (Young) Adults. *Circulation 92*, 785-9.

(52) Maron, B. J., Olivotto, I., Spirito, P., Casey, S. A., Bellone, P., Gohman, T. E., Graham, K. J., Burton, D. A., and Cecchi, F. (2000) Epidemiology of hypertrophic cardiomyopathy-related death: revisited in a large non-referral-based patient population. *Circulation 102*, 858-64.

(53) Mogensen, J., Klausen, I. C., Pedersen, A. K., Egeblad, H., Bross, P., Kruse, T. A., Gregersen, N., Hansen, P. S., Baandrup, U., and Borglum, A. D. (1999) Alpha-cardiac actin is a novel disease gene in familial hypertrophic cardiomyopathy. *J Clin Invest 103*, R39-43.

(54) Thierfelder, L., Watkins, H., MacRae, C., Lamas, R., McKenna, W., Vosberg, H. P., Seidman, J. G., and Seidman, C. E. (1994) Alpha-tropomyosin and cardiac troponin T mutations cause familial hypertrophic cardiomyopathy: a disease of the sarcomere. *Cell 77*, 701-12.

(55) Harada, K., and Morimoto, S. (2004) Inherited cardiomyopathies as a troponin disease. *Jpn J Physiol 54*, 307-18.

(56) Gomes, A. V., and Potter, J. D. (2004) Molecular and cellular aspects of troponin cardiomyopathies. *Ann N Y Acad Sci 1015*, 214-24.

(57) Tanigawa, G., Jarcho, J. A., Kass, S., Solomon, S. D., Vosberg, H. P., Seidman, J. G., and Seidman, C. E. (1990) A molecular basis for familial hypertrophic cardiomyopathy: an alpha/beta cardiac myosin heavy chain hybrid gene. *Cell 62*, 991-8.

(58) Geisterfer-Lowrance, A. A., Christe, M., Conner, D. A., Ingwall, J. S., Schoen, F. J., Seidman, C. E., and Seidman, J. G. (1996) A mouse model of familial hypertrophic cardiomyopathy. *Science 272*, 731-4.

(59) Poetter, K., Jiang, H., Hassanzadeh, S., Master, S. R., Chang, A., Dalakas, M. C., Rayment, I., Sellers, J. R., Fananapazir, L., and Epstein, N. D. (1996) Mutations in either the essential or regulatory light chains of myosin are associated with a rare myopathy in human heart and skeletal muscle. *Nat Genet 13*, 63-9.

(60) Oakley, C. E., Hambly, B. D., Curmi, P. M., and Brown, L. J. (2004) Myosin binding protein C: structural abnormalities in familial hypertrophic cardiomyopathy. *Cell Res 14*, 95-110.

(61) Alcalai, R., Seidman, J. G., and Seidman, C. E. (2008) Genetic basis of hypertrophic cardiomyopathy: from bench to the clinics. *J Cardiovasc Electrophysiol 19*, 104-10.

(62) Ashrafian, H., Redwood, C., Blair, E., and Watkins, H. (2003) Hypertrophic cardiomyopathy:a paradigm for myocardial energy depletion. *Trends Genet 19*, 263-8.

(63) Mirza, M., Marston, S., Willott, R., Ashley, C., Mogensen, J., McKenna, W., Robinson, P., Redwood, C., and Watkins, H. (2005) Dilated cardiomyopathy mutations in three thin filament regulatory proteins result in a common functional phenotype. *J Biol Chem 280*, 28498-506.

(64) Perry, S. V. (1998) Troponin T: genetics, properties and function. *J Muscle Res Cell Motil 19*, 575-602.

(65) Blumenschein, T. M., Tripet, B. P., Hodges, R. S., and Sykes, B. D. (2001) Mapping the interacting regions between troponins T and C. Binding of TnT and TnI peptides to TnC and NMR mapping of the TnT-binding site on TnC. *J Biol Chem 276*, 36606-12.

(66) Knollmann, B. C., and Potter, J. D. (2001) Altered regulation of cardiac muscle contraction by troponin T mutations that cause familial hypertrophic cardiomyopathy. *Trends Cardiovasc Med 11*, 206-12.

(67) Gomes, A. V., and Potter, J. D. (2004) Cellular and molecular aspects of familial hypertrophic cardiomyopathy caused by mutations in the cardiac troponin I gene. *Mol Cell Biochem 263*, 99-114.

(68) Hoffmann, B., Schmidt-Traub, H., Perrot, A., Osterziel, K. J., and Gessner, R. (2001) First mutation in cardiac troponin C, L29Q, in a patient with hypertrophic cardiomyopathy. *Hum Mutat 17*, 524.

(69) Lim, C. C., Yang, H., Yang, M., Wang, C. K., Shi, J., Berg, E. A., Pimentel, D. R., Gwathmey, J. K., Hajjar, R. J., Helmes, M., Costello, C. E., Huo, S., and Liao, R. (2008) A Novel Mutant Cardiac Troponin C Disrupts Molecular Motions Critical For Calcium Binding Affinity And Cardiomyocyte Contractility. *Biophys J.*

(70) Elliott, K., Watkins, H., and Redwood, C. S. (2000) Altered regulatory properties of human cardiac troponin I mutants that cause hypertrophic cardiomyopathy. *J Biol Chem 275*, 22069-74.

(71) Szczesna, D., Zhang, R., Zhao, J., Jones, M., Guzman, G., and Potter, J. D. (2000) Altered regulation of cardiac muscle contraction by troponin T mutations that cause familial hypertrophic cardiomyopathy. *J Biol Chem 275*, 624-30.

(72) Gomes, A. V., Venkatraman, G., Davis, J. P., Tikunova, S. B., Engel, P., Solaro, R. J., and Potter, J. D. (2004) Cardiac troponin T isoforms affect the Ca(2+) sensitivity of force development in the presence of slow skeletal troponin I: insights into the role of troponin T isoforms in the fetal heart. *J Biol Chem 279*, 49579-87.

(73) Hernandez, O., Szczesna-Cordary, D., Knollmann, B. C., Miller, T., Bell, M., Zhao, J., Sirenko, S. G., Diaz, Z., Guzman, G., Xu, Y., Wang, Y., Kerrick, W. G., and Potter, J. D. (2005) F110I and R278C troponin T mutations that cause familial hypertrophic cardiomyopathy affect muscle contraction in transgenic mice and reconstituted human cardiac fibers. *J Biol Chem.*

(74) Parvatiyar, M., Pinto, J. R., Jones, M. A., Ackerman, M. J., and Potter, J. D. (2008) in *Biophysical Society, Annual Meeting*, Long Beach, CA.

(75) Rayment, I., Holden, H. M., Sellers, J. R., Fananapazir, L., and Epstein, N. D. (1995) Structural interpretation of the mutations in the beta-cardiac myosin that have been implicated in familial hypertrophic cardiomyopathy. *Proc Natl Acad Sci U S A 92*, 3864-8.

(76) Idowu, S. M., Gautel, M., Perkins, S. J., and Pfuhl, M. (2003) Structure, stability and dynamics of the central domain of cardiac myosin binding protein C (MyBP-C): implications for multidomain assembly and causes for cardiomyopathy. *J Mol Biol 329*, 745-61.

(77) Lindhout, D. A., Boyko, R. F., Corson, D. C., Li, M. X., and Sykes, B. D. (2005) The role of electrostatics in the interaction of the inhibitory region of troponin I with troponin C. *Biochemistry 44*, 14750-9.

(78) Wuthrich, K. (1986) *NMR of Proteins and Nucleic Acids*, John Wiley & Sons, New York.

(79) Palmer, A. G., 3rd. (2004) NMR characterization of the dynamics of biomacromolecules. *Chem Rev 104*, 3623-40.

(80) Lipari, G., and Szabo, a. (1982) Model-Free Approach to the Interpretation of Nuclear Magnetic-Resonance Relaxation in Macromolecules.1. Theory and Range of Validity. *J Am Chem Soc 104*, 4546-4559.

CHAPTER II

The effect of L29Q and E59D/D75Y cardiomyopathy mutations on the function of cNTnC*

Outline

The cardiac specific N-terminus of cTnI is known to modulate the activity of troponin upon phosphorylation with PKA by decreasing its Ca^{2+} affinity and increasing the relaxation rate of the thin filament. The molecular details of this modulation have not been elaborated to date. We have established that the N-terminus ($cTnI_{1-29}$/$cTnI_{1-29}$PP) and the switch region of cTnI ($cTnI_{147-163}$) bind to cNTnC simultaneously, and that the PKA signal is transferred via the cTnI N-terminus modulating the cNTnC affinity towards $cTnI_{147-163}$ but not towards Ca^{2+}. The K_D of cNTnC for $cTnI_{147-163}$ was found to be 600 μM in the presence of $cTnI_{1-29}$ and 370 μM in the presence of $cTnI_{1-29}$PP, which can explain the difference in muscle relaxation rates upon the phosphorylation with PKA in experiments with cardiac fibers. In the light of newly found mutations in cNTnC, associated with cardiomyopathies, the role of the cTnI N-terminus is emerging also to be important in the development of heart disorders. The mutants studied, L29Q and E59D/D75Y, demonstrated unchanged Ca^{2+} affinity per se and in complex with the cTnI N-terminus ($cTnI_{1-29}$ and $cTnI_{1-29}$PP). The affinity of L29Q and E59D/D75Y towards $cTnI_{147-163}$ was significantly perturbed, both alone and in complex with $cTnI_{1-29}$ and $cTnI_{1-29}$PP, which is likely to be responsible for the development of malfunctions.

Introduction

Recent studies suggested the involvement of the N-terminal cTnI region (Fig. I-3) in the development of cardiomyopathies, in which the mutations in cTnC perturb interactions with the N-terminus of cTnI, giving rise to the malfunction of the heart (*1*, *2*). One of these cNTnC mutations, L29Q, has been found in a patient with hypertrophy of the heart (*3*) suggesting it to be a cause for FHC. L29Q is located on silent Ca^{2+} binding site I of cNTnC and is potentially capable of changing the Ca^{2+} affinity by reviving defunct site I. This hypothesis is especially attractive since the L29Q substitution was

---

* The version of this chapter has been published. Baryshnikova O.K., Li M.X., and Sykes B.D. (2008) *J Mol Biol 375*, 735-751.

found in cold water fish where it was proposed to increase the Ca^{2+} sensitivity of the cardiac muscle at low temperatures (*4*). It is also possible that L29Q affects the interaction with the switch region of cTnI (~residues 147-163) or, as suggested in literature, the interaction with the N-terminal region of cTnI (~residues 1-29) (Fig. I-3) (*1*). The latter will in turn affect the way $cTnI_{1-29}$ modulates the Ca^{2+} affinity of cTn, which might be responsible for the development of FHC.

The other cNTnC mutation mentioned in literature, E59D/D75Y, was connected to a dilated cardiomyopathy, DCM (*5, 6*). For this mutant, the change in Ca^{2+} affinity can be expected since residue 75 is mapped on the loop corresponding to functional Ca^{2+} binding site II. Residue 59 is located in close proximity to the bound $cTnI_{147-163}$ peptide (*7*), which if mutated might also affect the affinity towards the switch region of cTnI (~residues 147-163). In addition, the E59D/D75Y mutation might affect the binding of the cTnI N-terminus (~residues 1-29) and perturb its modulation of cNTnC interactions (Fig. I-3), leading to the development of DCM.

Since the molecular details of the effect of the cTnI N-terminus on the interactions of cNTnC have not been fully elaborated to date (*8*), we have addressed these questions. The affinities of cNTnC towards Ca^{2+} and $cTnI_{147-163}$ were measured in the presence of the phosphorylated and unphosphorylated cTnI peptides ($cTnI_{1-29}$PP and $cTnI_{1-29}$), where the minimal length of the peptides required to confer the modulation by PKA was determined previously (*9*). The nature of the binding site for $cTnI_{1-29}$ on cNTnC, the simultaneous binding of the cTnI N-terminus and the switch region, and the possible mechanisms by which the phosphorylation signal is transferred within cTn are discussed. Second, we have examined how the presence of mutations in cNTnC, L29Q and E59D/D75Y, affects the Ca^{2+} and $cTnI_{147-163}$ binding affinities per se and in the presence of $cTnI_{1-29}$ and $cTnI_{1-29}$PP.

Results

Titrations of L29Q and E59D/D75Y with Ca^{2+} using NMR spectroscopy

In a typical 2D {^{1}H, ^{15}N} HSQC NMR spectrum, the observed cross-peaks correlate the chemical shifts of backbone amide ^{15}N to the chemical shifts of backbone amide ^{1}H. Backbone amide chemical shifts are exquisitely sensitive to the changes in structure and dynamics of a protein. Therefore, a 2D NMR spectrum provides a high resolution residue specific probe to follow changes in a protein; for example, upon binding a ligand. This method has been called chemical shift mapping. The 2D {^{1}H, ^{15}N}

HSQC NMR spectra of L29Q and E59D/D75Y were very similar to the spectrum of cNTnC, implying that both mutant proteins have a similar structure to the native fold. This is also supported by the ^{15}N backbone amide NMR relaxation measurements discussed below.

As it can be seen from the overlay of 2D {^{1}H, ^{15}N} HSQC spectra obtained during Ca^{2+} titrations, Ca^{2+} binding to L29Q (Fig. II-1a) and E59D/D75Y (Fig. II-1b) causes gradual chemical shift changes that were very similar to each other and to the changes induced upon the Ca^{2+} binding to cNTnC (*7*), indicating binding to the same site and in a similar fashion. Several cross-peaks in Figure II-1 are labeled based on the assignments for cNTnC. In both cases, proportional movement of cross-peaks implies that the Ca^{2+} binding kinetics is in fast exchange on the NMR time scale. Linear movement of cross-peaks in titrations suggests that a single binding event is involved. Multiple Ca^{2+} binding sites would cause non-linear chemical shift changes. The movements of cross-peaks in Figure II-1 are primarily linear. The possibility for the weak second binding site, suggested for L29Q on the basis of comparison with cold water fish cTnC (*4*), will be considered further below.

Binding curves for L29Q and for E59D/D75Y are shown in Figures II-1a and II-1b (insets) respectively. When the curves were fitted with the single binding site model, the dissociation constants, K_D's, were found to be 1.5 μM for L29Q and 2 μM for E59D/D75Y (Table II-1). The upper boundary errors for the fitted K_D's were 2 μM, whereas the lower boundary errors could not be established since K_D's tighter than 1 μM cannot be discriminated within the current concentration conditions. When a second binding site was taken into account in the case of L29Q, the quality of fit was not noticeably improved as the chemical shifts almost completely stopped changing at the Ca^{2+} : protein ratio equal to 1. Within the limitations of this method, we assume that the K_D's determined (~2 μM for E59D/D75Y and ~1.5 μM for L29Q) were essentially the same as the K_D of 2.6 μM for cNTnC (*10*), with no indication of a weak second Ca^{2+} binding site in case of L29Q.

Ca^{2+} affinity towards cNTnC, L29Q, and E59D/D75Y determined using competition assays with the chromophoric chelator, 5,5'-Br_2-BAPTA

The NMR method for determining affinities is most accurate in 0.1-1.0 mM range, where K_D's and the concentrations of protein are of the same order of magnitude. To measure high affinity K_D's more accurately, we used competition assays with the

chromophoric chelator, 5,5'-Br_2-BAPTA. In this type of assays, the concentrations of proteins were ~20-30 μM. The chelator, 5,5'-Br_2-BAPTA, was chosen because its K_D for Ca^{2+} is close to the expected K_D's for the proteins of interest (*11*). Titration data for cNTnC, L29Q, and E59D/D75Y obtained in competitive assays are presented in Figure II-2. Using a single site binding model for curve fitting, determined K_D's for cNTnC, L29Q, and E59D/D75Y were 5 ± 4 μM, 4 ± 2.5 μM, and 6 ± 3 μM respectively (Table II-1). The errors in fitted K_D's reflect mostly the error in the K_D of Ca^{2+} binding to 5,5'-Br_2-BAPTA. Data obtained are in agreement with the results of NMR titrations, where the L29Q and E59D/D75Y mutants showed essentially the same Ca^{2+} affinity as cNTnC within the limitation of the technique.

Since the L29Q substitution occurs naturally in trout cTnC, which possesses the second weak Ca^{2+} binding site I (*12*), we attempted to fit the NMR data for Ca^{2+} titration of L29Q by a two site binding model, using K_{D1} for site II (determined in competitive assays) as a fixed parameter. Three curves corresponding to K_{D2} of 5 mM, 0.5 mM, and 0.05 mM shown in Figure II-3 imply that $K_{D2} \geq 5$ mM. Thus, if L29Q makes defunct site I slightly active, its affinity would be exceptionally low, on the order of 5 mM or higher.

It has been suggested that the Ca^{2+} affinity of cTn is dependent on the presence of the cardiac specific N-terminus of cTnI in phosphorylated state (*13*). Since the affinities of cNTnC towards Ca^{2+} in the presence of $cTnI_{1-29}$ and $cTnI_{1-29}PP$ have not been determined previously, we have performed Ca^{2+} titrations of cNTnC in the complex with $cTnI_{1-29}$ and $cTnI_{1-29}PP$ using competitive assays with 5,5'-Br_2-BAPTA. Complexes formed with $cTnI_{1-29}$ and $cTnI_{1-29}PP$ had the ratio of protein : peptide equal to 1:3. Figure II-4a demonstrates that the K_D's towards Ca^{2+} for cNTnC, cNTnC•$cTnI_{1-29}$, and cNTnC•$cTnI_{1-29}PP$ were indistinguishable and equal to 5 ± 3 μM (Table II-1).

Similar experiments were performed with the L29Q and E59D/D75Y mutants in the presence of $cTnI_{1-29}$ and $cTnI_{1-29}PP$. Figures II-4b and II-4c indicate that these mutations do not affect the Ca^{2+} affinity of L29Q and E59D/D75Y in 1:3 complex with $cTnI_{1-29}$ and $cTnI_{1-29}PP$ within the limitations of the method. Determined K_D's for L29Q, L29Q•$cTnI_{1-29}$, and L29Q•$cTnI_{1-29}PP$ were 4 ± 2 μM and K_D's for E59D/D75Y, E59D/D75Y•$cTnI_{1-29}$, and E59D/D75Y•$cTnI_{1-29}PP$ were 6 ± 3 μM (Table II-1).

$cTnI_{147-163}$ titrations of L29Q•Ca^{2+} and E59D/D75Y•Ca^{2+}

The switch region of cTnI (~residues 147-163) is an important binding partner of cNTnC, that binds in a Ca^{2+} dependent manner to cNTnC, relays the Ca^{2+} signal, and

relieves the inhibition of the actomyosin ATPase. To address the question whether the cardiomyopathy mutations confer the changes in the $cTnI_{147-163}$ binding, L29Q•Ca^{2+} and E59D/D75Y•Ca^{2+} were titrated with the $cTnI_{147-163}$ peptide using 2D {^1H, ^{15}N} HSQC NMR spectroscopy. The overlay of 2D {^1H, ^{15}N} HSQC NMR spectra obtained during titrations (Fig. II-5) demonstrated that induced chemical shift changes were remarkably similar to those observed for cNTnC•Ca^{2+} (*7*) indicating that $cTnI_{147-163}$ binds in a similar fashion to the same binding site. The per residue chemical shift changes caused by the $cTnI_{147-163}$ binding to L29Q•Ca^{2+} and E59D/D75Y•Ca^{2+} were averaged for several of the most perturbed residues and plotted against the peptide/protein ratio (Figs. II-5a and II-5b). The value of K_D obtained for L29Q•Ca^{2+} was 200 ± 20 μM, which is ~1.3-fold weaker than the value of 154 μM determined for cNTnC•Ca^{2+} earlier (*7*) (Table I-1). The value of K_D obtained for E59D/D75Y•Ca^{2+} was 60 ± 40 μM, which is ~2.6-fold tighter than that of for cNTnC•Ca^{2+} (Table I-1).

$cTnI_{147-163}$ titrations of cNTnC•Ca^{2+}, L29Q•Ca^{2+}, and E59D/D75Y•Ca^{2+} in complex with $cTnI_{1-29}$ or $cTnI_{1-29}$PP

The question whether the cardiac specific extension of cTnI in its phosphorylated or unphosphorylated state affects the affinity of cNTnC•Ca^{2+} towards $cTnI_{147-163}$ was addressed using 2D {^1H, ^{15}N} HSQC NMR spectroscopy. Residues that underwent chemical shift changes during the binding of $cTnI_{147-163}$ to cNTnC•Ca^{2+}•$cTnI_{1-29}$ and to cNTnC•Ca^{2+}•$cTnI_{1-29}$PP were essentially the same as that of for cNTnC•Ca^{2+} (Fig. II-6). This suggests that $cTnI_{147-163}$ binds in the same manner to the same binding site on cNTnC•Ca^{2+} alone and in complex with $cTnI_{1-29}$ or $cTnI_{1-29}$PP. However, binding affinities determined for cNTnC•Ca^{2+} in the presence of $cTnI_{1-29}$ or $cTnI_{1-29}$PP were substantially different from the K_D of 154 μM determined for cNTnC•Ca^{2+} (*7*). The K_D obtained for the $cTnI_{147-163}$ binding towards cNTnC•Ca^{2+}•$cTnI_{1-29}$ (Fig. II-7a and Table II-1) was equal to 600 ± 100 μM (~4 fold increase compared to cNTnC•Ca^{2+} alone) and the K_D obtained for the $cTnI_{147-163}$ binding towards cNTnC•Ca^{2+}•$cTnI_{1-29}$PP was 370 ± 30 μM (~2.4 fold increase compared to cNTnC•Ca^{2+} alone).

It has been proposed that the L29Q mutation of troponin C perturbs the interaction with $cTnI_{1-29}$ and $cTnI_{1-29}$PP, and thus is responsible for the development of FHC (*1*). We have measured whether the presence of $cTnI_{1-29}$ and $cTnI_{1-29}$PP affects the affinity towards $cTnI_{147-163}$ in case of L29Q and E59D/D75Y. 2D {^1H, ^{15}N} HSQC NMR

spectroscopy was employed to monitor the changes in chemical shifts of L29Q•Ca^{2+} and E59D/D75Y•Ca^{2+} in complex with unlabeled $cTnI_{1-29}$ or $cTnI_{1-29}PP$ during titrations with the $cTnI_{147-163}$ peptide. The overlay of 2D {^1H, ^{15}N} HSQC NMR spectra shows the similarity between $cTnI_{147-163}$ binding sites in case of L29Q•Ca^{2+}•$cTnI_{1-29}$, L29Q•Ca^{2+}•$cTnI_{1-29}PP$, E59D/D75Y•Ca^{2+}•$cTnI_{1-29}$, and E59D/D75Y•Ca^{2+}•$cTnI_{1-29}PP$ (Figs. II-6c, II-6d, II-6e, and II-6f). In spite of these similarities, determined affinities were noticeably different (Table II-1). The K_D obtained for $cTnI_{147-163}$ towards L29Q•Ca^{2+}•$cTnI_{1-29}$ was equal to 410 ± 30 μM and the K_D obtained for $cTnI_{147-163}$ towards L29Q•Ca^{2+}•$cTnI_{1-29}PP$ was 450 ± 130 μM (Fig. II-7b). The K_D obtained for $cTnI_{147-163}$ towards E59D/D75Y•Ca^{2+}•$cTnI_{1-29}$ was equal to 290 ± 100 μM and the K_D obtained for $cTnI_{147-163}$ towards E59D/D75Y•Ca^{2+}•$cTnI_{1-29}PP$ was 830 ± 150 μM (Fig. II-7c).

Table II-1. Binding affinities towards Ca^{2+} and $cTnI_{147-163}$ for cNTnC, L29Q, and E59D/D75Y determined by solution NMR and in competitive assays with the chelator 5,5'-Br_2-BAPTA.

	Ca^{2+} affinity determined by solution NMR (μM)	Ca^{2+} affinity determined using competitive assays with the chelator, 5,5'-Br_2-BAPTA (μM)	Ca^{2+} affinity determined using competitive assays with the chelator, 5,5'-Br_2-BAPTA (μM) in a complex with	
			$cTnI_{1-29}$	$cTnI_{1-29}PP$
cNTnC	2.6 (*10*)	5 ± 4	5 ± 3	5 ± 3
L29Q	1.5 ± 2	4 ± 2.5	4 ± 2	4 ± 2
E59D/D75Y	2 ± 2	6 ± 3	6 ± 3	6 ± 3
	$cTnI_{147-163}$ affinity determined using solution NMR (μM)		$cTnI_{147-163}$ affinity determined using solution NMR (μM) in a complex with	
			$cTnI_{1-29}$	$cTnI_{1-29}PP$
cNTnC•Ca^{2+}	154 (*7*)		600 ± 100	370 ± 30
L29Q•Ca^{2+}	200 ± 20		410 ± 30	450 ± 130
E59D/D75Y•Ca^{2+}	60 ± 40		290 ± 100	830 ± 150

^{15}N backbone relaxation data

The ^{15}N backbone NMR relaxation parameters T_1, T_2, and NOE depend on the motions of a protein, including the tumbling of a protein as a whole and the motions of its

independent parts. T_1, T_2, and NOE are the complex functions of protein motions; however, the interpretation of T_2 is more straightforward since the major contribution to T_2 is the tumbling of a protein as a whole, which makes T_2 directly proportional to the overall correlation time, τ_m, and therefore to the molecular weight of the species for a wide variety of conditions (*14*). The other significant contribution to T_2 arises from the chemical exchange processes including self-association. T_2 can be used to indicate the presence of chemical exchange or self-association if it is noticeably lower than the theoretical T_2 values, calculated using Model Free approach (*15*), where $S^2 \approx 0.85$ (the approximation valid for many proteins (*16*)) and the contribution of internal motions are considered negligible (τ_f < 100 μs) (*17*). T_1, T_2, and NOE were determined for apo cNTnC, cNTnC•Ca^{2+}, L29Q•Ca^{2+}, and E59D/D75Y•Ca^{2+} alone, and in the presence of $cTnI_{147-163}$, $cTnI_{1-29}$, and $cTnI_{1-29}$PP (Table II-2, data for T_1 and NOE are not shown). Experimental T_2 values are mostly in the same range as the theoretical T_2 values that are directly proportional to the molecular weight of the species (Table II-2), which indicates the absence of significant exchange processes or self-association. Care should be taken for E59D/D75Y, where T_2 is ~20 ms lower in the case of the Ca^{2+} and $cTnI_{147-163}$ bound forms. Line broadening observed during the $cTnI_{147-163}$ titration of E59D/D75Y•Ca^{2+} (for ex. residues 34, 73, 66, Fig. II-5a) argues that the change in the $cTnI_{147-163}$ binding kinetics from fast to slow on NMR time scale is likely to be responsible for the decrease in T_2, which brings the contribution from the chemical exchange to the T_2 relaxation rate. In case of the Ca^{2+} bound form, the decrease in T_2 can also result from the changes in Ca^{2+} binding kinetics but more likely it stems from the slight dimerization, supported also by the increase in the overall correlation time, τ_m, as discussed below.

The overall correlation time, τ_m, obtained from relaxation parameters T_1, T_2, and NOE (*17, 18*) often serves as a useful indicator of molecular weight of the species in solution (*19*). The increase in τ_m, as compared to the theoretical estimate, equal to MW(kDa)/2, can sometimes result from the presence of mobile domains that slows down the tumbling of a protein or from the dimerization (*20*), in which case the Model Free analysis is not strictly suitable (*21*) unless modified for the presence of two species. Based on T_2 data, the dimerization was absent for almost all species except for E59D/D75Y•Ca^{2+}. Based on the similarity between {^1H, ^{15}N} HSQC spectra (Figs. II-1, II-5, and II-6) for cNTnC, L29Q, and E59D/D75Y, we conclude that the proteins have a similar fold to that of cNTnC, for which no mobile domains or significantly long tails were found (*7, 22*). Thus, obtained τ_m's (Table II-3, Fig. II-8) serve as a direct indicator

of the increase in the molecular weight of species due to the formation of complexes with the cTnI peptides.

Table II-2. ^{15}N backbone amide NMR relaxation parameter, T_2, for cNTnC, L29Q, and E59D/D75Y in various complexes obtained at 500 MHz. T_2's were averaged over all residues and presented together with their standard deviations. The errors in T_2's represent the quality of the fit. Theoretical T_2's values were calculated for a protein of the same molecular weight using Model Free formalism, where S^2 is equal to 0.85 and internal motions are considered negligible (*15*).

	Average T_2 (ms)	T_2 error (ms)	Theoretical T_2 (ms)
apo cNTnC	134 ± 31	4	149
apo cNTnC•$cTnI_{1-29}$	113 ± 19	3	122
apo cNTnC•$cTnI_{1-29}$PP	137 ± 48	3	121
cNTnC•Ca^{2+}	142 ± 52	5	149
L29Q•Ca^{2+}	139 ± 15	4	149
E59D/D75Y•Ca^{2+}	130 ± 46	4	149
cNTnC•Ca^{2+}•$cTnI_{147-163}$	138 ± 27	8	132
L29Q•Ca^{2+}•$cTnI_{147-163}$	123 ± 49	4	132
E59D/D75Y•Ca^{2+}•$cTnI_{147-163}$	111 ± 47	2	132
cNTnC•Ca^{2+}•$cTnI_{1-29}$	118 ± 39	5	122
L29Q•Ca^{2+}•$cTnI_{1-29}$	128 ± 51	4	122
E59D/D75Y•Ca^{2+}•$cTnI_{1-29}$	114 ± 47	4	122
cNTnC•Ca^{2+}•$cTnI_{1-29}$PP	139 ± 57	5	121
L29Q•Ca^{2+}•$cTnI_{1-29}$PP	148 ± 55	4	121
E59D/D75Y•Ca^{2+}•$cTnI_{1-29}$PP	120 ± 45	5	121
cNTnC•Ca^{2+}•$cTnI_{1-29}$•$cTnI_{147-163}$	102 ± 47	3	110
L29Q•Ca^{2+}•$cTnI_{1-29}$•$cTnI_{147-163}$	111 ± 49	5	110
E59D/D75Y•Ca^{2+}•$cTnI_{1-29}$•$cTnI_{147-163}$	101 ± 51	4	110
cNTnC•Ca^{2+}•$cTnI_{1-29}$PP•$cTnI_{147-163}$	115 ± 51	4	109
L29Q•Ca^{2+}•$cTnI_{1-29}$PP•$cTnI_{147-163}$	121 ± 56	4	109
E59D/D75Y•Ca^{2+}•$cTnI_{1-29}$PP•$cTnI_{147-163}$	111 ± 47	4	109

Table II-3. Theoretical versus experimental overall correlation time τ_m for cNTnC, L29Q, and E59D/D75Y in various complexes. Theoretical τ_m values were calculated as MW(kDa)/2, similarly to the described previously (*19*).

	Overall correlation time, τ_m (ns)	Theoretical overall correlation time, τ_m (ns)
apo cNTnC	4.99	5.08
apo cNTnC•$cTnI_{1-29}$	6.66	6.66
apo cNTnC•$cTnI_{1-29}$PP	5.14	6.74
cNTnC•Ca^{2+}	4.95	5.08
cNTnC•Ca^{2+}•$cTnI_{147-163}$	5.79	5.98
cNTnC•Ca^{2+}•$cTnI_{1-29}$	6.05	6.66
cNTnC•Ca^{2+}•$cTnI_{1-29}$•$cTnI_{147-163}$	6.89	7.56
cNTnC•Ca^{2+}•$cTnI_{1-29}$PP	5.16	6.74
cNTnC•Ca^{2+}•$cTnI_{1-29}$PP•$cTnI_{147-163}$	6.09	7.64
L29Q•Ca^{2+}	5.07	5.09
L29Q•Ca^{2+}•$cTnI_{147-163}$	5.87	5.99
L29Q•Ca^{2+}•$cTnI_{1-29}$	5.81	6.67
L29Q•Ca^{2+}•$cTnI_{1-29}$•$cTnI_{147-163}$	6.44	7.57
L29Q•Ca^{2+}•$cTnI_{1-29}$PP	5.12	6.75
L29Q•Ca^{2+}•$cTnI_{1-29}$PP•$cTnI_{147-163}$	5.91	7.65
E59D/D75Y•Ca^{2+}	5.49	5.1
E59D/D75Y•Ca^{2+}•$cTnI_{147-163}$	6.39	6.00
E59D/D75Y•Ca^{2+}•$cTnI_{1-29}$	6.33	6.68
E59D/D75Y•Ca^{2+}•$cTnI_{1-29}$•$cTnI_{147-163}$	6.84	7.58
E59D/D75Y•Ca^{2+}•$cTnI_{1-29}$PP	5.82	6.76
E59D/D75Y•Ca^{2+}•$cTnI_{1-29}$PP•$cTnI_{147-163}$	6.37	7.67

Based on the τ_m data (Table II-3, Fig. II-8a), cNTnC•Ca^{2+} binds all three peptides $cTnI_{1-29}$, $cTnI_{1-29}$PP, and $cTnI_{147-163}$ independently. Apo cNTnC binds both $cTnI_{1-29}$ and $cTnI_{1-29}$PP as well, with similar avidity. The interaction of cNTnC•Ca^{2+} with $cTnI_{1-29}$ is more efficient than with $cTnI_{1-29}$PP since τ_m for cNTnC•Ca^{2+}•$cTnI_{1-29}$ is larger than τ_m for cNTnC•Ca^{2+}•$cTnI_{1-29}$PP and τ_m for apo cNTnC•$cTnI_{1-29}$ is larger than τ_m for apo cNTnC•$cTnI_{1-29}$PP (Table II-3, Fig. II-8a). Complexes with $cTnI_{1-29}$ and $cTnI_{1-29}$PP are formed with the stoicheometry less then 1:1 (τ_m's are smaller than the theoretical values in Table II-3 and below the diagonal in Figure II-8a), which indicates incomplete binding. cNTnC•Ca^{2+} in complex with $cTnI_{1-29}$ or $cTnI_{1-29}$PP binds $cTnI_{147-163}$ forming a triple complex (τ_m's for triple complexes are higher than τ_m's for the corresponding duplexes). The addition of $cTnI_{147-163}$ increases the weight of the cNTnC•Ca^{2+}•$cTnI_{1-29}$

complex to a smaller degree than that of cNTnC•Ca^{2+}•$cTnI_{1-29}$PP (Table II-3) supporting the titration data where $cTnI_{147-163}$ binds tighter to cNTnC•Ca^{2+}•$cTnI_{1-29}$PP.

Similar qualitative conclusions can be drawn for L29Q and E59D/D75Y (Table II-3, Figs. II-8b and II-8c). Both mutants bind three peptides, $cTnI_{1-29}$, $cTnI_{1-29}$PP, and $cTnI_{147-163}$, independently, and form triplexes with $cTnI_{1-29}$ or $cTnI_{1-29}$PP and $cTnI_{147-163}$. L29Q•Ca^{2+} binds $cTnI_{1-29}$ and $cTnI_{1-29}$PP less efficiently than cNTnC•Ca^{2+}. The L29Q•Ca^{2+} binding to $cTnI_{1-29}$PP is especially small (τ_m's for L29Q•Ca^{2+}•$cTnI_{1-29}$PP and L29Q•Ca^{2+}•$cTnI_{1-29}$PP•$cTnI_{147-163}$ are almost the same as the τ_m's for L29Q•Ca^{2+} and L29Q•Ca^{2+}•$cTnI_{147-163}$). The binding of $cTnI_{147-163}$ to L29Q•Ca^{2+}•$cTnI_{1-29}$PP is almost as efficient as binding to L29Q•Ca^{2+}•$cTnI_{1-29}$.

Since several τ_m's in Figure II-8c are above the theoretical values and possibly slightly distorted due to the dimerization, conclusions about the E59D/D75Y behavior should be drawn with care. It is likely that E59D/D75Y•Ca^{2+} binds $cTnI_{1-29}$ weaker than cNTnC•Ca^{2+} and binds $cTnI_{1-29}$PP stronger than cNTnC•Ca^{2+}. The binding of $cTnI_{147-163}$ to E59D/D75Y•Ca^{2+}•$cTnI_{1-29}$ might be as efficient as the binding of $cTnI_{147-163}$ to cNTnC•Ca^{2+}•$cTnI_{1-29}$PP not contradicting our titration data.

Discussion

Ca^{2+} and $cTnI_{147-163}$ binding affinity for cNTnC in the presence of $cTnI_{1-29}$ and $cTnI_{1-29}$PP

It has been established that the phosphorylation of cTnI at position 22 and 23 results in the decreased Ca^{2+} sensitivity of actomyosin ATPase (*23, 24*) and increased rates of muscle relaxation and cross-bridge cycling (*25, 26*). Ca^{2+} off-rates in phosphorylated Tn complex are increased as well (*27*), which might stem from the alterations in either equilibria involved in Scheme 1. Within the errors of the method our data demonstrates that the Ca^{2+} binding affinity of cNTnC is not affected by the presence of $cTnI_{1-29}$ or $cTnI_{1-29}$PP (Fig. II-4, Table II-1), suggesting that the interaction with $cTnI_{1-29}$ or $cTnI_{1-29}$PP does not interrupt Ca^{2+} ligation and does not significantly affect the structure and dynamics of cNTnC, which might also potentially perturb the Ca^{2+} binding energetics. The affinities towards $cTnI_{147-163}$ are instead decreased substantially: ~4 times for cNTnC•Ca^{2+}•$cTnI_{1-29}$ and ~2 times for cNTnC•Ca^{2+}•$cTnI_{1-29}$PP. The $cTnI_{147-163}$ binding affinity towards cNTnC•Ca^{2+} is decreasing in the following order: cNTnC•Ca^{2+} > cNTnC•Ca^{2+}•$cTnI_{1-29}$PP > cNTnC•Ca^{2+}•$cTnI_{1-29}$, which corresponds to the cTnI inhibition activity increasing in the similar order: cNTnC•Ca^{2+} < cNTnC•Ca^{2+}•$cTnI_{1-29}$PP < cNTnC•Ca^{2+}•$cTnI_{1-29}$. This is in excellent agreement with the physiological data

on muscle myofibrillar relaxation (*25*), where relaxation rates followed the similar trend: a muscle preparation from transgenic mice expressing ssTnI (where ssTnI is a slow skeletal version of cTnI lacking the first 32 residues) relaxed faster (~70 ms) than the phosphorylated preparation from wt mice muscle (~90 ms), which in turn relaxed faster than the unphosphorylated version (~150 ms). This serves as an evidence of the importance of the $cTnI_{147-163}$ binding kinetics in determining the rate of muscle relaxation. The more efficiently the switch region of cTnI (~residues 147-163) binds to cNTnC•Ca^{2+}, the more efficiently the inhibitory region of cTnI (~residues 128-147) is sequestered away from its binding site on actin, which is likely to accelerate the formation of cross-bridges, their cycling rate, and the relaxation rate of muscle, thus transferring the signal of phosphorylation by PKA.

The binding interactions between cNTnC•Ca^{2+} and $cTnI_{1-29}$ or $cTnI_{1-29}$PP are of enormous interest, but notoriously difficult to detect. The quenching of fluorescent Tyr^{25} and Tyr^{28} on cTnI and the changes in the CD spectra during titration with cNTnC•Ca^{2+} were negligible (data not shown). The signal in ITC titrations was remarkably small (*28*) and the majority of binding studies presented in literature had to utilize a label, AEDANS (*8*) or IAANS (*29, 30*), possibly affecting the charge distribution on the cNTnC surface and the binding equilibrium. Chemical shifts changes in the NMR spectra of the N-domain of cTnC•Ca^{2+} bound to $cTnI_{1-80}$ were exceptionally small (*31*), so that a binding curve plot was not possible to construct (our data not shown). In this work the following insights about the $cTnI_{1-29}$ and $cTnI_{1-29}$PP binding to cNTnC•Ca^{2+} have been obtained: <u>first</u>, based on the τ_m values, both, $cTnI_{1-29}$ and $cTnI_{1-29}$PP bind to cNTnC•Ca^{2+} and apo cNTnC. In agreement with literature data, $cTnI_{1-29}$ binds more efficiently than $cTnI_{1-29}$PP (*28, 30*). <u>Second</u>, the $cTnI_{1-29}$ ($cTnI_{1-29}$PP) binding to cNTnC•Ca^{2+}(apo cNTnC) does not induce significant conformational changes and most probably is driven by electrostatics since the changes in cNTnC•Ca^{2+} and apo cNTnC chemical shifts upon binding to $cTnI_{1-29}$ ($cTnI_{1-29}$PP) are very small, which is characteristic of a typical electrostatic interaction. In comparison, the $cTnI_{147-163}$ binding to cNTnC•Ca^{2+} is accompanied by the large chemical shift changes in NMR spectra, and induces the substantial conformation change in cNTnC from a closed to an opened conformation. <u>Third</u>, both complexes, cNTnC•Ca^{2+}•$cTnI_{1-29}$ and cNTnC•Ca^{2+}•$cTnI_{1-29}$PP, bind $cTnI_{147-163}$ into its original binding site and form triplexes, which implies that $cTnI_{147-163}$ and $cTnI_{1-29}$ ($cTnI_{1-29}$PP) have independent binding sites and can bind simultaneously. <u>Fourth</u>, the presence of $cTnI_{1-29}$ ($cTnI_{1-29}$PP) affects the affinity of cNTnC•Ca^{2+} towards $cTnI_{147-163}$, but not the

affinity of cNTnC towards Ca^{2+}. One of the hypotheses, explaining the change in the $cTnI_{147-163}$ affinity, proposes that the $cTnI_{1-29}$ and $cTnI_{1-29}PP$ binding sites on cNTnC•Ca^{2+} partially overlap with the binding site for $cTnI_{147-163}$. This overlap is small since the $cTnI_{147-163}$ peptide still binds fairly tightly and the $cTnI_{1-29}$ binding alone does not induce the open conformation of cNTnC•Ca^{2+}. This hypothesis would be in agreement with the cross-linking data, showing that cTnI residues 5 (or 8) and 154 are in close proximity (*32*). Another hypothesis proposes that $cTnI_{1-29}$ and $cTnI_{1-29}PP$ sites on cNTnC•Ca^{2+} do not overlap with the $cTnI_{147-163}$ binding site, however, $cTnI_{1-29}$ and $cTnI_{1-29}PP$ stabilize cNTnC•Ca^{2+} in a closed conformation, albeit with different strengths, thus requiring more energy for $cTnI_{147-163}$ to bind to the cleft on cNTnC•Ca^{2+}. The affinity of $cTnI_{147-163}$ will be lessened the most when $cTnI_{1-29}$ is bound unphosphorylated, since more $cTnI_{1-29}$ is bound to cNTnC•Ca^{2+}, locking cNTnC•Ca^{2+} in the closed conformation. This hypothesis is in agreement with the reported NMR data showing the line broadening in areas of β-sheets on cNTnC•Ca^{2+} bound to $cTnI_{1-80}$ (*31, 33*). The area of β-sheets on cNTnC•Ca^{2+} is located on the opposite side from the $cTnI_{147-163}$ binding site (*7*). We favor the model where $cTnI_{1-29}$ and $cTnI_{1-29}PP$ bind on cNTnC•Ca^{2+} without overlapping with $cTnI_{147-163}$; however, the distance between both cTnI regions when bound to cNTnC•Ca^{2+} should be short enough to afford the cross-linking between them (*32*). More detailed information on binding of $cTnI_{1-29}$ ($cTnI_{1-29}PP$) to cNTnC•Ca^{2+}, e.g. the nature of the forces driving the formation of the cNTnC•Ca^{2+}•$cTnI_{1-29}$ complex will be discussed in Chapter IV.

It is desirable to compare other binding data available with the K_D's obtained in this work. For instance, data on the binding of whole cTnI to cTnC has been reported (*8, 29*), however, upon phosphorylation one segment of cTnI should bind weaker (~residues 1-29) and another segment of cTnI should bind stronger (~residues 147-163), thus reported K_D's represent a complex function of several independent events that are difficult to dissect. This emphasizes the need for binding studies with independent peptides, where individual K_D's can be obtained and compared. In addition, the introduction of a charged label such as AEDANS, might perturb the charge distribution on the cNTnC surface, which similarly to E59D/D75Y might reverse the effect of the cTnI N-terminus (*8*), strengthening the binding towards $cTnI_{147-163}$ in the presence of TnI_{1-29} and weakening in the presence of $TnI_{1-29}PP$.

It is also highly attractive to explain the increase in Ca^{2+} off rates and the decrease in Ca^{2+} sensitivity upon phosphorylation. The Ca^{2+} sensitivity of force development decreases in the following order (Ca^{2+} required for 50% activation): ssTnI

(0.74 μM) < cTnI (1.52 μM) < cTnI-PP (2.15 μM). The Ca^{2+} off rates increase in the following order: cTnI (21 /s) < cTnI-PP (48 /s) (*27*). As it is known from literature, Ca^{2+} sensitivity and Ca^{2+} off-rates depends on the length of a sarcomere (*34*), on the presence of ATP and Mg^{2+} (*35*), and on the activation of cross-bridges (*36, 37*). Theoretical considerations advocate that "neither activation of force nor that of ATPase is proportional to Ca^{2+} absorption to the activating sites", which underlines the complexity of Ca^{2+} regulation in muscle (*38*). At this point, we are unable to provide a mechanistic explanation for the differences in Ca^{2+} off-rates and filament Ca^{2+} sensitivities in phosphorylated, unphosphorylated states, and without the N-terminus of cTnI due to the complexity of the system.

Ca^{2+} binding affinity for L29Q and E59D/D75Y

A consensus EF hand motif in Ca^{2+} binding proteins is composed of 12 residues, 6 of which are directly involved in the coordination of Ca^{2+} (Table II-4) (*39*). In cNTnC silent Ca^{2+} binding site I, 4 residues remain available for the coordination of Ca^{2+} out of 6 conserved residues, providing 5 out of 7 ligating atoms. Several consensus residues that do not directly interact with Ca^{2+} but provide the required rigidity and charge balance for a Ca^{2+} binding site are also substituted in cNTnC site I, and one residue preceding binding site I is inserted (Table II-4). The L29Q mutation in site I is potentially capable of providing the side chain for Ca^{2+} coordination, however, the amide group of Gln^{29} is a less potent ligand than the carboxylic group of consensus Asp^{29}, and the chain length for a ligand is slightly longer than that of Asp^{29}. Site II remained intact and the affinity of site II in L29Q should not be changed. The question of whether the L29Q substitution increases the overall Ca^{2+} affinity of cNTnC was addressed using two independent methods, NMR titrations and UV/VIS titrations with a chromophoric chelator, 5,5'-Br_2-BAPTA. Both methods yielded consistent results with the L29Q affinity towards Ca^{2+} essentially the same as that of for cNTnC. In fish cTnC, the engineered Q29L mutation was shown to decrease the originally high Ca^{2+} sensitivity to the level comparable with human cTnC, thus proving that the L29Q substitution in fish is required for the higher sensitivity towards Ca^{2+}, however, L29Q is not the only substitution necessary for a higher Ca^{2+} sensitivity (*40*). While the increase in Ca^{2+} sensitivity in fish cTnC is the most noticeable at cold temperatures, where it allows the fish to overcome the desensitization of the heart, the increase in Ca^{2+} affinity for human L29Q at 30°C was not significant enough to be recorded. Little evidence for a weak second Ca^{2+} binding site for

L29Q was observed and the estimated K_{D2} for this binding is ~5 mM or weaker, which limits its possible physiological consequences.

In case of E59D/D75Y, the Ca^{2+} affinity also did not noticeably change, although the slight decrease in Ca^{2+} affinity of site II might have been expected. The substitution of conserved Asp^{75} to Tyr^{75} should not affect Ca^{2+} coordination directly, however, it can disrupt electrostatic balance and the packing within the Ca^{2+} binding loop (Table II-4). In competition assays with a chelator, 5,5'-Br_2-BAPTA, and in NMR titrations E59D/D75Y showed no change in Ca^{2+} affinity within the errors of the method. It is still possible that the changes in affinities smaller than the resolution of the techniques used in this work could be physiologically significant.

Table II-4. Residues involved in the coordination of Ca^{2+} in the EF hand motifs of various TnC's.

Position	X		Y	Z		-Y	-X			-Z
Consensus sequence	D	Basic	D/N G	D/N	G	Any	hydro-phobic	D/E/T/S	Hydro-phobic	Acidic	E
Coordinating group	COO side chain		C=O COO side chain	C=O COO side chain		C=O back-bone		COO $CONH_2$ OH Water			COO
cNTnC (site I)	F^{27}	V^{28} **L^{29}**	G^{30}	A^{31} E^{32}	D^{33}	G^{34} S^{35}	I^{36}	S^{37}	T^{38}	K^{39}	E^{40}
L29Q	F^{27}	V^{28} **Q^{29}**	G^{30}	A^{31} E^{32}	D^{33}	G^{34} S^{35}	I^{36}	S^{37}	T^{38}	K^{39}	E^{40}
Trout cNTnC	F^{27}	I^{28} **Q^{29}**	D^{30}	A^{31} E^{32}	D^{33}	G^{34} S^{35}	I^{36}	S^{37}	T^{38}	K^{39}	E^{40}
sNTnC	F^{28}	– **D^{29}**	A^{30}	D^{31} G^{32}	D^{33}	G^{34} D^{35}	I^{36}	S^{37}	V^{38}	K^{39}	E^{40}
cNTnC (site II)	E^{63}	V^{64} D^{65}	E^{66}	D^{67} G^{68}	S^{69}	G^{70} T^{71}	V^{72}	D^{73}	F^{74}	**D^{75}**	E^{76}
E59D/D75Y	E^{63}	V^{64} D^{65}	E^{66}	D^{67} G^{68}	S^{69}	G^{70} T^{71}	V^{72}	D^{73}	F^{74}	**Y^{75}**	E^{76}
Trout cNTnC	E^{63}	V^{64} D^{65}	E^{66}	D^{67} G^{68}	S^{69}	G^{70} T^{71}	V^{72}	D^{73}	F^{74}	**D^{75}**	E^{76}
sNTnC	E^{63}	V^{64} D^{65}	E^{66}	D^{67} G^{68}	S^{69}	G^{70} T^{71}	I^{71}	D^{73}	F^{74}	**D^{75}**	E^{76}

$cTnI_{147-163}$ binding affinity for L29Q•Ca^{2+} and E59D/D75Y•Ca^{2+}

The slight decrease in affinity for L29Q•Ca^{2+} towards $cTnI_{147-163}$ was anticipated since the L29Q mutation is likely to perturb the binding interface with the $cTnI_{147-163}$ peptide. On the structure reported by Li et al. (7), the δ-hydrogen of Leu^{29} on cNTnC is positioned 6.3 Å away from the δ-proton and 6.6 Å away from the β-proton of Leu^{158} on $cTnI_{147-163}$, and 7.1 Å away from the δ-proton of Leu^{159} on $cTnI_{147-163}$. Although these residues do not directly interact with Leu^{29} on cNTnC, the decrease in the affinity of L29Q•Ca^{2+} towards $cTnI_{147-163}$ can stem from the perturbed bonding interactions within the hydrophobic core of the interface, for example, through Val^{44} and Ile^{26}.

The increase in the affinity of E59D/D75Y•Ca^{2+} towards $cTnI_{147-163}$ can be explained by the strengthening of the interaction between Asp^{59} on E59D/D75Y and Arg^{147} of $cTnI_{147-163}$ due to the shortening of the side chain in the position of residue 59. In the structure of cNTnC•Ca^{2+} in complex with $cTnI_{147-163}$ (*7*) the guanidine group of Arg^{147} on $cTnI_{147-163}$ is ~ 6 Å away from the carboxylic oxygen and ~ 4 Å away from the γ-protons of Glu^{59} on cNTnC. Thus, the shortening of the side chain of residue 59 is likely to result in a stronger electrostatic contact between E59D/D75Y•Ca^{2+} and $cTnI_{147-163}$.

Ca^{2+} and $cTnI_{147-163}$ binding affinity for L29Q, and E59D/D75Y in the presence of $cTnI_{1-29}$ and $cTnI_{1-29}PP$

Similarly to cNTnC, within the experimental error the affinities of L29Q and E59D/D75Y towards Ca^{2+} were not affected by the presence of $cTnI_{1-29}$ and $cTnI_{1-29}PP$. The affinity towards $cTnI_{147-163}$ was distinct for every mutant and different from that of cNTnC•Ca^{2+}. L29Q•Ca^{2+} affinity towards $cTnI_{147-163}$ was essentially the same in the presence of $cTnI_{1-29}$ and $cTnI_{1-29}PP$, which should confer the same cTnI inhibition of actin regardless of cTnI phosphorylation state. This is in accordance with the data showing that the impact of phosphorylation in L29Q was abolished, and both, ATPase activity and the sliding velocity of the thin filament, remained unaffected by cTnI phosphorylation (*1*). Based on our τ_m data, L29Q•Ca^{2+} binds both $cTnI_{1-29}$ and $cTnI_{1-29}PP$ less efficiently than cNTnC•Ca^{2+}, which might explain the absence of bound species on the binding plate in Schmidtmann et al. (*1*). A slight decrease in the Ca^{2+} sensitivity of force development (*41*) is in agreement with a decreased affinity towards $cTnI_{147-163}$ (in the absence of phosphorylation by PKA) that might increase the inhibition of actin and presumably decelerate the rate of cross-bridge formation. When phosphorylated, the L29Q containing fibers might demonstrate a decrease in inhibition of actin and increase in the rates of cross-bridge formation and muscle relaxation, for which physiological data is not available. The introduction of the L29Q mutation has brought the change in the $cTnI_{147-163}$ binding affinity per se, and the change in the interactions of L29Q•Ca^{2+} with $cTnI_{1-29}$ and $cTnI_{1-29}PP$, which affects their modulation of the $cTnI_{147-163}$ affinity with and without PKA phosphorylation. The interplay between these events is likely to be responsible for the development of FHC.

The E59D/D75Y mutation brings a drastic change in the $cTnI_{147-163}$ binding equilibrium to cNTnC•Ca^{2+} alone and in complex with $cTnI_{1-29}$ and $cTnI_{1-29}PP$. The strength of $cTnI_{147-163}$ binding becomes reversed: E59D/D75Y•Ca^{2+}•$cTnI_{1-29}$ binds $cTnI_{147-}$

$_{163}$ with higher affinity than E59D/D75Y•Ca^{2+}•$cTnI_{1-29}$PP. This data can be explained by the charge perturbation on the $cTnI_{1-29}$ and $cTnI_{1-29}$PP binding interface. In E59D/D75Y, the surface charge is changed to the less negative as compared to cNTnC, decreasing the electrostatic repulsion of $cTnI_{1-29}$PP. This leads to a slightly tighter binding towards $cTnI_{1-29}$PP as compared to cNTnC (qualitatively supported by the τ_m data) and a weaker binding towards $cTnI_{147-163}$ (supported by our titration data). When phosphorylated, the E59D/D75Y containing filaments are likely to exhibit the increased inhibition of actin, which is in agreement with the reduced ability to activate myosin ATPase activity (*42*). The surface charge perturbation of E59D/D75Y•Ca^{2+} should also lead to a weaker binding of $cTnI_{1-29}$ and consequently a tighter binding of $cTnI_{147-163}$ (supported by our titration data), which in muscle relaxation experiments is likely to result in the decreased muscle inhibition and accelerated relaxation rates. The combined effects of increased affinity towards $cTnI_{147-163}$ for uncomplexed E59D/D75Y•Ca^{2+} and perturbed modulation of the $cTnI_{147-163}$ affinity by $cTnI_{1-29}$ and $cTnI_{1-29}$PP are likely to result in the development of a heart disorder such as DCM.

Conclusions

The cTnI N-terminus is a crucial participant of the Ca^{2+} regulated cardiac muscle contraction. It binds to cNTnC simultaneously with the switch region of cTnI (~residues 147-163) and upon phosphorylation modulates the cNTnC affinity towards $cTnI_{147-163}$, thus transferring the PKA phosphorylation signal further along the thin filament. In case of the cNTnC mutants associated with cardiomyopathy, L29Q and E59D/D75Y, the interactions with the N-terminus and the switch region of cTnI are significantly perturbed, which underlines the importance of these regions in the development of malfunctions and advances our understanding of cardiac muscle regulation.

Materials and Methods

Protein Expression and Purification

The DNA encoding cNTnC (1-89) with the mutations C35S and C84S was subcloned previously into pET-3a expression vector as described in Pearlstone et al. (*43*). Using cNTnC(C35S, C84S) as a template, the L29Q and E59D/D75Y mutations were engineered using a site-directed mutagenesis kit (QuikChange purchased from Stratagene). *E. coli* strain BL21(DE3)pLysS was transformed with the expression vector and incubated at 37°C to the OD_{600} of 0.6-0.9. Cell cultures were induced with IPTG and harvested after incubation for 3 hours. Uniformly ^{15}N-labeled cNTnC, L29Q, and E59D/D75Y were expressed in a minimal media enriched with $(^{15}NH_4)_2SO_4$ (*44*). Cell pellet was lysed using French press and applied to a DEAE-sephadex (A25) column (50 mM Tris, 0.1 M NaCl, pH 8.0). Proteins were further purified using a Superdex-75 size exclusion column (50 mM Tris, 0.15 M NaCl, pH 8.0), desalted using Sephadex G25 column (10 mM NH_4HCO_3), decalcified as described previously (*45*), and lyophilized. Molecular masses for unlabeled proteins, cNTnC, L29Q, and E59D/D75Y, as determined by MALDI mass spectrometry were equal to the expected values for cNTnC (10,030 ± 1 Da), L29Q (10,045 ± 1 Da), and E59D/D75Y (10,064 ± 1 Da). Amino acid composition was confirmed independently by amino acid analysis.

Peptides

Synthetic peptides, $cTnI_{147-163}$ (acetyl-RISADAMMQALLGARAK-amide), $cTnI_{1-29}$ (acetyl-ADGSSDAAREPRPAPAPIRRRSSNYRAYA-amide), and $cTnI_{1-29}PP$ (acetyl-ADGSSDAAREPRPAPAPIRRRS(P)S(P)NYRAYA-amide) were prepared using standard methodology for a typical TnI peptide (*46*). The sequences were confirmed by amino acid analysis and the masses were verified by electrospray mass spectrometry.

Ca^{2+} titrations of ^{15}N-L29Q and ^{15}N-E59D/D75Y monitored by 2D {^1H, ^{15}N} HSQC NMR spectroscopy

Decalcified ^{15}N-L29Q and ^{15}N-E59D/D75Y, respectively, were dissolved in 500 µl of NMR buffer containing 100 mM KCl, 10 mM imidazole, 5 mM NaN_3, and 0.2 mM DSS in 90% H_2O/10% D_2O. The pH was adjusted to 6.8 for both samples. Solutions of 50 mM and 100 mM $CaCl_2$ in water used in titrations of both samples, were prepared from 1.0 M $CaCl_2$ solution purchased from Sigma-Aldrich. The concentration of L29Q (0.9 mM) and E59D/D75Y (1 mM) were determined by amino acid analysis. Changes in protein concentration due to dilution were taken into account during data analysis. To plot the binding curve, per residue chemical shift changes, Δ_{total}, were obtained using the following equation: $\Delta_{total} = \sqrt{(0.2\Delta\delta_{15N})^2 + (\Delta\delta_{1H})^2}$, where $\Delta\delta_{15N}$ is the chemical shift change in ppm in ^{15}N dimension and $\Delta\delta_{1H}$ is the chemical shift change in ppm in ^1H dimension. The coefficient of 0.2 accounts for the difference between sensitivities of ^{15}N and ^1H nuclei. The per residue chemical shift changes for the most perturbed residues (with large chemical shift changes, Δ_{total}) were averaged and analyzed using the program xcrvfit (www.bionmr.ualberta.ca).

Ca^{2+} titrations of cNTnC, L29Q, and E59D/D75Y monitored by UV/VIS spectroscopy using competition assays with the chromophoric chelator, 5,5'-Br_2- BAPTA

A buffer containing 150 mM KCl and 10 mM imidazole (pH 6.8) was decalcified with Chelex-100 resin (BioRad). The affinity of a chelator towards Ca^{2+} was determined by titrating of 40-50 µM of tetra potassium salt of 5,5'-Br_2-BAPTA (CalBiochem) with

$CaCl_2$. 3 μL aliquots of 3 mM $CaCl_2$ were added at every titration point. The UV absorbance was recorded at λ=263 nm. The initial concentration of 5,5'-Br_2-BAPTA (Ca^{2+} free) was calculated using the extinction coefficient of $2 \cdot 10^4$ $L \cdot mol^{-1} \cdot cm^{-1}$ at λ=263 nm (*47*). The K_D for 5,5'-Br_2-BAPTA under experimental conditions was determined to be 0.5 ± 0.3 μM from the average of five independent titrations, which is comparable to the literature data (*11, 47*).

In competition assays, the mixture of a chelator and a protein (or its complex with $cTnI_{1-29}$ and $cTnI_{1-29}PP$) in a total volume of 1 mL was titrated with Ca^{2+}. 3 μL aliquots of 3 mM $CaCl_2$ were added at every titration point. In order to assure the equal concentration of proteins during titrations alone and in complexes with $cTnI_{1-29}$ and $cTnI_{1-29}PP$, protein stock solutions were divided in three portions, into which $cTnI_{1-29}$ or $cTnI_{1-29}PP$ were subsequently added. The concentrations of protein stock solutions were determined by amino acid analysis. The K_D of a protein was deconvoluted from obtained binding curves using Microsoft Excel and xcrvfit software using the K_D of the chelator and the concentrations of individual components as known parameters during the fitting (*11*).

$cTnI_{147-163}$ titration of L29Q•Ca^{2+} and E59D/D75Y•Ca^{2+} monitored by 2D {^1H, ^{15}N} HSQC NMR spectroscopy

The synthetic peptide, $cTnI_{147-163}$, was added in the form of powder during titration of the solution of 0.9 mM L29Q•Ca^{2+} and 0.6 mM E59D/D75Y•Ca^{2+} respectively. The buffer was the same as the buffer used for the NMR Ca^{2+} titrations. $CaCl_2$ was added to a concentration of 35 μM. pH of solutions was adjusted to 6.75 ± 0.1. The concentration of proteins and peptides was determined by amino acid analysis at every titration point.

$cTnI_{147-163}$ titration of cNTnC•Ca^{2+}, L29Q•Ca^{2+} and E59D/D75Y•Ca^{2+} in complex with $cTnI_{1-29}$ or $cTnI_{1-29}PP$ monitored by 2D {^1H, ^{15}N} HSQC NMR spectroscopy

The complexes of cNTnC•Ca^{2+}, L29Q•Ca^{2+} and E59D/D75Y•Ca^{2+} with $cTnI_{1-29}$ or $cTnI_{1-29}PP$ were prepared to the ratio 1 : 2.3. The concentration of proteins was equal to 0.6 mM in the same NMR buffer described above, containing 35 μM of $CaCl_2$. The concentration of peptides was equal to 1.4 ± 0.05 mM in all samples. The formation of complexes was verified using the measurements of ^{15}N backbone amide NMR relaxation rates. During titrations, $cTnI_{147-163}$ was added in the form of powder until the ratio of cNTnC•Ca^{2+} (L29Q•Ca^{2+} or E59D/D75Y•Ca^{2+}) : $cTnI_{147-163}$ was equal to 1 : ~3.5. The pH of solutions was kept at 6.75 ± 0.1. The results of amino acid analysis for the mixture of three components gave rise to a less accurate estimation of concentrations as compared to the concentrations determined by weight. Thus, in these experiments, the weight of added peptide powder was used to calculate the concentration of $cTnI_{147-163}$.

^{15}N backbone amide NMR relaxation data

Relaxation data were acquired from ^{15}N-T_1, ^{15}N-T_2, and {^1H-^{15}N} NOE experiments (Biopack, Varian Associates) for 500 μL samples containing in all experiments 0.6 mM of cNTnC, L29Q, and E59D/D75Y. T_1 data were acquired using relaxation delays of 10, 50, 100, 200, 300, and 400 ms, and T_2 data were acquired using relaxation delays of 10, 30, 50, 70, 90, and 110 ms. The delays between transients in ^{15}N-T_2 and ^{15}N-T_1 experiments were set to 3 s. {^1H-^{15}N} NOE experiments were performed using delays of 5 s for spectra recorded without proton saturation and delays of 2 s for spectra recorded with proton saturation. The proton saturation was set to 3 s so that the total time between transients was equal to 5 s. NMR experiments were conducted at 30

°C on a Varian Inova 500 MHz spectrometer equipped with a z-axis pulsed field gradient triple resonance probe. Acquired spectra were processed using NMRPipe (*48*) and visualized using NMRView (*49*). Relaxation parameters, T_1, T_2, and NOE, were extracted using the rate analysis module built in NMRView. The overall rotational tumbling τ_m was averaged from the per residue fitting of the relaxation data to the Lipari-Szabo S^2-τ_m-τ_f model (*15*). In this method of τ_m calculation, the relaxation data for residues with significant internal motions, as judged by NOE<0.65, and the data for residues with possible slow motions, as judged by significantly decreased T_2, were excluded. Mathematica scripts used for the analysis of relaxation data were provided by Dr. Leo Spyracopuolos (www.bionmr.ualberta.ca/~lspy/) (*50*).

Figure II-1. The overlay of 2D {^{1}H, ^{15}N} HSQC NMR spectra obtained during the Ca^{2+} titrations of L29Q (a) and E59D/D75Y (b). Residue assignments are shown for resonances with significant chemical shift changes. Binding curves (insets) represent the average of chemical shift changes for indicated residues versus the ratio of the total calcium to protein concentrations. The results of fitting are shown for one binding site model.

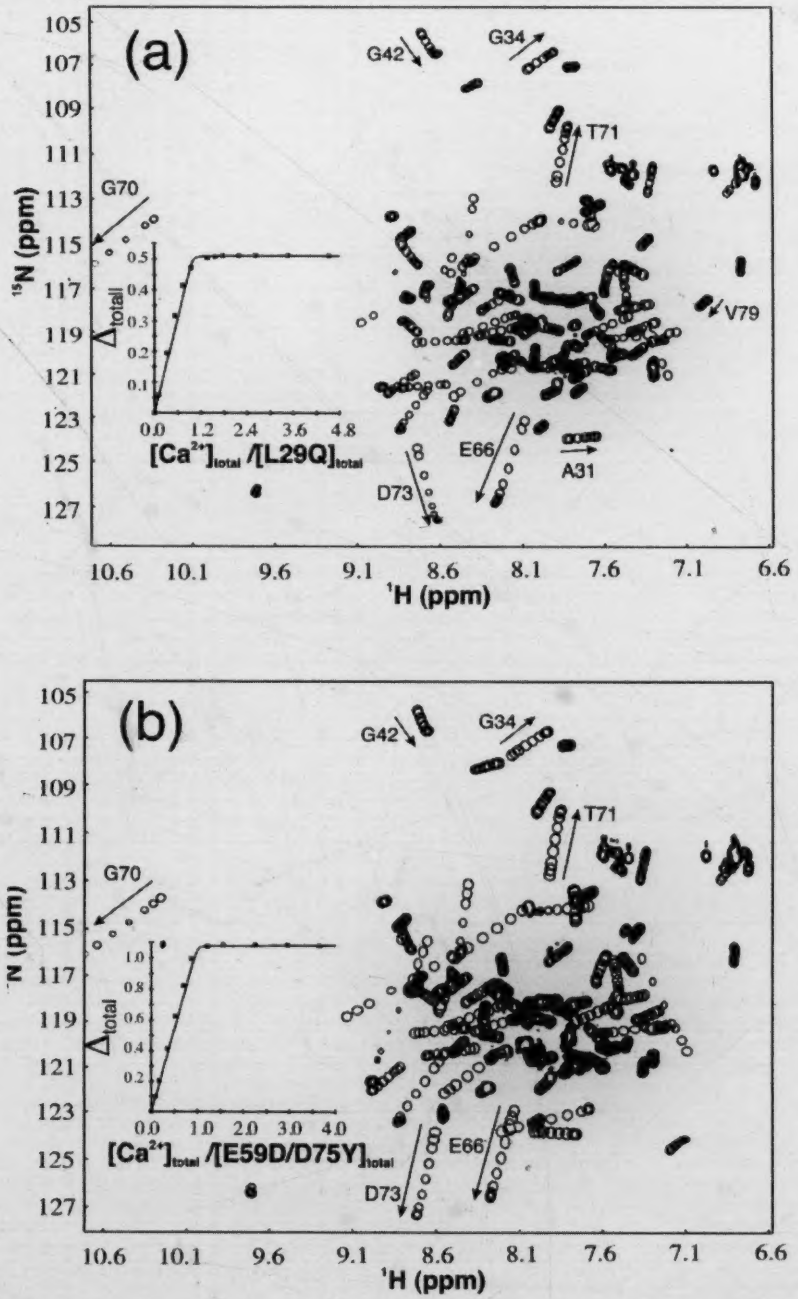

Figure II-2. Normalized absorbance changes during Ca^{2+} titrations for cNTnC (a), L29Q (b), and E59D/D75Y (c) obtained in competitive assays with the chromophoric chelator, 5,5'-Br_2-BAPTA. Two independent binding experiments (triangles and squares) for each protein are shown to demonstrate reproducibility of the method.

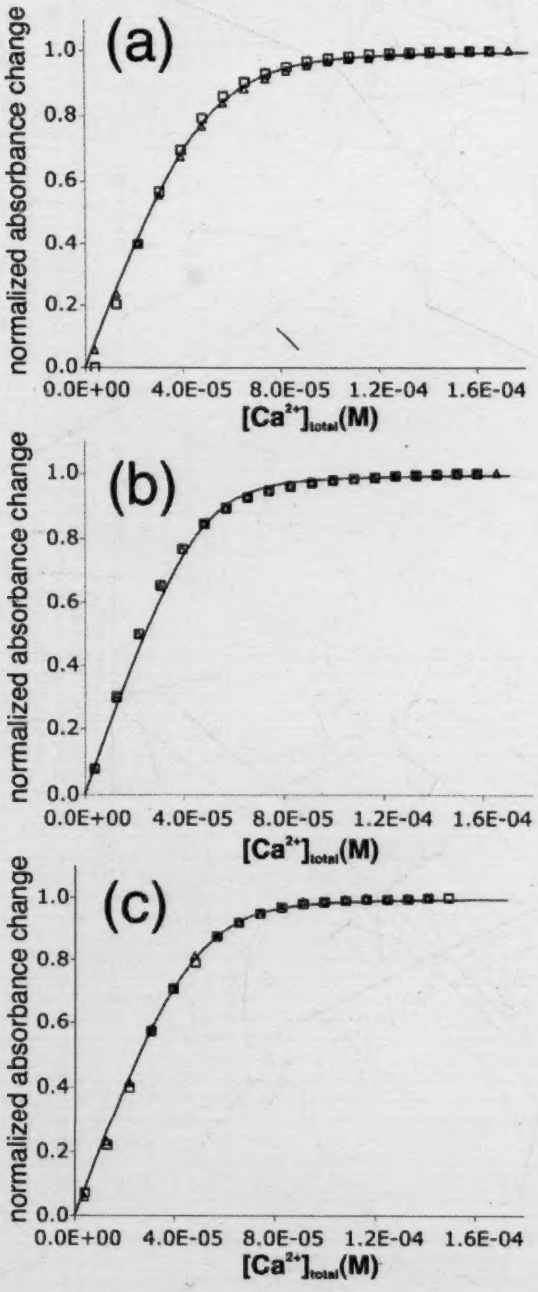

Figure II-3. Ca^{2+} titration of L29Q determined by NMR and analyzed using the two binding site model. Affinity for the first binding site (K_{D1} = 5 μM) was taken as a fixed parameter during the fitting. Examples of the curves obtained with different K_{D2}'s are shown for comparison.

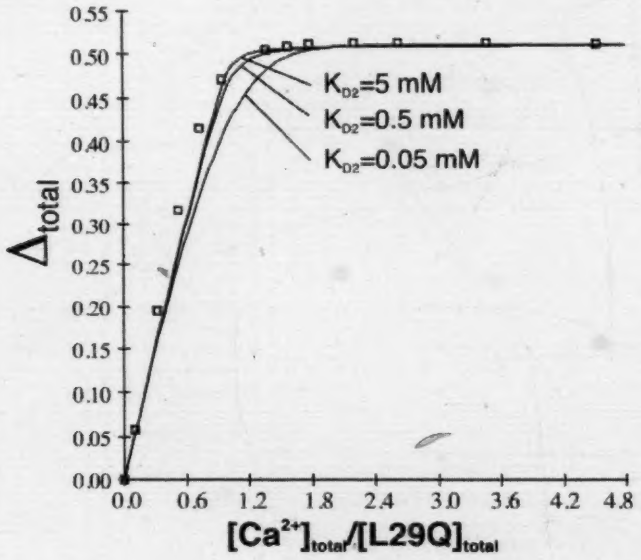

Figure II-4. Normalized absorbance changes during Ca^{2+} titrations for cNTnC (triangles), cNTnC•$cTnI_{1-29}$ (squares), and cNTnC•$cTnI_{1-29}$PP (circles) (a), L29Q (triangles), L29Q•$cTnI_{1-29}$ (squares), and L29Q•$cTnI_{1-29}$PP (circles) (b), and E59D/D75Y (triangles), E59D/D75Y•$cTnI_{1-29}$ (squares), and E59D/D75Y•$cTnI_{1-29}$PP (circles) (c) obtained in competitive assays with the chromophoric chelator, 5,5'-Br_2-BAPTA.

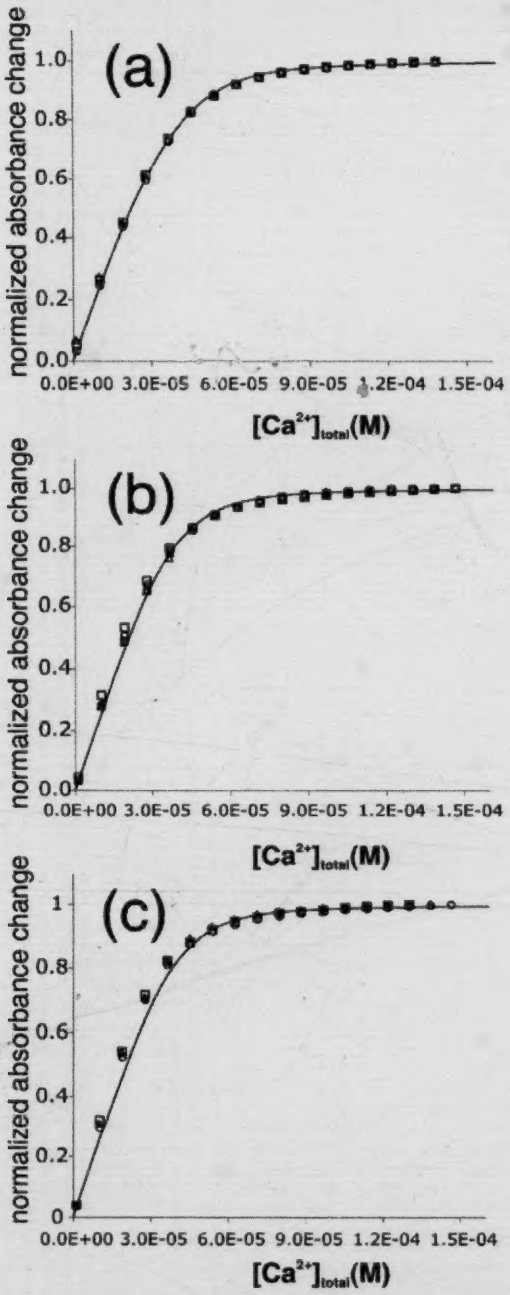

Figure II-5. The overlay of 2D {^{1}H, ^{15}N} HSQC NMR spectra acquired during titration of L29Q•Ca^{2+} (a) and E59D/D75Y•Ca^{2+} (b) with $cTnI_{147-163}$. The contour level for spectra was chosen to demonstrate the fact of line broadening in the middle of titration in case of E59D/D75Y. Binding curves (insets) are averaged over the several residues with substantial chemical shift changes, for which the residue assignments are indicated.

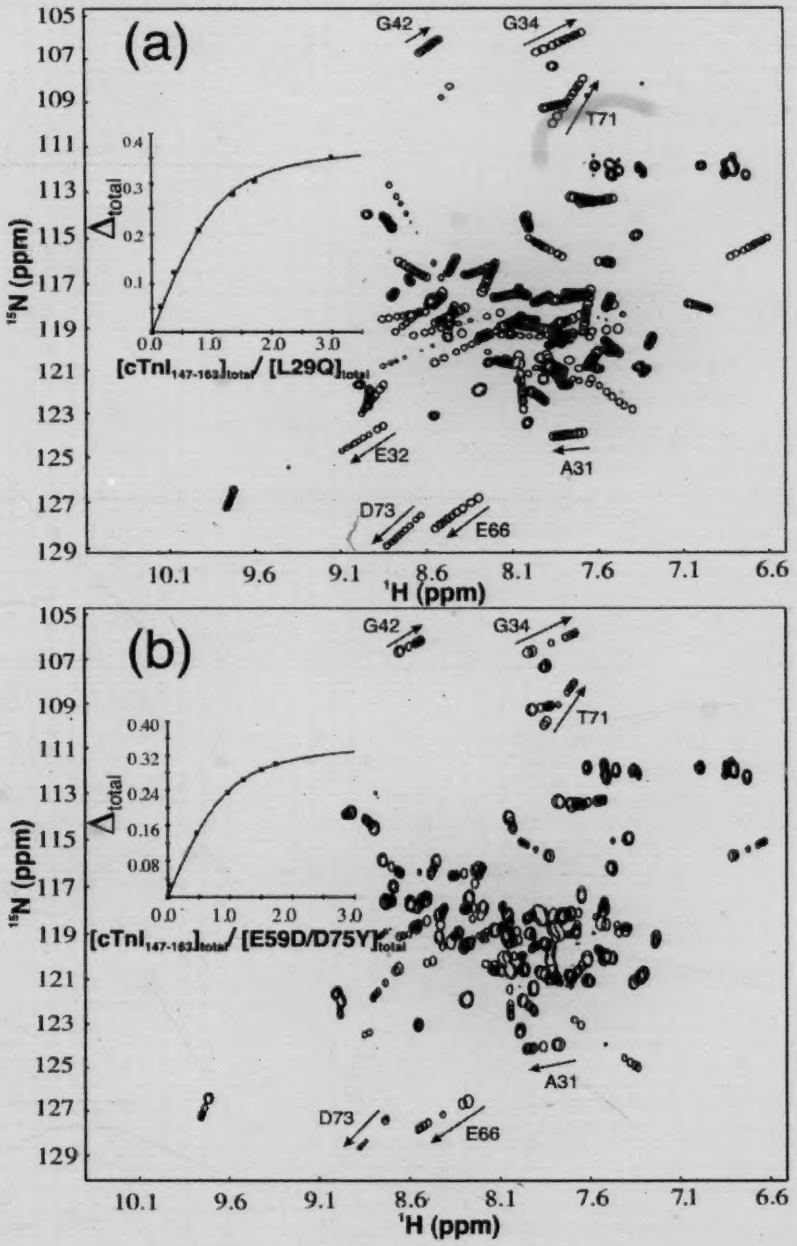

Figure II-6. The overlay of 2D {^{1}H, ^{15}N} HSQC NMR spectra acquired during the $cTnI_{147-163}$ titration of cNTnC•Ca^{2+} in the presence of $cTnI_{1-29}$ (a) and $cTnI_{1-29}$PP (b), L29Q•Ca^{2+} in the presence of $cTnI_{1-29}$ (c) and $cTnI_{1-29}$PP (d), and E59D/D75Y•Ca^{2+} in the presence of $cTnI_{1-29}$ (e) and $cTnI_{1-29}$PP (f). Residue assignments are indicated for the same resonances in each panel.

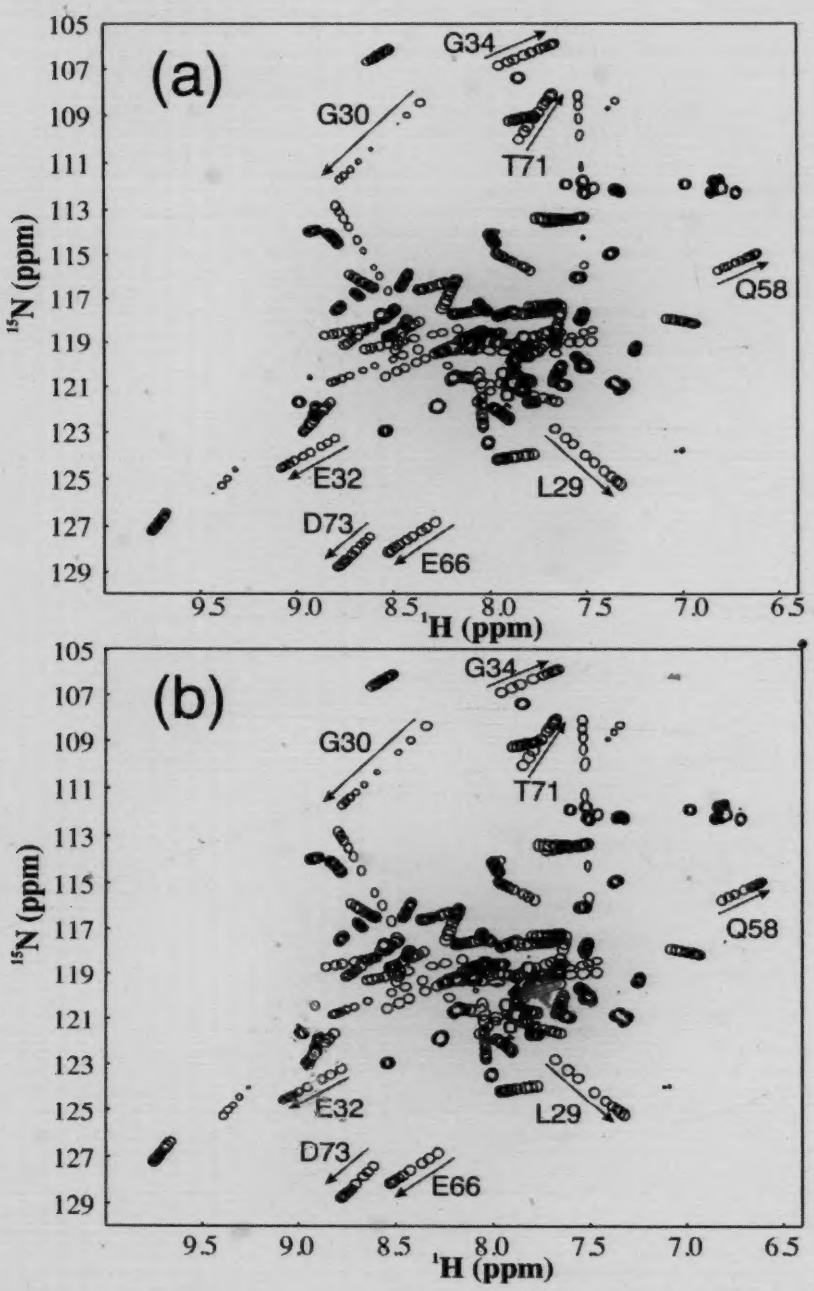

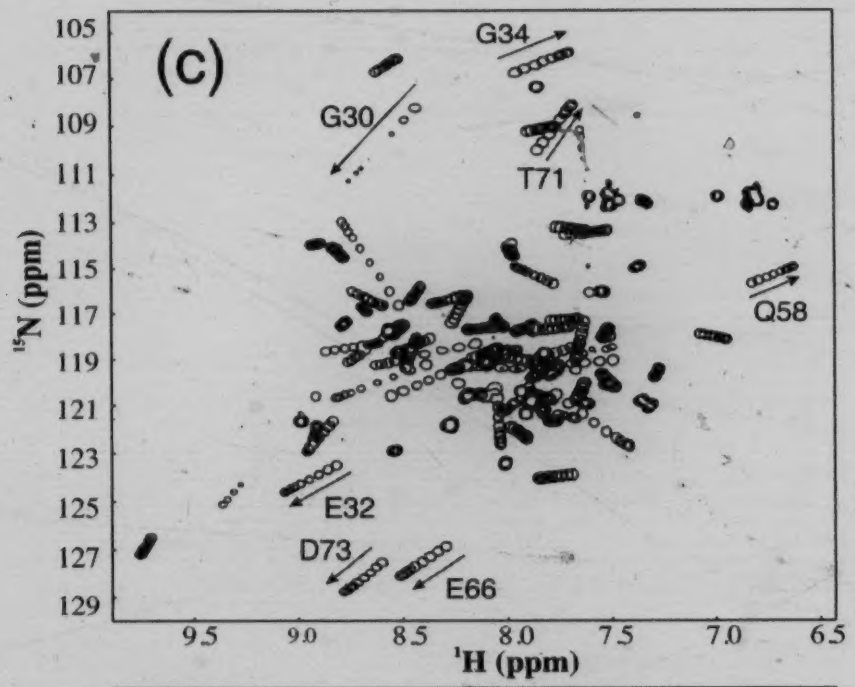
(c)
G34
G30
T71
Q58
E32
D73
E66
105
107
109
111
113
115
117
119
121
123
125
127
129
^{15}N (ppm)
9.5
9.0
8.5
8.0
7.5
7.0
6.5
^{1}H (ppm)

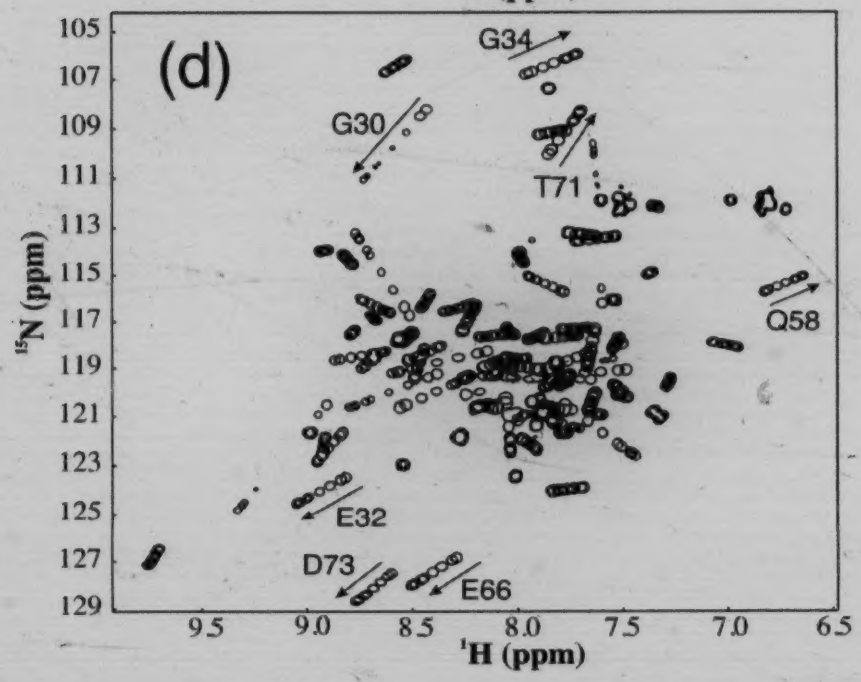
(d)
G34
G30
T71
Q58
E32
D73
E66
105
107
109
111
113
115
117
119
121
123
125
127
129
^{15}N (ppm)
9.5
9.0
8.5
8.0
7.5
7.0
6.5
^{1}H (ppm)

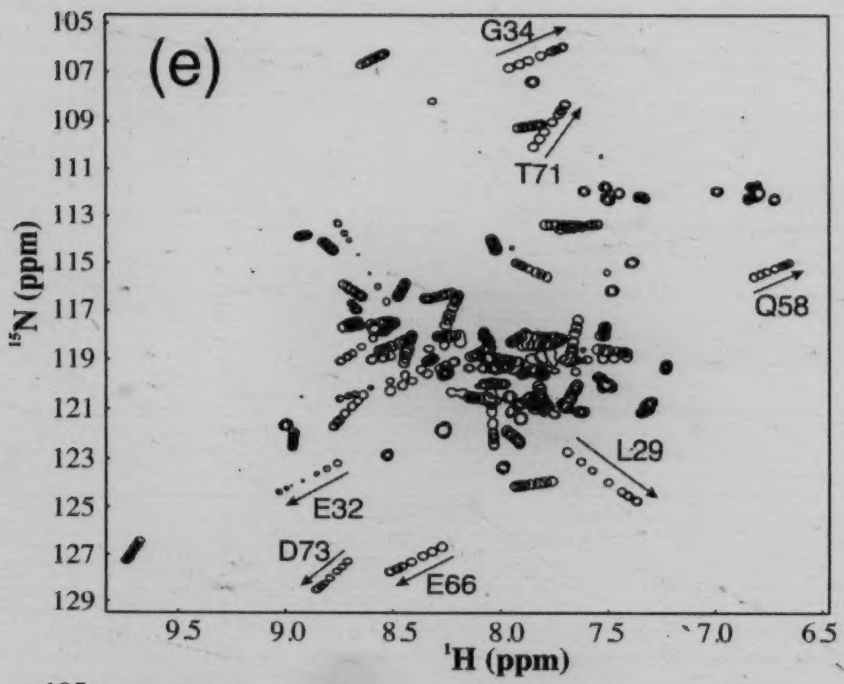
(e)
G34
T71
Q58
L29
E32
D73
E66
^{15}N (ppm)
^{1}H (ppm)

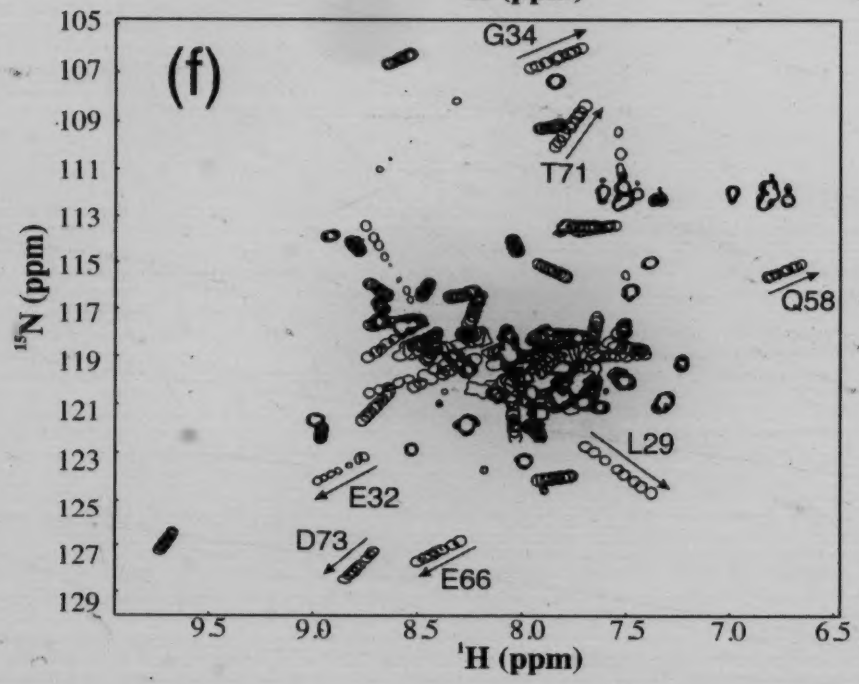
(f)
G34
T71
Q58
L29
E32
D73
E66
^{15}N (ppm)
^{1}H (ppm)

Figure II-7. Binding curves obtained during the $cTnI_{147-163}$ titrations of cNTnC•Ca^{2+} in the complex with $cTnI_{1-29}$ (circles) and $cTnI_{1-29}$PP (squares) (a), L29Q•Ca^{2+} in complex with $cTnI_{1-29}$ (circles) and $cTnI_{1-29}$PP (squares) (b), and E59D/D75Y•Ca^{2+} in complex with $cTnI_{1-29}$ (circles) and $cTnI_{1-29}$PP (squares) (c).

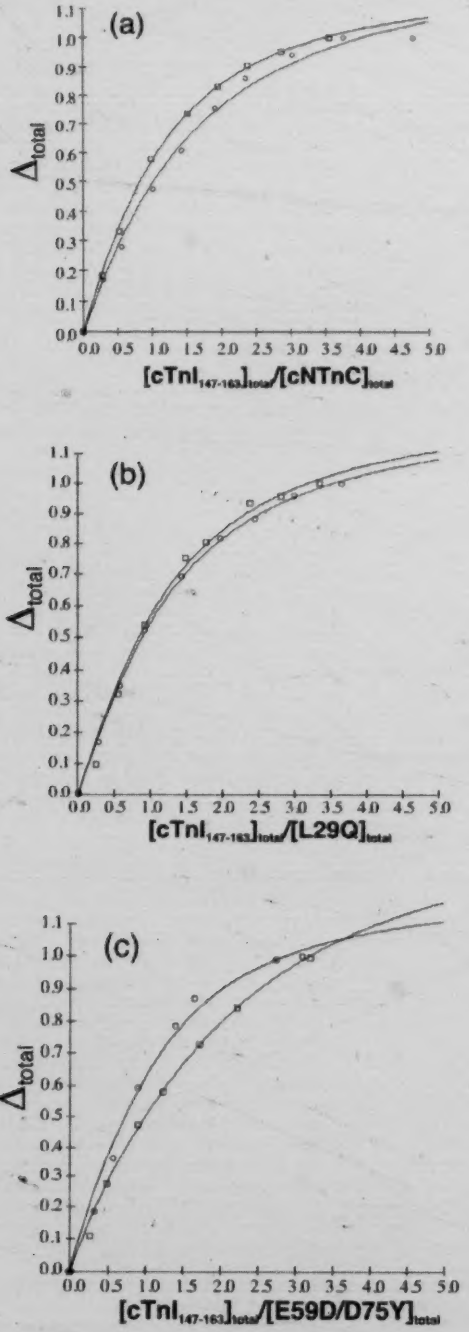

Figure II-8. Experimental NMR rotational correlation times plotted versus theoretical estimates calculated based on the expected molecular weights for cNTnC (a), L29Q (b), and E59D/D75Y (d) in various complexes. Complexes below diagonal line are formed with the stoicheometry less then 1:1. Complexes above diagonal line most likely undergo dimerization. In the case of E59D/D75Y, the suspected dimerization is mild.

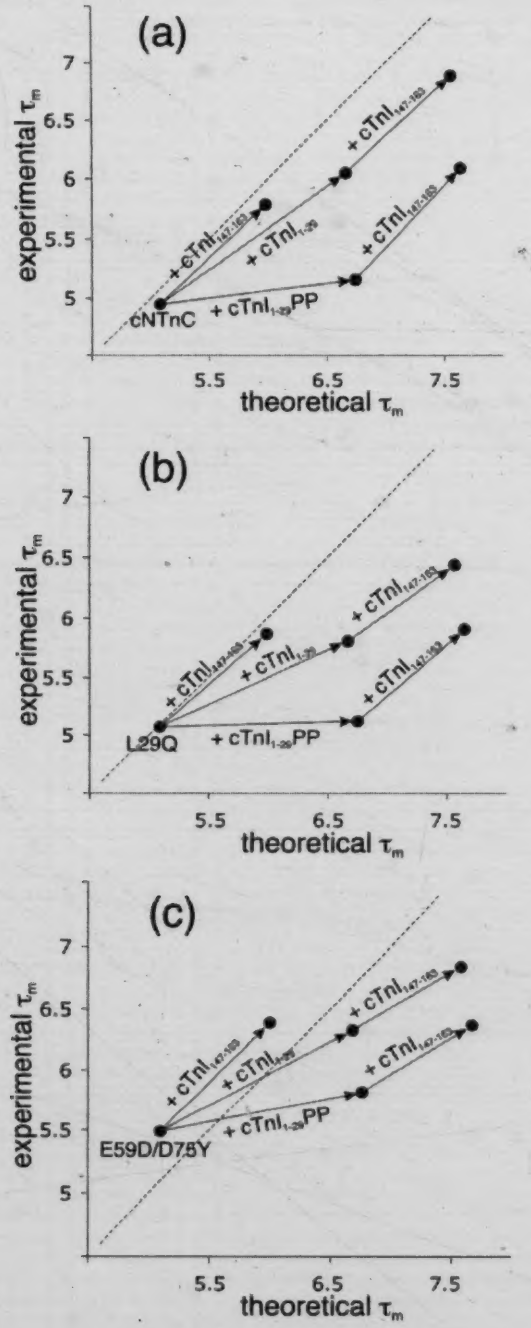

References

(1) Schmidtmann, A., Lindow, C., Villard, S., Heuser, A., Mugge, A., Gessner, R., Granier, C., and Jaquet, K. (2005) Cardiac troponin C-L29Q, related to hypertrophic cardiomyopathy, hinders the transduction of the protein kinase A dependent phosphorylation signal from cardiac troponin I to C. *Febs J 272*, 6087-97.

(2) Biesiadecki, B. J., Kobayashi, T., Walker, J. S., John Solaro, R., and de Tombe, P. P. (2007) The Troponin C G159D Mutation Blunts Myofilament Desensitization Induced by Troponin I Ser23/24 Phosphorylation. *Circ Res 100*, 1486-1493.

(3) Hoffmann, B., Schmidt-Traub, H., Perrot, A., Osterziel, K. J., and Gessner, R. (2001) First mutation in cardiac troponin C, L29Q, in a patient with hypertrophic cardiomyopathy. *Hum Mutat 17*, 524.

(4) Churcott, C. S., Moyes, C. D., Bressler, B. H., Baldwin, K. M., and Tibbits, G. F. (1994) Temperature and pH effects on Ca2+ sensitivity of cardiac myofibrils: a comparison of trout with mammals. *Am J Physiol 267*, R62-70.

(5) Gomes, A. V., and Potter, J. D. (2004) Molecular and cellular aspects of troponin cardiomyopathies. *Ann N Y Acad Sci 1015*, 214-24.

(6) Lim, C. C., Yang, H., Yang, M., Wang, C. K., Shi, J., Berg, E. A., Pimentel, D. R., Gwathmey, J. K., Hajjar, R. J., Helmes, M., Costello, C. E., Huo, S., and Liao, R. (2008) A Novel Mutant Cardiac Troponin C Disrupts Molecular Motions Critical For Calcium Binding Affinity And Cardiomyocyte Contractility. *Biophys J 94*, 3577-89.

(7) Li, M. X., Spyracopoulos, L., and Sykes, B. D. (1999) Binding of cardiac troponin-I147-163 induces a structural opening in human cardiac troponin-C. *Biochemistry 38*, 8289-98.

(8) Abbott, M. B., Dong, W. J., Dvoretsky, A., DaGue, B., Caprioli, R. M., Cheung, H. C., and Rosevear, P. R. (2001) Modulation of cardiac troponin C-cardiac troponin I regulatory interactions by the amino-terminus of cardiac troponin I. *Biochemistry 40*, 5992-6001.

(9) Ward, D. G., Cornes, M. P., and Trayer, I. P. (2002) Structural consequences of cardiac troponin I phosphorylation. *J Biol Chem 277*, 41795-801.

(10) Li, M. X., Gagne, S. M., Spyracopoulos, L., Kloks, C. P., Audette, G., Chandra, M., Solaro, R. J., Smillie, L. B., and Sykes, B. D. (1997) NMR studies of Ca2+ binding to the regulatory domains of cardiac and E41A skeletal muscle troponin C reveal the importance of site I to energetics of the induced structural changes. *Biochemistry 36*, 12519-25.

(11) Linse, S. (2002) in *Methods in Molecular Biology* (Vogel, H. J., Ed.), Humana Press, Totowa, New Jersey.

(12) Blumenschein, T. M., Gillis, T. E., Tibbits, G. F., and Sykes, B. D. (2004) Effect of temperature on the structure of trout troponin C. *Biochemistry 43*, 4955-63.

(13) Solaro, R. J., Moir, A. J., and Perry, S. V. (1976) Phosphorylation of troponin I and the inotropic effect of adrenaline in the perfused rabbit heart. *Nature 262*, 615-7.

(14) Palmer, A. G., 3rd. (2004) NMR characterization of the dynamics of biomacromolecules. *Chem Rev 104*, 3623-40.

(15) Lipari, G., and Szabo, a. (1982) Model-Free Approach to the Interpretation of Nuclear Magnetic-Resonance Relaxation in Macromolecules.1. Theory and Range of Validity. *J Am Chem Soc 104*, 4546-4559.

(16) Goodman, J. L., Pagel, M. D., and Stone, M. J. (2000) Relationships between protein structure and dynamics from a database of NMR-derived backbone order parameters. *J Mol Biol 295*, 963-78.

(17) Kay, L. E., Torchia, D. A., and Bax, A. (1989) Backbone dynamics of proteins as studied by 15N inverse detected heteronuclear NMR spectroscopy: application to staphylococcal nuclease. *Biochemistry 28*, 8972-9.

(18) Farrow, N. A., Muhandiram, R., Singer, A. U., Pascal, S. M., Kay, C. M., Gish, G., Shoelson, S. E., Pawson, T., Forman-Kay, J. D., and Kay, L. E. (1994) Backbone dynamics of a free and phosphopeptide-complexed Src homology 2 domain studied by 15N NMR relaxation. *Biochemistry 33*, 5984-6003.

(19) Lindhout, D. A., Boyko, R. F., Corson, D. C., Li, M. X., and Sykes, B. D. (2005) The role of electrostatics in the interaction of the inhibitory region of troponin I with troponin C. *Biochemistry 44*, 14750-9.

(20) Baryshnikova, O. K., and Sykes, B. D. (2006) Backbone dynamics of SDF-1alpha determined by NMR: interpretation in the presence of monomer-dimer equilibrium. *Protein Sci 15*, 2568-78.

(21) Schurr, J. M., Babcock, H. P., and Fujimoto, B. S. (1994) A test of the model-free formulas. Effects of anisotropic rotational diffusion and dimerization. *J Magn Reson B 105*, 211-24.

(22) Sia, S. K., Li, M. X., Spyracopoulos, L., Gagne, S. M., Liu, W., Putkey, J. A., and Sykes, B. D. (1997) Structure of cardiac muscle troponin C unexpectedly reveals a closed regulatory domain. *J Biol Chem 272*, 18216-21.

(23) Ray, K. P., and England, P. J. (1976) Phosphorylation of the inhibitory subunit of troponin and its effect on the calcium dependence of cardiac myofibril adenosine triphosphatase. *FEBS Lett 70*, 11-6.

(24) Holroyde, M. J., Howe, E., and Solaro, R. J. (1979) Modification of Calcium requirements for activation of cardiac myofibrillar ATPase by cyclic AMP dependent phosphorylation. *Biochim Biophys Acta 586*, 63-69.

(25) Kentish, J. C., McCloskey, D. T., Layland, J., Palmer, S., Leiden, J. M., Martin, A. F., and Solaro, R. J. (2001) Phosphorylation of troponin I by protein kinase A accelerates relaxation and crossbridge cycle kinetics in mouse ventricular muscle. *Circ Res 88*, 1059-65.

(26) Herron, T. J., Korte, F. S., and McDonald, K. S. (2001) Power output is increased after phosphorylation of myofibrillar proteins in rat skinned cardiac myocytes. *Circ Res 89*, 1184-90.

(27) Robertson, S. P., Johnson, J. D., Holroyde, M. J., Kranias, E. G., Potter, J. D., and Solaro, R. J. (1982) The effect of troponin I phosphorylation on the Ca2+-binding properties of the Ca2+-regulatory site of bovine cardiac troponin. *J Biol Chem 257*, 260-3.

(28) Ward, D. G., Brewer, S. M., Cornes, M. P., and Trayer, I. P. (2003) A cross-linking study of the N-terminal extension of human cardiac troponin I. *Biochemistry 42*, 10324-32.

(29) Dong, W. J., Chandra, M., Xing, J., She, M., Solaro, R. J., and Cheung, H. C. (1997) Phosphorylation-induced distance change in a cardiac muscle troponin I mutant. *Biochemistry 36*, 6754-61.

(30) Chandra, M., Dong, W. J., Pan, B. S., Cheung, H. C., and Solaro, R. J. (1997) Effects of protein kinase A phosphorylation on signaling between cardiac troponin I and the N-terminal domain of cardiac troponin C. *Biochemistry 36*, 13305-11.

(31) Finley, N., Abbott, M. B., Abusamhadneh, E., Gaponenko, V., Dong, W., Gasmi-Seabrook, G., Howarth, J. W., Rance, M., Solaro, R. J., Cheung, H. C., and

Rosevear, P. R. (1999) NMR analysis of cardiac troponin C-troponin I complexes: effects of phosphorylation. *FEBS Lett 453*, 107-12.

(32) Warren, C. M., Kobayashi, T., and Solaro, R. J. (2007) in *Biophysical Society, Annual Meeting* pp 473a, Baltimore, Maryland.

(33) Gaponenko, V., Abusamhadneh, E., Abbott, M. B., Finley, N., Gasmi-Seabrook, G., Solaro, R. J., Rance, M., and Rosevear, P. R. (1999) Effects of troponin I phosphorylation on conformational exchange in the regulatory domain of cardiac troponin C. *J Biol Chem 274*, 16681-4.

(34) Wang, Y. P., and Fuchs, F. (1995) Osmotic compression of skinned cardiac and skeletal muscle bundles: effects on force generation, Ca2+ sensitivity and Ca2+ binding. *J Mol Cell Cardiol 27*, 1235-44.

(35) Pan, B. S., and Solaro, R. J. (1987) Calcium-binding properties of troponin C in detergent-skinned heart muscle fibers. *J Biol Chem 262*, 7839-49.

(36) Engel, P. L., Kobayashi, T., Biesiadecki, B., Davis, J., Tikunova, S., Wu, S., and Solaro, R. J. (2007) Identification of a region of troponin I important in signaling cross-bridge-dependent activation of cardiac myofilaments. *J Biol Chem 282*, 183-93.

(37) Solzin, J., Iorga, B., Sierakowski, E., Gomez Alcazar, D. P., Ruess, D. F., Kubacki, T., Zittrich, S., Blaudeck, N., Pfitzer, G., and Stehle, R. (2007) Kinetic mechanism of the Ca2+-dependent switch-on and off of cardiac troponin in myofibrils. *Biophys J 93*, 3917-31

(38) Shiner, J. S., and Solaro, R. J. (1982) Activation of thin-filament-regulated muscle by calcium ion: considerations based on nearest-neighbor lattice statistics. *Proc Natl Acad Sci U S A 79*, 4637-41.

(39) Strynadka, N. C., and James, M. N. (1989) Crystal structures of the helix-loop-helix calcium-binding proteins. *Annu Rev Biochem 58*, 951-98.

(40) Gillis, T. E., Moyes, C. D., and Tibbits, G. F. (2003) Sequence mutations in teleost cardiac troponin C that are permissive of high Ca2+ affinity of site II. *Am J Physiol Cell Physiol 284*, C1176-84.

(41) Muir, L. A., Tschirgi, M. L., Rajapakse, I., and Chandra, M. (2006) in *Biophysical Society, Annual Meeting* pp 529, Salt Lake City, Utah.

(42) Dweck, D., Gomes, A. V., and Potter, J. D. (2005) in *Biophysical Society, Annual Meeting* pp 317a, Long Beach, CA.

(43) Pearlstone, J. R., Chandra, M., Sorenson, M. M., and Smillie, L. B. (2000) Biological function and site II Ca2+-induced opening of the regulatory domain of skeletal troponin C are impaired by invariant site I or II Glu mutations. *J Biol Chem 275*, 35106-15.

(44) Li, M. X., Corson, D. C., and Sykes, B. D. (2002) Structure determination by NMR. Isotope labeling. *Methods Mol Biol 173*, 255-65.

(45) Li, M. X., Gagne, S. M., Tsuda, S., Kay, C. M., Smillie, L. B., and Sykes, B. D. (1995) Calcium binding to the regulatory N-domain of skeletal muscle troponin C occurs in a stepwise manner. *Biochemistry 34*, 8330-40.

(46) Tripet, B., Van Eyk, J. E., and Hodges, R. S. (1997) Mapping of a second actin-tropomyosin and a second troponin C binding site within the C terminus of troponin I, and their importance in the Ca2+-dependent regulation of muscle contraction. *J Mol Biol 271*, 728-50.

(47) Tsien, R. Y. (1980) New calcium indicators and buffers with high selectivity against magnesium and protons: design, synthesis, and properties of prototype structures. *Biochemistry 19*, 2396-404.

(48) Delaglio, F., Grzesiek, S., Vuister, G. W., Zhu, G., Pfeifer, J., and Bax, A. (1995) NMRPipe: a multidimensional spectral processing system based on UNIX pipes. *J Biomol NMR 6*, 277-93.

(49) Johnson, B. A., and Blevins, R. A. (1994) NMRView: A computer program for the visualization and analysis of NMR data. *J Biomol NMR 4*, 603-614.

(50) Spyracopoulos, L. (2006) A suite of Mathematica notebooks for the analysis of protein main chain 15N NMR relaxation data. *J Biomol NMR 36*, 215-24.

CHAPTER III

Consequences of the DCM mutation G159D on the structure and dynamics of cardiac troponin C and its interaction with troponin I*

Outline

NMR spectroscopy has been employed to elucidate the molecular consequences of the DCM mutation G159D on structure and dynamics of troponin C, and its interaction with troponin I. Since the effects of this human mutation are expected to be subtle, all NMR experiments were run as direct side-by-side comparisons of the wild type and G159D mutant proteins. The affinity of G159D towards the anchoring region of cTnI ($cTnI_{34-71}$) was reduced ($K_D = 6 \pm 3$ μM) as compared to that for cCTnC ($K_D < 1$ μM). The overall structure and dynamics of the G159D•$cTnI_{34-71}$ complex were very similar to those of cCTnC•$cTnI_{34-71}$. There were, however, significant changes in the ^1H, ^{13}C, and ^{15}N NMR chemical shifts of troponin C in the complex, especially for the residues involved in the direct contact with $cTnI_{34-71}$, and changes in the NOE connectivity patterns between G159D and $cTnI_{34-71}$. Thus, one possibility is that the development of disease results from the poor anchoring of the cTnI to cCTnC, with the resulting increase in acto-myosin inhibition in agreement with physiological data. Another possibility is that long range electrostatic interactions affect the binding of the switch region of cTnI ($cTnI_{147-163}$) and/or the cardiac specific N-terminus of cTnI ($cTnI_{1-29}$) to the N-domain of cTnC. These important interactions are all spatially close in the X-ray structure of the core of cardiac TnC (*1*).

Introduction

Ca^{2+} regulation of contraction in cardiac muscle is a fine tuned process that depends on the reliable function of its protein parts. The development of cardiac malfunctions can be caused by the presence of mutations in contractile proteins. Indeed, as revealed by genetic analysis, a large number of mutations in β-myosin, α-tropomyosin, cardiac troponin I (cTnI), and cardiac troponin T (cTnT) causes various forms of cardiomyopathy (*2, 3*). Cardiac troponin C (cTnC), the protein directly responsible for Ca^{2+} sensitivity of the thin filament, is highly conserved among mammals and thought to have fewer mutations until recently (*4-7*).

cTnC consists of two domains: the structural domain, cCTnC, and the regulatory domain, cNTnC. At all times, cCTnC, stays saturated with Ca^{2+} and bound to the anchoring region of cTnI (~ residues 34-71), which tethers cTn to the thin filament. The regulatory domain, cNTnC, binds Ca^{2+} only at high Ca^{2+} concentration upon muscle stimulation. In Ca^{2+} form, cNTnC binds to the switch region of cTnI (~ residues 147-163), which pulls the inhibitory region of cTnI (~ residues 128-147) away from its binding site on actin, triggering contraction (for reviews see (*8, 9*)).

Two mutations found in cNTnC, L29Q and E59D/D75Y, were linked to hypertrophic cardiomyopathy (FHC) and dilated cardiomyopathy (DCM), respectively (*4, 5*). In Chapter II, the physiological consequences of the L29Q and E59D/D75Y mutations were linked to the impaired thermodynamics of the cNTnC interactions with its binding partners, $cTnI_{1-29}$ and $cTnI_{147-163}$. Another mutation, G159D, associated with DCM, was found in cCTnC (*7*). In reconstituted rat (*10*) and rabbit (*11*) cardiac trabeculae, the presence of G159D did not significantly alter myofilament Ca^{2+} sensitivity. However, the presence of G159D in guinea pig trabeculae resulted in the reduced Ca^{2+} sensitivity (*12*). Available physiological data on G159D reported the reduced activity of ATPase (*12*); however, the Ca^{2+} sensitivity of ATPase was not affected (*10*). It might be difficult to interpret physiological results on the molecular level, especially since Ca^{2+} sensitivity is a complex function of many consequent events, such as the binding of Ca^{2+}, binding of $cTnI_{147-163}$ and attachment of cross-bridges, and since the reproducibility of results was mentioned to be dependent on the muscle fiber type (*11*). We have attempted to address this question using the G159D mutant of cCTnC and the cTnI peptide ($cTnI_{34-71}$), so that the interactions between troponin parts can be unambiguously traced. The knowledge of these interactions can be afterwards compiled into the overall picture assisting the interpretation of the physiological data.

There are several functions attributed to cCTnC, which could be affected by the presence of G159D: first, in its Ca^{2+} bound form, cCTnC binds to the anchoring region of cTnI (~ residues 34-71) and tethers the entire troponin complex to the thin filament; second, cCTnC binds the inhibitory region of cTnI (~ residues 128-147), the location of which has not been visualized in available crystal structures (*1*) and is suspected to be driven by electrostatics (*13, 14*). The binding of $cTnI_{128-147}$ occurs without replacement of $cTnI_{34-71}$ and is hypothesized to be localized next to the highly charged E-D linker connecting the two domains of cTnC. Third, cCTnC was also shown to interact with cTnT (*15*). Fourth, G159D might affect the interaction with the cardiac specific N-

terminus of cTnI (~ residues 1-29), as was suspected in experiments with skinned rat trabeculae (*10*) and with reconstituted troponin complex (*16*). In the crystal structure, Gly^{159} is located at the very end of the H-helix, 5 Å away from Leu^{47} of the anchoring region of cTnI (~residues 34-71) (*1*). This suggests that the presence of mutation might first of all affect the interaction with $cTnI_{34-71}$, which has not been addressed previously. Using NMR spectroscopy, we have determined the affinity of G159D towards $cTnI_{34-71}$ and examined the consequences of this mutation on structure and dynamics of the G159D•$cTnI_{34-71}$ complex. Based on NOE connectivity patterns, NMR chemical shifts changes, dynamics, and determined 3D structures, we conclude that, compared to cCTnC, G159D binds to $cTnI_{34-71}$ in a similar fashion, albeit with a lower affinity. This interaction is a key function of cCTnC, and when impaired, can perturb the function of the entire Tn complex and lead to severe physiological consequences, such as the development of cardiomyopathy.

Results

$cTnI_{34-71}$ titrations of cCTnC and G159D

In a 2D {^{1}H, ^{15}N} HSQC NMR spectrum, cross peaks correlate the ^{15}N and ^{1}H chemical shifts of backbone amide NH. Chemical shifts are exceptionally sensitive to changes in the structure and dynamics of a protein. 2D {^{1}H, ^{15}N} HSQC spectra obtained for G159D (Fig. III-1a) and cCTnC (Fig. III-1b), with and without their binding partner, $cTnI_{34-71}$, demonstrate the difference in the positions of several {^{1}H, ^{15}N} HSQC cross peaks, corresponding to the residues adjacent to the site of mutation. The rest of the amide chemical shifts, and the changes they undergo during the titration with $cTnI_{34-71}$, are similar, suggesting resemblance in the overall structural folds for G159D and cCTnC, in agreement with the structures determined herein (see below). The kinetics of the binding of $cTnI_{34-71}$ to G159D (Fig. III-1a) and cCTnC (Fig. III-1b) is on the NMR slow exchange time scale, in which the intensities of cross-peaks for complexed and uncomplexed species vary depending on the degree of binding. Binding curves were obtained by measuring the intensity decrease for several representative cross-peaks corresponding to the unliganded protein, which were averaged and fit to a single binding site model (Fig. III-1, insets). K_D's were found to be 6 ± 3 μM in the case of G159D and < 1 μM in the case of cCTnC. The later is in agreement with literature data (*17*). K_D's tighter than 1 μM cannot be determined precisely within the concentration limits of NMR.

^{15}N backbone relaxation data

^{15}N backbone NMR relaxation parameters, T_1, T_2, and NOE, are the functions of the protein motions, including the tumbling of a protein as a whole, the motions of its independent parts, and the chemical exchange processes. Per residue T_1, T_2, and NOE were determined for G159D and cCTnC alone, and in complex with $cTnI_{34-71}$ (Fig. III-2). T_1, T_2, and NOE for cCTnC•$cTnI_{34-71}$ and G159D•$cTnI_{34-71}$ were virtually identical within the errors of the experiments (Fig. III-2), implying that the presence of the mutation did not affect the dynamic properties, as well as the conformational flexibility, of the complex. Importantly, ^{15}N backbone T_1, T_2, and NOE for cCTnC•$cTnI_{34-71}$ and G159D•$cTnI_{34-71}$ were also similar in the area adjacent to the mutation site. Relaxation data for cCTnC was in agreement with qualitative data presented earlier (*18, 19*).

T_1, T_2, and NOE are per residue parameters, whereas the overall correlation time, τ_m, calculated from T_1, T_2, and NOE (Table III-1), is the function of the hydrated radius of the entire protein, r_h, and consequently its molecular weight. According to the Stokes-Einstein-Debye theory (*20*),

$$\tau_m = \frac{4}{3}\pi\eta r_h^3 / k_B T,$$

where η is the solvent viscosity, k_B is the Boltzmann constant, and T is temperature. As a rule of thumb, τ_m (ns) is approximated to the half of the molecular weight of a protein (kDa), provided that the protein tumbling is mostly isotropic. This can serve as a good estimate of the molecular weight of a protein or its complexes (*13*). An increase in τ_m as compared to the calculated molecular weight can result from issues such as dimerization (*21*), which is the case for skeletal protein, sCTnC (*22*). We have determined τ_m's for G159D and cCTnC alone, and in complex with $cTnI_{34-71}$ (Table III-1). For cCTnC and G159D, τ_m's are comparable to each other and smaller than the rule of thumb estimate, which could be explained by a lesser degree of bound water, for example (*23, 24*). The values of τ_m's determined for G159D•$cTnI_{34-71}$ and cCTnC•$cTnI_{34-71}$ were comparable to each other and to the theoretical estimate, which suggests the formation of 1:1 complexes in both cases, and the absence of dimerization and significant conformational exchange.

Table III-1. NMR relaxation parameters T_1, T_2, and τ_m determeters determined for G159D and cCTnC alone and in complexes with $cTnI_{34-71}$. Theoretical estimate for correlation time τ_m is equal to the half of the molecular weight in kDa.

	Average of per residue T_1 (ms)	Average of per residue T_2 (ms)	Overall correlation time, τ_m (ns)	Theoretical estimate for correlation time, τ_m (ns)
G159D	356 ± 47	193 ± 31	3.3	4.2
G159D•$cTnI_{34-71}$	436 ± 46	112 ± 9	6.6	6.4
cCTnC	348 ± 42	185 ± 25	3.4	4.2
cCTnC•$cTnI_{34-71}$	438 ± 53	109 ± 13	6.5	6.4

Differences in the chemical shifts of cCTnC and G159D in the complexes with $cTnI_{34-71}$

Chemical shifts changes are uniquely indicative of changes in chemical environment of nuclei and hence, in protein structure and dynamics. We have calculated the chemical shift changes of ^{15}N, ^{13}C, and ^{1}H for G159D and cCTnC in complexes with $cTnI_{34-71}$ (Figs. III-3 and III-4). Backbone amide ^{15}N chemical shifts underwent the most significant perturbations at the end of the H-helix near to the mutation site (Figs. III-3a and III-4a). ^{15}N chemical shifts in the region where the H-helix is contacting the E-helix (residues 93-97) are also affected by the presence of mutation but to a much lesser degree. As demonstrated by ^{15}N chemical shifts changes, the overall fold of G159D and cCTnC remains similar with the only significant perturbation being near to the mutation site. Changes in ^{1}H and ^{13}C chemical shifts, especially those for the side chains, are sensitive not only to the changes in overall fold but also to the changes in the configurational patterns, e.g. the number, energetics, and the geometry of connections that stabilize protein core or protein complex. As demonstrated by ^{13}C chemical shifts changes (Figs. III-3b and III-4b), the major perturbations occurred at the several hydrophobic residues (for example Leu^{100}, Met^{120}, Leu^{121}, and Ile^{128}) known to be responsible for the interaction with $cTnI_{34-71}$ (*1*). ^{1}H, atoms directly responsible for the majority of van der Waals and hydrophobic contacts in proteins, are the most sensitive indicators of changes in protein core and binding interfaces. As demonstrated by ^{1}H chemical shifts differences (Figs. III-3c and III-4c), significant changes occurred with the residues forming the interface between cCTnC and $cTnI_{34-71}$ (for example Leu^{100}, Met^{103}, Met^{120}, Leu^{121}, Ile^{128}, Leu^{136}), implying that the binding of $cTnI_{34-71}$ to cCTnC is perturbed in the presence of the mutation (*1*). Interestingly, the chemical shifts of two interior residues, Ile^{148} and Ile^{112}, which form the hydrophobic core of cCTnC, have also been affected.

Differences in the NOE connectivities of cCTnC and G159D in the complex with $cTnI_{34-71}$

NOE connectivites obtained from 3D ^{13}C NOESY HSQC and ^{15}N NOESY HSQC NMR spectra are typically used as distance restraints during structure calculations. It is often informative therefore to make pair-wise comparisons of NOE patterns. NOE, however, is a less sensitive parameter to long range perturbations as compared to a chemical shift since the intensity of NOE decreases rapidly with the distance between two nuclei: $NOE \propto \frac{1}{r^6}$ (25). We have compared strips from 3D ^{13}C NOESY HSQC and ^{15}N NOESY HSQC NMR spectra for G159D and cCTnC for residues with the significant chemical shift changes. Spectra were acquired using identical parameters, such as mixing time, which is crucial for such a comparison. The vast majority of contacts in the cCTnC spectra were accurately reproduced in the G159D spectra; however, there were some differences (Fig. III-5). For example, in the ^{13}C NOESY HSQC spectrum, the γ-proton of Met^{103} has more contacts in cCTnC compared to G159D, with some of these contacts being tentatively assigned to the peptide resonances (Fig. III-5a). The γ-proton of Ile^{112} contacted the α-proton of Asp^{149} in G159D, and the α-proton of Asp^{105} and the δ-proton of Tyr^{150} in cCTnC (Fig. III-5b). The α-proton of Gly^{140} contacted the γ-proton of Glu^{152} in cCTnC but not in G159D (Fig. III-5c). The γ-proton of Val^{160} contacted the ε-proton of Phe^{156} in G159D but not in cCTnC (Fig. III-5d). In the ^{15}N NOESY HSQC NMR spectrum, the differences in NOE patterns were less significant, with the noticeable change observed in the amide proton of Ala^{108}, which had contacts with the β-protons of Lys^{106} and Asn^{107} in G159D but not in cCTnC. These results demonstrate that the residues with the large chemical shift differences (Fig. III-5) had also distinct NOE connectivities in ^{13}C NOESY HSQC and ^{15}N NOESY HSQC spectra.

Structures of cCTnC and G159D in the complexes with $cTnI_{34-71}$

The ensemble containing 20 best NMR structures out of 50 calculated was analyzed for G159D and cCTnC. All structures had a good geometry after water refinement with > 92 % in most favorable and > 7 % in additional allowed regions of the Ramachandran plot for G159D and cCTnC (Table III-2). Structures of both proteins converged with rmsd < 1.4 Å for all atoms for residues 95-155, including loops. The overall topology and the secondary structure for G159D and cCTnC were similar to the cCTnC structure obtained by X-ray crystallography, PDB code 1J1D (*1*) and previously by NMR, PDB code 1FI5 (*19*). Rmsd's for backbone atoms between cCTnC and 1J1D

was 1.2 Å for all residues, and between cCTnC and 1FI5 1.4 Å (Fig. III-6a). Similar rmsd of 1.7 Å was between reported 1FI5 and 1J1D. The G159D structure, although similar overall, overlapped with 1J1D with rmsd of 1.7 Å for backbone atoms for all residues (Fig. III-6b). G159D overlapped with cCTnC with rmsd of 1.4 Å and with 1FI5 with 1.3 Å (Fig. III-6b). The resolution of X-ray diffraction data for 1J1D was 2.6 Å (*1*), within which, structures determined in this work and reported previously have similar folds.

Table III-2. Statistics for 20 NMR structures of G159D and cCTnC in complex with $cTnI_{34-71}$. Structures were calculated using CYANA (*26*), refined using XPLOR-NIH (*27*, *28*), and analyzed using PROCHECK (*29*) and WHATCHECK (*30*).

	G159D	cCTnC
NOE restraints	1075	957
Short range ($\|i-j\|=1$)	624	561
Medium range ($1<\|i-j\|<5$)	231	215
Long range ($\|i-j\|\geq 5$)	220	181
Ca^{2+} binding restraints	16	16
Dihedral restraints (ϕ/ψ)[a]	84	86
NOE violations		
> 0.5 Å	0.15 ± 0.37	0.0 ± 0.0
> 0.3 Å	0.25 ± 0.55	1.8 ± 1.20
> 0.1 Å	6.3 ± 1.95	10.45 ± 2.28
Dihedral Violations (°)	0.0 ± 0.0	0.0 ± 0.0
Ramachadran plot statistics[b]		
ϕ/ψ in most favorable regions (%)	93 ± 4	92 ± 4
ϕ/ψ in additionally allowed regions (%)	7 ± 3	7 ± 3
ϕ/ψ in generously allowed regions (%)	0 ± 1	1 ± 1
ϕ/ψ in disallowed regions (%)	0 ± 1	1 ± 1
Pairwise RMSD (Å)[c]		
Before water refinement	0.71 ± 0.13	0.59 ± 0.12
After water refinement	1.29 ± 0.28	1.31 ± 0.24
WHAT CHECK structure Z-scores after water refinement		
Second-generation packing quality	-0.9 ± 0.4	-0.9 ± 0.3
Ramachandran plot appearance	0.9 ± 0.7	1.8 ± 0.8

[a]Predicted from chemical shifts using TALOS
[b]PROCHECK was used over all the residues (90-161)
[c]Main chain nuclei over the residues 95-155

The packing of the cCTnC core occurs between the hydrophobic residues of α-helical regions (Leu^{97}, Phe^{101}, Leu^{117}, Met^{120}, Leu^{121}, Ile^{133}, Leu^{136}, Phe^{153}, and Met^{157}) and the two residues of the β-sheet region (Ile^{112} and Ile^{148}). Orientation of these key residues did not change in the cCTnC and G159D structures calculated in this work as compared

to 1J1D and 1FI5. Several residues such as Phe^{104} and Phe^{156} in cCTnC and G159D are lacking the restraints with the peptide and thus their positions are more flexible, but are in the good agreement with the NMR structure, 1FI5. The packing interactions between helices and the protein cores of cCTnC have not been affected by the presence of G159D as demonstrated by the resultant structures. In spite of some differences in NOE contacts for Ile^{112} and Ile^{148}, the calculated structures were similar within the limits of the method. This demonstrates that among the restraints used (Table III-2), many were identical, which determined the similarity between the structures.

Differences in the NOE connectivities between cCTnC (and G159D) and cTnI$_{34-71}$ in ^{13}C-edited, filtered NOESY spectra

The NOE connectivities between ^{15}N, ^{13}C-labeled cCTnC and the unlabeled peptide cTnI$_{34-71}$ were obtained using the ^{13}C-edited, filtered NOESY pulse sequence (*31*) optimized in our laboratory for this particular complex (*32*). In this experiment, each cross peak corresponds to a ^{1}H protein resonance on the vertical axis and to a ^{1}H peptide resonance on the horizontal axis. ^{13}C resonance in the third dimension connects to the corresponding ^{1}H resonances on the protein, which allows for the assignment. Peptide ^{1}H assignments can be typically obtained with the 2D ^{15}N, ^{13}C-edited TOCSY and 2D ^{15}N, ^{13}C-edited NOESY (*33-35*); however, in our case, few resonances can be unambiguously assigned due to the poor dispersion of peptide chemical shifts, which precluded the structure calculation for the entire complex. Similarly to previous NMR studies (*19, 22, 36*), structure determination of the entire complex was difficult to achieve without the additional restraints between a protein and a peptide, which might be found in crystal structures but are not always desirable to use due to possible introduction of artifacts. The peptide in complex is predominantly α-helical, which is supported by the values of peptide chemical shifts in 2D ^{15}N, ^{13}C-edited TOCSY and 2D ^{15}N, ^{13}C-edited NOESY and their poor dispersion. The superposition of ^{13}C-edited, filtered NOESY spectra for G159D and cCTnC in complexes with cTnI$_{34-71}$ shows a similarity between contacts formed (Fig. III-7). Some contacts are virtually identical, for example, the contacts between Ala^{57} of cTnI$_{34-71}$ and Leu^{100} and Met^{120} of cCTnC and G159D (Fig. III-7a) or the contact between Leu^{62} of cTnI$_{34-71}$ and Met^{103} of cCTnC and G159D (Fig. III-7c). Some contacts were slightly changed, for example, the contacts between Ile^{56} of cTnI$_{34-71}$ and Thr^{124} of cCTnC and G159D (Fig. III-7c). One contact, between Leu^{54} of cTnI$_{34-71}$ and Val^{160} of cCTnC, was clearly missing in G159D (Fig. III-7b). No contacts were observed

in the spectrum of G159D that were missing in case of cCTnC. Also, the intensities of existing connectivities were not stronger in the case of G159D. This demonstrates that G159D interacts with $cTnI_{34-71}$ similarly to cCTnC, without making new connections between the protein and the peptide and with the existing connections being qualitatively not stronger.

Discussion

The task of defining the effect of mutations on protein behavior represents a substantial challenge, especially for human mutations where the effect on the protein has to be mild to allow an individual to function even in disease. Structural approaches, including the determination of structure using NMR or crystallography might not bring conclusive answers when the differences in structures of mutant and wild type proteins are not significant enough to be resolved within the resolution of the chosen technique. Often the affinities of mutated and wild type proteins for their targets and/or ligands are unchanged. It remains unknown, therefore, whether the mutant phenotype has been brought about by the changes undetectable within the limits of methods. However, the necessity to study individual human mutations is evident by the growing interest in genetically tailored nutrition and medicine, and overall will be beneficial to our understanding of current biochemical models, in our example, cardiac muscle contraction.

We have attempted to dissect the effect of the G159D mutation on the structure, dynamics, and interactions of troponin C using solution state NMR. This technique allows not only for the structure determination but also provides a wealth of information pertaining to the chemical environment and dynamics of individual residues. Since the effects are expected to be subtle, all NMR experiments were run as direct side-by-side comparisons of the wild type and G159D mutant proteins. We have found that the secondary structure, tertiary structure, and the packing of the protein core did not changed for G159D•$cTnI_{34-71}$ in comparison to cCTnC•$cTnI_{34-71}$. Dynamic behavior for G159D was also unaffected, even in the vicinity of the mutation. However, the affinity of G159D towards $cTnI_{34-71}$ was reduced, and the NMR chemical shifts of protein residues were perturbed. The differences in NMR chemical shifts were well beyond the resolution in ^{1}H dimension (0.03 ppm), ^{13}C dimension (0.3 ppm), and ^{15}N dimension (0.2 ppm) in our experiments, with the most significant changes observed for residues directly involved in binding to $cTnI_{34-71}$. The K_D of G159D towards $cTnI_{34-71}$ has been increased >

6 fold. We have also observed the changes in NOE connectivities between the protein and the peptide, with some connectivities changed or missing. All of the above evidence indicates the weakened binding and perturbed interaction between G159D and $cTnI_{34-71}$. The structure and dynamics of the protein core remain the same, however, in agreement with the G159D mutation locating at the very end of the H-helix, away from the protein core.

The binding of cCTnC to $cTnI_{34-71}$ is a key function of the C-domain of cTnC. In skeletal TnC, the binding of the inhibitory region of sTnI is dependent upon the presence of the anchoring region of sTnI, with the anchoring region modulating the binding of the inhibitory region (*37-39*) which directly influences contractility. In insect flight muscle, the regulation of contraction is achieved entirely through the C-domain of TnC without the involvement of the N-domain and its binding to the region analogous to the switch region of cTnI (*40*). Our data supports the possibility that G159D might lead to the impaired contractility and the disease through the impaired anchoring of cTnC and enhanced inhibition of acto-myosin. When this interaction is impaired in G159D, the weaker binding to $cTnI_{34-71}$ might lead to a weaker anchoring of troponin C to the thin filament, lower k_{on} for the switch region of cTnI (~residues 147-163) due to the decrease in proximity effect, and a more pronounced inhibition of contraction. This is in agreement with a slower activation kinetics in rabbit psoas fibers (*11*), which might be a more important parameter than the steady state force development (*41, 42*). Our conclusions are also in agreement with the decrease in actin-tropomyosin activated ATPase rate and the decrease in sliding velocity (*12*).

The second possibility is that the presence of G159D impaired the function of cNTnC via the perturbations in the long-range electrostatic interactions. Electrostatic potential drops off as a function of $\frac{1}{r}$, where r is the distance from the charge, so that it can be active 10-20 Å away from the site of mutation. In crystal structure (*1*), the N-domain of cTnC is folded over the C-domain of cTnC (Fig. III-8), so that Gly^{159} is in proximity to the binding site for the switch region of cTnI (~residues 147-163) (*43*), to the possible binding site for the cardiac specific N-terminus of cTnI (~ residues 1-29) (*44, 45*), and to the binding site of the inhibitory region of cTnI (~residues 128-147). The binding of the cardiac specific N-terminus and the inhibitory regions of TnI are suspected to be electrostatically driven (14,18), as well as influenced by phosphorylation (*46*), and the change in electrostatic potential of cCTnC might affect these interactions. A

perturbed interaction of G159D with the N-terminus of cTnI has been reported (*10, 16*), which resulted in blunting the effect of PKA phosphorylation. Interestingly, the L29Q mutation has also blunted the effect of PKA phosphorylation (*16, 47, 48*) but lead to hypertrophy instead (*4*). The physical parameter crucial for the development of hyper- vs hypocontractility may be the resultant affinity towards the switch region of cTnI (~residues 147-163) (*47*) and the kinetics of this binding interaction (*16*).

In this work, we have determined that G159D binds to $cTnI_{34-71}$ with weaker affinity, supported by structural data, such as changes in chemical shifts and NOE connectivities. This weakened interaction may impair the anchoring of troponin C, with the resulting increase of acto-myosin inhibition. The G159D mutation may also perturb the binding of the adjacent N-terminus of cTnI (~ residues 1-29) to cNTnC through the long range electrostatic interactions, which will affect the cNTnC binding of the switch region of cTnI (~ residues 147-163) and overall contractility.

Materials and methods

Protein Expression and Purification

The DNA encoding cCTnC (91-161) was subcloned previously into pET-3a expression vector similarly to Pearlstone et al. (*49*). Using cCTnC as a template, the G159D mutation was engineered using a site-directed mutagenesis kit (QuikChange purchased from Stratagene). *E. coli* strain BL21(DE3)pLysS was transformed with the expression vector and incubated at 37°C to the OD_{600} of 0.6-0.9. Cell cultures were induced with IPTG and harvested after incubation for 3 hours. Uniformly ^{15}N-labeled cCTnC and G159D were expressed in a minimal media enriched with $(^{15}NH_4)_2SO_4$ (*50*). Cell pellet was lysed using French press and applied to a DEAE column (50 mM Tris, 0.1 M NaCl, pH 8.0). Proteins were further purified using a Superdex-75 size exclusion column (50 mM Tris, 0.15 M NaCl, pH 8.0), desalted using Sephadex G25 column (10 mM NH_4HCO_3), and lyophilized. Molecular masses for unlabeled proteins, cCTnC and G159D, as determined by MALDI mass spectrometry were equal to the expected values. Amino acid composition was confirmed independently by amino acid analysis.

$cTnI_{34-71}$ titration of cCTnC and G159D monitored by 2D {^1H, ^{15}N} HSQC NMR spectroscopy

The peptide, $cTnI_{34-71}$, (acetyl-AKKKSKISASRKLQLKTLLLQIAKQELEREA-EERRGEK-amide) was synthesized using standard methodology for a typical TnI peptide (*51*). The sequence was confirmed by amino acid analysis and the mass was verified by electrospray mass spectrometry. During titration, the peptide was added in the form of powder to the 500 µL solution of 0.57 mM cCTnC and 0.56 mM G159D. The buffer consisted of 100 mM KCl, 10 mM imidazole, 2 mM $CaCl_2$, 5 mM NaN_3, and 0.2 mM DSS in 90% H_2O/10% D_2O. The pH was adjusted to 6.7 ± 0.05 at every titration point. Concentrations of proteins and peptides were determined by weight and confirmed by amino-acid analysis. Since the reaction proceeds within the slow exchange limits for both cCTnC and G159D, the chemical shifts for two species (cCTnC or G159D alone and in

complex with $cTnI_{34-71}$) were observed during titrations. The decreasing intensities of uncomplexed cCTnC or G159D were used to calculate K_D.

^{15}N backbone amide NMR relaxation data

Relaxation data were acquired at 30 °C on a Varian Inova 500 MHz spectrometer from ^{15}N-T_1, ^{15}N-T_2, and {^1H-^{15}N} NOE experiments (Biopack, Varian Associates) for 500 µL samples containing 0.57 mM of cCTnC or 0.56 mM G159D and 1.2 mM of $cTnI_{34-71}$. T_1 data were acquired using relaxation delays of 10, 50, 100, 200, 300, and 400 ms, and T_2 data were acquired using relaxation delays of 10, 30, 50, 70, 90, and 110 ms. Delays between transients in ^{15}N-T_2 and ^{15}N-T_1 experiments were set to 3 s. {^1H-^{15}N} NOE experiments were performed using delays of 5 s for spectra recorded without proton saturation and delays of 2 s for spectra recorded with proton saturation. Proton saturation was set to 3 s so that the total time between transients was equal to 5 s. Relaxation parameters, T_1, T_2, and NOE, were extracted using the rate analysis module built in NMRView (*52*) and analyzed using Mathematica scripts provided by Dr. Leo Spyracopuolos (www.bionmr.ualberta.ca/~lspy/) (*53*). Overall rotational tumbling time, τ_m, was averaged from the per residue fitting of relaxation data to the Lipari-Szabo S^2-τ_m-τ_f model (*54*). Relaxation data for residues with significant internal motions, as judged by NOE<0.65, and data for residues with possible slow motions, as judged by significantly decreased T_2, were excluded in this method of τ_m calculation.

Assignment and structure calculation for cCTnC•$cTnI_{34-71}$ and G159D•$cTnI_{34-71}$

Samples used for NMR data acquisition contained ~0.5 mM of G159D or cCTnC, ~1.2 mM of $cTnI_{34-71}$ in the buffer consisted of 100 mM KCl, 10 mM imidazole, 2 mM $CaCl_2$, 5 mM NaN_3, and 0.2 mM DSS in 90% H_2O/10% D_2O. Buffer used for data acquisition in D_2O contained 100 mM KCl, 0.5 mM imidazole, 9.5 mM deuterated imidazole, 2 mM $CaCl_2$, 5 mM NaN_3, and 0.2 mM DSS. NMR spectra were acquired at 30°C on Varian INOVA 500, Unity 600, or INOVA 800 spectrometers equipped with 5 mm triple resonance probes and *z* axis pulsed field gradients (Table III-3). NMR data was processed using NMRPipe (*55*) and analyzed with NMRView (*52*). The backbone resonances for cCTnC and G159D in the |^{13}C,^{15}N| cCTnC•$cTnI_{34-71}$ and |^{13}C,^{15}N| G159D•$cTnI_{34-71}$ complexes were assigned using SmartNotebook v5.1.3 (*56*). Side chain assignment was carried out using HCCH-TOCSY, HCCONH, CCONH, HNHA, HNHB, and ^{15}N TOCSY HSQC. The majority of side chain resonances were unambiguously assigned. Resonances for aromatic residues were assigned using 2D homonuclear DQF-COSY and NOESY experiments in D_2O. Resonances for the $cTnI_{34-71}$ peptide were not dispersed well enough in 2D ^{13}C/^{15}N-filtered TOCSY and NOESY experiments to allow for the assignment of many residues except for amide protons, HN, for residues 41-64, Hα for residues 41-59, Hβ for residues 41-43, 50, 53, 56, and Hδ/γ for residues 46-53, 55, and 58-60.

Structure calculations were performed with CYANA (*26*) using the 'noeassign' automatic assignment procedure (*57*) and distance restraints from ^{13}C NOESY HSQC and ^{15}N NOESY HSQC experiments. Unambiguous restraints were assigned manually and were forced to keep their assignments during the first four runs of CYANA calculations, after which they were open for automatic assignment by CYANA. Distance restraints were calibrated with CYANA standard procedure using upper limits of 6 Å. TALOS dihedral restraints for helical regions for G159D and cCTnC (*58*), and Ca^{2+} restraints for Ca^{2+} binding loops were obtained from X-ray crystallographic data and added into the calculation (Table III-3). TALOS restraints did not affect the overall fold of the structures (data not shown), however, in case of G159D, in final structure calculations the restraints

were truncated up to residue 151, to avoid artifactual secondary structure. CYANA was used to calculate 50 structures, and the 20 conformers with the lowest target function were refined in explicit solvent by XPLOR-NIH (*27, 28*) with a water box of 18.856 Å. The final ensembles were averaged and refined using the same water refinement protocol as done previously, and are the structures discussed herein and deposited (PDBs). Structures were validated using PROCHECK (*29*) and WHATCHECK (*30*).

Table III-3. NMR experiments acquired for structure calculations and chemical shift assignments.

Experiment	Nuclei[a]	^{1}H	x-pts[b]	y-pts	z-pts	x-sw	y-sw	z-sw	Mix (ms)
^{15}N-HSQC	^{1}H, ^{15}N	500	1074	192		8384.9		2026.3	–
HCCH-TOCSY	^{1}H, ^{13}C, ^{1}H	500	1024	128	104	8384.9	5998.5	10057.8	–
CBCA(CO)NNH	^{1}H, ^{13}C, ^{15}N	500	1024	118	64	8384.9	10057.2	2026.3	–
HNCACB	^{1}H, ^{13}C, ^{15}N	500	1024	118	64	8384.9	10057.2	2026.3	–
HCCONH	^{1}H, ^{13}C, ^{15}N	600	1024	160	64	8398.1	5998.5	2431.6	–
CCONH	^{1}H, ^{13}C, ^{15}N	600	1024	184	64	8398.1	12067.2	2431.6	–
^{13}C NOESY HSQC	^{1}H, ^{1}H, ^{13}C	600	1024	160	80	8398.1	5998.7	6033.7	100
^{15}N NOESY HSQC	^{1}H, ^{1}H, ^{15}N	600	1024	160	80	8398.1	5998.7	2431.6	150
^{15}N TOCSY HSQC	^{1}H, ^{1}H, ^{15}N	600	1024	160	64	8398.1	5998.7	2431.6	50
HNHA	^{1}H, ^{1}H, ^{15}N	600	1024	160	64	8398.1	5998.7	2431.6	–
HNHB	^{1}H, ^{1}H, ^{15}N	500	1024	160	64	8384.9	4998.8	2026.3	–
DQF-COSY ($D_2$0)	^{1}H, ^{1}H	800							
NOESY ($D_2$0)	^{1}H, ^{1}H	800							
^{13}C/^{15}N-filt. TOCSY	^{1}H, ^{1}H	600	4096	512	–	8384.9	8385.7	–	0.06
^{13}C/^{15}N-filt. NOESY	^{1}H, ^{1}H	600	4096	512	–	8384.9	8385.7	–	0.25
^{13}C-filt., ed. NOESY	^{1}H, ^{1}H, ^{13}C	600	1024	240	64	3595.9	3595.9	3014.0	0.15

[a] The nucleus acquired in each dimension (e.g., ^{1}H, ^{15}N indicates proton *x*, nitrogen *y*). [b] x-, y-, and z-pts and -sw are the number of complex points and the sweep width in each respective dimension (x is the directly detected dimension).

Figure III-1. Titration of G159D (a) and cCTnC (b) with $cTnI_{34-71}$ using 2D {^1H, ^{15}N} HSQC NMR spectroscopy. Closed cross-peaks correspond to uncomplexed cCTnC or G159D and open cross-peaks correspond to the complex of cCTnC or G159D with $cTnI_{34-71}$. Corresponding binding curves are shown in the insets. Annotated residues have the largest ^{15}N backbone chemical shift differences and are adjacent to the mutation site.

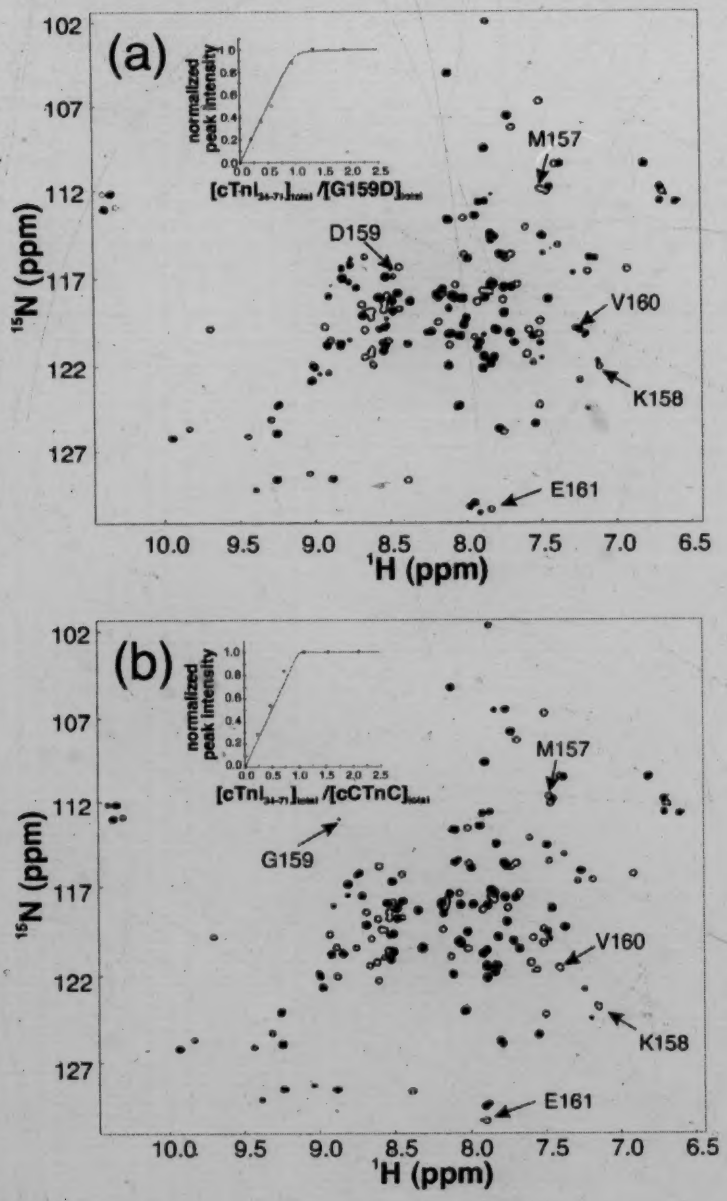

Figure III-2. Per residue NMR relaxation parameters T_2 (a), T_1 (b), NOE (c) for G159D (closed circles) and cCTnC (open circles) in complexes with $cTnI_{34-71}$.

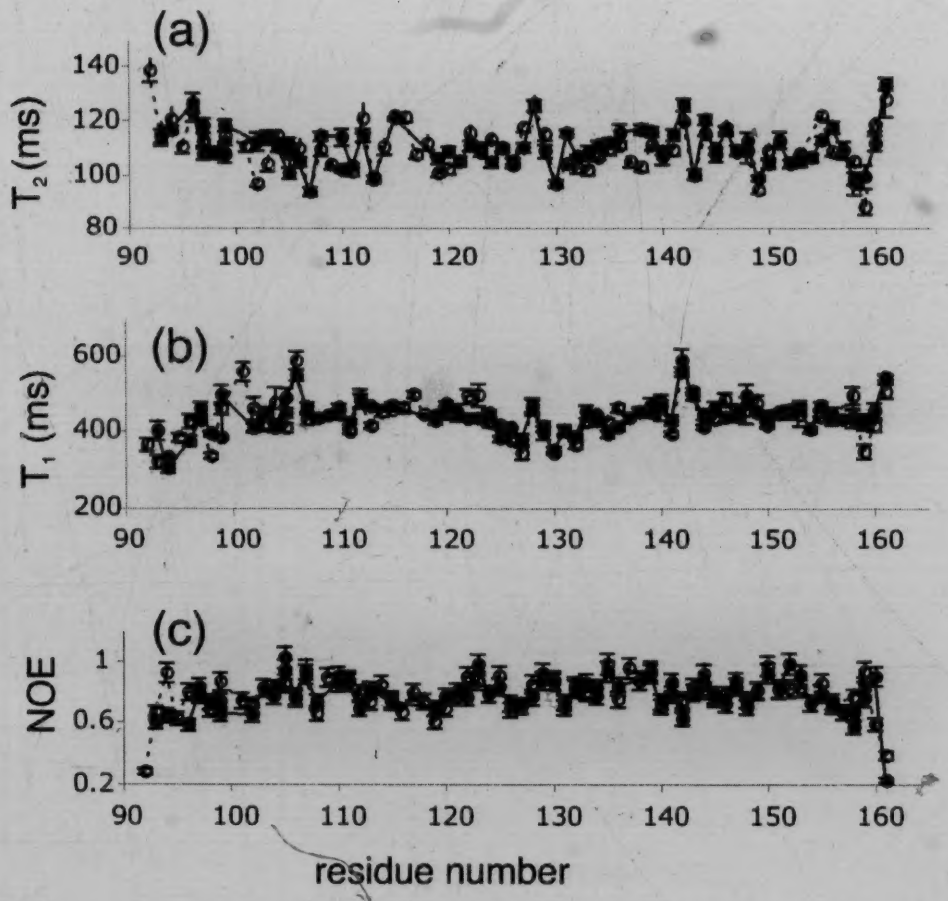

Figure III-3. Chemical shifts differences between G159D and cCTnC in complexes with $cTnI_{34-71}$ for backbone amide ^{15}N (a), side chain ^{13}C (b), and side chain ^{1}H (c). Side chain chemical shift changes for ^{13}C and ^{1}H are added together for every residue, with Cα and Hα in black, Cβ and Hβ in white, Cδ and Hδ in red, Cε and Hε in dark blue, and Cδ and Hδ in green. Horizontal lines correspond to the average value plus one standard deviation.

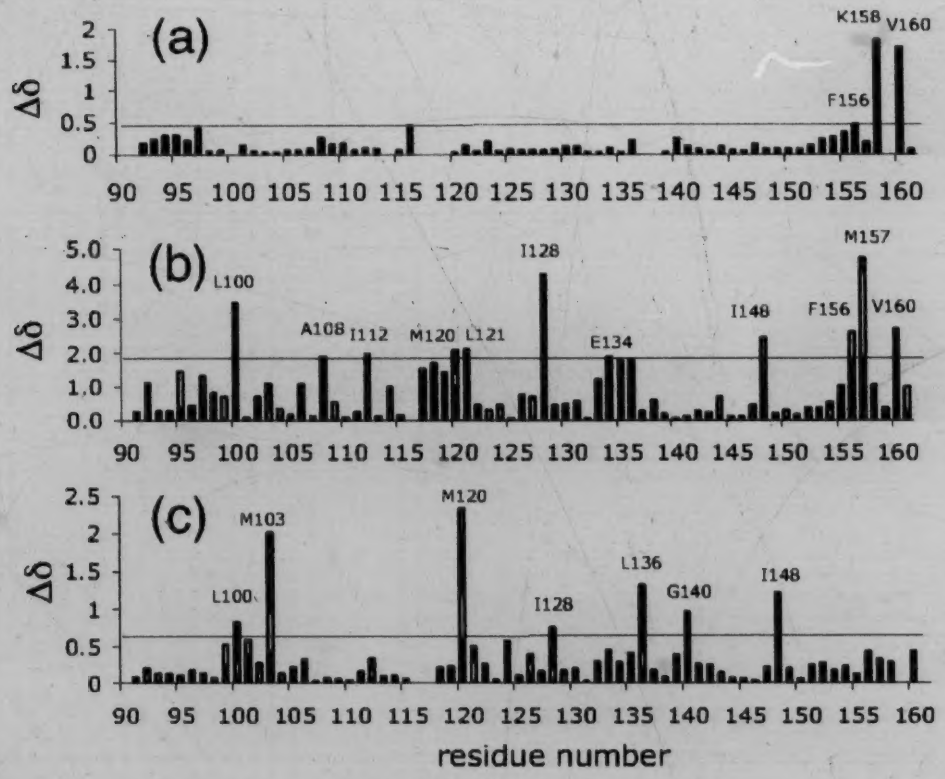

Figure III-4. Residues with chemical shift changes visualized on the structure of cCTnC determined by X-ray crystallography (1J1D). Residues with the significant ^{15}N chemical shift changes are shown in black (a). Residues with the significant side chain ^{13}C chemical shift changes are shown in green (b). Residues with the significant side chain ^{1}H chemical shift changes are shown in red (c). Gly^{159} is shown in yellow in all three panels.

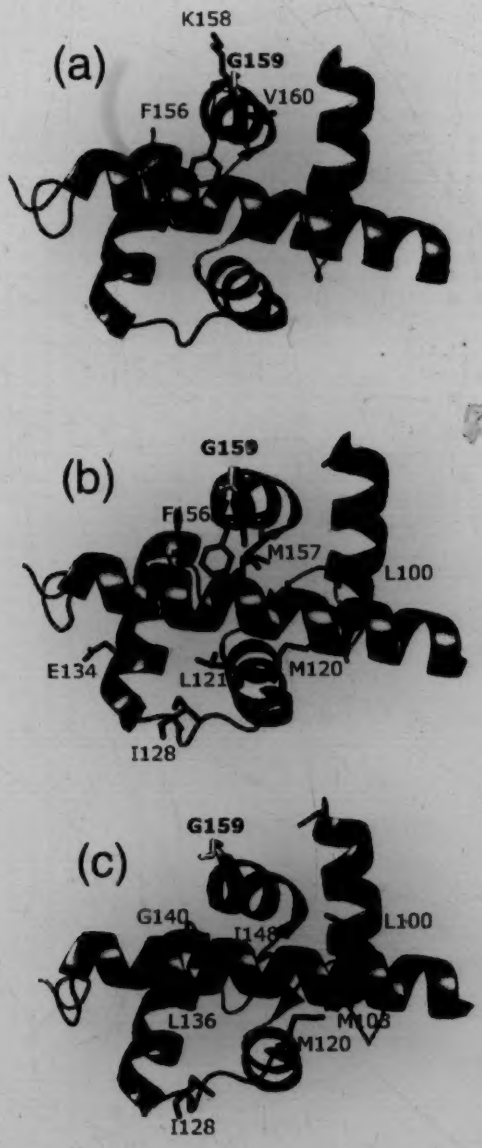

Figure III-5. NOE strips for G159D (left) and cCTnC (right) in complexes with $cTnI_{34-71}$ obtained in 3D ^{13}C NOESY HSQC NMR experiments (a-d) and in ^{15}N NOESY HSQC NMR experiments (e), where stars represent the resonances tentatively assigned to the peptide, and double stars represent resonances tentatively assigned to the protein. Assignments are indicated below each pair of plots.

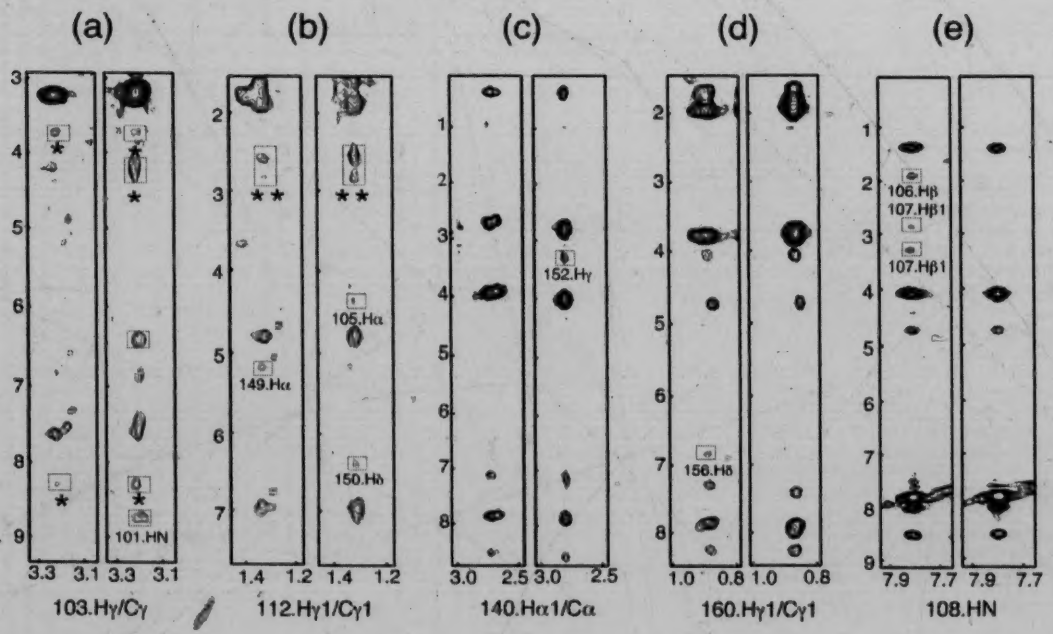

Figure III-6. Secondary structures of cCTnC (a) and G159D (b) in complexes with the anchoring region of cTnI (or $cTnI_{34-71}$) in comparison with the previously determined structures 1J1D (grey) and 1FI5 (green). The structure of cCTnC determined in this work is shown on both panels in red and the structure of G159D is in yellow.

(a)

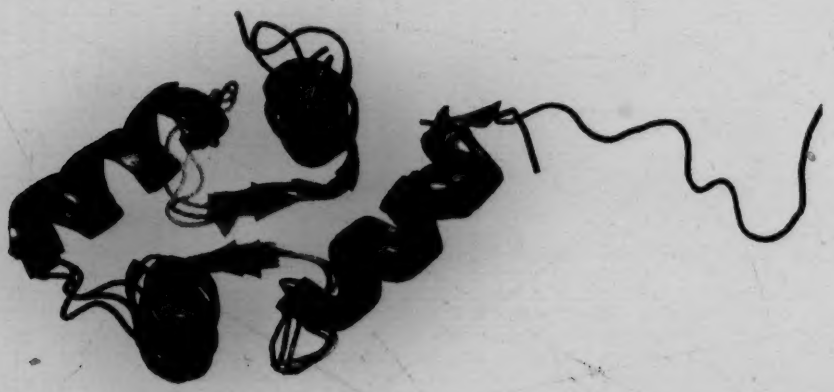

(b)

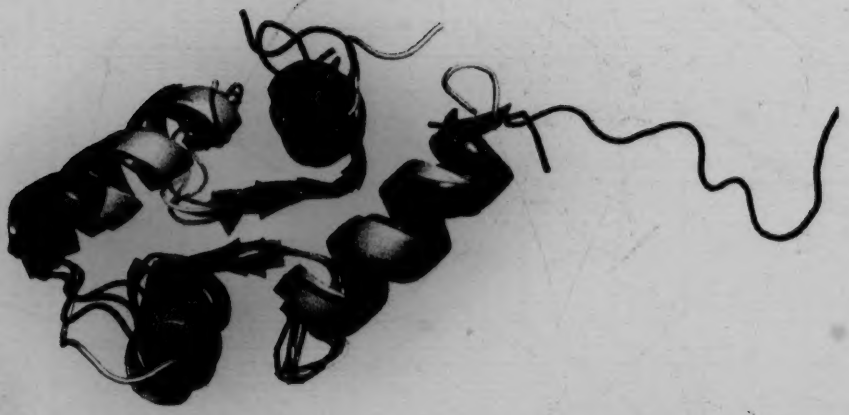

Figure III-7. Overlay of the regions of ^{13}C-filtered, edited NOESY spectra showing the direct contacts between G159D (black contours) and cCTnC (red contours) with $cTnI_{34-71}$. The resonances of proteins are shown with the horizontal solid arrows, the resonances for the peptide are shown with the vertical dashed arrows. The contact for G159D in the panel B is missing.

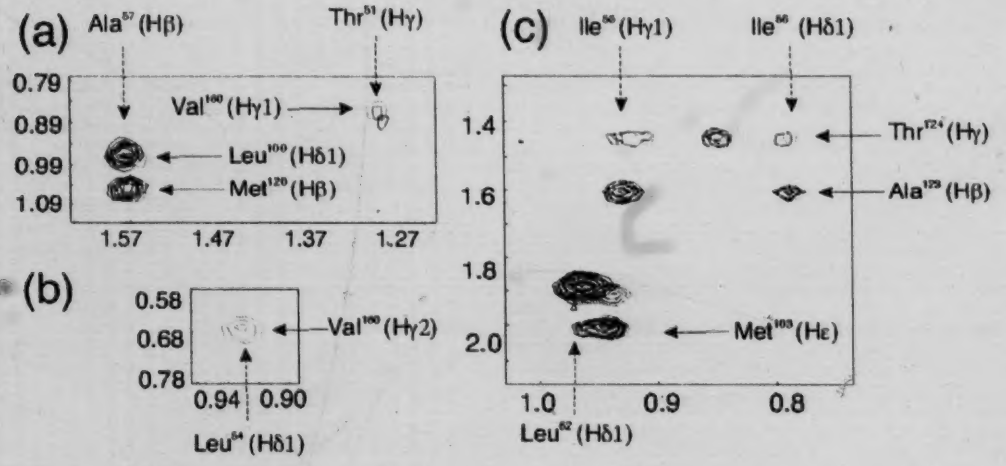

Figure III-8. The X-ray structure of the core of cardiac troponin complex (1JID) overlaid with the G159D structure to demonstrate the proximity of Asp^{159} to cNTnC. Ribbon diagram is shown for cTnC (green), cTnI (red), cTnT (grey), and G159D (yellow). The cNTnC binding site for $cTnI_{147-163}$ and the possible cNTnC binding site for $cTnI_{1-29}$ are indicated. Electrostatic residues of cNTnC in close proximity to Asp^{159} are shown in sticks (Asp^{87} and Asp^{3}).

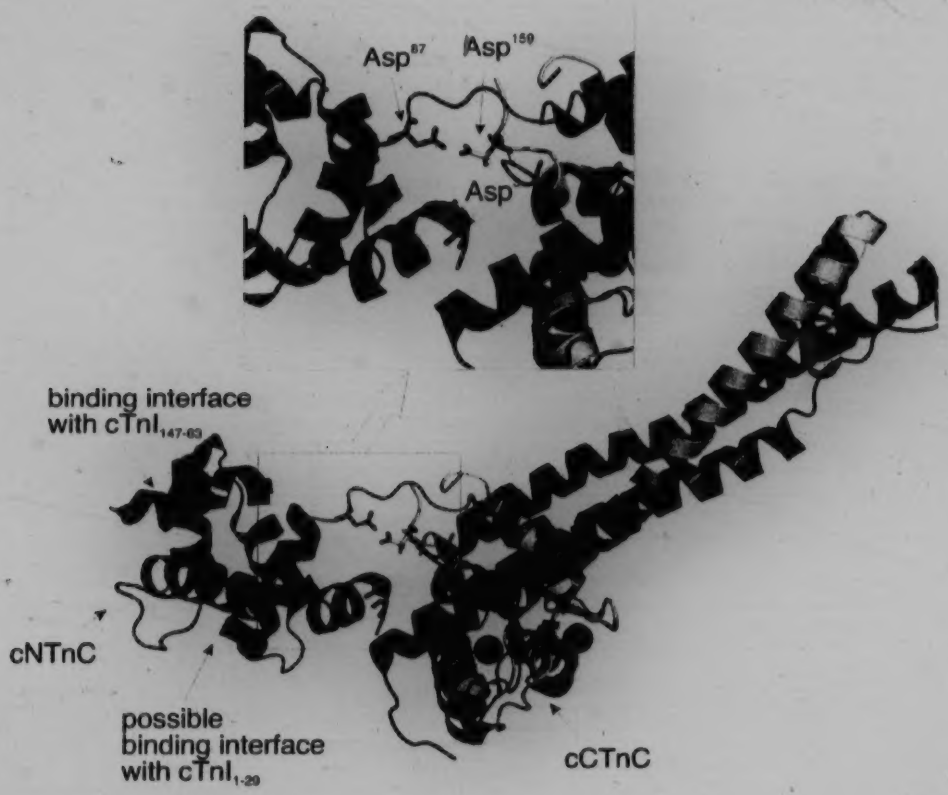

References

(1) Takeda, S., Yamashita, A., Maeda, K., and Maeda, Y. (2003) Structure of the core domain of human cardiac troponin in the Ca(2+)-saturated form. *Nature 424*, 35-41.

(2) Redwood, C. S., Moolman-Smook, J. C., and Watkins, H. (1999) Properties of mutant contractile proteins that cause hypertrophic cardiomyopathy. *Cardiovasc Res 44*, 20-36.

(3) Seidman, J. G., and Seidman, C. (2001) The genetic basis for cardiomyopathy: from mutation identification to mechanistic paradigms. *Cell 104*, 557-67.

(4) Hoffmann, B., Schmidt-Traub, H., Perrot, A., Osterziel, K. J., and Gessner, R. (2001) First mutation in cardiac troponin C, L29Q, in a patient with hypertrophic cardiomyopathy. *Hum Mutat 17*, 524.

(5) Lim, C. C., Yang, H., Yang, M., Wang, C. K., Shi, J., Berg, E. A., Pimentel, D. R., Gwathmey, J. K., Hajjar, R. J., Helmes, M., Costello, C. E., Huo, S., and Liao, R. (2008) A Novel Mutant Cardiac Troponin C Disrupts Molecular Motions Critical For Calcium Binding Affinity And Cardiomyocyte Contractility. *Biophys J 94*, 3577-89.

(6) Parvatiyar, M., Pinto, J. R., Jones, M. A., Ackerman, M. J., and Potter, J. D. (2008) in *Biophysical Society, Annual Meeting*, Long Beach, CA.

(7) Mogensen, J., Murphy, R. T., Shaw, T., Bahl, A., Redwood, C., Watkins, H., Burke, M., Elliott, P. M., and McKenna, W. J. (2004) Severe disease expression of cardiac troponin C and T mutations in patients with idiopathic dilated cardiomyopathy. *J Am Coll Cardiol 44*, 2033-40.

(8) Li, M. X., Wang, X., and Sykes, B. D. (2004) Structural based insights into the role of troponin in cardiac muscle pathophysiology. *J Muscle Res Cell Motil 25*, 559-79.

(9) Sykes, B. D. (2003) Pulling the calcium trigger. *Nat Struct Biol 10*, 588-9.

(10) Biesiadecki, B. J., Kobayashi, T., Walker, J. S., John Solaro, R., and de Tombe, P. P. (2007) The Troponin C G159D Mutation Blunts Myofilament Desensitization Induced by Troponin I Ser23/24 Phosphorylation. *Circ Res 100*, 1486-1493.

(11) Preston, L. C., Ashley, C. C., and Redwood, C. S. L. (2007) DCM troponin C mutant Gly159Asp blunts the response to troponin phosphorylation. *Biochem Biophys Res Commun 360*, 27-32.

(12) Mirza, M., Marston, S., Willott, R., Ashley, C., Mogensen, J., McKenna, W., Robinson, P., Redwood, C., and Watkins, H. (2005) Dilated cardiomyopathy mutations in three thin filament regulatory proteins result in a common functional phenotype. *J Biol Chem 280*, 28498-506.

(13) Lindhout, D. A., Boyko, R. F., Corson, D. C., Li, M. X., and Sykes, B. D. (2005) The role of electrostatics in the interaction of the inhibitory region of troponin I with troponin C. *Biochemistry 44*, 14750-9.

(14) Vinogradova, M. V., Stone, D. B., Malanina, G. G., Karatzaferi, C., Cooke, R., Mendelson, R. A., and Fletterick, R. J. (2005) Ca(2+)-regulated structural changes in troponin. *Proc Natl Acad Sci U S A 102*, 5038-43.

(15) Blumenschein, T. M., Tripet, B. P., Hodges, R. S., and Sykes, B. D. (2001) Mapping the interacting regions between troponins T and C. Binding of TnT and TnI peptides to TnC and NMR mapping of the TnT-binding site on TnC. *J Biol Chem 276*, 36606-12.

(16) Dong, W. J., Xing, J., Ouyang, Y., An, J., and Cheung, H. C. (2008) Structural kinetics of cardiac troponin C mutants linked to familial hypertrophic and dilated cardiomyopathy in troponin complexes. *J Biol Chem 283*, 3424-32.

(17) Li, M. X., Wang, X., Lindhout, D. A., Buscemi, N., Van Eyk, J. E., and Sykes, B. D. (2003) Phosphorylation and mutation of human cardiac troponin I deferentially destabilize the interaction of the functional regions of troponin I with troponin C. *Biochemistry 42*, 14460-8.

(18) Lindhout, D. A., and Sykes, B. D. (2003) Structure and dynamics of the C-domain of human cardiac troponin C in complex with the inhibitory region of human cardiac troponin I. *J Biol Chem 278*, 27024-34.

(19) Gasmi-Seabrook, G. M., Howarth, J. W., Finley, N., Abusamhadneh, E., Gaponenko, V., Brito, R. M., Solaro, R. J., and Rosevear, P. R. (1999) Solution structures of the C-terminal domain of cardiac troponin C free and bound to the N-terminal domain of cardiac troponin I. *Biochemistry 38*, 8313-22.

(20) Bloembergen, N., Purcell, E. M., and Pound, R. V. (1948) Relaxation Effects in Nuclear Magnetic Resonance Absorption. *Physical Review 73*, 679-712.

(21) Baryshnikova, O. K., and Sykes, B. D. (2006) Backbone dynamics of SDF-1alpha determined by NMR: interpretation in the presence of monomer-dimer equilibrium. *Protein Sci 15*, 2568-78.

(22) Mercier, P., Spyracopoulos, L., and Sykes, B. D. (2001) Structure, dynamics, and thermodynamics of the structural domain of troponin C in complex with the regulatory peptide 1-40 of troponin I. *Biochemistry 40*, 10063-77.

(23) Cantor, C. R., and Schimmel, P. R. (1980) *Biophysical Chemistry, Part II, Techniques for the study of biological structure and function*, W.H. Freeman, New York.

(24) Tanford, C. (1961) *Physical chemistry of macromolecules*, John Wiley & Sons, Inc., New York.

(25) Wuthrich, K. (1986) *NMR of Proteins and Nucleic Acids*, John Wiley & Sons, New York.

(26) Guntert, P. (2004) Automated NMR strucutre calculation with CYANA. *Methods Mol Biol 278*, 353-78.

(27) Linge, J. P., Williams, M. A., Spronk, C. A., Bonvin, A. M., and Nilges, M. (2003) Refinement of protein structures in explicit solvent. *Proteins 50*, 496-506.

(28) Schwieters, C. D., Kuszewski, J. J., Tjandra, N., and Clore, G. M. (2003) The Xplor-NIH NMR molecular structure determination package. *J Magn Reson 160*, 65-73.

(29) Laskowski, R. A., MacArthur, M. W., Moss, D. S., and Thornton, J. M. (1993) PROCHECK: a program to check the stereochemical quality of protein structures. *J Appl Cryst 26P*, 283-291.

(30) Hooft, R. W., Vriend, G., Sander, C., and Abola, E. E. (1996) Errors in protein structures. *Nature 381*, 272.

(31) Lee, W., Revington, M. J., Arrowsmith, C., and Kay, L. E. (1994) A pulsed field gradient isotope-filtered 3D 13C HMQC-NOESY experiment for extracting intermolecular NOE contacts in molecular complexes. *FEBS Lett 350*, 87-90.

(32) Robertson, I. M., Spyracopoulos, L., and Sykes, B. D. (2007) in *Proceedings for the international School of Biological Magnetic Resonanse, 8th Course on Biophysics and the Challenges of Emerging Threats* (Puglisi, J. D., Ed.), NATO Science Series: Life and Behavioural Sciences, IOS press, The Nethrlands.

(33) Gemmecker, G., Olejniczak, E. T., and Fesik, S. W. (1992) An Improved Method for Selectively Observing Protons Attached to C-12 in the Presence of H-1-C-13 spin Pairs. *J Mag Res 96*, 199-204.

(34) Ikura, M., and Bax, A. (1992) Isotope-Filtered 2d NMR of a Protein Peptide Complex - Study of a Skeletal-Muscle Myosin Light Chain Kinase Fragment Bound to Calmodulin. *J Am Chem Soc 114*, 2433-2440.

(35) Ogura, K., Terasawa, H., and Inagaki, F. (1996) An improved double-tuned and isotope-filtered pulse scheme based on a pulsed field gradient and a wide-band inversion shaped pulse. *J Biomol NMR 8*, 492-498.

(36) Finley, N. L., Howarth, J. W., and Rosevear, P. R. (2004) Structure of the Mg2+-loaded C-lobe of cardiac troponin C bound to the N-domain of cardiac troponin I: comparison with the Ca2+-loaded structure. *Biochemistry 43*, 11371-9.

(37) Sheng, Z., Pan, B. S., Miller, T. E., and Potter, J. D. (1992) Isolation, expression, and mutation of a rabbit skeletal muscle cDNA clone for troponin I. The role of the NH2 terminus of fast skeletal muscle troponin I in its biological activity. *J Biol Chem 267*, 25407-13.

(38) Potter, J. D., Sheng, Z., Pan, B. S., and Zhao, J. (1995) A direct regulatory role for troponin T and a dual role for troponin C in the Ca2+ regulation of muscle contraction. *J Biol Chem 270*, 2557-62.

(39) Tripet, B., De Crescenzo, G., Grothe, S., O'Connor-McCourt, M., and Hodges, R. S. (2003) Kinetic analysis of the interactions between troponin C (TnC) and troponin I (TnI) binding peptides: evidence for separate binding sites for the 'structural' N-terminus and the 'regulatory' C-terminus of TnI on TnC. *J Mol Recognit 16*, 37-53.

(40) De Nicola, G., Burkart, C., Qiu, F., Agianian, B., Labeit, S., Martin, S., Bullard, B., and Pastore, A. (2007) The structure of Lethocerus troponin C: insights into the mechanism of stretch activation in muscles. *Structure 15*, 813-24.

(41) Cheng, H., Lederer, M. R., Lederer, W. J., and Cannell, M. B. (1996) Calcium sparks and [Ca2+]i waves in cardiac myocytes. *Am J Physiol 270*, C148-59.

(42) Takamatsu, T., and Wier, W. G. (1990) Calcium waves in mammalian heart: quantification of origin, magnitude, waveform, and velocity. *Faseb J 4*, 1519-25.

(43) Li, M. X., Spyracopoulos, L., and Sykes, B. D. (1999) Binding of cardiac troponin-I147-163 induces a structural opening in human cardiac troponin-C. *Biochemistry 38*, 8289-98.

(44) Finley, N., Abbott, M. B., Abusamhadneh, E., Gaponenko, V., Dong, W., Gasmi-Seabrook, G., Howarth, J. W., Rance, M., Solaro, R. J., Cheung, H. C., and Rosevear, P. R. (1999) NMR analysis of cardiac troponin C-troponin I complexes: effects of phosphorylation. *FEBS Lett 453*, 107-12.

(45) Gaponenko, V., Abusamhadneh, E., Abbott, M. B., Finley, N., Gasmi-Seabrook, G., Solaro, R. J., Rance, M., and Rosevear, P. R. (1999) Effects of troponin I phosphorylation on conformational exchange in the regulatory domain of cardiac troponin C. *J Biol Chem 274*, 16681-4.

(46) Keane, N. E., Quirk, P. G., Gao, Y., Patchell, V. B., Perry, S. V., and Levine, B. A. (1997) The ordered phosphorylation of cardiac troponin I by the cAMP-dependent protein kinase--structural consequences and functional implications. *Eur J Biochem 248*, 329-37.

(47) Baryshnikova, O. K., Li, M. X., and Sykes, B. D. (2008) Modulation of cardiac troponin C function by the cardiac-specific N-terminus of troponin I: influence of PKA phosphorylation and involvement in cardiomyopathies. *J Mol Biol 375*, 735-51.

(48) Schmidtmann, A., Lindow, C., Villard, S., Heuser, A., Mugge, A., Gessner, R., Granier, C., and Jaquet, K. (2005) Cardiac troponin C-L29Q, related to hypertrophic cardiomyopathy, hinders the transduction of the protein kinase A

dependent phosphorylation signal from cardiac troponin I to C. *Febs J 272*, 6087-97.

(49) Pearlstone, J. R., Chandra, M., Sorenson, M. M., and Smillie, L. B. (2000) Biological function and site II Ca2+-induced opening of the regulatory domain of skeletal troponin C are impaired by invariant site I or II Glu mutations. *J Biol Chem 275*, 35106-15.

(50) Li, M. X., Corson, D. C., and Sykes, B. D. (2002) Structure determination by NMR. Isotope labeling. *Methods Mol Biol 173*, 255-65.

(51) Tripet, B., Van Eyk, J. E., and Hodges, R. S. (1997) Mapping of a second actin-tropomyosin and a second troponin C binding site within the C terminus of troponin I, and their importance in the Ca2+-dependent regulation of muscle contraction. *J Mol Biol 271*, 728-50.

(52) Johnson, B. A., and Blevins, R. A. (1994) NMRView: A computer program for the visualization and analysis of NMR data. *J Biomol NMR 4*, 603-614.

(53) Spyracopoulos, L. (2006) A suite of Mathematica notebooks for the analysis of protein main chain 15N NMR relaxation data. *J Biomol NMR 36*, 215-24.

(54) Lipari, G., and Szabo, a. (1982) Model-Free Approach to the Interpretation of Nuclear Magnetic-Resonance Relaxation in Macromolecules.1. Theory and Range of Validity. *J Am Chem Soc 104*, 4546-4559.

(55) Delaglio, F., Grzesiek, S., Vuister, G. W., Zhu, G., Pfeifer, J., and Bax, A. (1995) NMRPipe: a multidimensional spectral processing system based on UNIX pipes. *J Biomol NMR 6*, 277-93.

(56) Slupsky, C. M., Boyko, R. F., Booth, V. K., and Sykes, B. D. (2003) Smartnotebook: a semi-automated approach to protein sequential NMR resonance assignments. *J Biomol NMR 27*, 313-21.

(57) Jee, J., and Guntert, P. (2003) Influence of the completeness of chemical shift assignments on NMR structures obtained with automated NOE assignment. *J Struct Funct Genomics 4*, 179-89.

(58) Cornilescu, G., Delaglio, F., and Bax, A. (1999) Protein backbone angle restraints from searching a database for chemical shift and sequence homology. *J Biomol NMR 13*, 289-302.

CHAPTER IV

Exploring the interaction between cNTnC and the N-terminus of cTnI

Outline

In Chapter II we have investigated the interaction between $cTnI_{1-29}$ and cNTnC and demonstrated that it is important in modulation of cTnC function. This modulation is perturbed in the presence of cardiomyopathy mutations studied, and therefore suggests that it may be involved in the development of cardiomyopathies. Various lines of evidence suggest that electrostatic interactions play a major role in the binding of $cTnI_{1-29}$ to cNTnC. Using NMR relaxation data as a function of ionic strength, we have obtained experimental evidence supporting the hypothesized electrostatic nature of the interaction between cNTnC•Ca^{2+} and $cTnI_{1-29}$.

Introduction

There is an increasing amount of evidence for interaction between the N-terminus of cTnI (~residues 1-29) and cNTnC (with and without Ca^{2+}) (*1-5*), which was not visualized in crystal structures (*6*) nor in NMR studies (*1, 7*). This may be due to the fairly weak binding and/or flexibility of this region of cTnI. Estimation of binding affinity for $cTnI_{1-29}$ has proven to be difficult. This interaction, however, plays a paramount role in the modulation of the cTnC function in response to β-adrenergic stimulation (*8-10*), and in disease, for example in the presence of FHC and DCM mutations (*11-13*). Visualization of this interaction, as well as others that occur with intrinsically disordered and/or charged protein fragments, remains both technically challenging and of the outmost biological interest (*14, 15*).

As mentioned in Chapter II, a major contribution to the interaction between cNTnC and the N-terminus of cTnI ($cTnI_{1-29}$) is thought to come from electrostatics based on following facts: first, the backbone chemical shift changes induced by the binding of $cTnI_{1-29}$/ $cTnI_{1-29}$PP to cNTnC are very small upon the formation of complex (*1*), similar to the interaction of the inhibitory region of cTnI (~residues 128-147) with cCTnC•Ca^{2+} (*16*). The lack of the large backbone chemical shift changes is indicative of electrostatic interactions between sidechains, in which the core of the protein is not significantly affected and the backbone chemical shifts remain unchanged. Second, line broadening in the NMR study of backbone dynamics for the cTnC•$cTnI_{1-80}$ complex indicated that the

possible site of binding was located in the region of β-sheets, opposite to the hydrophobic cleft, which is the binding site for the switch region of cTnI (~residues 147-163) (*17*). Formation of the triple complex was confirmed by the increase in the overall correlation time, supporting the notion of the independent binding site for $cTnI_{1-29}$, different from the binding site for $cTnI_{147-163}$ (*5*). Third, the N-terminus of cTnI is positively charged, with the first 29 residues being ADGSSDAAREPRPAPAPIRRRSSNYRAYA, where the three consequent arginines (underlined) are suspected to interact with the negatively charged residues on cNTnC (*3, 7*). Upon phosphorylation, as shown by the NMR studies of phosphorylated peptides, the conformation of the cTnI N-terminus changes so that two phosphogroups screen the charges on the arginines, possibly precluding strong electrostatic contacts to be formed and promoting the dissociation of the cTnI N-terminus from cNTnC (*18*).

In Debye-Huckel formalism, the presence of electrolyte has a screening effect on the electric field of individual ions, which varies with the square root of the ionic strength (*19*). Coulomb potential has the following form:

$$\varphi_C(r) = \frac{z}{4\pi\varepsilon} \bullet \frac{1}{r},$$

where the elementary charge is equal to 1, z is a charge of the ion, ε is the medium permittivity, and r is the distance from the center of ion. The effect of charge shielding of the central ion is denoted as following:

$$\varphi_C(r) = \frac{ze^{-\frac{r}{r_D}}}{4\pi\varepsilon} \bullet \frac{1}{r},$$

where r_D is the Debye radius with the following dependence on ionic strength:

$$r_I = \sqrt{\frac{\varepsilon_0 \varepsilon_r kT}{2NI}},$$

where ε_0 is the permittivity of free space, ε_r is the dielectric constant, k is Boltzmann's constant, T is the absolute temperature, N is Avogadro's number, and I is the ionic strength. Ionic strength is expressed as a function of concentration of all ions in solution:

$$I = \frac{1}{2}\sum_A c_A z_A^2$$

where c_A is the concentration of ion A and z_A is the charge of ion A in solution. Thus, the higher the concentration of salt and ionic strength are, the greater the shielding, and the weaker electrostatic potential.

One of the methods to probe electrostatic interactions is to vary the ionic strength of the solution. While this method gives straightforward results for some systems (*20, 21*), electrostatic interactions in proteins can contribute not only to the formation of interfaces but in some cases to the stabilization of a protein core complicating the interpretation of results (*22, 23*). We have determined the dependence of the ^{15}N NMR relaxation parameter T_2 as a function of ionic strength for different ^{15}N labeled cNTnC complexes, apo cNTnC, cNTnC•Ca^{2+}, cNTnC•$cTnI_{1-29}$, and cNTnC•Ca^{2+}•$cTnI_{1-29}$, in order to probe electrostatic interactions between $cTnI_{1-29}$ and cNTnC. Average T_2 values (obtained by averaging the per residue T_2's) as a function of ionic strength provided evidence for the decrease in binding of $cTnI_{1-29}$ to apo cNTnC and cNTnC•Ca^{2+} in high salt, supporting the hypothesis of electrostatic interaction. Per residue T_2 trends, together with chemical shift changes, demonstrate that increased flexibility and possibly K^+ binding to Ca^{2+} binding site of apo-cNTnC take place at low salt. In case of cNTnC•Ca^{2+}, per residue T_2 trends and chemical shift changes show that cNTnC•Ca^{2+} remains essentially unchanged (up to ionic strength of ~400 mM) and therefore serve as a fairly good control in our experiments. Decrease in T_2 upon the addition of $cTnI_{1-29}$ in low salt substantiated the hypothesis of electrostatic interactions between $cTnI_{1-29}$ and cNTnC•Ca^{2+}.

Results and Discussion

Dependence of per residue and average T_2 on ionic strength for apo cNTnC, cNTnC•Ca^{2+}, cNTnC•$cTnI_{1-29}$, and cNTnC•Ca^{2+}•$cTnI_{1-29}$

Relaxation parameter T_2 is a complex function of protein motions (*24, 25*), but can be used to correlate with the increase in molecular weight of the protein (*16, 26*). Average T_2 data is presented in Figure IV-1 as a function of ionic strength. For cNTnC•Ca^{2+} the dependence on ionic strength was minimal (open red squares) as compared to cNTnC•Ca^{2+}•$cTnI_{1-29}$ (closed red squares), which underwent a decrease in T_2 values in lower salt. At high salt, the average T_2 for cNTnC•Ca^{2+}•$cTnI_{1-29}$ was almost equal to the average T_2 for cNTnC•Ca^{2+}, which implies that complex formation is very weak at high salt and therefore provides direct evidence for electrostatic interactions playing the major role in stabilizing the complex between cNTnC•Ca^{2+} and $cTnI_{1-29}$.

Similar results were observed for apo cNTnC, with average T_2 values remained approximately independent of salt concentration (open black circles), whereas for cNTnC•$cTnI_{1-29}$ (closed black circles), the dependence on ionic strength is clearly

noticeable. This data similarly supports the notion of electrostatic interactions playing the major role in the complex between $cTnI_{1-29}$ and cNTnC, since contacts are stronger in lower salt and therefore, the complex is heavier as demonstrated by lower values for T_2. The average T_2 data for cNTnC•Ca^{2+}•$cTnI_{1-29}$ and cNTnC•$cTnI_{1-29}$ are in agreement at ionic strength >100 mM, supporting the notion of formation similar complexes.

Per residue T_2 trends followed similar dependences to the average T_2's for cNTnC•Ca^{2+}, cNTnC•Ca^{2+}•$cTnI_{1-29}$, and cNTnC•$cTnI_{1-29}$ (Figs. IV-2a, IV-2b, and IV-2d). The control, cNTnC•Ca^{2+}, could be considered roughly unperturbed by ionic strength based on per residue and average T_2 data. Per residue T_2 trends for apo cNTnC followed patterns different from the average T_2 (Fig. IV-2c), demonstrating that the addition of KCl affected the conformational flexibility of cNTnC. Some residues of apo cNTnC in low salt became more flexible (higher T_2 values) and some residues were likely to be involved in conformational exchange (lower T_2 values). The possibility of aggregation for apo cNTnC can be ruled out since the average T_2 values remain high. It is possible that electrostatic repulsion within the protein has been increased leading to the conformational flexibility. It is also possible that at high concentration of KCl, K^+ might occupy the Ca^{2+} binding site on cNTnC. This complicates the interpretation of data pertaining to the apo cNTnC complex with $cTnI_{1-29}$. At low salt, the T_2 values for cNTnC•$cTnI_{1-29}$ are very low suggesting aggregation, possibly triggered by the increased flexibility of apo cNTnC.

2D {^1H, ^{15}N} HSQC NMR spectroscopy of apo cNTnC, cNTnC•Ca^{2+}, cNTnC•$cTnI_{1-29}$, and cNTnC•Ca^{2+}•$cTnI_{1-29}$ in varying ionic strength

Chemical shift changes are sensitive parameters that can be also used to monitor protein changes upon changing the ionic strength of solution. 2D {^{1}H, ^{15}N} HSQC NMR spectra for apo cNTnC, cNTnC•Ca^{2+}, cNTnC•$cTnI_{1-29}$, and cNTnC•Ca^{2+}•$cTnI_{1-29}$ were acquired in varying ionic strength and are shown in Figures IV-3 and IV-4. The spectrum of cNTnC•Ca^{2+} underwent no or very slight perturbation as a function of ionic strength (Fig. IV-3b), with only a few charged residues moving slightly, as it is shown with arrows. Overall chemical shift changes were small, barely above the resolution in the {^{1}H, ^{15}N} HSQC spectrum, which was ~0.02 ppm (Fig. IV-4). Small changes in chemical shifts accompanied also the addition of salt to apo cNTnC, cNTnC•$cTnI_{1-29}$, and cNTnC•Ca^{2+}•$cTnI_{1-29}$ (Figs. IV-3a, IV-3c, and IV-3d). For cNTnC•$cTnI_{1-29}$, the changes in chemical shift were the largest (Fig. IV-4). Interestingly, in case of apo cNTnC, some

chemical shift changes followed curved trajectory, supporting the existence of several processes. Based on chemical shift changes, the structure of cNTnC•Ca^{2+} was essentially unaffected by the increase in ionic strength, and thus, cNTnC•Ca^{2+} can serve as a good control in our experiments. Changes observed for cNTnC•$cTnI_{1-29}$ and cNTnC•Ca^{2+}•$cTnI_{1-29}$ were similar, demonstrating the similarity between formed complexes, however, since the behavior of apo cNTnC as a function of ionic strength is more complex, the data related to cNTnC•$cTnI_{1-29}$ should be treated with caution.

Conclusions

Varying ionic strength is a common method to probe electrostatic interactions within the complexes. However, protein folding may also be dependent to a some degree on particular ionic conditions. Based on our data, the structure of cNTnC•Ca^{2+} was largely unaffected by the differences in ionic strength (up to ~400 mM), and thus, the changes observed with cNTnC•Ca^{2+}•$cTnI_{1-29}$ can be directly attributed to the changes in interactions between cNTnC•Ca^{2+} and $cTnI_{1-29}$. For cNTnC•Ca^{2+}•$cTnI_{1-29}$ we have observed a decrease in T_2 values at low salt, and an increase in T_2 at high salt. At high ionic strength T_2 for the complex is almost equal to T_2 for cNTnC•Ca^{2+}, suggesting that the complex is not formed under these conditions and providing the evidence for the hypothesis that electrostatic interactions play a major role in the interaction between cNTnC•Ca^{2+} and $cTnI_{1-29}$.

In case of apo cNTnC, the dependence of average T_2 and chemical shifts on ionic strength for cNTnC•$cTnI_{1-29}$ shows generally similar trends to cNTnC•Ca^{2+}•$cTnI_{1-29}$; however, these results should be treated with care since the per residue T_2 for apo cNTnC demonstrated a dependence on ionic strength in the absence of $cTnI_{1-29}$.

The binding of $cTnI_{1-29}$ to cNTnC is of substantial interest due to its involvement in the regulation of cardiac contraction and the development of cardiac malfunctions. The data presented here provides experimental support for the electrostatic nature of the interaction between $cTnI_{1-29}$ and cNTnC•Ca^{2+}.

Materials and Methods

Protein Expression and Purification

The DNA encoding cNTnC (1-89) with the mutations C35S and C84S was used in pET-3a expression vector. *E. coli* strain BL21(DE3)pLysS was transformed and incubated at 37°C to the OD_{600} of 0.6-0.9. Cell cultures were induced with IPTG and harvested after incubation for 3 hours. Uniformly ^{15}N-labeled cNTnC was expressed in a

minimal media enriched with $(^{15}NH_4)_2SO_4$ (*27*). Cell pellet was lysed using French press and applied to a DEAE-sephadex (A25) column (50 mM Tris, 0.1 M NaCl, pH 8.0). Protein wa further purified using a Superdex-75 size exclusion column (50 mM Tris, 0.15 M NaCl, pH 8.0), decalcified, and desalted using Sephadex G25 column (10 mM NH_4HCO_3), decalcified as described previously (*28*), and lyophilized. Molecular mass for the unlabeled protein was confirmed with mass spectrometry.

Peptides

Synthetic peptide, $cTnI_{1-29}$ (acetyl-ADGSSDAAREPRPAPAPIRRRSSNYRAYA -amide), was synthesized using standard methodology (*29*). The sequence was confirmed by amino acid analysis and the masses were verified by electrospray mass spectrometry.

NMR spectroscopy

NMR samples were prepared in 500 µl of NMR buffer containing 10 mM imidazole, 5 mM NaN_3, and 0.2 mM DSS in 90% H_2O/10% D_2O. In case of cNTnC•Ca^{2+}, 1 ml of 1M $CaCl_2$ was added. Concentration of cNTnC in all experiments was ~0.6 mM and the concentration of $cTnI_{1-29}$ was ~1.8 mM. The increase in ionic strength was achieved by adding solid KCl. Whenever needed, pH was adjusted to 6.75. At every salt concentration the following experiments were acquired: ^1H 1D, 2D {^1H, ^{15}N} HSQC, and the T_2 series using relaxation delays of 10, 30, 50, 70, 90, and 110 ms. NMR experiments were conducted at 30 °C on a Varian Inova 500 MHz spectrometer equipped with a z-axis pulsed field gradient triple resonance probe. Acquired spectra were processed using NMRPipe (*30*) and visualized using NMRView (*31*). Per residue relaxation parameters, T_2, were extracted using the rate analysis module built in NMRView and presented along with the T_2 averaged over a dataset. Per residue chemical shift changes, $\Delta\delta$, were obtained using the following equation: $\Delta\delta = \sqrt{(0.2\Delta\delta_{5N})^2 + (\Delta\delta_H)^2}$, where $\Delta\delta_{5N}$ is the chemical shift change in ppm in ^{15}N dimension and $\Delta\delta_H$ is the chemical shift change in ppm in ^1H dimension. The coefficient of 0.2 accounts for the difference between sensitivities of ^{15}N and ^1H nuclei. Easily traceable changes in chemical shifts for several residues were analyzed and presented as an averaged value.

Figure IV-1. Average T_2 values for apo cNTnC (open black circles), cNTnC•Ca^{2+} (open red squares), cNTnC•$cTnI_{1-29}$ (closed black circles), and cNTnC•Ca^{2+}•$cTnI_{1-29}$ (closed red squares).

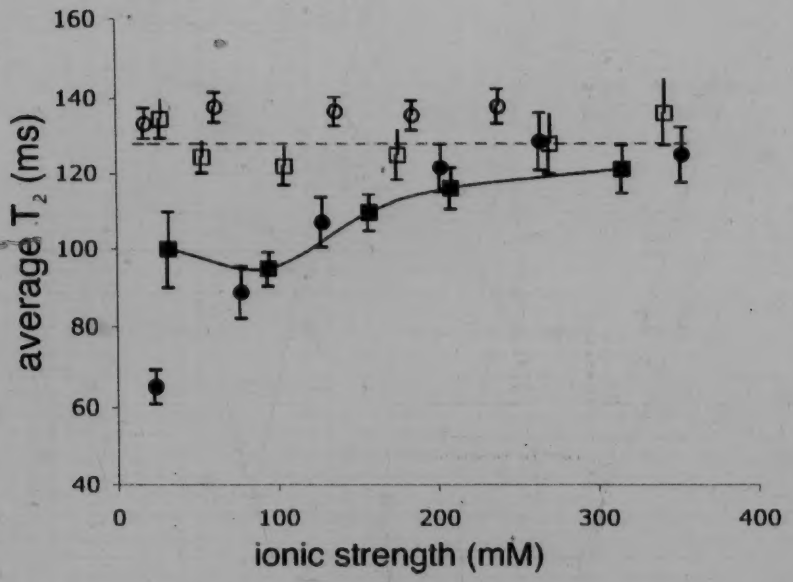

Figure IV-2. Dependence of per residue T_2's on ionic strength. Data is shown for several residues to demonstrate the range of T_2 values for cNTnC•Ca^{2+} (a), cNTnC•Ca^{2+}•$cTnI_{1-29}$ (b), apo cNTnC (c), and cNTnC•$cTnI_{1-29}$ (d). Notice the spread in individual T_2's for apo cNTnC in low salt (c).

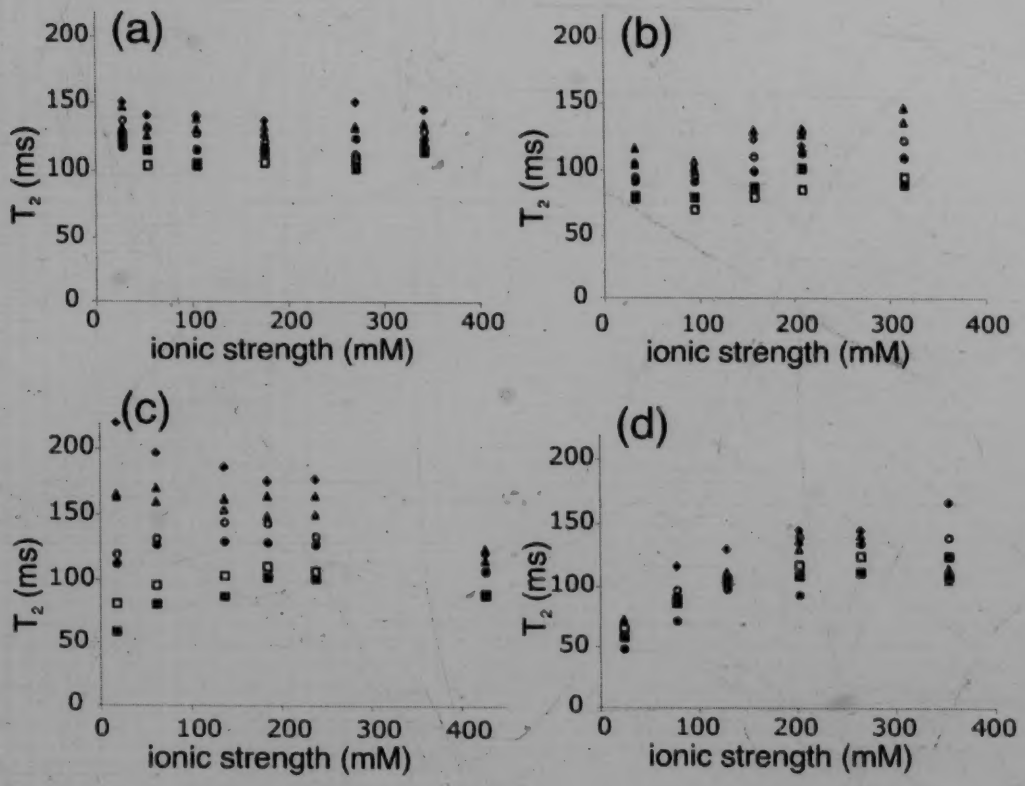

Figure IV-3. Overlays of 2D {^{1}H, ^{15}N} HSQC NMR spectra obtained for apo cNTnC (a), cNTnC•Ca^{2+}(b), cNTnC•$cTnI_{1-29}$ (c), and cNTnC•Ca^{2+}•$cTnI_{1-29}$ (d) as a function of ionic strength. Assignments are taken from (*32*).

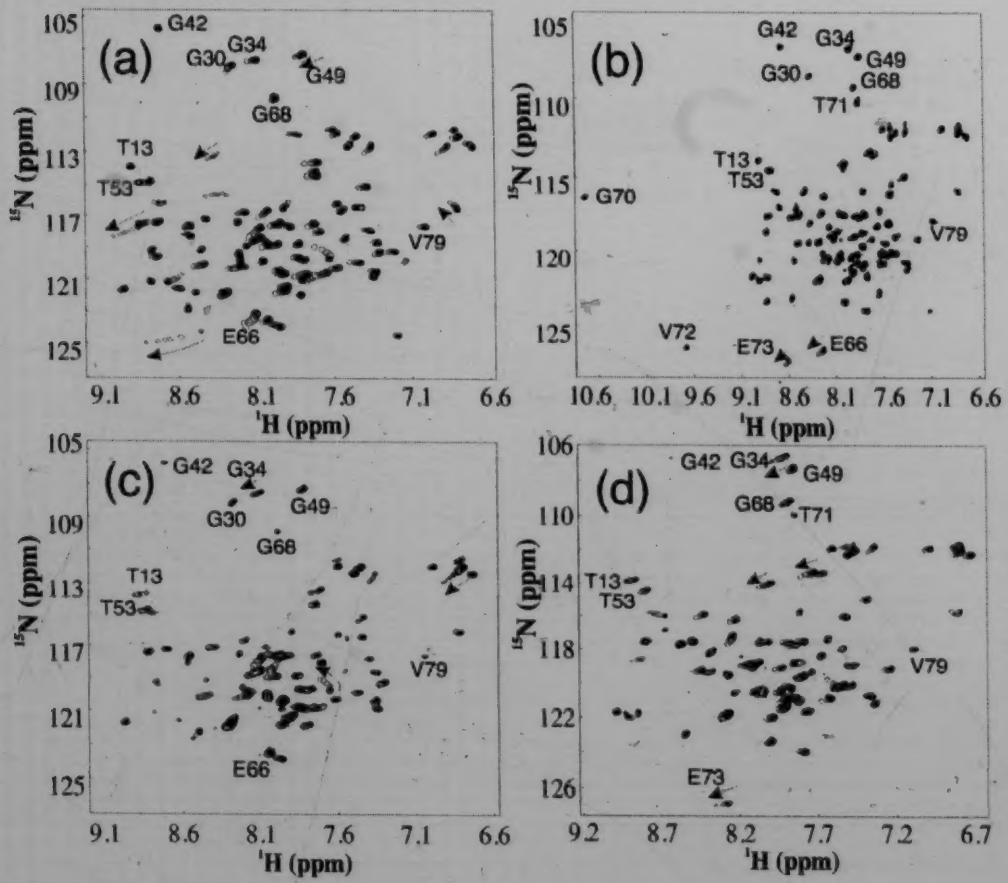

Figure IV-4. Chemical shift difference as a function of ionic strength for several easily traceable residues for apo cNTnC (open circles), cNTnC•Ca^{2+} (open squares), cNTnC•$cTnI_{1-29}$ (closed circles), and cNTnC•Ca^{2+}•$cTnI_{1-29}$ (closed squares).

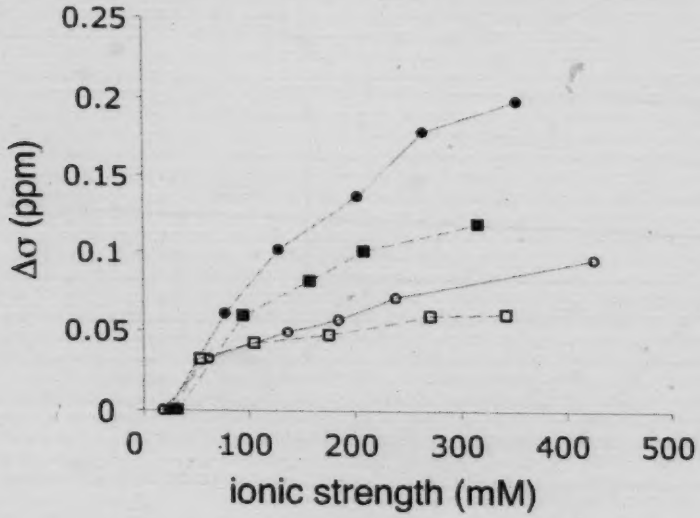

References

(1) Finley, N., Abbott, M. B., Abusamhadneh, E., Gaponenko, V., Dong, W., Gasmi-Seabrook, G., Howarth, J. W., Rance, M., Solaro, R. J., Cheung, H. C., and Rosevear, P. R. (1999) NMR analysis of cardiac troponin C-troponin I complexes: effects of phosphorylation. *FEBS Lett 453*, 107-12.

(2) Abbott, M. B., Dong, W. J., Dvoretsky, A., DaGue, B., Caprioli, R. M., Cheung, H. C., and Rosevear, P. R. (2001) Modulation of cardiac troponin C-cardiac troponin I regulatory interactions by the amino-terminus of cardiac troponin I. *Biochemistry 40*, 5992-6001.

(3) Ward, D. G., Cornes, M. P., and Trayer, I. P. (2002) Structural consequences of cardiac troponin I phosphorylation. *J Biol Chem 277*, 41795-801.

(4) Ward, D. G., Brewer, S. M., Cornes, M. P., and Trayer, I. P. (2003) A cross-linking study of the N-terminal extension of human cardiac troponin I. *Biochemistry 42*, 10324-32.

(5) Baryshnikova, O. K., Li, M. X., and Sykes, B. D. (2008) Modulation of cardiac troponin C function by the cardiac-specific N-terminus of troponin I: influence of PKA phosphorylation and involvement in cardiomyopathies. *J Mol Biol 375*, 735-51.

(6) Takeda, S., Yamashita, A., Maeda, K., and Maeda, Y. (2003) Structure of the core domain of human cardiac troponin in the Ca(2+)-saturated form. *Nature 424*, 35-41.

(7) Ward, D. G., Brewer, S. M., Gallon, C. E., Gao, Y., Levine, B. A., and Trayer, I. P. (2004) NMR and mutagenesis studies on the phosphorylation region of human cardiac troponin I. *Biochemistry 43*, 5772-81.

(8) Robertson, S. P., Johnson, J. D., Holroyde, M. J., Kranias, E. G., Potter, J. D., and Solaro, R. J. (1982) The effect of troponin I phosphorylation on the Ca2+-binding properties of the Ca2+-regulatory site of bovine cardiac troponin. *J Biol Chem 257*, 260-3.

(9) Holroyde, M. J., Howe, E., and Solaro, R. J. (1979) Modification of Calcium requirements for activation of cardiac myofibrillar ATPase by cyclic AMP dependent phosphorylation. *Biochim Biophys Acta 586*, 63-69.

(10) Chandra, M., Dong, W. J., Pan, B. S., Cheung, H. C., and Solaro, R. J. (1997) Effects of protein kinase A phosphorylation on signaling between cardiac troponin I and the N-terminal domain of cardiac troponin C. *Biochemistry 36*, 13305-11.

(11) Schmidtmann, A., Lindow, C., Villard, S., Heuser, A., Mugge, A., Gessner, R., Granier, C., and Jaquet, K. (2005) Cardiac troponin C-L29Q, related to hypertrophic cardiomyopathy, hinders the transduction of the protein kinase A dependent phosphorylation signal from cardiac troponin I to C. *Febs J 272*, 6087-97.

(12) Dong, W. J., Xing, J., Ouyang, Y., An, J., and Cheung, H. C. (2008) Structural kinetics of cardiac troponin C mutants linked to familial hypertrophic and dilated cardiomyopathy in troponin complexes. *J Biol Chem 283*, 3424-32.

(13) Biesiadecki, B. J., Kobayashi, T., Walker, J. S., John Solaro, R., and de Tombe, P. P. (2007) The Troponin C G159D Mutation Blunts Myofilament Desensitization Induced by Troponin I Ser23/24 Phosphorylation. *Circ Res 100*, 1486-1493.

(14) Dyson, H. J., and Wright, P. E. (2005) Intrinsically unstructured proteins and their functions. *Nat Rev Mol Cell Biol 6*, 197-208.

(15) Fink, A. L. (2005) Natively unfolded proteins. *Curr Opin Struct Biol 15*, 35-41.

(16) Lindhout, D. A., Boyko, R. F., Corson, D. C., Li, M. X., and Sykes, B. D. (2005) The role of electrostatics in the interaction of the inhibitory region of troponin I with troponin C. *Biochemistry 44*, 14750-9.

(17) Gaponenko, V., Abusamhadneh, E., Abbott, M. B., Finley, N., Gasmi-Seabrook, G., Solaro, R. J., Rance, M., and Rosevear, P. R. (1999) Effects of troponin I phosphorylation on conformational exchange in the regulatory domain of cardiac troponin C. *J Biol Chem 274*, 16681-4.

(18) Keane, N. E., Quirk, P. G., Gao, Y., Patchell, V. B., Perry, S. V., and Levine, B. A. (1997) The ordered phosphorylation of cardiac troponin I by the cAMP-dependent protein kinase--structural consequences and functional implications. *Eur J Biochem 248*, 329-37.

(19) Debye, P., and Huckel, E. (1923) The theory of electolytes. I. Lowering of freezing point and related phenomena. *Physikalische Zeitschrift 24*, 185-206.

(20) Suh, J. Y., Tang, C., and Clore, G. M. (2007) Role of electrostatic interactions in transient encounter complexes in protein-protein association investigated by paramagnetic relaxation enhancement. *J Am Chem Soc 129*, 12954-5.

(21) Davis, S. J., Davies, E. A., Tucknott, M. G., Jones, E. Y., and van der Merwe, P. A. (1998) The role of charged residues mediating low affinity protein-protein recognition at the cell surface by CD2. *Proc Natl Acad Sci U S A 95*, 5490-4.

(22) Dill, K. A. (1990) Dominant forces in protein folding. *Biochemistry 29*, 7133-55.

(23) Stigter, D., Alonso, D. O., and Dill, K. A. (1991) Protein stability: electrostatics and compact denatured states. *Proc Natl Acad Sci U S A 88*, 4176-80.

(24) Palmer, A. G., 3rd. (2004) NMR characterization of the dynamics of biomacromolecules. *Chem Rev 104*, 3623-40.

(25) Palmer, A. G., 3rd. (1997) Probing molecular motion by NMR. *Curr Opin Struct Biol 7*, 732-7.

(26) Blumenschein, T. M., Stone, D. B., Fletterick, R. J., Mendelson, R. A., and Sykes, B. D. (2005) Calcium-dependent changes in the flexibility of the regulatory domain of troponin C in the troponin complex. *J Biol Chem 280*, 21924-32.

(27) Li, M. X., Corson, D. C., and Sykes, B. D. (2002) Structure determination by NMR. Isotope labeling. *Methods Mol Biol 173*, 255-65.

(28) Li, M. X., Gagne, S. M., Tsuda, S., Kay, C. M., Smillie, L. B., and Sykes, B. D. (1995) Calcium binding to the regulatory N-domain of skeletal muscle troponin C occurs in a stepwise manner. *Biochemistry 34*, 8330-40.

(29) Tripet, B., Van Eyk, J. E., and Hodges, R. S. (1997) Mapping of a second actin-tropomyosin and a second troponin C binding site within the C terminus of troponin I, and their importance in the Ca2+-dependent regulation of muscle contraction. *J Mol Biol 271*, 728-50.

(30) Delaglio, F., Grzesiek, S., Vuister, G. W., Zhu, G., Pfeifer, J., and Bax, A. (1995) NMRPipe: a multidimensional spectral processing system based on UNIX pipes. *J Biomol NMR 6*, 277-93.

(31) Johnson, B. A., and Blevins, R. A. (1994) NMRView: A computer program for the visualization and analysis of NMR data. *J Biomol NMR 4*, 603-614.

(32) Li, M. X., Spyracopoulos, L., and Sykes, B. D. (1999) Binding of cardiac troponin-I147-163 induces a structural opening in human cardiac troponin-C. *Biochemistry 38*, 8289-98.

CHAPTER V

Towards the determination of the pKa's of side chain carboxyl groups involved in electrostatic interactions on the interface between cNTnC and the N-terminus of cTnI

Outline

Side chain pKa's for residues forming an interface with a ligand are often shifted from their typical values in solution. This information can be used to delineate residues participating in the interface, and to understand the interactions that stabilize the protein complex. We attempted to determine the pKa's of side chain carboxyl groups of cNTnC using a 2D HBHG(CBCG)CO NMR pulse sequence, which we developed on the basis of 3D $^{13}C'$–(^{13}C)–^{1}H HSQC/HSQC (*1*). Although the pulse sequence was successful, the pH titrations of cNTnC had to be discontinued due to the precipitation of cNTnC below pH ~5. The approach should be useful, however, for other studies.

Introduction

One approach to probe electrostatic interactions in a complex involves the determination of side chain pKa's for residues suspected to participate in the formation of the interface. It is known that catalytically important residues (*2-7*), as well as residues that determine protein folding (*8-10*), often have side chain pKa's different from those of the individual amino acids in solution. Residues forming interfaces were shown to have different pKa's in the absence and presence of a binding partner (*11*). The electrostatic nature of the interaction between the N-terminus of cTnI ($cTnI_{1-29}$) and cNTnC was investigated in Chapter IV. Possible contacts between $cTnI_{1-29}$ and cNTnC can exist between Arg^{19}, Arg^{20}, and Arg^{21} of $cTnI_{1-29}$ and Glu^{32}, Glu^{40}, Glu^{55}, Glu^{63}, Glu^{66}, Asp^{33}, Asp^{62}, and Asp^{75} of cNTnC. Determination of pKa's of side chain carboxyl groups in cNTnC should provide direct evidence for their involvement in the formation of the interface with $cTnI_{1-29}$. Similarly, the identification of ionization constants for guanidinium groups in arginines of $cTnI_{1-29}$ might provide the evidence for their participation in the formation of the interface with cNTnC.

A common and straightforward method for the determination of side chain pKa's involves the pH titration of a protein monitored by the solution state NMR spectroscopy. In one of the earliest applications of biomacromolecular NMR spectroscopy, 1D ^{1}H NMR

experiments were employed to study the pKa's of histidines of ribonuclease (*2*). With the development of multidimensional multinuclear NMR methods and protein isotope labeling techniques, other experiments became available for determining the pKa of side chains carboxyl groups; for example, 2D {^{13}C, ^{1}H} H(C)CO TOCSY (*11*), 2D homonuclear TOCSY (*4, 9*), 1D ^{13}C (*12-14*), and $^{13}C'$–(^{13}C)–^{1}H HSQC/HSQC (*1, 3, 5*). New experiments are emerging for detecting arginine side chain resonances, such as the Arg-$H^{\varepsilon}(N^{\varepsilon}C^{\delta})H^{\delta}$, Arg-$H^{\varepsilon}(N^{\varepsilon}C^{\zeta})H^{\eta}$, and Arg-$H^{\eta}(N^{\eta}C^{\zeta})H^{\varepsilon}$ pulse sequences (*15, 16*). Lysine side chains have been recently studied using an HISQC pulse sequence (*17*).

We attempted to determine the pKa's of side chain carboxyl groups for cNTnC•Ca^{2+} using the HBHG(CBCG)CO pulse sequence, developed on the basis of 3D $^{13}C'$–(^{13}C)–^{1}H HSQC/HSQC (*1*). The modified and tested pulse sequence worked well. However, the lower limit of pH where cNTnC•Ca^{2+} remain a folded protein with the known structure was ~5, below which cNTnC•Ca^{2+} precipitated. Thus, the NMR method for identification of pKa's of side chain carboxyl groups was not suitable for studying cNTnC•Ca^{2+}. However, the HBHG(CBCG)CO pulse sequence, might find applications in further studies in Dr. Sykes' laboratory.

Results and Discussion

HBHG(CBCG)CO pulse sequence

To follow the side chain carboxyl groups of cNTnC, we have modified the 3D pulse sequence $^{13}C'$–(^{13}C)–^{1}H HSQC/HSQC from Yamazaki et al. (*1*) to create a 2D pulse sequence, referred herein as HBHG(CBCG)CO, in which H^{β}/C^{β} (or H^{γ}/C^{γ}) and carboxyl resonances (C′) are correlated. $^{13}C'$–(^{13}C)–^{1}H HSQC/HSQC was developed similarly to the HCACO pulse sequence, in which H^{α}, C^{α}, and C′ are correlated (*18*). At time point *a* (Fig. V-1), the single quantum coherence $C^{\beta}{}_{y}H^{\beta}{}_{z}$ (or $C^{\gamma}{}_{y}H^{\gamma}{}_{z}$) is generated as a result of INEPT. During evolution for a total time period of $1/2J_{C\beta C'}$, the C^{β} (C^{γ}) coherences evolve with the $C^{\beta}C'$ ($C^{\gamma}C'$) J-couplings active and the carbon chemical shifts inverted and refocused by the composite Shaka pulse (*19, 20*). The magnetization is thus transferred on the carboxyl carbon C′ (point *b*). C′ coherences are labeled with the chemical shift during evolution time t_1, while the chemical shifts for H and C^{β} are refocused (point *c*). After this, magnetization from C′ is transferred to C^{β} (C^{γ}) during the evolution under the active C^{β}-C′ (C^{γ}-C′) J-couplings, with chemical shifts inverted and refocused by the composite Shaka pulse (point *d*). Reversed INEPT is used to transfer the magnetization from C^{β} (C^{γ}) to the observable magnetization on H^{β} (H^{ε}), point *e*, followed

by the acquisition of FID. Pulse sequence was coded and complied for VnmrJ, with its code presented in Appendix A. HBHG(CBCG)CO was tested on the previously assigned complex of cCTnC with EMD57033 (*21*). The carboxyl ^{13}C NMR chemical shifts were in agreement with those previously assigned (data not shown).

pH titration of cNTnC•Ca^{2+} monitored by HBHG(CBCG)CO spectroscopy

The lower pH limit for these experiments was determined by the precipitation of cNTnC•Ca^{2+}, which became pronounced at pH ~5. Ionization constants for glutamates and aspartates are typically found in the range of pKa ≈ 2–5. The majority of cross peaks correlating the H^{β} (H^{γ}) resonance on the x-axis and the carboxyl ^{13}C resonance on the y-axis did not shift significantly within the pH range used (Fig. V-2). Interestingly, a few cross peaks changed their chemical shifts starting from pH ~7–8. These residues are glutamates (left panel) and aspartates (right panel) with pKa's higher than typical, which might suggest their biological significance. However, protein precipitation precluded further pH titrations, and pKa's were not determined.

pH titration of cNTnC•Ca^{2+} monitored by {^{1}H, ^{15}N} NMR spectroscopy

2D {^{1}H, ^{15}N} HSQC NMR spectroscopy provides a useful insight on protein integrity due to the unique sensitivity of backbone amide chemical shifts. In acidic and basic conditions the exchange of labile amide protons is often facilitated, which renders the observation of labile protons difficult (*22*). The general trend of pH dependences (Fig. V-3) supported the previous assignment and correlates with the known secondary structure of the protein (*23*). Residues involved in hydrogen bonding interactions, such as elements of α-helices, are protected against ^{1}H exchange the most; for example, Leu^{12}, Ile^{26}, Met^{47} Glu^{56}, and Phe^{77} (Figs. V-3a and V-3b), whose intensities have not significantly decreased up to pH ~9. Residues belonging to the loops, for example, Glu^{32}, Gln^{50}, and Gly^{68}, disappeared from the 2D {^{1}H, ^{15}N} HSQC spectra earlier in titrations (Fig. V-3c). At high pH, the chemical shifts for remaining observable amides remained the same (data not shown), which indicates that the overall structure of cNTnC•Ca^{2+} remained unchanged up to ~ pH 9.5. In spite of the fact that many amides were not observable (50% cross-peaks were missing at pH 9.8), ^{13}C and ^{1}H NMR of side chain atoms can be still used to explore the behavior of cNTnC•Ca^{2+} at these pH conditions. At pH ~5 and lower, cNTnC•Ca^{2+} underwent conformational changes, as demonstrated by

the shifting of some cross-peaks and appearance of new cross-peaks in 2D {^{1}H, ^{15}N} HSQC spectra (data not shown).

Conclusions

Typically, studies of troponin C has been carried out within the physiological range of pH from ~6.7 to ~7 (*23-26*). In experiments aiming to determine the pKa of side chain carboxyl groups and their role in electrostatic interactions, the limits of pH in which cNTnC•Ca^{2+} is studied have to be expanded. As it was determined here, the range of pH within which cNTnC•Ca^{2+} exists as a folded protein with the known structure was limited by pH ~5, thus making the chosen method for determination of pKa's unsuitable. The modified and tested pulse sequence HBHG(CBCG)CO might find its application in the studies of different protein complexes.

Materials and Methods

Titrations were performed on the sample containing 0.6 mM of ^{15}N labeled cNTnC, in a buffer consisted of 100 mM KCl, 5% of D_2O, and 0.2 mM DSS and 2 mM of each, formate, imidazole, tris, and piperazine, that were used as internal pH indicators. The protein, cNTnC•Ca^{2+}, was expressed and purified as it is described earlier (*27*). Aliquots of 1N NaOH or HCl were added in order to adjust the pH of a sample. 1D ^{1}H, 2D {^{1}H, ^{15}N} HSQC NMR and 2D HBHG(CBCG)CO spectra were acquired at 30 ^{0}C on a Varian Unity 600 MHz spectrometer. ^{1}H chemical shifts in 1D ^{1}H NMR spectra corresponding to pH indicators (formate, tris, imidazole and piperazine (Appendix B)) were used to determine pH.

Figure V-1. Pulse scheme for the experiment employed to correlate the C^{β}/H^{β} (or C^{γ}/H^{γ}) and carboxyl carbon coherences (C´). Narrow and wide pulses correspond to 90^0 and 180^0 flip angles. Phases are as indicated. The carrier is set to 35 ppm for the C^{β} (or C^{γ}) pulses and to 180 ppm for the carboxyl pulses. Phase cycling is the following: Φ_1=(x, -x), Φ_2=(2x, 2(-x)), Φ_3=Φ_4=(4x, 4(-x)), Ψ_1=(x,y), Ψ_1=(x,-y).

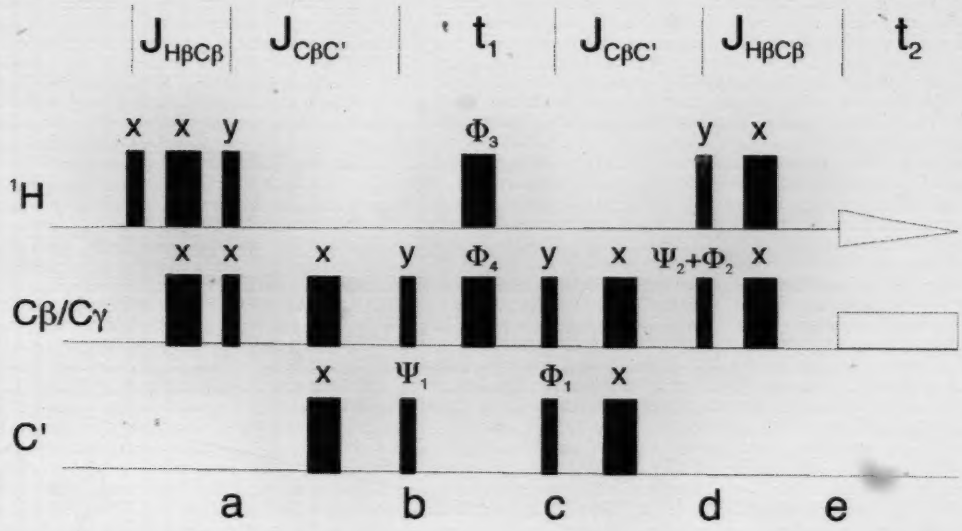

Figure V-2. Expanded regions of the 2D HBHG(CBCG)CO NMR spectra of cNTnC•Ca^{2+} obtained at different pH values. Cross peaks that demonstrate little or no movement are shown inside the boxes, cross peaks that undergo some movement are shown inside the ovals. First signs of possible precipitation were observed at pH of 5.68. The assignment of some side chain carboxyl groups is indicated.

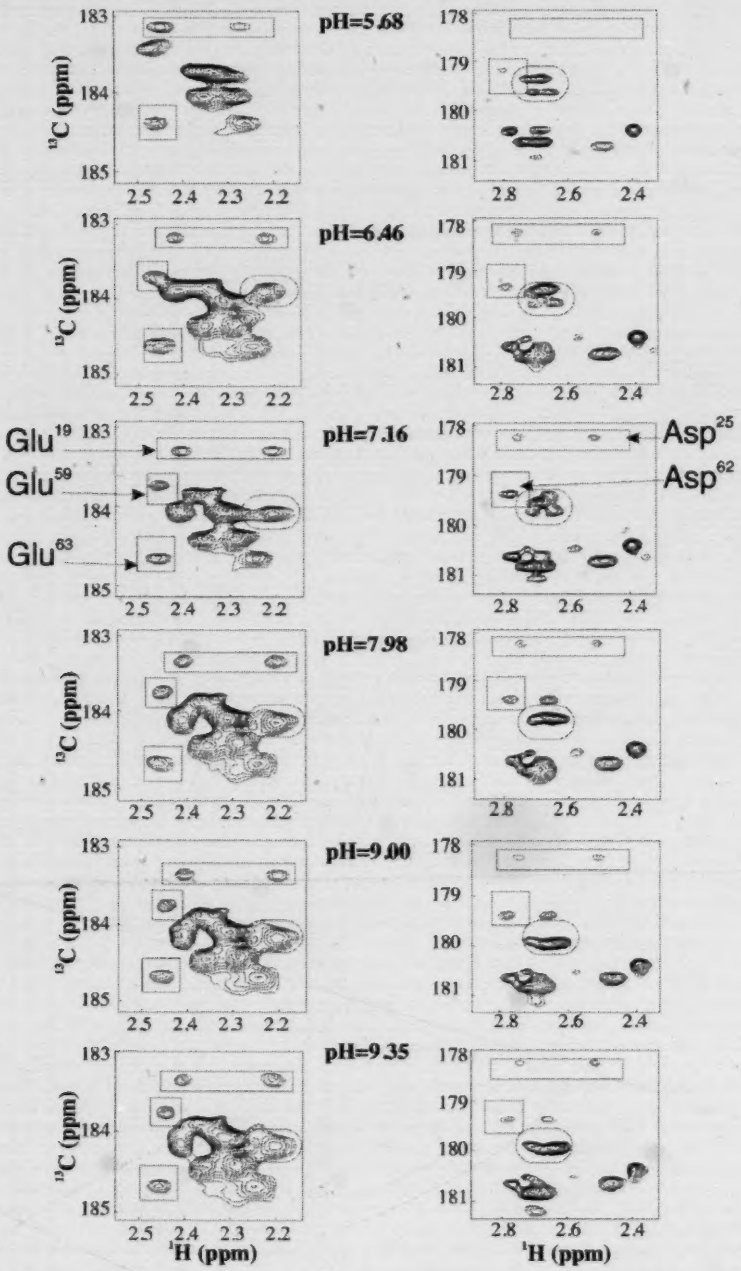

Figure V-3. The pH dependence of backbone amide cross peak intensities for residues Leu^{12} (open square), Ile^{26} (closed circle), and Met^{47} (open circle) located on the helices N, A, and B respectively (a); for residues Glu^{56} (open triangle) and Phe^{77} (closed diamond) located on the helices C and D respectively (b), and for residues Glu^{32} (closed circle), Gln^{50} (open triangle), and Gly^{68} (open circle) located on the loops, including the Ca^{2+} binding loop for residue Gly^{68} (c). Solid and dashed lines represent the fits of the data using equations from (*28*). Resonances were assigned previously (*23*).

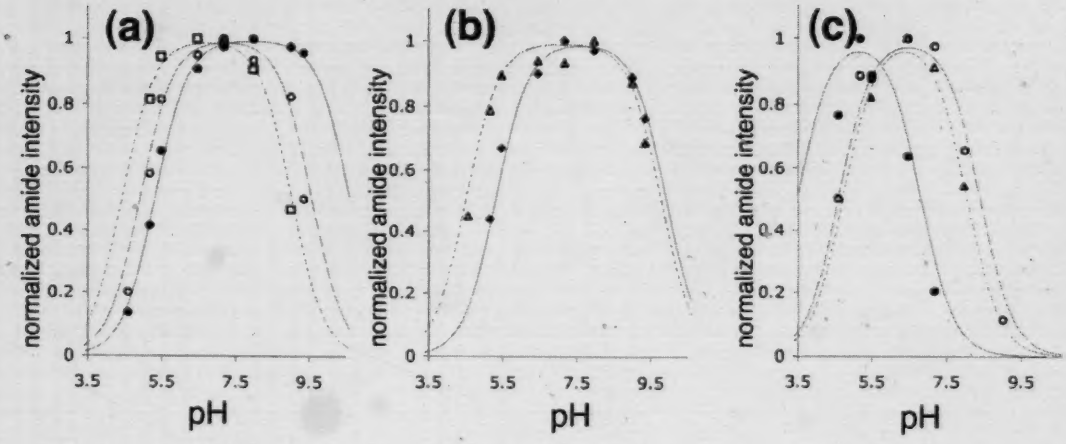

References

(1) Yamazaki, T., Yoshida, M., and Nagayama, K. (1993) Complete assignments of magnetic resonances of ribonuclease H from Escherichia coli by double- and triple-resonance 2D and 3D NMR spectroscopies. *Biochemistry 32*, 5656-69.

(2) Bradbury, J. H., and Scheraga, H. A. (1966) Structural studies of ribonuclease. XXIV. The application of Nuclear Magnetic Resonanse spectroscopy to distinguish between the histidine residues of ribonuclease. *J Am Chem Soc 88*, 4240.

(3) Jeng, M. F., and Dyson, H. J. (1996) Direct measurement of the aspartic acid 26 pKa for reduced Escherichia coli thioredoxin by 13C NMR. *Biochemistry 35*, 1-6.

(4) Perez-Canadillas, J. M., Campos-Olivas, R., Lacadena, J., Martinez del Pozo, A., Gavilanes, J. G., Santoro, J., Rico, M., and Bruix, M. (1998) Characterization of pKa values and titration shifts in the cytotoxic ribonuclease alpha-sarcin by NMR. Relationship between electrostatic interactions, structure, and catalytic function. *Biochemistry 37*, 15865-76.

(5) Oda, Y., Yamazaki, T., Nagayama, K., Kanaya, S., Kuroda, Y., and Nakamura, H. (1994) Individual ionization constants of all the carboxyl groups in ribonuclease HI from Escherichia coli determined by NMR. *Biochemistry 33*, 5275-84.

(6) Forman-Kay, J. D., Clore, G. M., and Gronenborn, A. M. (1992) Relationship between electrostatics and redox function in human thioredoxin: characterization of pH titration shifts using two-dimensional homo- and heteronuclear NMR. *Biochemistry 31*, 3442-52.

(7) Joshi, M. D., Hedberg, A., and McIntosh, L. P. (1997) Complete measurement of the pKa values of the carboxyl and imidazole groups in Bacillus circulans xylanase. *Protein Sci 6*, 2667-70.

(8) Kohda, D., Sawada, T., and Inagaki, F. (1991) Characterization of pH titration shifts for all the nonlabile proton resonances a protein by two-dimensional NMR: the case of mouse epidermal growth factor. *Biochemistry 30*, 4896-900.

(9) Kuhlman, B., Luisi, D. L., Young, P., and Raleigh, D. P. (1999) pKa values and the pH dependent stability of the N-terminal domain of L9 as probes of electrostatic interactions in the denatured state. Differentiation between local and nonlocal interactions. *Biochemistry 38*, 4896-903.

(10) Khare, D., Alexander, P., Antosiewicz, J., Bryan, P., Gilson, M., and Orban, J. (1997) pKa measurements from nuclear magnetic resonance for the B1 and B2 immunoglobulin G-binding domains of protein G: comparison with calculated values for nuclear magnetic resonance and X-ray structures. *Biochemistry 36*, 3580-9.

(11) Chen, H. A., Pfuhl, M., McAlister, M. S., and Driscoll, P. C. (2000) Determination of pK(a) values of carboxyl groups in the N-terminal domain of rat CD2: anomalous pK(a) of a glutamate on the ligand-binding surface. *Biochemistry 39*, 6814-24.

(12) McIntosh, L. P., Hand, G., Johnson, P. E., Joshi, M. D., Korner, M., Plesniak, L. A., Ziser, L., Wakarchuk, W. W., and Withers, S. G. (1996) The pKa of the general acid/base carboxyl group of a glycosidase cycles during catalysis: a 13C-NMR study of bacillus circulans xylanase. *Biochemistry 35*, 9958-66.

(13) Pascal, S. M., Singer, A. U., Yamazaki, T., Kay, L. E., and Forman-Kay, J. D. (1995) Structural and dynamic characterization of an SH2 domain-phosphopeptide complex by NMR approaches. *Biochem Soc Trans 23*, 729-33.

(14) Joshi, M. D., Sidhu, G., Nielsen, J. E., Brayer, G. D., Withers, S. G., and McIntosh, L. P. (2001) Dissecting the electrostatic interactions and pH-dependent activity of a family 11 glycosidase. *Biochemistry 40*, 10115-39.

(15) Pascal, S. M., Yamazaki, T., Singer, A. U., Kay, L. E., and Forman-Kay, J. D. (1995) Structural and dynamic characterization of the phosphotyrosine binding region of a Src homology 2 domain--phosphopeptide complex by NMR relaxation, proton exchange, and chemical shift approaches. *Biochemistry 34*, 11353-62.

(16) Yamazaki, T., Pascal, S. M., Singer, A. U., Forman-Kay, J. D., and Kay, L. E. (1995) NMR Pulse Schemes for the Sequence-Specific Assignement of Arginine Guanidino 15N and 1H Chemical Shifts in Proteins. *J Am Chem Soc 117*, 3556-3564.

(17) Iwahara, J., Jung, Y. S., and Clore, G. M. (2007) Heteronuclear NMR spectroscopy for lysine NH(3) groups in proteins: unique effect of water exchange on (15)N transverse relaxation. *J Am Chem Soc 129*, 2971-80.

(18) Grzesiek, S., and Bax, A. (1993) The origin and removal of artifacts in 3D HCACO spectra of proteins uniformly enriched with 13C. *J Mag Res B 102*, 103-106.

(19) Shaka, A. J. (1985) Composite pulses for ultra-broadband spin inversion. *Chem Phys Lett 120*, 201-205.

(20) Mohebbi, A., and Shaka, A. J. (1991) Improvements in carbon-13 broadband homonuclear cross-polarization for 2D and 3D NMR. *Chem Phys Lett 178*, 374-378.

(21) Wang, X., Li, M. X., Spyracopoulos, L., Beier, N., Chandra, M., Solaro, R. J., and Sykes, B. D. (2001) Structure of the C-domain of human cardiac troponin C in complex with the Ca2+ sensitizing drug EMD 57033. *J Biol Chem 276*, 25456-66.

(22) Wuthrich, K. (1986) *NMR of Proteins and Nucleic Acids*, John Wiley & Sons, New York.

(23) Sia, S. K., Li, M. X., Spyracopoulos, L., Gagne, S. M., Liu, W., Putkey, J. A., and Sykes, B. D. (1997) Structure of cardiac muscle troponin C unexpectedly reveals a closed regulatory domain. *J Biol Chem 272*, 18216-21.

(24) Li, M. X., Spyracopoulos, L., and Sykes, B. D. (1999) Binding of cardiac troponin-I147-163 induces a structural opening in human cardiac troponin-C. *Biochemistry 38*, 8289-98.

(25) Lindhout, D. A., and Sykes, B. D. (2003) Structure and dynamics of the C-domain of human cardiac troponin C in complex with the inhibitory region of human cardiac troponin I. *J Biol Chem 278*, 27024-34.

(26) Gagne, S. M., Tsuda, S., Li, M. X., Smillie, L. B., and Sykes, B. D. (1995) Structures of the troponin C regulatory domains in the apo and calcium-saturated states. *Nat Struct Biol 2*, 784-9.

(27) Li, M. X., Corson, D. C., and Sykes, B. D. (2002) Structure determination by NMR. Isotope labeling. *Methods Mol Biol 173*, 255-65.

(28) O'Neil, J. D., and Sykes, B. D. (1989) NMR studies of the influence of dodecyl sulfate on the amide hydrogen exchange kinetics of a micelle-solubilized hydrophobic tripeptide. *Biochemistry 28*, 699-707.

CHAPTER VI

Conclusions

The aim of this thesis was to provide an insight on the mechanism by which cardiomyopathy mutations in troponin C disrupt its normal function and may lead to the development of the disease. We have established, first, that the L29Q and E59D/D75Y mutants have unperturbed affinity to Ca^{2+}. Instead their affinity towards the switch region of cTnI ($cTnI_{147-163}$) has been significantly changed especially in the presence of the N-terminus of cTnI ($cTnI_{1-29}$). This points to the complex nature of the interactions on the biochemical scale where Ca^{+2} binding leads to the conformational changes in cTnC, which modulates and being modulated by the interactions with cTnI. Second, we have determined that the G159D mutation results in the weakened interaction with the anchoring region of cTnI ($cTnI_{34-71}$), which might lead to a weaker anchoring of cTn to the thin filament. Third, we have established the important role played by the N-terminus of cTnI ($cTnI_{1-29}$/$cTnI_{1-29}$PP) in modulating the binding of the switch region of cTnI ($cTnI_{147-163}$). Fourth, we have determined that the interaction between the N-terminus of cTnI and the N-domain of cTnC is Ca^{2+} independent and electrostatically driven.

Results pertaining to the modulation of the cNTnC binding to the switch region of cTnI can be summarized as the following (Fig. VI-1): the N-terminus of cTnI in unphosphorylated form is bound to cNTnC (Fig. VI-1a) which lessens the cNTnC affinity towards the switch region of cTnI. In original model, this interaction was not present. Upon PKA phosphorylation, the N-terminus of cTnI partially or completely dissociates from cNTnC, resulting in the increased affinity of cNTnC towards the switch region of cTnI (Fig. VI-1b). This would likely result in the increased muscle contractility induced by PKA phosphorylation as a response to β-adrenergic stimulation. Thus, as a result of PKA phosphorylation, the cNTnC affinity towards the switch region of cTnI is modulated, whereas the affinity towards Ca^{2+} remains unperturbed. These findings compliment the existing model proposed to explain the mechanism of PKA signaling in cTn (*1*, *2*).

Within the cTn complex, some of the interactions between cTnC and cTnI remain to be visualized at the molecular level. For example, the binding of cTnC to the N-terminus or the inhibitory region of cTnI, which occur within the poorly structured regions of cTnI, are not easily amenable to traditional structural techniques. A major advance in technology might be needed in order to visualize the complete interactions

between the contractile proteins in the Tn complex. Without understanding of the molecular details of these interactions, the picture of cardiac contractility, as well as the effect of mutations, will remain incomplete.

As it is becoming more evident, the dynamics and conformational flexibility of proteins or their domains play a major role in the functioning of biological molecules. In order for cNTnC to reach the N-terminus of cTnI, the N-domain of cTnC must be folded onto the C-domain of cTnC as was observed in the crystal structure of the cTn core (*3*). This 3D quaternary arrangement was not emphasized previously, and our data (Chapters II and IV) provide evidence for such an arrangement. However, in order to interact with other regions of cTnI, the central linker of cTnC might need to be straighter similar to sTnC (*4*). This suggests the possibility of the large conformational change for cTnC during the relaxation-contraction cycle (Fig. VI-2) and the need for the additional states in the overall model of Ca^{2+} regulated cardiac contraction. The attempt to visualize individual conformations along the relaxation-contraction cycle might increase the level of complexity of the Ca^{2+} regulated cardiac contraction mechanism, but might help explain special features of cardiac muscle such as the effect of mechanical activation (*5*).

The organization of contractile proteins within the sarcomere, although studied in much detail, is not yet completely understood. For example, the interaction of cTnT with tropomyosin is not well studied (*6*). The mechanism of stretch activation is just beginning to be understood (*5, 7*). The effects of PKA, PKC, PKG, and PKD phosphorylation on the molecular interactions within the contractile machinery remain in rudimentary stage (*8*). The understanding of the interplay between the expression patterns of particular cTnI and cTnT isoforms during the development (and in disease) and the molecular details of cardiac muscle contraction during the development will require much future effort (*9*). In addition, cardiomyocytes vary in appearance and function depending on their location in the heart (*10*), the molecular details of which the current model of cardiac contraction does not explain. In spite of tremendous amount of research in this field and many keyston[illegible]iscoveries, we still have a partially illuminated picture, with many pieces of the puzzle missing and poorly connected.

The mathematical reconstruction of the individual events of the relaxation-contraction cycle, from Ca^{2+} release by the sarcolemmal Ca^{2+} channel to the binding of cross-bridges, with the understanding of thermodynamics and kinetics of every individual steps, would allow us to answer many questions regarding the perturbed contractility in a quantitative manner. There is a large body of thermodynamic and kinetic data presented

in literature, which is often obtained with different techniques providing partially or completely incompatible results. Due to the differences in solution compositions, pH, ionic strength, viscosity, etc, thermodynamic and kinetic data obtained *in vitro* might be very different from the *in vivo* values. Such a mathematical model will also require the consideration of non-equilibrium conditions and appears to be a major endeavor, not easily feasible. Recent computational efforts used global parameters such as the Ca^{2+} sensitivity of the myofilament in order to simulate the effect of FHC mutations on the development of force (*11*), without considering the fine tuned machinery of the Ca^{2+} regulation.

Studies of individual cardiomyopathy mutations greatly promote the expansion of our knowledge pertaining to the Ca^{2+} regulated contraction. As it was demonstrated in Chapter II, the effects of L29Q and E59D/D75Y mutations needed to be considered in the context of the N-terminus of cTnI. However, there are following challenges in dissecting the effects of mutations on contractility. First, traditional methods have their limitations and associated errors, within which physiologically important differences might remain undetected. It is noteworthy, that human mutations with severe effects would be lethal, and only mild mutations or polymorphisms are expected. Second, the model of Ca^{2+} contraction is incomplete, and therefore the differences found in protein functions might not be important in the overall picture of contraction or compensated by other mechanisms. Third, the number of human mutations is increasingly large and is expected to increase even more, which indicates the need for technological advances, where these mutations can be studied in throughput manner, side-by-side, and with careful controls.

Understanding of human mutations is an exciting quest, which may help us to unravel the basis of individual differences in human pathology and physiology. With the knowledge of mutation effects and their interplay with the environment, we might approach in every individual case the understanding of the role of nature vs nurture. In future, it might be possible to predict and treat health issues, control dieting and exercising, deal with psychological problems, etc, in a genetically tailored manner. As a field of science, biochemistry might eventually exhaust the range of problems traditionally addressed by biochemists, but the biochemical approach should spread into other fields of science: medicine, nutrition, psychology, etc. Using biochemistry as a platform in other fields of sciences, human curiosity will find even more unanswered questions. This thesis is a part of the ongoing process undertaken by humankind aimed towards the understanding of ourselves and the world around us.

Figure VI-1. The model of Ca^{2+} regulated cardiac muscle contraction with the results of our work added. Two states of contractility are considered, with the first state in the absence of PKA phosphorylation (a), and the second in the presence of PKA phosphorylation (b). Phosphorylation is denoted as a yellow dot. Notice that in both states, the switch region of cTnI binds to cNTnC, however, with different affinities.

(a)

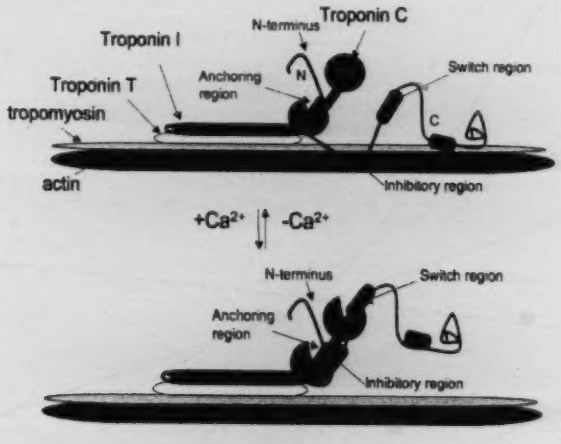

(b)

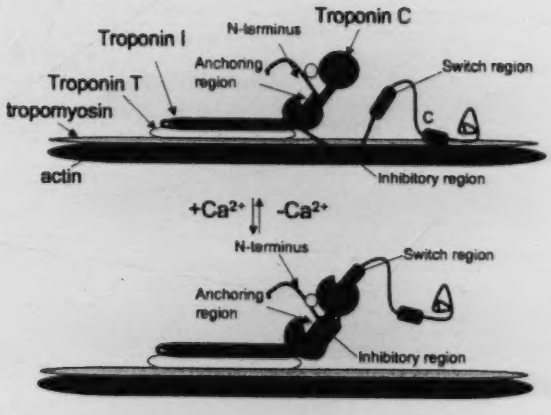

Figure VI-2. Possible conformational change of cTnC during the contraction-relaxing cycle. Crystallographic structures of sTn and cTn (*3*, *4*) are aligned over their cTnI subunits (grey). The C-domain of skeletal TnC (green) and cardiac TnC (red) are well overlapped, however the N-domains are oriented differently. The conformational change needed to bring cNTnC to overlap with sNTnC is shown with the arrow. In cardiac structure, the N-terminus of cTnI is positioned next to cNTnC, making possible the interaction with cNTnC (shown as a dashed line). If cNTnC moved similarly to sNTnC, such an interaction would be impossible.

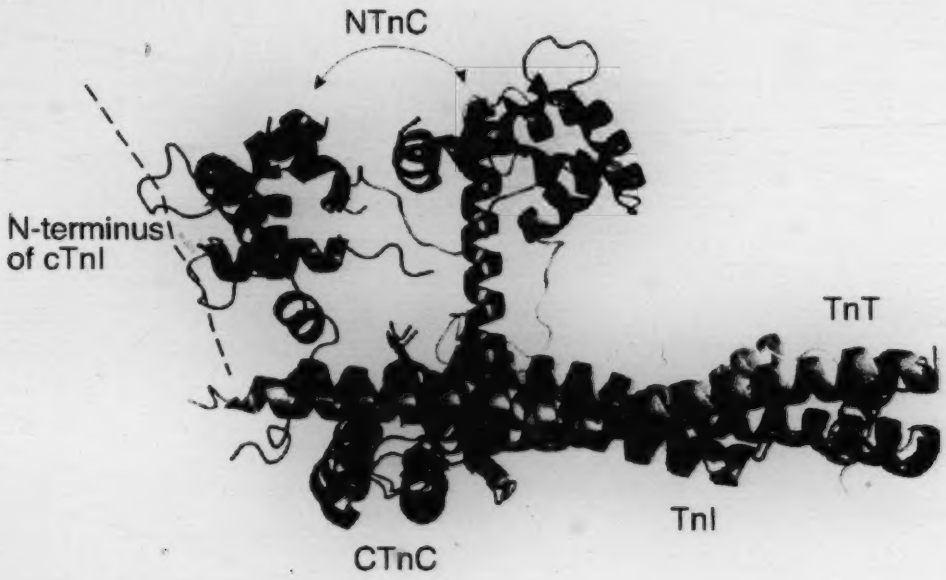

References

(1) Howarth, J. W., Meller, J., Solaro, R. J., Trewhella, J., and Rosevear, P. R. (2007) Phosphorylation-dependent conformational transition of the cardiac specific N-extension of troponin I in cardiac troponin. *J Mol Biol 373*, 706-22.

(2) Solaro, R. J., Rosevear, P., and Kobayashi, T. (2008) The unique functions of cardiac troponin I in the control of cardiac muscle contraction and relaxation. *Biochem Biophys Res Commun 369*, 82-7.

(3) Takeda, S., Yamashita, A., Maeda, K., and Maeda, Y. (2003) Structure of the core domain of human cardiac troponin in the Ca(2+)-saturated form. *Nature 424*, 35-41.

(4) Vinogradova, M. V., Stone, D. B., Malanina, G. G., Karatzaferi, C., Cooke, R., Mendelson, R. A., and Fletterick, R. J. (2005) Ca(2+)-regulated structural changes in troponin. *Proc Natl Acad Sci U S A 102*, 5038-43.

(5) De Nicola, G., Burkart, C., Qiu, F., Agianian, B., Labeit, S., Martin, S., Bullard, B., and Pastore, A. (2007) The structure of Lethocerus troponin C: insights into the mechanism of stretch activation in muscles. *Structure 15*, 813-24.

(6) Perry, S. V. (1998) Troponin T: genetics, properties and function. *J Muscle Res Cell Motil 19*, 575-602.

(7) Fukuda, N., and Granzier, H. L. (2005) Titin/connectin-based modulation of the Frank-Starling mechanism of the heart. *J Muscle Res Cell Motil 26*, 319-23.

(8) Metzger, J. M., and Westfall, M. V. (2004) Covalent and noncovalent modification of thin filament action: the essential role of troponin in cardiac muscle regulation. *Circ Res 94*, 146-58.

(9) Gomes, A. V., Venkatraman, G., Davis, J. P., Tikunova, S. B., Engel, P., Solaro, R. J., and Potter, J. D. (2004) Cardiac troponin T isoforms affect the Ca(2+) sensitivity of force development in the presence of slow skeletal troponin I: insights into the role of troponin T isoforms in the fetal heart. *J Biol Chem 279*, 49579-87.

(10) Bootman, M. D., Higazi, D. R., Coombes, S., and Roderick, H. L. (2006) Calcium signalling during excitation-contraction coupling in mammalian atrial myocytes. *J Cell Sci 119*, 3915-25.

(11) Kataoka, A., Hemmer, C., and Chase, P. B. (2007) Computational simulation of hypertrophic cardiomyopathy mutations in troponin I: influence of increased myofilament calcium sensitivity on isometric force, ATPase and |Ca2+|i. *J Biomech 40*, 2044-52.

APPENIDIX A

The code for the HBHG(CBCG)CO pulse sequence

```
/* gChsqc_Chsqc.c
Sequence for CB/CG CO HB/HG experiment for Asp and Glu
            F2  F1  F3  (Presently F1F3 2D experiment)
Modified from Yamazaki et al. Biochem 32 5656 (1994)
Original pulse sequence is called 3D Y-X-1H HSQC/HSQC

  set dof for F2 to  35.0 ppm (centered on CB/CG)
  F1 is set to 175.0 ppm (centered on CO)

 Set:   tauHC = 1/(4JHC)
        tauCC  = 1/(4 JCC)
        pwC90 for selective CB/CG or CO pulse depending upon dof
        pwC180 for selective SLP CB/CG 180 null at CO, decpwr same as pwC90 pulse
above

satmode = 'ynn' for presat
satdly = length of presaturation period
satpwr = power level for presat `*/

#include <standard.h>
#include "Pbox_bio.h"  /* Pbox Bio Pack Pulse Shaping Utilities */

shaka6(pwC90)
double pwC90;
{
   /* Shaka composite (10.9333*pwC90)   */
decrgpulse(pwC90*158.0/90.0, zero, 0.0, 0.0);
decrgpulse(pwC90*171.2/90.0, two, 0.0, 0.0);
decrgpulse(pwC90*342.8/90.0, zero, 0.0, 0.0);
decrgpulse(pwC90*145.5/90.0, two, 0.0, 0.0);
decrgpulse(pwC90*81.2/90.0, zero, 0.0, 0.0);
decrgpulse(pwC90*85.3/90.0, two, 0.0, 0.0);
}

static double d2_init=0.0;

static int
 phi1[2] = {0,2},       /* phi 123&5 as per Yamazaki */
 phi2[4] = {0,0,2,2},
 phi3[8] = {0,0,0,0,2,2,2,2},
 phi5[16]= {0,0,0,0,0,0,0,0,2,2,2,2,2,2,2,2},
 phi11[1]= {0},         /* psi 1 as per Yamazaki  */
 rec[4]  = {0,2,2,0};

pulsesequence()
{
```

```
/* Declare variables */
char
   satmode[MAXSTR];

 getstr("satmode",satmode);

int
 t1_counter = 0,
 phase = getval("phase");

double
 d0  = getval("d0"),
 satdly = getval("satdly"),
 satpwr = getval("satpwr"),
 satfrq = getval("satfrq"),
 tauHC = getval("tauHC"),
 tauCC = getval("tauCC"),
 pwC    = getval("pwC"),
 pwClvl = getval("pwClvl"),
 compC  = getval("compC"),
 pwC90  = getval("pwC90"),    /* 90 deg CB/CG or CO pulse at dpwrf rf2*/ pwC180,
 pwN    = getval("pwN"),
 pwNlvl = getval("pwNlvl"),
 gt0    = getval("gt0"),
 gt1  = getval("gt1"),
 gt3  = getval("gt3"),
 gt5  = getval("gt5"),
 gzlvl0  = getval("gzlvl0"),
 gzlvl1  = getval("gzlvl1"),
 gzlvl3  = getval("gzlvl3"),
 gzlvl5  = getval("gzlvl5"),
 rf0,
 rf2;   /* fine dec power for CB/CG region selective pulse*/
   /* also used for fine dec power for CO 90 deg pulse at CB/CG */
 pwC180=2*pwC90;

/*  Parameter checks    */
if ( pw > 20e-6 )
     {
     printf( "your pw seems too long !!!  ");
     printf( "  pw must be <= 20 usec \n");
     psg_abort(1);
     }
    if ( pwC > 30e-6 )
     {
     printf( "your pwC seems too long !!!  ");
     printf( "  pwC must be <= 30 usec \n");
     psg_abort(1);
     }
  if ( pwN > 50e-6 )
```

```
    {
    printf( "your pwN seems too long !!!  ");
    printf( "  pwN must be <= 50 usec \n");
    psg_abort(1);
    }
  if ( dm[C] == 'y')
  {
 if ( at > 0.11 )
  {
 printf( " acquisition time is too long for decoupling !!!\n");
 psg_abort(1);
 }
 if ( dpwr > 46  )
  {
 printf( "incorrect power for dpwr !!!  ");
 printf( " must limit dpwr <= 46 \n");
 psg_abort(1);
 }
}
 if ( ( dm[A] == 'y') || ( dm[B] == 'y'))
  {
printf( "no decoupling should be done during status periods A or B !!!\n");
psg_abort(1);
}
 if ( gt1 > 1.5e-3  ) { printf( "gt1 is too long !!!\n");
 psg_abort(1);
 }

/* Set variables  */
settable(t1,  2, phi1);
settable(t2,  4,  phi2);
settable(t3,  8, phi3);
settable(t5,  16,  phi5);
settable(t11,  1,  phi11);
settable(t60,  4, rec);

/* Phase incrementation for hypercomplex data */
if ( phase == 2 )
{
tsadd(t11,1,4);
 }

 if( ix == 1) d2_init = d2;
 t1_counter = (int) ( (d2-d2_init)*sw1 + 0.5 );
 if(t1_counter % 2)
{ tsadd(t11,2,4); tsadd(t60,2,4); }

/* 90 degree pulse at C0 (175ppm) null at CB/CG (35ppm) */
/* 90 degree regional selective pulse at CB/CG (35ppm) */
 rf0 = 4095.0;
 rf2 = (compC*4095.0*pwC)/pwC90; /* power level for CB/CG pulses */
```

```
rf2 = (int) (rf2 + 0.5);

/* Begin the actual pulse sequence  */
status(A);
 delay(d0);
 txphase(zero);
 obspower(tpwr);
 decphase(zero);
 decpower(pwClvl);
 dec2phase(zero);
 dec2power(pwNlvl);

  if ( satmode[A] == 'y' )
 {
 obspower(satpwr);
 obsoffset(satfrq);
 rgpulse(satdly,zero,rof1,rof2);
 obspower(tpwr);
 obsoffset(tof);
 delay(1.0e-3);
 }
  else
 {
 delay(d1);
 }
 rcvroff();
status(B);

 if(gt1>0.2e-6)
 {
  delay(10.0e-6);
  decrgpulse(pwC,zero,0.0,0.0);
  delay(0.2e-6);
  zgradpulse(gzlvl1,gt1);
   }
 delay(1.0e-3);

   rgpulse(pw,zero,0.0,0.0);    /* INEPT section HA->CA, HB->CB, HG->CG */
delay(2.0e-6);
zgradpulse(gzlvl0,gt0);
delay(tauHC-gt0-2.0e-6);
simpulse(2.0*pw,2*pwC,zero,zero,0.0,0.0);
delay(tauHC-gt0-500.0e-6);
zgradpulse(gzlvl0,gt0);
txphase(one);
delay(500.0e-6);
rgpulse(pw,one,0.0,0.0);
delay(2.0e-6);
zgradpulse(gzlvl3,gt3);
delay(200.0e-6);
decrgpulse(pwC,zero,0.0,0.0);
```

```
delay(tauCC-0.5*10.9333*pwC);
shaka6(pwC);  /*  Shaka composite 180 refocusing and inversion pulse  */
decpwrf(rf2);
delay(tauCC-0.5*10.9333*pwC);
decrgpulse(pwC90,one,0.0,0.0);
delay(2.0e-6);
decoffset(dof+(180-35)*dfrq);
delay(10.0e-6);
decrgpulse(pwC90, t11, 0.0, 0.0);    /* CO SQC */

if (d2 > pwC180)
{
 delay(d2/2);
 simshaped_pulse("","cocb180",2*pw, pwC180, t3,t3,0.0,0.0);
 delay(d2/2);
  }
else
 delay(d2);

decrgpulse(pwC90, t1, 0.0, 0.0);
delay(2.0e-6);
decoffset(dof);
delay(10.0e-6);
decrgpulse(pwC90,one,0.0,0.0);
decpwrf(rf0);
decphase(zero);
delay(tauCC-0.5*10.9333*pwC);
shaka6(pwC);  /*  Shaka composite 180 refocusing and inversion pulse  */
delay(tauCC-0.5*10.9333*pwC);

simpulse(pw,pwC,one,t2,0.0,0.0);
delay(2.0e-6);
txphase(zero);
decphase(zero);
zgradpulse(gzlvl5,gt5);
delay(tauHC-pwC -gt5 - 2.0e-6);
simpulse(2*pw,2*pwC,zero,zero,0.0,0.0);
delay(tauHC-pwC-gt5-500.0e-6-2.0*POWER_DELAY);
zgradpulse(gzlvl5,gt5);
decpower(dpwr);
dec2power(dpwr2);
delay(500.0e-6);

status(C);          /* Aquire the fid in t3 */
rcvron();
delay(rof2);
setreceiver(t60);
}
```

APPENIDIX B

Buffer components as internal pH indicators for biomolecular NMR*

Outline

During NMR experiments, pH of the sample can be determined using a non-invasive convenient technique where the components of the buffer serve as internal pH indicators. Formate, tris, piperazine, and imidazole, whose ^{1}H NMR chemical shifts are sensitive to pH in a range from 2.5 to 9.8, were used to report pH of the sample in this work. This method is suitable for a wide range of applications where samples are handled intensively during NMR titrations or in high throughput analysis in structural genomics or metabolomics.

Introduction

The vast majority of biological processes occur under a stringent control of pH, which should be reproduced during *in vitro* experiments. The most common method to report pH *in vitro* employs a pH sensitive glass electrode. This method, although well established and widely used, has significant disadvantages in solution state biological NMR experiments. First, positively charged proteins and peptides are frequently nonspecifically absorbed by a negatively charged glass surface of an electrode, which leads to the loss of a protein, contamination of the glass surface, and as a result to the distortion of pH calibration. Second, due to the moistening of the electrode surface, a fraction of protein solution is retained on the walls of an electrode, leading to an error in the determination of sample volume, which is especially significant when amplified during repeated pH measurements. Third, the measurement of pH with an electrode is an invasive technique, during which the impurities affecting equilibria and promoting sample degradation might be introduced. This is especially important for rare samples or for the samples particularly sensitive to denaturants and degradation. Fourth, in the case of high throughput analysis, pH measurements with an electrode amount to a substantial time cost.

---

* The version of this appendix was published. Baryshnikova O.K., Williams T.C., and Sykes B.D. (2008) *J Biomol NMR.* 41(1): 5-7.

The idea of monitoring pH using NMR chemical shifts of ^{19}F, ^{13}C, and ^{31}P has found numerous biological (*1-4*) and chemical applications (*5*). Several compounds were proposed as pH indicators with their ^{1}H NMR chemical shifts sensitive to pH: hydroxylammonium chloride (*6*), which is a reducing agent that might react with protein solution; phosphoric acid (*7*), which has limited solubility in the presence of biologically relevant metals, precipitating as a salt; mixture of methylated imidazoles (*8*), that covers mostly basic pH range; guanidinium chloride (*6*), which might promote highly undesirable protein unfolding; cacodylate (*9*), which is an arsenic compound and potentially toxic. While many compounds can be employed, common buffers are the most convenient to use as pH indicators. Tris, formate, piperazine, and imidazole were employed as internal reporters of pH, since they demonstrate a dependence of ^{1}H NMR chemical shifts on pH and their 1D ^{1}H NMR spectra are relatively simple, showing one or two peaks, so that the resonances of a protein or a peptide of question would be minimally obstructed. These compounds are also biologically inert including the lack of interactions with metal ions such as Ca^{2+} and Mg^{2+}, which is important in case of Ca^{2+} binding proteins for example troponin C. In Dr. Sykes' laboratory, an imidazole based buffer sensitive to pH in a region of 5.6-8.6 with a pKa of imidazole equal to 7.11 (100 mM KCl, 10 mM imidazole, 30°C) has been previously developed (T.C. Williams, unpublished data). This buffer has proved to be useful in a large number of NMR studies of troponin C performed in Dr. Sykes' laboratory over a period of more than a decade (*10-12*). In order to control pH over a wider range, a combination of four pH reporters (tris, formate, piperazine, and imidazole) has been developed.

Results and Discussion

The buffer containing 100 mM KCl, 2 mM tris, 2 mM formate, 2 mM piperazine, 2 mM imidazole, 0.2 mM DSS, and 5% D_2O was calibrated using a standard pH-sensitive glass electrode (purchased from Radiometer America Inc.) in a 30°C thermostat. Solutions of 1 M HCl or NaOH were added to adjust the pH of a buffer. 1D ^{1}H NMR spectra were recorded on a Varian Inova 500 MHz spectrometer at 30 °C using a standard 1D pulse sequence provided by BioPack. Calibrations were repeated three times with an example calibration shown in Figure B-1. ^{1}H chemical shifts for formate were found to range from 8.236 to 8.442 for protonated and deprotonated forms correspondingly (Fig. B-1a, Table B-1), and the value of pKa was found to be 3.56 ± 0.05, as determined using xcrvfit program (http://www.bionmr.ualberta.ca/bds/software/index.html). ^{1}H chemical

shift for the H2 proton of imidazole ranged from 8.672 to 7.765 for protonated and deprotonated forms (Fig. B-1a, Table B-1) with the pKa of 7.08 ± 0.08. ^{1}H chemical shifts for tris ranged from 3.732 to 3.509 for protonated and deprotonated forms (Fig. B-1b, Table B-1) with the pKa value of 8.23 ± 0.08. ^{1}H chemical shifts for piperazine ranged from 3.585 to 3.113 for protonated and deprotonated forms (Fig. B-1b, Table B-1) with the pKa_1 value of 5.61 ± 0.07.

The values of pKa's and ^{1}H chemical shifts for protonated and deprotonated forms determined during calibration were used in a macro written for VnmrJ and available on-line (http://www.bionmr.ualberta.ca/mc/). The macro utilizes the following relationship: $pH = pKa - \lg\left(\frac{\delta_{obs} - \delta_{HA}}{\delta_A - \delta_{obs}}\right)$, where δ_{HA} and δ_A, are the chemical shifts for protonated and deprotonated forms correspondingly, and δ_{obs} is the ^{1}H chemical shift observed for the solution with unknown pH. The most precise determination of pH is achieved when δ_{obs} lies within the linear portion of chemical shift dependence on pH (Fig. B-1). The limits within which pH indicators provide the most reliable information were truncated for formate to pH of 2.5 (δ of 8.246) and 4.7 (δ of 8.427), for piperazine to pH 4.4 (δ of 3.542) and 6.4 (δ of 3.175), for imidazole to pH 5.8 (δ of 8.635) and 8.6 (δ of 7.803), and for tris to pH 6.7 (δ of 3.725) and 9.8 (δ of 3.516) (Table B-1). Thus, the overall pH range covered by these four compounds spans from 2.5 to 9.8, which can be easily extended if needed by adding another buffer component with an appropriate pKa value. Within these limits, the pH of solution can be determined with the error of ± 0.05 provided that the spectrum was correctly referenced to DSS and the error of a standard glass electrode used during calibration was of the same order or less.

Table B-1. pKa values, ^{1}H chemical shifts for protonated and deprotonated forms of internal pH reporters and the limits of their applicability.

	pKa	σ_{HA}	σ_{A^-}	applicability regions	
formate	3.56 ± 0.05	8.236	8.442	2.5 (δ of 8.246)	4.7 (δ of 8.427)
piperazine	5.61 ± 0.07	3.585	3.113	4.4 (δ of 3.542)	6.4 (δ of 3.175)
imidazole	7.08 ± 0.08	8.672	7.765	5.8 (δ of 8.635)	8.6 (δ of 7.803)
tris	8.23 ± 0.08	3.732	3.509	6.7 (δ of 3.725)	9.8 (δ of 3.516)

This method requires a calibration that needs to be performed only once for a particular set of conditions, such as temperature, salt concentration, etc. Parameters pKa, δ_{HA}, and δ_A for the buffers chosen do not change greatly over the typical range of conditions for biological NMR samples. For example, over the temperature of 25 to 40 °C, the pKa of piperazine changes by 0.3, the pKa of tris changes by 0.2, the pKa of formate changes by 0.2, and the pKa of imidazole, the most stable among studied compounds, changes by 0.1. The changes in pKa's with ionic strength ranging from ~ 20 mM to 100 mM were negligible within the errors of experiment; however, it is desirable to calibrate against a glass electrode for a particular set of conditions to achieve the best detection accuracy. Once the calibration has been performed, pH can be determined from the ^{1}H chemical shifts of buffer compounds.

It might seem that the measuring of pH using NMR chemical shifts vs glass electrode is a more time consuming during the initial preparation of the sample due to the necessity for shimming and re-equilibrating each time after adjusting pH. However, the use of a glass electrode also requires that the sample and buffer are equilibrated at all temperatures, and that pH meter calibration curves are done at all temperatures, which is a tedious procedure and often not done properly. Once the sample is prepared, the NMR method is far easier to quickly measure pH within the sample due to any changes that might occur with time, reaction, or degradation, for example.

Conclusions

The method described here utilized the pH dependence of ^{1}H chemical shifts of buffer components such as formate, tris, imidazole, and piperazine to determine pH of the NMR sample. This method is devoid of many disadvantages of a glass electrode. It affords a better reproducibility of results, consistency among users, and availability for after the fact validation. It can be conveniently used for measuring pH in kinetic experiments or when monitoring long-term stability of a sample. It is indispensable when proteins are in shigemi style tubes or when pH is measured against temperature. Most importantly this method is highly beneficial during NMR titrations when samples are intensively handled or during high throughput analysis in proteomics, metabolomics, and structural genomics.

Figure B-1. 1D 500 MHz ^{1}H NMR spectra of the buffer containing four internal pH indicators (formate (a), imidazole (a), tris (b), and piperazine (b)) as a function of pH. Protons that give rise to peaks in ^{1}H 1D NMR spectra are shown in boxes and connected to the corresponding resonances with arrows. The triplet on panel b corresponds to a CH_2 resonance arising from DSS that served as a reference compound.

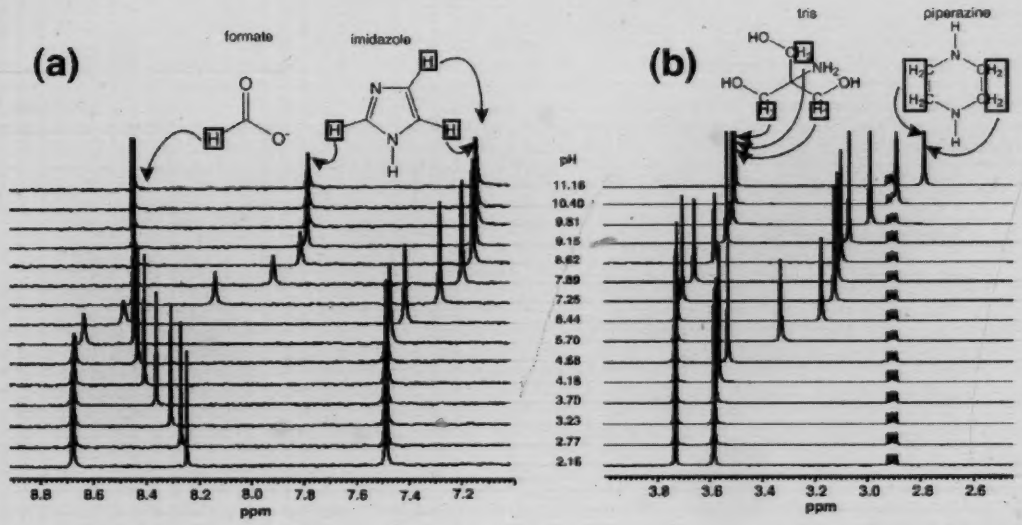

References

(1) Taylor, J., and Deutsch, C. (1988) 19F-nuclear magnetic resonance: measurements of [O2] and pH in biological systems. *Biophys J 53*, 227-33.

(2) DeFronzo, M., and Gillies, R. J. (1987) Characterization of methylphosphonate as a 31P NMR pH indicator. *J Biol Chem 262*, 11032-7.

(3) Pietri, S., Miollan, M., Martel, S., Le Moigne, F., Blaive, B., and Culcasi, M. (2000) alpha - and beta -phosphorylated amines and pyrrolidines, a new class of low toxic highly sensitive 31P NMR pH indicators. Modeling of pKa and chemical shift values as a function of substituents. *J Biol Chem 275*, 19505-12.

(4) Pietri, S., Martel, S., Culcasi, M., Delmas-Beauvieux, M. C., Canioni, P., and Gallis, J. L. (2001) Use of diethyl(2-methylpyrrolidin-2-yl)phosphonate as a highly sensitive extra- and intracellular 31P NMR pH indicator in isolated organs. Direct NMR evidence of acidic compartments in the ischemic and reperfused rat liver. *J Biol Chem 276*, 1750-8.

(5) Vistad, O. B., Akporiaye, D. E., Taulelle, F., and Lillerud, K. P. (2003) Morpholine, an in situ C-13 NMR pH meter for hydrothermal crystallogenesis of SAPO-34. *Chemistry of Materials 15*, 1650-1654.

(6) Rabenstein, D. L., and Fan, S. Y. (1986) Proton nuclear magnetic resonance spectroscopy of aqueous solutions: complete elimination of the water resonance by spin-spin relaxation. *Anal Chem 58*, 3178-84.

(7) Szakacs, Z., Hagele, G., and Tyka, R. (2004) 1H/31P NMR pH indicator series to eliminate the glass electrode in NMR spectroscopic pKa determinations. *Analytica Chimica Acta 522*, 247-258.

(8) Sorkin, D. L., and Miller, A. F. (1997) Spectroscopic measurement of a long-predicted active site pK in iron-superoxide dismutase from Escherichia coli. *Biochemistry 36*, 4916-24.

(9) Valcour, a. a., and Woodworth, R. C. (1986) Internal Proton Magnetic-Resonance Probes for Ph Titration of Proteins. *Journal of Magnetic Resonance 66*, 536-541.

(10) Sia, S. K., Li, M. X., Spyracopoulos, L., Gagne, S. M., Liu, W., Putkey, J. A., and Sykes, B. D. (1997) Structure of cardiac muscle troponin C unexpectedly reveals a closed regulatory domain. *J Biol Chem 272*, 18216-21.

(11) Li, M. X., Spyracopoulos, L., and Sykes, B. D. (1999) Binding of cardiac troponin-I147-163 induces a structural opening in human cardiac troponin-C. *Biochemistry 38*, 8289-98.

(12) Lindhout, D. A., and Sykes, B. D. (2003) Structure and dynamics of the C-domain of human cardiac troponin C in complex with the inhibitory region of human cardiac troponin I. *J Biol Chem 278*, 27024-34.

APPENIDIX C

Structures of peptide agonists derived on the basis of SDF-1α reveal a common motif possibly implicated in the binding to the CXCR4 receptor*

Outline

CXCR4 is an important pharmacological target due to its involvement in HIV-1 pathogenesis and cancer metastasis. Two recently discovered allosteric agonists (17-mers) that bind and activate CXCR4, the ASLW and RSVM peptides, were analyzed using solution NMR spectroscopy. Both peptides assumed an extended backbone conformation with several well defined local motifs in the regions from residues 5 to 8 and 9 to 12. Similar examples in literature suggest the relevance of nascent structures in peptides to their biologically relevant conformations. The local structure in the region 9 to 12 was adopted by the entire ensemble of the ASLW peptide structures and by the subset of conformations for the RSVM peptide. The same turn was found in full length SDF-1α and in the small family of the SDF-1α N-terminal 17-mer. The significance of found local structures and implications for further drug design are discussed.

Introduction

Chemokine receptors belong to a family of G-protein coupled receptors (GPCRs) that are especially attractive as therapeutic targets (*1-5*). The chemokine receptor CXCR4, through interactions with the stromal derived factor, SDF-1α, mediates trafficking of lymphocytes, memory immune responses (*6, 7*), vascular and germ cell development (*8, 9*), haematopoieses and lymphopoiesis (*10*), and neuronal patterning (*11*). CXCR4 has a crucial role in metastasis of various cancers (*2, 12-17*) and in HIV-1 pathogenesis (*18*), which provides a strong impetus for studying this system on a molecular level.

A number of approaches have been used to address the structural determinants of interactions between GPCRs and their ligands (*19*). Membrane bound proteins, such as GPCRs, represent a substantial challenge for traditional structural approaches using NMR and X-ray techniques. One approach employs structural studies of isolated biologically active peptides in order to infer information about the interactions with their cognate

---

* The version of this chapter was published. Baryshnikova O.K., Rainey J.K., and Sykes B.D. (2005) *J Pep Res* 66 (S1), 12-21.

receptors and possible binding modes (*19*). In the majority of cases, isolated peptides are considered to be disordered in solution. However, within apparently unstructured conformations it is often possible, especially at lower temperatures, to find regions with local structures that have been demonstrated to be biologically relevant (*20, 21*). With the decrease of temperature, according to Gibb's equation for free energy, the favorable intramolecular enthalpic contacts that determine the conformation of a peptide will play an increasingly more important role since the entropic component is lowered. In the bound form, the conformation of a peptide is also determined to a considerable degree by enthalpic contacts, including intermolecular contacts. Thus, the conformations obtained for both conditions should demonstrate some similarity (*21*). We applied this methodology to study at lower temperature the conformations of unbound peptides, which might provide information regarding possible binding modes and a valuable starting point for rational drug design especially for a system with very low structural information available.

A number of compounds have been shown to bind CXCR4 and inhibit the binding of its natural ligand SDF-1α. Some compounds act as agonists of CXCR4 activity and activate the signalling cascade upon binding to the receptor (*22, 23*), while others act as antagonists and bind to CXCR4 without triggering the downstream biological response (*23*). The best known inhibitor, the bicyclam AMD3100, is remarkably specific as a CXCR4 inhibitor, and the potential for its use in clinical applications including AIDS, cancer, rheumatoid arthritis, and stem cell transplantation is very promising (*24*). In spite of the success of AMD3100, due to its inhibition of CXCR4, concerns have often arisen about possible detrimental effects, such as defects in bone-marrow myelopoiesis, haematopoeiesis, and cardiogenesis (*24*). It is often desirable that an inhibitor could not only bind to a receptor but also induce its biological activity so that the detrimental effects of receptor silencing were minimal during the inhibition. Two peptides were recently reported that act in this manner (*22*). These peptides, designated as RSVM and ASLW, are 17-mers derived from the SDF-1α N-terminus and differ only in the four N-terminal residues. It was shown that the RSVM and ASLW peptides bind to CXCR4 and trigger the signalling of a receptor. Noteworthy, they bind to CXCR4 via a different binding site from that of AMD3100 and SDF-1α thus demonstrating allosterism (*22*).

We used solution NMR spectroscopy to study the conformations of the ASLW and RSVM peptides at 5^0C. The studied peptides adopted several local structures or

motifs that were compared with each other and with motifs described in literature. In the region from residues 5 to 8 the structures of the ASLW and RSVM peptides adopted local structures, which were unique and not comparable to other described motifs or each other. In the region from 9 to 12, the ASLW peptide formed a local structure that was also present in full length SDF-1α, and in a subset of the RSVM and the SDF-1α N-terminal 17-mer structures. The structures of two allosteric peptides, their relevance to bound conformations and implications for future drug design are discussed further.

Results

Structural characterization of the ASLW and RSVM peptides: chemical shifts, J-coupling constants, and NOE connectivities

The sequential assignment of proton resonances for two allosteric peptides agonists was accomplished using standard methods described by Wüthrich (*25*). NH and Hα chemical shifts obtained for both peptides were shown to be similar to each other and to the chemical shifts for the SDF-1α N-terminal 17-mer (*26*) (Table C-1).

The signs and values of NMR chemical shift deviations (CSD) from random coil chemical shifts are often characteristic of the secondary structure adopted by a polypeptide (*27*). CSD values for Hα and NH NMR chemical shifts are mostly negative in helices and positive in β-sheets. The alternating signs and small values of CSD for the ASLW and RSVM peptides and the SDF-1α 17-mer (Table C-2) indicate that under experimental conditions all three peptides do not adopt either extensive helical nor β-strand conformations on average.

J-coupling constants are correlated with torsion angles ϕ and therefore provide the information on secondary structure of polypeptides. For the studied peptides, J-coupling measurements from 1D spectra ranged from 5.6 to 8.6 Hz, which suggests that torsion angles can adopt a variety of values. This renders J-coupling constants less useful for structure calculations.

NOE patterns are also useful indicators of the elements of secondary structure adopted by polypeptides. For example the presence of β-turns is often accompanied by connectivities between $d_{NN}(2,3)$, $d_{NN}(3,4)$, $d_{\alpha N}(2,3)$, $d_{\alpha N}(3,4)$ and $d_{\alpha N}(2,4)$, where the numbers refer to the position of a residue in the turn. The summary of NOE connectivities for the ASLW peptide (Fig. C-1a) suggests the possible formation of a local turn-like structure in the region from Tyr^7 to Phe^{13}. The $d_{\alpha N}(i,i+2)$ connectivity between Ser^2 and Trp^4 may also suggest a β-turn in the region from Ala^1 to Trp^4. The

RSVM peptide is less structured with one medium range connectivity between Ser^6 and Arg^8 (Fig. C-1b). Missing $d_{\alpha N}(i,i+1)$ connectivities (Figs. C-1a and C-1b) next to Pro^{10} in the RSVM peptide and Ser^6 in the ASLW peptide, were not included due to ambiguity in their assignments. In general, both peptides adopt flexible conformations with possible local structures as indicated by NOE pattern.

Table C-1. NMR chemical shifts for the ASLW and RSVM peptides and the NH and Hα chemical shifts for the SDF-1α 17-mer. NMR data was obtained at 5°C for the ASLW and RSVM peptides in this study and at 8°C for the SDF-1α N terminal 17-mer as described earlier (*26*).

NH chemical shifts			Hα chemical shifts			Chemical shifts for proton nuclei other than NH and Hα		Primary sequence for SDF-1α 17-mer
ASLW peptide	RSVM peptide	SDF-1α 17-mer	ASLW peptide	RSVM peptide	SDF-1α 17-mer	ASLW peptide	RSVM peptide	
			4.10	4.08	4.35		Hβ 1.94, 1.93	Lys^1
8.79	8.95		4.43	4.57	4.53		γCH_2 1.65, 1.65	Pro^2
8.58	8.55	8.52	4.26	4.13	4.07		δCH_2 3.22, 3.22	Val^3
8.19	8.58	8.51	4.63	4.48	4.46		εNH_3^+ 7.28	Ser^4
7.96	8.47	8.56	4.26	4.38	4.37	Hβ 3.72, 3.64	Hβ 3.85, 3.85	Leu^5
8.08	8.33	8.31	4.28	4.37	4.39	Hβ 1.55, 1.51	Hβ 2.07	Ser^6
8.08	8.29	8.17	4.49	4.52	4.51	γCH_2 1.45	γCH_2 0.95, 0.95	Tyr^7
8.08	8.16	8.11	4.23	4.25	4.24	δCH_2 0.87, 0.82		Arg^8
8.37	8.45	8.41	4.61	4.64	4.63	Hβ 3.29, 3.19	Hβ 2.07, 1.97	Cys^9
			4.41	4.42	4.40	2H 7.20	gCH_2 2.57, 2.51	Pro^{10}
8.48	8.52	8.48	4.38	4.40	4.39	4H 7.60		Cys^{11}
8.50	8.53	8.48	4.25	4.24	4.24	5H 7.13		Arg^{12}
8.23	8.27	8.23	4.55	4.56	4.55	6H 7.23		Phe^{13}
8.22	8.24	8.20	4.53	4.53	4.53	7H 7.48		Phe^{14}
8.30	8.31	8.28	4.21	4.21	4.21	indole NH 10.22		Glu^{15}
8.42	8.43	8.39	4.33	4.33	4.33	Hβ 1.53, 1.50	Hβ 1.63, 1.63	Ser^{16}
8.71	8.72	8.68	4.69	4.69	4.70	γCH_2 1.41	Hβ 1.49	His^{17}

One might expect the formation of a hydrophobic core around residues Tyr^7, Phe^{13}, and Phe^{14} similarly to the structural studies reported previously (*28*). The experiment spectral resolution was sufficient to resolve frequencies for the majority of

aromatic residues for both peptides. Surprisingly, the ring protons for both peptides failed to give rise to medium range inter-residue NOEs (data not shown). Trp^4 in the ASLW peptide also demonstrated no contacts to the aromatic residues Tyr^7, Phe^{13}, and Phe^{14} through either its backbone atoms or ring protons.

Table C-2. NH and Hα NMR chemical shifts deviations. CSD values were calculated as $\sigma_{obs}-\sigma_{ref}$, where NH σ_{ref} obtained for 25°C (*29*) were corrected using NH temperature gradient of -7.6 ppb/°C reported for random coil (*30*) and σ_{obs} is the observed chemical shift. Hα σ_{ref} were assumed to stay unaltered for temperatures of interest (*29*). CSD for the SDF-1α 17-mer were taken from previous work (*26*).

Hα CSD			NH CSD		
ASLW peptide	RSVM peptide	SDF-1α 17-mer	ASLW peptide	RSVM peptide	SDF-1α 17-mer
-0.21	-0.26	-0.24			
-0.04	0.10	0.12	0.32	0.48	
-0.08	0.01	-0.05	0.27	0.37	0.19
-0.03	0.00	0.00	-0.22	0.15	0.1
-0.08	0.03	0.03	-0.35	0.16	0.19
-0.19	-0.10	-0.08	-0.38	-0.13	-0.11
-0.06	-0.02	-0.04	-0.19	0.01	-0.27
-0.11	-0.09	-0.10	-0.30	-0.22	-0.29
0.06	0.09	-0.18	-0.10	-0.02	0.08
-0.01	0.00	-0.05			
-0.17	-0.15	-0.16	0.01	0.05	0.13
-0.09	-0.10	-0.11	0.12	0.15	0.09
-0.07	-0.06	-0.07	-0.22	-0.18	-0.20
-0.09	-0.09	-0.09	-0.23	-0.21	-0.23
-0.14	-0.14	-0.14	-0.27	-0.26	-0.19
-0.14	-0.14	-0.13	-0.04	-0.03	-0.03
-0.03	-0.04		0.13	0.14	0.28

Due to the presence of *cis-* and *trans-* isomerism of X-Pro^{10} peptide bond, the resonances in the proton NMR spectra for peptides containing Pro is often doubled, so that minor and major conformations can be identified. In case of the ASLW and RSVM peptides, the doubling of resonances was negligible, which together with the characteristic NOEs from β-hydrogens of Cys^9 to δ-hydrogens of Pro^{10} present for both peptides indicates that these were the *trans* isomers of Cys^9-Pro^{10} peptide bond.

Structure Calculation and Clustering Analysis

Two regions on the ASLW peptide, residues 5 to 8 and residues 9 to 12, can be superimposed over their backbone atoms with the rmsd less then 0.7 Å for an entire

ensemble (Table C-3 and Figs. C-2a and C-2b). Regions other than 5-8 and 9-12 gave poor superposition statistics, with rmsd values of no less then 1.2 Å. The observed local structures were in agreement with NOE connectivity data except for the region around Ser^2 where, even in the presence of connectivity (Fig. C-2a), local structure was not observed. The RSVM peptide had only one pronounced local feature for an entire ensemble, which is a turn in the region 5-8 with the superposition of 0.64 Å (Table C-3 and Figs. C-2c and C-2d). For both peptides, the regions with low rmsd were further analyzed with NMRCLUST (*31*) to extract individual subsets of conformations with even lower rmsd values (Table C-3).

Table C-3. The results of cluster analysis for the ensembles of structures of the ASLW and RSVM peptides, the SDF-1α 17-mer, and full length SDF-1α. The data for major families (more than 10% of an entire ensemble) is shown.

	rmsd for backbone atoms for ensemble, Å	Cluster 1		Cluster 2		Cluster 3	
		rmsd for backbone atoms, Å	Relative population of a cluster, %	rmsd for backbone atoms, Å	Relative population of a cluster, %	rmsd for backbone atoms, Å	Relative population of a cluster, %
ASLW peptide 5-8 region	0.71±0.24	0.51±0.15	43	0.51±0.13	25	–	–
ASLW peptide 9-12 region Motif II	0.67±0.21	0.21±0.07	25	0.29±0.12	25	0.24±0.09	18
RSVM peptide 5-8 region	0.64±0.31	0.41±0.14	68	0.99±0.24	23	–	–
RSVM peptide 9-12 region	1.17±0.52	0.70±0.22	33	0.55±0.18	30	0.74±0.20	20
SDF-1α 17-mer 5-8 region Motif I	0.56±0.27	0.22±0.09	34	0.12±0.09	28	0.13±0.04	15
SDF-1α 17-mer 9-12 region	1.22±0.40	0.53±0.16	28	0.59±0.23	28	0.51±0.18	26
full length SDF-1α 5-8 region	1.11±0.30	1.00±0.22	63	1.06±0.16	12	–	–
full length SDF-1α 9-12 region	0.29±0.08	–	–	–	–	–	–

Clustering analysis for the SDF-1α N-terminal 17-mer was repeated and the results were essentially the same as reported earlier (*26*). The ensemble of SDF-1α 17-mer structures at 8^0C adopted a local turn in a region 5-8 with rmsd equal to 0.56 Å for an ensemble, which can be clustered into the families with rmsd values smaller than 0.22 Å.

The local structure for Cluster 1 shown to be shared with several other CXCR4 ligands such as the ITAC 1-8 peptide and the vMipII 1-10 peptide (*21*) is referred here as Motif I. The region 9-12 of the SDF-1α 17-mer was weakly convergent for an entire family; however clustering analysis revealed individual subsets of structures with rmsd lower than 0.59 Å (Table C-3).

The ensemble of full length SDF-1α structures determined at 30°C (*32*) was subjected to similar analysis. The region 9-12 was very well defined with the rmsd of 0.27 Å for an ensemble of 30 structures. The region 5-8 was convergent with the rmsd of 1.03 Å for an ensemble and individual clusters obtained with NMRCLUST showed rmsd's no less then 1.00 Å (Table C-3).

Comparison of motifs

The local structures found for the two allosteric peptides were compared to each other and to the corresponding regions of SDF-1α and the SDF-1α 17-mer (Tables C-4 and C-5, Figs. C-3a and C-3b). The conformation in the region of residues 5-8 was distinct for every peptide under investigation. The RSVM peptide formed a unique structure, which is quite different from the ASLW peptide and the SDF-1α 17-mer. The same is true about the ASLW peptide, which is well converged in the region of interest, but unique in its conformation (Fig. C-3a). Motif I found for the SDF-1α N-terminal 17-mer (*21*) as it is shown in Figure C-3a is not comparable to the conformations of allosteric peptides.

The local structures in the region 9-12 for the ASLW peptide and full length SDF-1α were identical and will be referred here as Motif II (Fig. C-3b). In full length SDF-1α this region is constrained not only by nonbonding interactions with the core of the protein but also by two disulphide bonds at Cys^{9}-Cys^{34} and Cys^{11}-Cys^{50}. Interestingly, the ASLW peptide adopts the same local structure without long range constraints. The conformations for 20% of the RSVM peptide structures (Table C-5, Cluster 3) and 28% of the SDF-1α 17-mer (Table C-5, Cluster 2) were comparable to Motif II in this region (Fig. C-3b), although the rmsd for these superpositions were higher (0.9 – 1.14 Å).

Discussion

The structural information regarding CXCR4 inhibitors is of certain value for the development of novel agents capable of blocking and modulating CXCR4 activity. In spite of the great importance of CXCR4 as a pharmacological target, the number of

available agents remains limited. We obtained the NMR structures of two potent allosteric agonists, the ASLW and RSVM peptides, that might be considered for further biochemical characterization and subsequent clinical applications or might serve as a useful platform for designing new inhibitors on their base. The studied peptides adopted an extended conformation suggested by the values of J-couplings, low numbers of medium and long range NOEs, and chemical shifts deviations. However, it was shown theoretically and experimentally that the conformational space sampled by a peptide is significantly restricted (*33*). It is thought that a polypeptide is never a completely random coil but instead exists as an ensemble of preferential conformations (*33, 34*). Indeed, the analysis of obtained structures for the ASLW and RSVM peptides revealed the presence of local structuring in several areas of a backbone. In the region of residues 5-8, well-defined local structures were present for each peptide under investigation. Also, in the region of residues 9-12, the ASLW peptide adopted a well-defined motif, which was also present in a subset of structures for the RSVM peptide. The same local structure was found in the region of residues 9-12 for full length SDF-1α and for a subset of structures of the N-terminal SDF-1α 17-mer.

It was proposed that the local structures found for peptides in solution might indicate the similar structural features present in its bound conformation (*21*). The thermodynamical rational behind this assumption is based on the consideration of the enthalpy and entropy interplay during a binding event. The entropic cost to fold a polypeptide is thought to be paid by enthalpic contributions generated upon binding (*35*). Thus, ligands, which are folded prior to binding, or possess a correct nascent structure, should have an advantage in terms of their binding energy. However, the exact contributions of free energy are not known and numerous examples in literature were reviewed where solution conformations are similar to their bound states (*36*) and where conformations are globally different (*37*). The insights from protein folding studies stresses the importance of the correct minimal structure in the denatured state that propagates the correct folding (*38-40*) and in our own experience local motifs in the Hox peptide, in solution, were demonstrated to be analogous to the bound conformations (*20*). If the structures of the RSVM and ASLW peptides in solution are indeed related to the conformations in their bound states one might propose that the dissimilarity in local structures in the regions of residues 5-8 indicates the dissimilarity in their binding modes. The formation of the same structure in the region 9-12 for allosteric peptides and natural ligands (Motif II) argues for at least partial overlapping of the binding interfaces.

In the context of the full length SDF-1α structure, Motif II formed between two cysteine bonds is concave, which renders the side chains of the residues composing the motif (Cys^9, Pro^{10}, Cys^{11}) unavailable for binding (Fig. C-4). It is also known that those residues are rarely involved in the formation of protein - protein interfaces (*41*). However, arginine side chains often form electrostatic interactions on interfaces and the formation of a rigid motif similar to Motif II can position the side chains of Arg^8 and Arg^{12}, flanking the region 9-12, more rigidly by constraining the backbone between them. A number of compounds have been shown to bind CXCR4 through electrostatic interactions. AMD3100, a well known inhibitor, binds to CXCR4 through the interaction of positively charged cyclam rings with carboxylic moieties on Asp^{171}, Asp^{262}, and Glu^{288} (*42, 43*). ALX40-4C is another highly charged and efficient inhibitor of CXCR4 that consists of nine arginine residues (*44*). Since arginine residues have a propensity to appear frequently on protein - protein interfaces (*41*) and since electrostatic interactions play a significant role in binding of CXCR4 inhibitors we believe that Motif II might serve to position the two arginine side chains in close proximity to each other against their electrostatic repulsion and to orient them favorably for the consequent binding to CXCR4 (Fig. C-4). The fact that the RSVM peptide is eight times less potent than the ASLW peptide as an inhibitor of CXCR4 (*22*) might be also relevant to the formation of Motif II prior to binding since the initial structuring of the RSVM peptide is less pronounced.

Materials and Methods

Peptide Synthesis and NMR Sample Preparation

The peptides H-ASLWLSYRCPCRFFESH-NH_2 and H-RSVMLSYRCPCRFFE-SH-NH_2 were synthesized by stepwise solid phase peptide synthesis using t-butoxycarbonyl protection chemistry. NMR samples contained ~3 mM of a peptide, 20 mM CD_3COONa, 15 mM deuterated DTT, 1 mM NaN_3, 1 mM DSS in 500 μl of 90% H_2O/10% D_2O. The pH was adjusted to 5.0±0.05.

NMR Spectroscopy

^1H 1D and TOCSY 2D NMR spectra for both peptides were acquired at Varian Unity 600 spectrometer. 2D NOESY NMR spectra were acquired at 5°C with the mixing time 500 ms at Varian Unity 600 spectrometer for the RSVM peptide and at Varian Inova 800 spectrometer for the ASLW peptide. NOESY spectra were used for integration of NOE cross peaks, which were consequently converted into the distance restraints using Bin module in NMRVIEW (*45*). NOE connectivities were grouped as weak, medium, and strong corresponding to upper distance restraints of 5.0, 3.4, and 2.8 Å respectively. In total, to calculate structures we used 79 inter-residue and 59 intra-residue connectivities for the ASLW peptide and 37 inter-residue and 63 intra-residue connectivities for the RSVM peptide.

Structure Calculations and Clustering Analysis

In case of partially unfolded proteins, the procedure commonly used for calculating structures of folded proteins is not applicable since long distance NOE restraints observed in different conformations cannot be satisfied simultaneously in one structure (*38, 46*). This generally results in a high total energy of structures and significant number of NOE violations. There are also examples in literature when the structures of smaller unfolded proteins or peptides were successfully calculated using standard NOE based approach where the entire set of NOE restraints is used to generate the family of conformers (*21, 26, 28, 47, 48*). In our case, the structures obtained using standard simulated annealing protocol implemented in CNS version 1.1 (*49*) demonstrated neither dihedral violations more than 5° nor NOE violations higher than 0.2 Å and the energies for the calculated structures did not exceed 35 kcal/mol and 15 kcal/mol for the ASLW and RSVM peptides respectively. The calculations were performed in torsion angle space using square well potential and the force constant for the NOE term equal to 1.0. The scaling factors for high temperature annealing stage (T=50000K) were 150 for NOE energy term and 100 for dihedral energy term. The scaling factors for the slow-cool annealing stage (T=50000K) were 150 for NOE energy term and 200 for dihedral energy term. For the final minimization stage, the scaling factor for NOE energy term was 75 and for dihedral energy term the scale factor was 400. PROCHECK (*50*) test showed 0.4% ad 4.3% of residues in disallowed regions for the ASLW and RSVM peptides correspondingly.

For further analysis, the 40 structures with the lowest energies were chosen out of 80 calculated structures. In order to locate regions that adopt similar conformations the families of 40 structures were superimposed in regions of 3-6 residues in length scanning the entire peptide and examined. Clustering was performed using NMRCLUST (*31*) software. Both superposition and clustering included backbone atoms for specific regions.

Table C-4. The convergence of individual clusters between each other in the region of residues from 5 to 8. Representative structures for individual clusters of peptides were obtained with NMRCLUST program and superimposed with their backbone atoms in the region of interest. The relative population of a cluster is indicated as a percent of the total number of structures in ensemble.

	RSVM peptide Cluster 1 67.5%	RSVM peptide Cluster 2 22.5%	ASLW peptide Cluster 1 42.5%	ASLW peptide Cluster 2 25%	SDF-1 17-mer Cluster 1 34.0% **Motif I**	SDF-1 17-mer Cluster 2 27.7%	SDF-1 17-mer Cluster 3 14.9%
RSVM peptide Cluster 1 67.5%	–	–	–	–	–	–	–
RSVM peptide Cluster 2 22.5%	1.12 Å	–	–	–	–	–	–
ASLW peptide Cluster 1 42.5%	1.89 Å	1.63 Å	–	–	–	–	–
ASLW Cluster 2 25%	1.73 Å	1.35 Å	1.18 Å	–	–	–	–
SDF-1 17-mer Cluster 1 **Motif I** 34.0%	1.19 Å	1.37 Å	1.51 Å	1.73 Å	–	–	–
SDF-1 17-mer Cluster 2 27.7%	1.58 Å	1.32 Å	1.60 Å	1.35 Å	1.05 Å	–	–
SDF-1 17-mer Cluster 3 14.9%	1.46 Å	1.71 Å	1.33 Å	1.79 Å	0.69 Å	1.47 Å	–

Table C-5. Convergence of individual clusters between each other in the region of residues from 9 to 12. Representative structures for every individual cluster of peptides were obtained with NMRCLUST. Rmsd values were calculated for backbone atoms of representative structures superimposed in the region of interest. The relative population of a cluster is indicated as a percentage of the total number of structures. The values in bold were considered as good or moderately good convergence.

	RSVM peptide Cluster 1 32.5%	RSVM peptide Cluster 2 30.0%	RSVM peptide Cluster 3 20.0%	ASLW peptide Cluster 1 25% **Motif II**	ASLW peptide Cluster 2 25% **Motif II**	ASLW peptide Cluster 3 17.5%	SDF-1α 17-mer Cluster 1 27.7%	SDF-1α 17-mer Cluster 2 27.7%	SDF-1α 17-mer Cluster 3 25.5%
RSVM peptide Cluster 1, 32.5%	–	–	–	–	–	–	–	–	–
RSVM peptide Cluster 2, 30.0%	1.36 Å	–	–	–	–	–	–	–	–
RSVM peptide Cluster 3, 20.0%	2.12 Å	2.19 Å	–	–	–	–	–	–	–
ASLW peptide Cluster 1 25% **Motif II**	1.53 Å	2.00 Å	1.42 Å	–	–	–	–	–	–
ASLW peptide Cluster 2 25% **Motif II**	1.66 Å	1.89 Å	**1.12** Å	**0.52** Å	–	–	–	–	–
ASLW peptide Cluster 3, 17.5%	1.85 Å	1.98 Å	1.45 Å	0.96 Å	1.09 Å	–	–	–	–
SDF-1α 17-mer Cluster 1, 27.7%	1.39 Å	1.37 Å	1.91 Å	**1.05** Å	1.36 Å	1.39 Å	–	–	–
SDF-1α 17-mer Cluster 2 27.7%	1.43 Å	2.06 Å	1.36 Å	1.18 Å	1.14 Å	1.35 Å	1.47 Å	–	–
SDF-1α 17-mer Cluster 3, 25.5%	1.20 Å	1.06 Å	2.07 Å	1.89 Å	1.89 Å	2.05 Å	1.43 Å	1.69 Å	–
SDF-1α full length ensemble	1.80 Å	2.06 Å	**0.90** Å	**0.78** Å	**0.49** Å	1.14 Å	1.48 Å	**1.04** Å	1.93 Å

Figure C-1. Summary of sequential and medium range NOE connectivities identified for the ASLW (a) and RSVM peptides (b). The width of the line indicates the relative magnitude for NOEs observed in NOESY experiment with 500 ms mixing time.

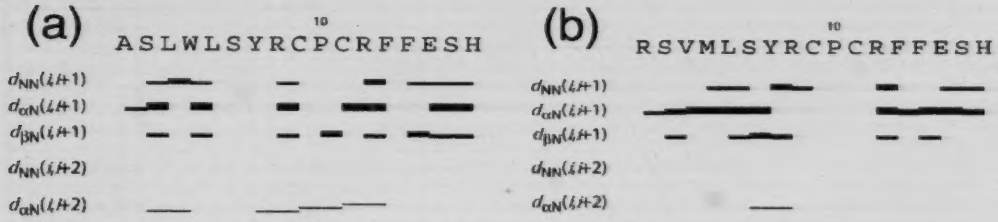

Figure C-2. The ensemble of the ASLW peptide structures backbone aligned in a region 5-8 (a) and 9-12 (b) and the ensemble of the RSVM peptide structures backbone aligned in a region 5-8 (c) and 9-12 (d). The ensemble of structures (in grey) is truncated from 4 to 9 residue (a and c) and from 8 to 13 residue (b and d) with the exception for one representative structure (in black) that is shown in its full length with side chain heavy atoms. Rmsd for the ensembles aligned with its backbone atoms in selected regions was 0.71±0.24 Å (a), 0.67±0.21 Å (b), 0.63±0.31 Å (c), and 1.17±0.52 Å (d).

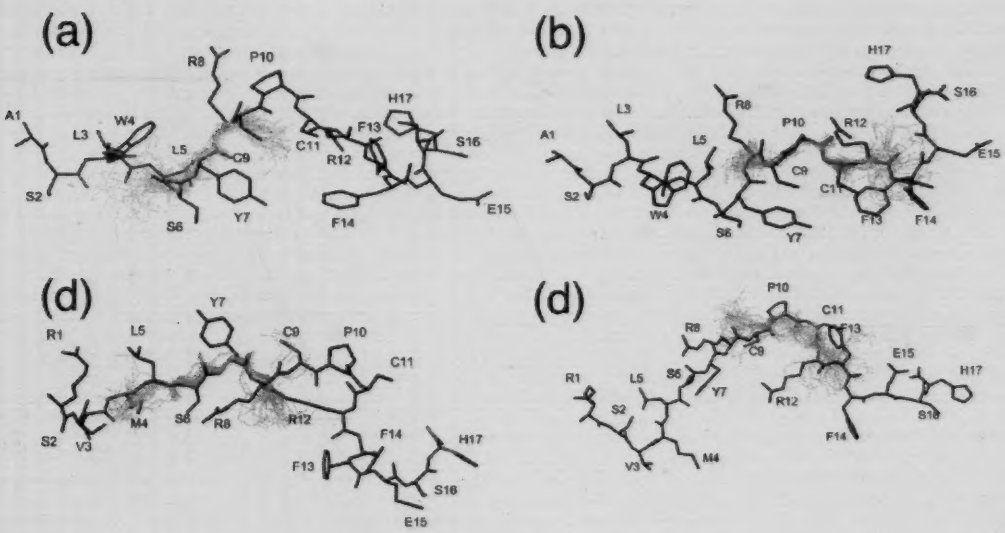

Figure C-3. The superposition of the ASLW and RSVM peptides with the SDF-1α 17-mer in the region 5-8 (a) and with the full length SDF-1α in the region 9-12 (b). (a), The structures shown are Cluster 1 for the SDF-1α 17-mer (Motif I) and the most convergent families of the ASLW peptide (Cluster 1) and the RSVM peptide (Cluster 1). (b), The entire ensemble of full length SDF-1α structures is shown together with the most convergent families of the ASLW peptide (Cluster 1 and 2) and the RSVM peptide (Cluster 3). Backbone atoms for residues 4-9 (a) and 8-14 (b) are shown in black for SDF-1α 17-mer (a) or SDF-1α (b), in red for the RSVM peptide, and in blue for the ASLW peptide.

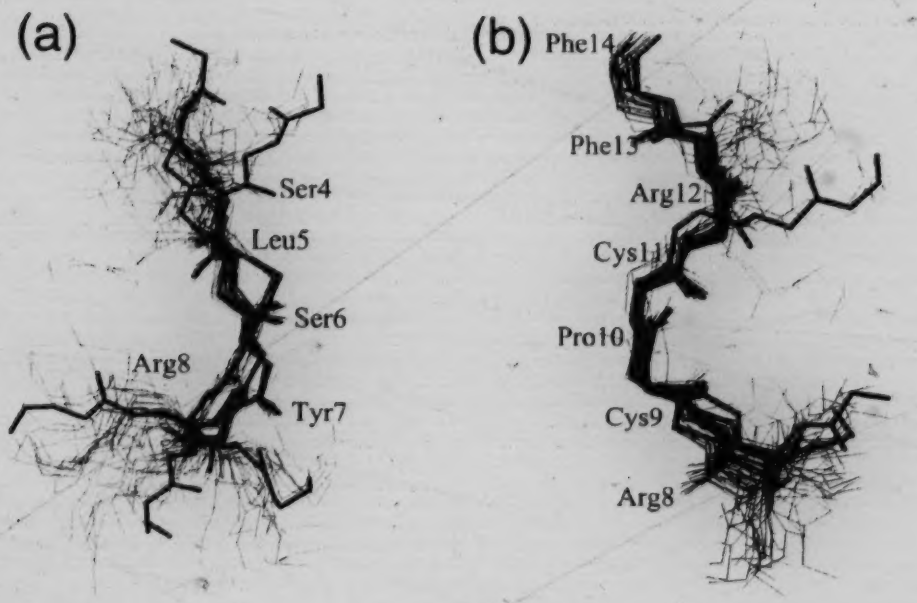

Figure C-4. Motif II in the context of SDF-1α structure. Motif II, formed by the backbone atoms of residues from 9 to 12 is shown in red. Pro^{10} side chain in the middle of Motif II is also shown in red in sticks representation. Residues Cys^{9}, Cys^{11}, Cys^{34}, and Cys^{50} that form disulphide bonds constraining Motif II are shown in yellow. Side chain arginines, Arg^{8} and Arg^{12}, are shown in stick representation and colored according to their atoms.

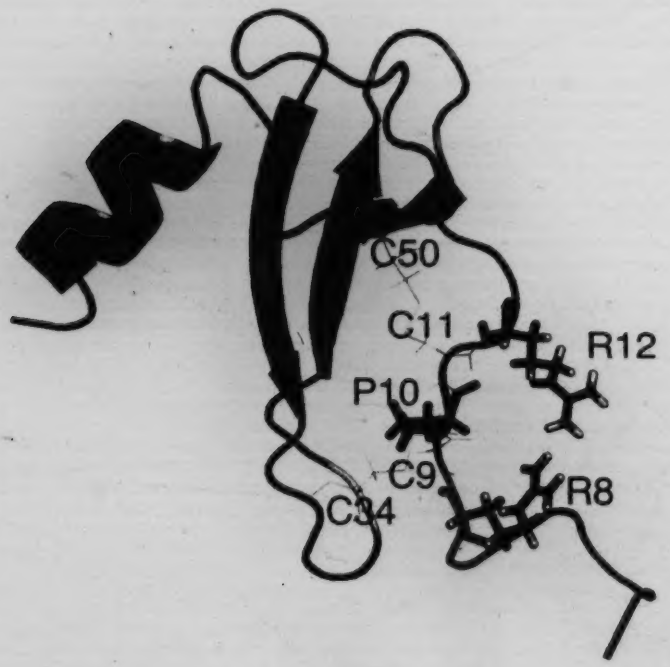

Reference

(1) Onuffer, J. J., and Horuk, R. (2002) Chemokines, chemokine receptors and small-molecule antagonists: recent developments. *Trends Pharmacol Sci. 23*, 459-67.

(2) Murphy, P. M. (2001) Chemokines and the molecular basis of cancer metastasis. *N Engl J Med. 345(11)*, 833-5.

(3) Fernandez, E. J., and Lolis, E. (2002) Structure, function, and inhibition of chemokines. *Annu Rev Pharmacol Toxicol. 42*, 469-99.

(4) Baggiolini, M. (2001) Chemokines in pathology and medicine. *J Intern Med. 250(2)*, 91-104.

(5) Horuk, R. (1998) Chemokines beyond inflammation. *Nature 393*, 524-5.

(6) Baggiolini, M. (1998) Chemokines and leukocyte traffic. *Nature 392(6676)*, 565-8.

(7) Sallusto, F., Mackay, C. R., and Lanzavecchia, A. (2000) The role of chemokine receptors in primary, effector, and memory immune responses. *Annu Rev Immunol 18*, 593-620.

(8) Tachibana, K., Hirota, S., Iizasa, H., Yoshida, H., Kawabata, K., Kataoka, Y., Kitamura, Y., Matsushima, K., Yoshida, N., Nishikawa, S., Kishimoto, T., and Nagasawa, T. (1998) The chemokine receptor CXCR4 is essential for vascularization of the gastrointestinal tract. *Nature 393*, 591-4.

(9) Knaut, H., Werz, C., Geisler, R., Nusslein-Volhard, C., and Consortium., T. S. (2003) A zebrafish homologue of the chemokine receptor Cxcr4 is a germ-cell guidance receptor. *Nature 421*, 279-82.

(10) Ma, Q., Jones, D., Borghesani, P. R., Segal, R. A., Nagasawa, T., Kishimoto, T., Bronson, R. T., and Springer, T. A. (1998) Impaired B-lymphopoiesis, myelopoiesis, and derailed cerebellar neuron migration in CXCR4- and SDF-1-deficient mice. *Proc Natl Acad Sci U S A 95*, 9448-53.

(11) Zou, Y. R., Kottmann, A. H., Kuroda, M., Taniuchi, I., and Littman, D. R. (1998) Function of the chemokine receptor CXCR4 in haematopoiesis and in cerebellar development. *Nature 393*, 595-9.

(12) Muller, A., Homey, B., Soto, H., Ge, N., Catron, D., Buchanan, M. E., McClanahan, T., Murphy, E., Yuan, W., Wagner, S. N., Barrera, J. L., Mohar, A., Verastegui, E., and Zlotnik, A. (2001) Involvement of chemokine receptors in breast cancer metastasis. *Nature 410*, 50-6.

(13) Burger, J. A., Burger, M., and Kipps, T. J. (1999) Chronic lymphocytic leukemia B cells express functional CXCR4 chemokine receptors that mediate spontaneous migration beneath bone marrow stromal cells. *Blood 94*, 3658-67.

(14) Juarez, J., Bradstock, K. F., Gottlieb, D. J., and Bendall, L. J. (2003) Effects of inhibitors of the chemokine receptor CXCR4 on acute lymphoblastic leukemia cells in vitro. *Leukemia 17*, 1294-300.

(15) Rubin, J. B., Kung, A. L., Klein, R. S., Chan, J. A., Sun, Y., Schmidt, K., Kieran, M. W., Luster, A. D., and Segal, R. A. (2003) A small-molecule antagonist of CXCR4 inhibits intracranial growth of primary brain tumors. *Proc Natl Acad Sci U S A 100*, 13513-8.

(16) Phillips, R. J., Burdick, M. D., Lutz, M., Belperio, J. A., Keane, M. P., and Strieter, R. M. (2003) The stromal derived factor-1/CXCL12-CXC chemokine receptor 4 biological axis in non-small cell lung cancer metastases. *Am J Respir Crit Care Med. 167(12)*, 1676-86.

(17) Cooper, C. R., Chay, C. H., Gendernalik, J. D., Lee, H. L., Bhatia, J., Taichman, R. S., McCauley, L. K., Keller, E. T., and Pienta, K. J. (2003) Stromal factors involved in prostate carcinoma metastasis to bone. *Cancer. 97(3 Suppl)*, 739-47.

(18) Berson, J. F., Long, D., Doranz, B. J., Rucker, J., Jirik, F. R., and Doms, R. W. (1996) A seven-transmembrane domain receptor involved in fusion and entry of T-cell-tropic human immunodeficiency virus type 1 strains. *J Virol. 70(9)*, 6288-95.

(19) Marshall, G. R. (2001) Peptide interactions with G-protein coupled receptors. *Biopolymers 60(3)*, 246-77.

(20) Slupsky, C. M., Sykes, D. B., Gay, G. L., and Sykes, B. D. (2001) The HoxB1 hexapeptide is a prefolded domain: implications for the Pbx1/Hox interaction. *Protein Sci. 10(6)*, 1244-53.

(21) Booth, V., Slupsky, C. M., Clark-Lewis, I., and Sykes, B. D. (2003) Unmasking ligand binding motifs: identification of a chemokine receptor motif by NMR studies of antagonist peptides. *J Mol Biol. 327*, 329-34.

(22) Sachpatzidis, A., Benton, B. K., Manfredi, J. P., Wang, H., Hamilton, A., Dohlman, H. G., and Lolis, E. (2003) Identification of allosteric peptide agonists of CXCR4. *J Biol Chem. 278*, 896-907.

(23) Heveker, N., Montes, M., Germeroth, L., Amara, A., Trautmann, A., Alizon, M., and Schneider-Mergener, J. (1998) Dissociation of the signalling and antiviral properties of SDF-1-derived small peptides. *Curr Biol. 8*, 369-76.

(24) De Clercq, E. (2003) The bicyclam AMD3100 story. *Nat Rev Drug Discov.*, 581-7.

(25) Wuthrich, K. (1986) *NMR of Proteins and Nucleic Acids*, John Wiley & Sons, New York.

(26) Elisseeva, E. L., Slupsky, C. M., Crump, M. P., Clark-Lewis, I., and Sykes, B. D. (2000) NMR studies of active N-terminal peptides of stromal cell-derived factor-1. Structural basis for receptor binding. *J Biol Chem. 275*, 26799-805.

(27) Wishart, D. S., Sykes, B. D., and Richards, F. M. (1991) Relationship between nuclear magnetic resonance chemical shift and protein secondary structure. *J Mol Biol. 222*, 311-33.

(28) Fairbrother, W. J., McDowell, R. S., and Cunningham, B. C. (1994) Solution conformation of an atrial natriuretic peptide variant selective for the type A receptor. *Biochemistry 33*, 8897-904.

(29) Wishart, D. S., Bigam, C. G., Holm, A., Hodges, R. S., and Sykes, B. D. (1995) 1H, 13C and 15N random coil NMR chemical shifts of the common amino acids. I. Investigations of nearest-neighbor effects. *J Biomol NMR. 5*, 67-81.

(30) Merutka, G., Dyson, H. J., and Wright, P. E. (1995) 'Random coil' 1H chemical shifts obtained as a function of temperature and trifluoroethanol concentration for the peptide series GGXGG. *J Biomol NMR. 5*, 14-24.

(31) Kelley, L. A., Gardner, S. P., and Sutcliffe, M. J. (1996) An automated approach for clustering an ensemble of NMR-derived protein structures into conformationally related subfamilies. *Protein Eng. 9*, 1063-5.

(32) Crump, M. P., Gong, J. H., Loetscher, P., Rajarathnam, K., Amara, A., Arenzana-Seisdedos, F., Virelizier, J. L., Baggiolini, M., Sykes, B. D., and Clark-Lewis, I. (1997) Solution structure and basis for functional activity of stromal cell-derived factor-1; dissociation of CXCR4 activation from binding and inhibition of HIV-1. *EMBO J. 16*, 6996-7007.

(33) Pappu, R. V., Srinivasan, R., and Rose, G. D. (2000) The Flory isolated-pair hypothesis is not valid for polypeptide chains: implications for protein folding. *Proc Natl Acad Sci U S A 97*, 12565-70.

(34) Baldwin, R. L., and Rose, G. D. (1999) Is protein folding hierarchic? I. Local structure and peptide folding. *Trends Biochem Sci 24*, 26-33.

(35) Dyson, H. J., and Wright, P. E. (2005) Intrinsically unstructured proteins and their functions. *Nat Rev Mol Cell Biol 6*, 197-208.

(36) Baldwin, R. L., and Rose, G. D. (1999) Is protein folding hierarchic? II. Folding intermediates and transition states. *Trends Biochem Sci 24*, 77-83.

(37) Dyson, H. J., and Wright, P. E. (2002) Coupling of folding and binding for unstructured proteins. *Curr Opin Struct Biol 12*, 54-60.

(38) Wright, P. E., Dyson, H. J., and Lerner, R. A. (1988) Conformation of peptide fragments of proteins in aqueous solution: implications for initiation of protein folding. *Biochemistry 27*, 7167-75.

(39) Daggett, V., and Fersht, A. (2003) The present view of the mechanism of protein folding. *Nat Rev Mol Cell Biol 4*, 497-502.

(40) Dobson, C. M., and Karplus, M. (1999) The fundamentals of protein folding: bringing together theory and experiment. *Curr Opin Struct Biol 9*, 92-101.

(41) Jones, S., and Thornton, J. M. (1996) Principles of protein-protein interactions. *Proc Natl Acad Sci U S A. 93*, 13-20.

(42) Rosenkilde, M. M., Gerlach, L. O., Jakobsen, J. S., Skerlj, R. T., Bridger, G. J., and Schwartz, T. W. (2004) Molecular mechanism of AMD3100 antagonism in the CXCR4 receptor: transfer of binding site to the CXCR3 receptor. *J Biol Chem. 279*, 3033-41.

(43) Trent, J. O., Wang, Z. X., Murray, J. L., Shao, W., Tamamura, H., Fujii, N., and Peiper, S. C. (2003) Lipid bilayer simulations of CXCR4 with inverse agonists and weak partial agonists. *J Biol Chem. 278*, 47136-44.

(44) Doranz, B. J., Grovit-Ferbas, K., Sharron, M. P., Mao, S. H., Goetz, M. B., Daar, E. S., Doms, R. W., and O'Brien, W. A. (1997) A small-molecule inhibitor directed against the chemokine receptor CXCR4 prevents its use as an HIV-1 coreceptor. *J Exp Med. 186*, 1395-400.

(45) Johnson, B. A., and Blevins, R. A. (1994) NMRView: A computer program for the visualization and analysis of NMR data. *J Biomol NMR 4*, 603-614.

(46) Choy, W. Y., and Forman-Kay, J. D. (2001) Calculation of ensembles of structures representing the unfolded state of an SH3 domain. *J Mol Biol 308*, 1011-32.

(47) Tamamura, H., Hiramatsu, K., Miyamoto, K., Omagari, A., Oishi, S., Nakashima, H., Yamamoto, N., Kuroda, Y., Nakagawa, T., Otaka, A., and Fujii, N. (2002) Synthesis and evaluation of pseudopeptide analogues of a specific CXCR4 inhibitor, T140: the insertion of an (E)-alkene dipeptide isostere into the betaII'-turn moiety. *Bioorg Med Chem Lett 12*, 923-8.

(48) Crump, M. P., Elisseeva, E., Gong, J., Clark-Lewis, I., and Sykes, B. D. (2001) Structure/function of human herpesvirus-8 MIP-II (1-71) and the antagonist N-terminal segment (1-10). *FEBS Lett 489*, 171-5.

(49) Brunger, A. T., Adams, P. D., Clore, G. M., DeLano, W. L., Gros, P., Grosse-Kunstleve, R. W., Jiang, J. S., Kuszewski, J., Nilges, M., Pannu, N. S., Read, R. J., Rice, L. M., Simonson, T., and Warren, G. L. (1998) Crystallography & NMR system: A new software suite for macromolecular structure determination. *Acta Crystallogr D Biol Crystallogr. 54*, 905-21.

(50) Laskowski, R. A., MacArthur, M. W., Moss, D. S., and Thornton, J. M. (1993) PROCHECK: a program to check the stereochemical quality of protein structures. *J Appl Cryst 26P*, 283-291.

APPENDIX D

Dimerization of SDF-1α studied by NMR relaxation methods*

Outline

The structures of SDF-1α determined by NMR spectroscopy have been shown to be monomeric while X-ray structures are dimeric. Biochemical data and *in vivo* studies suggest that dimerization is likely to be important for the function of chemokines. We determined the dynamics of SDF-1α using the backbone ^{15}N NMR relaxation methods. Data were obtained at several concentrations of SDF-1α and used to determine K_d of ~5 mM for a monomer-dimer equilibrium. K_d obtained was used to extrapolate relaxation data to monomeric SDF-1α. Experimental and extrapolated data were analyzed using Model Free approach. Effects of protein dimerization on relaxation parameters are discussed. Our results help rationalize the apparent discrepancies between solution NMR structures obtained under different conditions, clearly indicating the importance of the knowledge of oligomerization degree in the calculation of solution structures.

Introduction

SDF-1α is a member of the chemokine family, which is responsible for the trafficking of lymphocytes and numerous reactions in the immune system (*1*, *2*). SDF-1α is particularly interesting due to its involvement in HIV pathogenesis (*3*) and in a variety of cancers (*4-8*). It is generally expected that the inhibition of the interaction of SDF-1α with its receptor CXCR4 will be an important therapeutic breakthrough that will reduce the propagation rate of a variety of cancers and HIV-1 (*9*). SDF-1α exerts its biological function through interaction with the G-protein coupled receptor, CXCR4, in two steps. The first step includes the recruitment of a chemokine from solution and the second step involves the insertion of the SDF-1α N-terminus into the seven-helix bundle of the receptor and the initiation of a signaling cascade (*10*).

The interaction of a chemokine with its receptor can be modulated in several ways. One of them is through the interaction of a chemokine with the components of extracellular matrix such as glycosaminoglycans. These have a noticeable affinity for chemokines and help to bring the chemokines from bulk solution and concentrate them in

---

* The version of this chapter was published. Baryshnikova O.K., and Sykes B.D. (2006) *Prot Sci* 15, 2568-2578.

the proximity to membrane surface (*11*). Another possible way to modulate chemokine signaling is through multivalency, which is a well-known strategy employed by nature (*12*). Multivalency leads to the increase in the local concentration of a ligand on a surface and hence increases the observed affinity for its receptor. Several chemokines are known to exist as oligomers in concentrated solutions (*13*). If chemokines are also oligomeric *in vivo* at physiological concentrations, this might enhance the efficiency of recruitment and bring an additional level of regulation of signaling. Some *in vivo* studies suggested that dimerization is not required for the activation of a receptor (for example, IL-8) (*14*). Other studies demonstrated that at least in certain cases the ability of chemokines to dimerize influences the magnitude of signaling efficiency (for example, CCL2, CCL4 and CCL5) (*15*).

The oligomerization behavior of SDF-1α *in vitro* in terms of monomer-dimer equilibrium is controversial. The first NMR structure reported by Crump and coworkers characterized SDF-1α as a monomer under experimental conditions based on the following observations: no NOE contacts corresponding to a dimer interface were found; no slowly exchanging protons at the dimer interface were observed; and the molecular weights obtained with sedimentation equilibrium centrifugation were consistent with that expected for the monomeric species (*10*). In the two reported crystal structures SDF-1α was dimeric, with the dimer interface similar to the interface formed by IL-8 (*16, 17*). The original NMR structure of SDF-1α determined by Crump and coworkers (*10*) was slightly different from the structures of determined by crystallography, especially in the position of the C-helix. The most recent NMR structure of SDF-1α (*18*) determined under different experimental conditions was instead very similar to the individual subunits of SDF-1α in the crystal structure. The dimerization of SDF-1α can account for differences between these structures.

Monomer-dimer equilibrium for SDF-1α has been characterized by several biophysical methods, including solution state NMR, with K_d values in the range of ~150 μM to ~3 mM (*19, 20*). In the study by Veldkamp et al., special emphasis was drawn to the role of experimental conditions, e.g. pH and buffer content, on the monomer-dimer equilibrium (*20*). Given that oligomerization of chemokines may be crucial for enhancement of signaling by increasing the affinity of the chemokine-receptor interaction, a thorough investigation of the nature of SDF-1α oligomerization is important.

Results

^{15}N-T_1, T_2, and NOE data

Backbone amide ^{15}N relaxation parameters were obtained using 2D {^{1}H, ^{15}N} correlation NMR spectroscopy with a typical spectrum of 1.5 mM SDF-1α shown in Figure D-1. Backbone ^{15}N and ^{1}H chemical shifts for SDF-1α were assigned using 3D NOESY-HSQC and 3D TOCSY-HSQC spectra (*21*), and were in good agreement with ^{1}H chemical shifts obtained previously using homonuclear 2D NMR spectroscopy (*10*). ^{1}H chemical shifts were found to be dependent on protein concentration. Relaxation properties were determined for 56 of the 67 backbone amide ^{1}H-^{15}N pairs. Residues that could not be analyzed include: Lys^1, due to exchange with solvent; Phe^{13} and Cys^{34}, whose chemical shifts overlap; Pro^2, Pro^{10}, Pro^{32} and Pro^{53} lacking backbone amide protons; Leu^{26}, due to line broadening; and Gln^{37}, whose chemical shifts were not assigned. In several cases, Tyr^{61}, Leu^{62}, Phe^{14}, and Val^4 were excluded due to peak overlap. In most diluted samples, resonances for Phe^{13} and Cys^{34} could be discriminated and were therefore included in the analysis.

^{15}N-T_1, T_2, and NOE data for a sample of 1.5 mM recombinant ^{15}N labeled SDF-1α were obtained at 500 and 600 MHz, and 30 °C (Table D-1, Fig. D-2). The average NOE^{600}/NOE^{500} ratio was 1.04 ± 0.20 (Fig. D-2d). T_1^{500} and T_1^{600} followed similar per residue patterns with average T_1^{600}/T_1^{500} = 1.29 ± 0.07 (Fig. D-2e). T_2^{500} and T_2^{600} also showed similar per residue patterns with average T_2^{600}/T_2^{500} = 0.87 ± 0.06 (Fig. D-2f).

The N- and C-terminal regions (residues 3-8 and 62-67) of SDF-1α were more flexible than the protein core (Fig. D-2). This was in agreement with the unstructured N-terminus in NMR structure and the lack of electron density in X-ray structures (*10, 17*). Residues 23-27 and 30-31 had NOE's and T_2's lower than the average and may be more flexible than the protein core. However, the per residue profile for T_1/T_2 ratios (Fig. D-2g) shows an increase in this region, suggesting the presence of chemical exchange. Regions of residue 36-42, 49-51, and 65-67 had also high T_1/T_2's and low T_2's indicative of chemical exchange.

Concentration dependence of ^{15}N-T_2 values

Theoretical values for monomeric SDF-1α are T_2^{500}=176 ms and T_2^{600}=181 ms (S^2 = 0.85 (*22*), and τ_m = 3.9 ns) (*23*) (in-house script written by Stéphane Gagné). These values are significantly larger than experimental T_2^{500} of 109 ms and T_2^{600} of 130 ms. For

dimeric SDF-1α, theoretical values were T_2^{500}=102 ms and T_2^{600}=107 ms. Thus in fast exchange limit, SDF-1α in solution is likely to be partially dimeric, which resulted in a decrease of experimental T_2's. To explore this further, we measured T_2^{500} for a range of concentrations (2.6, 1.5, 0.9, 0.5, and 0.3 mM). The data shows a clear dependence of T_2^{500} on concentration, with the lowest T_2^{500} value observed for the most concentrated sample (Fig. D-3). This dependence is also highlighted in the plot of average R_2^{500} ($1/T_2^{500}$) for the core residues of SDF-1α as a function of concentration (Fig. D-4). Core residues included 15, 16, 18-22, 33, 35, 39, 41-43, 46, 50, 52, and 54-60.

Table D-1. NMR relaxation measurements obtained for 1.5 mM SDF-1α.

Frequency (MHz)	T_1 (all residues)	T_2 (all residues)	T_1 (protein core)[a]	T_2 (protein core)	NOE (all residues)	NOE (protein core)
500	446 ± 71[b]	130 ± 91[d]	432 ± 41[f]	107 ± 22[h]	0.50 ± 0.24	0.68 ± 0.05
600	576 ± 97[c]	109 ± 56[e]	550 ± 50[g]	90 ± 22[i]	0.57 ± 0.24	0.74 ± 0.04

[a] The excluded residues were the following: 3-14, 17, 23-25, 27, 29, 31, 38, 45, 48, 66-67 for the data set acquired at 500 MHz and 3-9, 12, 18, 29-31, 35-36, 64-67 for the data set acquired at 600 MHz. Residues were excluded if NOE^{500}<0.60 and NOE^{600}<0.65. [b] An average error of fitting was 15 ms. [c] An average error of fitting was of 32 ms. [d] An average error fitting was of 3 ms. [e] An average error of fitting was 6 ms. [f] An average error of fitting was 12 ms. [g] An average error of fitting was 25 ms. [h] An average error of fitting was 2 ms. [i] An average error of fitting was 4 ms.

Observed transverse relaxation rate R_2^{obs} can be written in terms of dimerization as following:

$$R_2^{obs} = f_m R_2^m + 2 f_d R_2^d \qquad (1),$$

where R_2^m and R_2^d are related to pure monomer and dimer, respectively, and the fractions of monomers and dimers are:

$$f_m = \frac{[mon]}{P_{total}} \quad \text{and} \quad f_d = \frac{[dim]}{P_{total}} \qquad (2).$$

Total concentration of the protein is:

$$P_{total} = [mon] + 2[dim] \qquad (3).$$

Substitution of eq.2 and eq.3 into eq.1 yields:

$$R_2^{obs} = \frac{[mon]}{P_{total}} R_2^m + 2\frac{[dim]}{P_{total}} R_2^d \qquad (4).$$

Concentrations of monomers and dimers can be derived by solving eq. 3 and the equation for K_d:

$$[mon] = \frac{1}{4}(-K_d + \sqrt{K_d}\sqrt{K_d + 8P_{total}}) \qquad (5),$$

$$[dim] = \frac{1}{8}(K_d + 4P_{total} - \sqrt{K_d}\sqrt{K_d + 8P_{total}}) \qquad (6).$$

Substitution of eq.6 and eq.7 into eq.4 and simplification yields

$$R_2^{obs} = \frac{(K_d(R_2^d - R_2^m) + 4R_2^d P_{total} + \sqrt{K_d}(R_2^m - R_2^d)\sqrt{K_d + 8P_{total}})}{4P_{total}} \qquad (7).$$

Experimental R_2 data were fit to eq.7 (www.pence.ca/~software) yielding the following best fit parameters: K_d = 9 mM, R_2^m = 7 s^{-1} and R_2^d = 18 s^{-1} (Fig. D-4). The quality of the fit at lower concentrations was significantly better. We also evaluated K_d using other methods as described below to obtain a more reliable value.

Dimerization constant calculated using 1D ^{1}H NMR spectroscopy

Chemical shifts are sensitive to changes in molecular structure and local environment. Chemical shifts obtained from 1D ^{1}H spectra offer advantages of being very accurate, since the resolution in 1D ^{1}H experiment at 500 MHz is normally below 1 Hz. However, due to peak overlap, only a few resonances can be easily traced. Changes in chemical shifts as a function of SDF-1α concentration for clearly distinguishable peaks (indole NH of Trp^{57}, 2,6H and 3,5H of Tyr^7, and 2,6H of Phe^{13} and Phe^{14}) were fit to eq.8 derived similarly to eq.7:

$$\sigma = \sigma_m f_m + 2\sigma_d f_d = \sigma_m \frac{[mon]}{P_{total}} + 2\sigma_d \frac{[dim]}{P_{total}} \qquad (8),$$

where σ_m and σ_d are chemical shifts for monomer and dimer. The average K_d was 5 ± 1 mM (Table D-2, Fig D-5a)

Dimerization constant calculated using 2D {^{1}H, ^{15}N} HSQC NMR spectroscopy

Chemical shift changes as a function of SDF-1α concentration were also followed with 2D {^{1}H, ^{15}N} HSQC NMR spectra. The resolution for the ^{1}H dimension in these spectra was ~20 Hz, which is significantly less than in 1D ^{1}H spectra. However, chemical shifts for a larger number of peaks could be traced. Data was fit to eq.8 (Table D-2, Fig. D-5b) with the average K_d of 7 ± 4 mM.

Table D-2. The values of dissociation constant as determined by chemical shift changes in 1D and 2D HSQC spectroscopy for indicated residues.

Residue	K_d values as estimated by chemical shifts changes in 1D spectra	Residue	K_d values as estimated by chemical shifts changes in 2D HSQC spectra
2,6 H Tyr^7	4.7 ± 3.9	Ala^{19}	10.9 ± 3.7
3,5 H Tyr^7	4.7 ± 3.9	Val^{23}	9.8 ± 12.8
2,6 Phe^{13}	7.3 ± 5.8	Ile^{38}	3.1 ± 3.6
2,6 Phe^{14}	4.7 ± 3.9	Val^{39}	9.7 ± 7.4
indole H of Trp^{57}	5.2 ± 3.1	Leu^{42}	2.1 ± 2.3
		Cys^{50}	13.4 ± 8.5
		Ile^{51}	3.0 ± 1.2
		Asp^{52}	6.1 ± 5.1
		Leu^{55}	5.5 ± 7.6
		Trp^{57}	6.0 ± 1.7
		Glu^{60}	6.1 ± 6.9
	average 5 ± 4		average 7 ± 5

Extrapolation of per residue T_1^{500} and T_2^{500} values to infinite dilution

Per residue T_2^{500} and T_1^{500} at infinite dilution were obtained using eq.7 and K_d of 5 mM. Datasets used for extrapolation included T_2^{500} data for 2.6, 1.5, 0.9, 0.5, and 0.3 mM SDF-1α, and T_1^{500} data for 2.6, 1.5, 0.9 and 0.3 mM SDF-1α. The average for extrapolated data for protein core was: T_2^{500} = 158 ± 24 ms (Fig. D-6a) and T_1^{500} = 364 ± 40 ms (Fig. D-6b), which is close within determined errors to the theoretical values for monomeric SDF-1α, which are 388 ms for T_1^{500} and 181 ms for T_2^{500}. Extrapolated T_2 and T_1 followed the same per residue trend as the experimentally obtained T_2^{500} and T_1^{500} (Fig. D-2).

Model free analysis of backbone dynamics

Backbone amide ^{15}N-T_1, T_2, and NOE datasets acquired at 500 and 600 MHz for 1.5 mM and 0.3 mM SDF-1α were examined by model free analysis. This approach affords the interpretation of relaxation data in terms of the overall correlation time, generalized order parameters, and local motions (*23, 24*). The overall tumbling of SDF-1α was assumed to be isotropic, given that rotational diffusion anisotropy was found to be negligible in previous backbone ^{15}N relaxation studies of monomeric chemokines (*25, 26*) and the dimeric chemokine, IL-8 (*27*). Overall correlation times determined using T_1, T_2, and NOE data (*28*) were the following: τ_m^{500} = 6.79 ns and τ_m^{600} = 7.24 ns for 1.5 mM

SDF-1α, and τ_m^{500} = 5.04 ns and τ_m^{600} = 7.17 ns for 0.3 mM SDF-1α. These values appeared to be overestimated in comparison to the expected values for monomeric SDF-1α (7.8 kDa), even for the most diluted sample where the fraction of dimer is ~5%. This observation is consistent with previous studies, where even the slight dimerization/aggregation can influence the interpretation of relaxation data (*29*). τ_m^{500} was also determined using extrapolated T_1^{500} and T_2^{500}, and NOE^{500} data for 1.5 mM SDF-1α (used due to unchanged NOE^{500} spectra and minimal error). τ_m^{500} obtained in this manner was 4.42 ns.

Generalized order parameters (S^2), chemical exchange terms (R_{ex}), and correlation times (τ_m and τ_s) are obtained from five different dynamic models in Lipari-Zhabo formalism (*23, 30*). Average S^2 was equal to 0.77 ± 0.04 (500 MHz) and 0.81 ± 0.05 (600 MHz) for 1.5 mM SDF-1α; 0.79 ± 0.09 (500 MHz) and 0.86 ± 0.07 (600 MHz) for 0.3 mM SDF-1α; and 0.77 ± 0.09 for the extrapolated dataset (Fig. D-7). S^2 for the core residues were 0.81 ± 0.03 (500 MHz) and 0.87 ± 0.03 (600 MHz) for 1.5 mM SDF-1α; 0.87 ± 0.07 (500 MHz) and 0.91 ± 0.06 (600 MHz) for 0.3 mM SDF-1α; and 0.83 ± 0.07 for the extrapolated dataset. Residues in the unstructured regions, the N- and C-termini and loops, displayed smaller values of S^2, indicating larger amplitudes of motions. Experimental error in relaxation measurements increased with SDF-1α dilution as a result of decreasing signal to noise ratio. Average S^2 was slightly smaller for the extrapolated dataset, but similar to average experimental S^2 for 1.5 and 0.3 mM SDF-1α (Fig. D-7).

Values for R_{ex} typically indicate the presence of chemical exchange. The trend for R_{ex} shows the highest values for regions of residues 23-31, 36-40, 50-51, and at the C-terminus (Fig. D-8). Residues with the largest R_{ex} are directly involved in the formation of dimer interface (*16, 17*). R_{ex} terms decreased upon dilution from ~20 s^{-1} for 1.5 mM SDF-1α to ~10 s^{-1} for 0.3 mM SDF-1α. R_{ex} terms were also present in extrapolated case for residues 17, 20 (the N-terminus), 24, 27, 28, 30 (the first β strand), 36, 38, 40 (the second β strand), 50-51 (the third β strand) and 64 (the C-terminal helix). If the rate of interconversion of exchanging species is fast relative to the chemical shift difference, the value of $R_{ex}^{600}/R_{ex}^{500}$ should be equal to $600^2/500^2$, or 1.44. Residues with $R_{ex}^{600}/R_{ex}^{500}$ values within the range 1.44 ± 0.28 (20% of error) included 23, 25, 27, 28, 50, and 65 for 1.5 mM SDF-1α, and 25, 27, 28, 29, 38, 41, and 65 for 0.3 mM SDF-1α.

Discussion

SDF-1α exists in monomer-dimer equilibrium

Experimental relaxation data demonstrates the existence of monomer-dimer equilibrium for SDF-1α. Proton chemical shifts observed in both 1D and 2D NMR experiments, and per residue transverse relaxation rates, R_2, demonstrated a dependence on the concentration of SDF-1α. Determined K_d of 5 ± 1 mM indicates a weaker self-association than previously reported (*19*), and agrees with the K_d dependence on buffer composition (*20*). In our study, the buffer was of low ionic strength, containing only 20 mM acetate and negligibly small amounts of azide and chloride. This buffer was optimized previously to minimize dimerization (*10*). High ionic strength buffers are expected to neutralize the positively charged residues on the first β-sheet of SDF-1α (Lys^{24}, His^{25}, Lys^{27}), reducing the repulsion between monomers, and favoring dimer formation (*20*). In our experiments, the percentage of dimer was 27.4% in the most concentrated sample (2.6 mM SDF-1α), 19.2% and 5.2% in the sample containing 1.5 mM and 0.3 mM SDF-1α, respectively.

Model free analysis

Protein dimerization often complicates the interpretation of relaxation measurements (*31, 32*), causing significant overestimations of the generalized order parameter and internal motions, as shown by simulations (*29*). The model free analysis, appropriate for the interpretation of relaxation data of purely monomeric or dimeric species, is not strictly suitable if both species are present in substantial quantities. There are a number of approaches that account for monomer-dimer equilibrium in model free analysis (*33-36*). One of them presents relaxation data only qualitatively (*36*). Another requires approximations such as equivalent local motions for both dimeric and monomeric species (*33*). We have extrapolated relaxation parameters to infinite dilution to obtain T_1 and T_2 for monomeric species, similarly to the approach of Pfuhl and coworkers, who extrapolated their data to infinite dilution where only a pure dimer existed (*34*). Model free analysis was performed on datasets obtained for two different concentrations of SDF-1α and on a dataset extrapolated to infinite dilution. The value of the overall correlation time for SDF-1α decreased with the decreasing fraction of dimer, as previously observed (*33, 34, 37*). The value of 4.42 ns for τ_m^{500} obtained using extrapolated dataset was reasonable for a 7.8 kDa protein containing flexible termini. This is consistent with hydrodynamic calculations performed on the dynamin pleckstrin

homology (PH) domain, where the presence of flexible tail slightly decreased the rate of overall rotational tumbling (*33*).

Generalized order parameters obtained for 1.5 and 0.3 mM SDF-1α, and for the extrapolated dataset showed similar trends with the N-terminus (residues 1-9) and the C-terminus (residues 63-67) being flexible. S^2 can be substantially overestimated for proteins that self-associate (*29*). However, the results presented in our work were similar to the results of previous experiments (*34*) and showed that the increases in S^2 in the presence of dimerization was not drastic.

Interestingly, residues 8-12 have been suggested to interact with the cognate SDF-1α receptor (*16*, *38*). The N-terminus of SDF-1α (residues 1-17) adopts an extended conformation with two cysteines, Cys^9 and Cys^{11}, constraining the region 8-12 by the two disulphide bonds Cys^9-Cys^{34} and Cys^{11}-Cys^{50}. S^2 values of 0.91 ± 0.09 and 0.87 ± 0.1 for Cys^{11} and Arg^{12} indicate that the flexibility of this region is restricted on the ps timescale. For comparison, the average S^2 value for Arg^8 was found to be 0.43 ± 0.05. Restriction of flexibility within this region may contribute favorably to the energy of the interaction with a receptor.

The number of residues requiring R_{ex} terms to properly account for relaxation data and the magnitude of R_{ex} terms showed a clear dependence on protein concentration similarly to reported data (*34*). This dependence was not linear, as expected from theoretical (*39*) and experimental (*40*) studies. Given that relaxation data for residues 25, 26, and 29 were missing due to the line broadening or due to the poor quality of extrapolations, it is possible that the entire first β-strand is involved in the conformational exchange. The second set of residues with R_{ex} terms was mapped to the second β-strand, the third β-strand, and the C-terminus. Residues belonging to the first β-strand and the C-helix directly participate in the formation of dimer interface. Residues with R_{ex} terms in the second and third β-strands interact directly with the residues comprising interface.

In the absence of monomer-dimer exchange, e.g. in the purely monomeric case, some residues still required R_{ex} terms in the model free analysis. These are generally the same residues involved in dimerization (Fig. D-9), and must reflect conformational flexibility within the monomer. The mechanism consistent with this data is:

$$M \Leftrightarrow M^*$$

$$M^* + M^* \Leftrightarrow D$$

where M represents a conformation of the monomer less prone to dimerization, M* a conformation more prone to dimerization, and D is the dimer. Such a mechanism would help explain the apparent discrepancies in the solution structures of SDF-1α determined by NMR. The NMR structure determined by Gozansky et al. (*18*) is similar to dimeric structures determined using X-ray crystallography (*16, 17*), and would represent the species M*; whereas the Crump et al. structure (*10*) would represent the species M. The phosphate buffer used by Gozansky et al. is expected to favor dimerization as compared to the acetate buffer used by Crump et al. (*20*).

Comparison with other chemokines and implications for receptor interaction

Chemokines were found to undergo dimerization using two major subclasses of binding modes. The first group dimerizes in a fashion similar to IL-8, utilizing residues on the first β-strand to establish the dimer interface, and the second group dimerizes similar to vMIP-I, utilizing residues from N-terminal loops (*41*). It would be interesting to compare the parameters obtained from relaxation measurements, especially R_{ex} terms, with respect to the different dimerization modes utilized by chemokines. In case of IL-8, which exists predominantly in dimeric form, the existence of monomer-dimer equilibrium resulted in line broadening in the regions of residues that make intersubunit contacts, even if the concentration of a monomer was negligible (*27*). In the case of eotaxin, eotaxin-2, and eotaxin-3 (*25, 42, 43*), the information about dimer interface is lacking and therefore, R_{ex} terms cannot be ascribed to self-association. In case of fractalkine, residues involved in crystal packing and those with R_{ex} terms are partially overlapped (*26*). These studies suggest a correlation between oligomerization behavior of proteins and the requirement for R_{ex} terms to account for the relaxation data. The detailed studies of relaxation and its concentration dependence for larger protein groups might be interesting.

The biological relevance of chemokine oligomerization may differ among the various members of the chemokine family that includes more than 60 members with a broad range of oligomerization behavior. The dependence of SDF-1α dimerization on pH and buffer composition was studied recently (*20*). SDF-1α, with a physiological concentration of 25-50 ng/ml (*44*) and a dimerization constant from ~150 μM in PBS buffer (*19*) to ~5 mM in acetate buffer (in our work), is unlikely to dimerize under physiological conditions. However, high ionic strength and interactions between SDF-1α and glycosaminoglycans at the cell surface can increase the fraction of dimeric SDF-1α.

Therefore it is reasonable to expect that SDF-1α *in vivo* can function both as a monomer and as a dimer under certain conditions. The intrinsic ability of SDF-1α to dimerize, and the interplay with the cell surface environment may play role in modulating the interaction of SDF-1α with its cognate receptor.

Materials and Methods

Protein expression and purification

The DNA encoding human SDF-1α (residue 1-67) was purchased from InvivoGen and subcloned into the pET-3a expression vector from Novagen. *E. coli* strain BL21(DE3)pLysS was transformed with the expression vector and incubated at 37 °C to an OD_{600} of 0.6-0.8. Cell cultures were induced with IPTG and harvested after 3 hours. Uniformly ^{15}N-labelled SDF-1α was expressed similarly in a media enriched with ^{15}N ammonium sulfate (*45*). Cell pellet was lysed using French press, centrifuged (10000 rpm, 10 min), homogenized, and solubilized in 8M urea buffer (50 mM Tris, pH 8.0). Homogenate was centrifuged again to remove cell walls and membrane debris (18000 rpm, 1 hour), and applied to a cation exchange CM-Sepharose column (50 mM Tris, pH 8.0). Protein was refolded by overnight dialysis against 10 mM NH_4HCO_3 and the first methionine residue was cleaved with CNBr as described earlier (*46*). The protein was purified on a size exclusion column (Superdex 75), dialyzed against 10 mM NH_4HCO_3, and lyophilized. The molecular weight determined by MALDI mass-spectroscopy was equal to the expected (7831 ± 1 for reduced species). The amino acid composition was confirmed by the amino acid analysis. Biological activity of recombinant SDF-1α was tested in the chemotaxis assay using mice spleenocytes Recombinant SDF-1α demonstrated chemotactic response similar to the commercially available control SDF-1α sample (data not shown).

Sample preparation

NMR samples were prepared in 500 μl of buffer containing 20 mM CD_3COONa, 1 mM NaN_3, and 1 mM DSS in 90% H_2O/10% D_2O. The pH was adjusted to 4.9. The two most concentrated samples were prepared by dissolving the lyophilized powder of recombinant SDF-1α. The rest of the samples were serially diluted from the sample containing 1.5 mM of SDF-1α, where the concentration was verified by amino acid analysis. The concentrations of recombinant SDF-1α analyzed in this work were equal to 2.6, 1.5, 0.9, 0.5, 0.3, and 0.1 mM.

NMR spectroscopy (data acquisition and processing)

All NMR data were acquired at 30 °C on a Varian Inova 500 MHz spectrometer and a Varian Unity 600 MHz spectrometer equipped with z-axis pulsed field gradient triple resonance probes. In order to assign the backbone and side chain ^1H and ^{15}N chemical shifts, 3D NOESY-HSQC, 3D TOCSY-HSQC, and 2D {^1H,^{15}N} HSQC were acquired at 500 MHz for 1.5 mM SDF-1α. Relaxation data were obtained from ^{15}N-T_1, ^{15}N-T_2, and ^1H–^{15}N NOE experiments conducted at 500 and 600 MHz for samples containing 2.6, 1.5, 0.8, 0.5, and 0.3 mM SDF-1α. At 500 and 600 MHz, T_1 data were acquired using relaxation delays of 10, 50, 100, 200, 300, and 400 ms, and T_2 data were acquired using relaxation delays equal to 10, 30, 50, 70, 90, and 110 ms. The delays between transients in T_1 and T_2 experiments were set to 3.5 s for 600 MHz and 2.5 s and 3.5 s in T_1 and T_2 experiments respectively for 500 MHz. A sufficiently long delay

between transients was necessary to prevent sample from heating as previously shown (47). $\{^1H,^{15}N\}$ NOE experiments were conducted using delays of 5 s for spectra recorded without proton saturation at both fields and delays of 2 s for spectra recorded with proton saturation. The proton saturation time was equal to 3 s and the total time between acquisitions was equal to 5 s. In addition, to follow the chemical shift changes as a function of SDF-1α concentration, 1D ^1H spectra and 2D $\{^1H,^{15}N\}$ HSQC spectra were acquired for every sample. Processing of NMR data was accomplished with NMRPipe software. Relaxation parameters T_1 and T_2 were obtained using NMRview and were in agreement with T_1 and T_2 values calculated using Mathematica scripts provided by Leo Spyracopoulos.

Figure D-1. 2D {^{1}H, ^{15}N} HSQC correlation spectrum of 1.5 mM SDF-1α. Assigned residues are indicated on the spectrum with labels. Arginine and glutamaine side chains amide protons as well as the indole NH of Trp^{57} are indicated with an asterisk. The resonance marked with a double asterisk was not assigned.

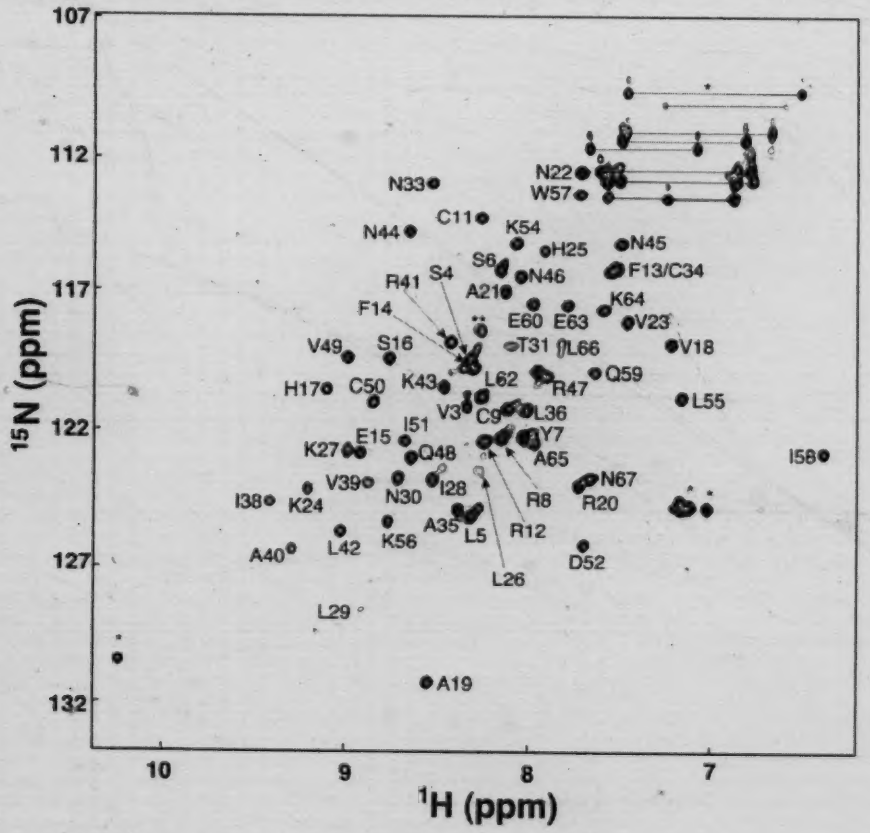

Figure D-2. Relaxation data obtained at two magnetic fields for 1.5 mM SDF-1α. (a) T_1^{600} (O) and T_1^{500} (●), (b) T_2^{600} (O) and T_2^{500}(●), (c) NOE^{600} (O) and NOE^{500} (●), (d) NOE^{600}/NOE^{500} ratio, (e) T_1^{600}/T_1^{500} ratio, (f) T_2^{600}/T_2^{500} ratio, and (g) T_1^{600}/T_2^{600} ratio (✧) and T_1^{500}/T_2^{500} ratio (●). Elements of secondary structure were determined from the coordinates of the crystal structure (*17*).

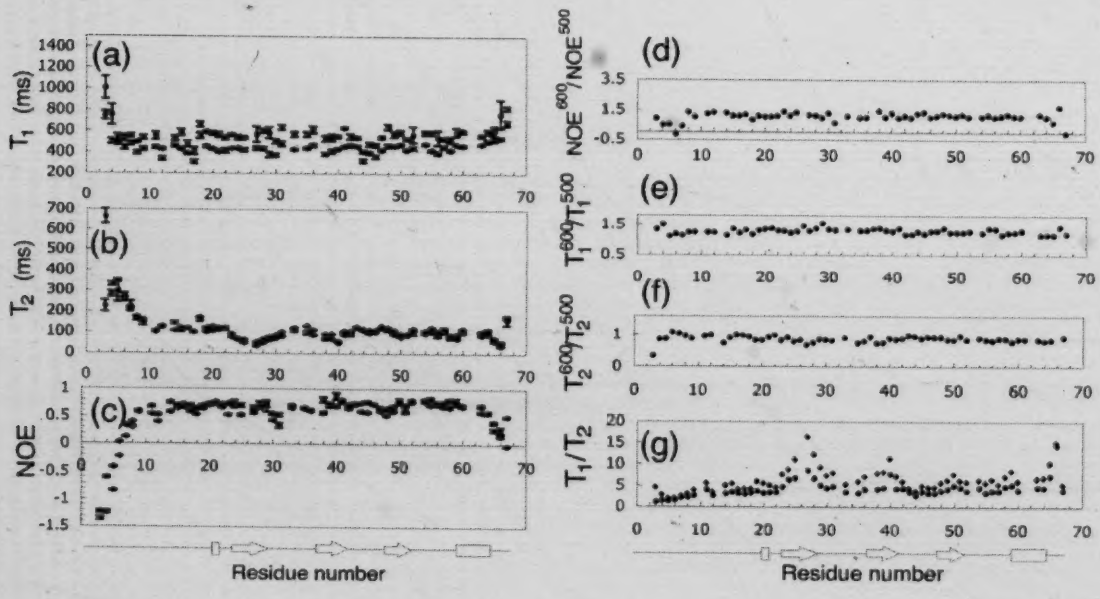

Figure D-3. ^{15}N-T_2^{500} relaxation data for SDF-1α samples containing different concentrations. ^{15}N-T_2^{500} relaxation data is shown for 2.6 mM (●), 0.9 mM (○), and 0.3 mM (▲) SDF-1α. Only three T_2^{500} datasets from a total of five are shown for clarity.

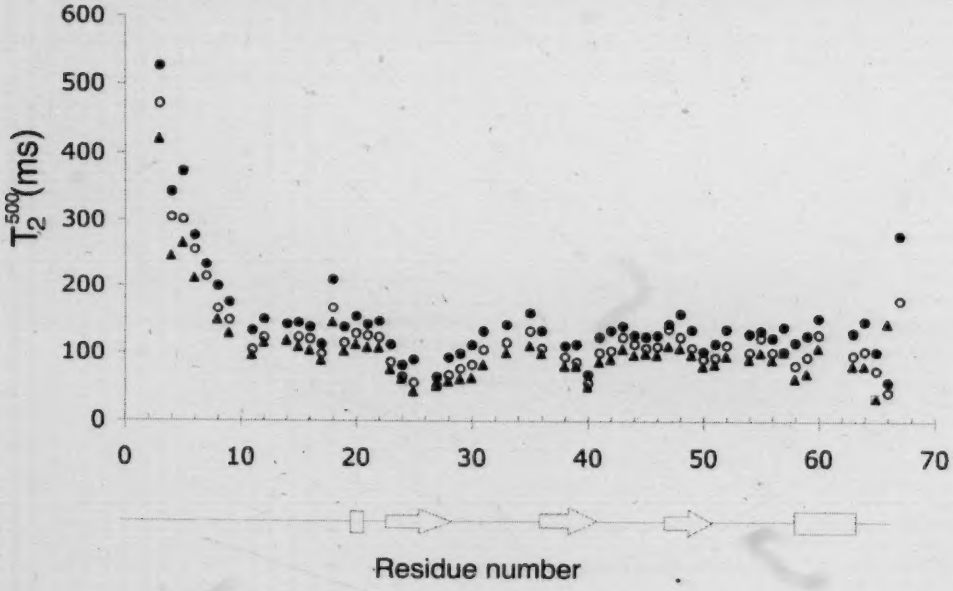

Figure D-4. ^{15}N-R_2^{500} relaxation data obtained for residues in the structured core of SDF-1α. R_2 values were averaged and plotted as a function of the concentration of SDF-1α. The best fit to eq.7 yielded $K_d = 9 \pm 24$ mM, $R_2^m = 7 \pm 1\ s^{-1}$ and $R_2^d = 18 \pm 15\ s^{-1}$.

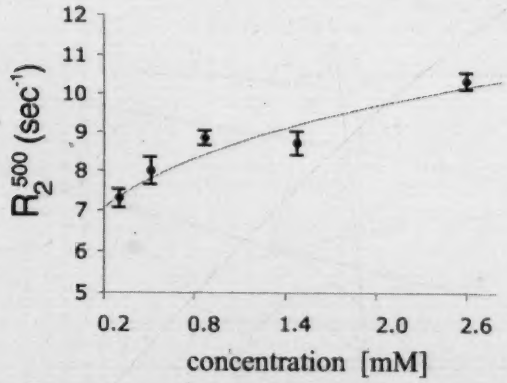

Figure D-5. Chemical shift changes obtained using 1D ^1H (a) and 2D {^1H, ^{15}N} HSQC NMR spectroscopy (b) plotted as a function of SDF-1α concentration for 3,5H of Tyr^7 (●) and 2,6H of Phe^{14} (□) (a) and for Val^{39} (■) and Trp^{57} (●) (b).

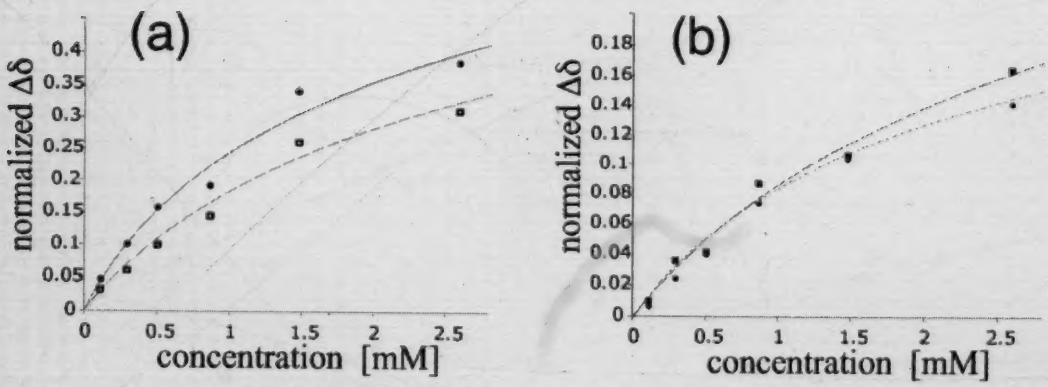

Figure D-6. Relaxation parameters, T_1^{500} (a), T_2^{500} (b), and T_1^{500}/T_2^{500} (c), extrapolated to infinite dilution. Elements of secondary structure were determined from the coordinates of the crystal structure (*17*).

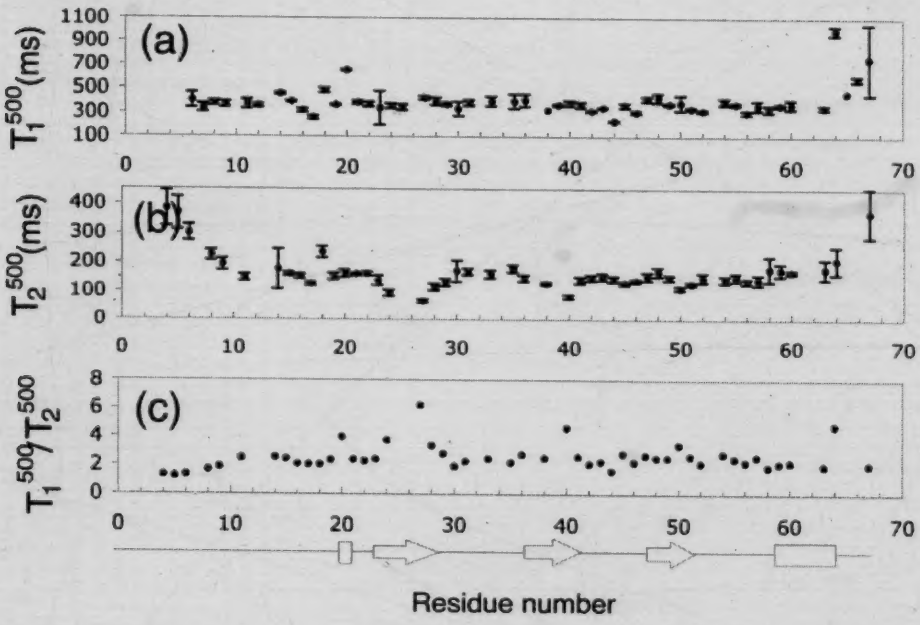

Figure D-7. Generalized order parameters, S^2, for samples containing different concentrations of SDF-1α, and relaxation data extrapolated to infinite dilution. Generalized order parameters for 1.5 mM SDF-1α at 500 (●) and 600 (○) MHz (a). Generalized order parameters for 0.3 mM SDF-1α at 500 (●) and 600 (○) MHz (b). Generalized order parameters obtained using T_1^{500} and T_2^{500} values extrapolated to infinite dilution (c).

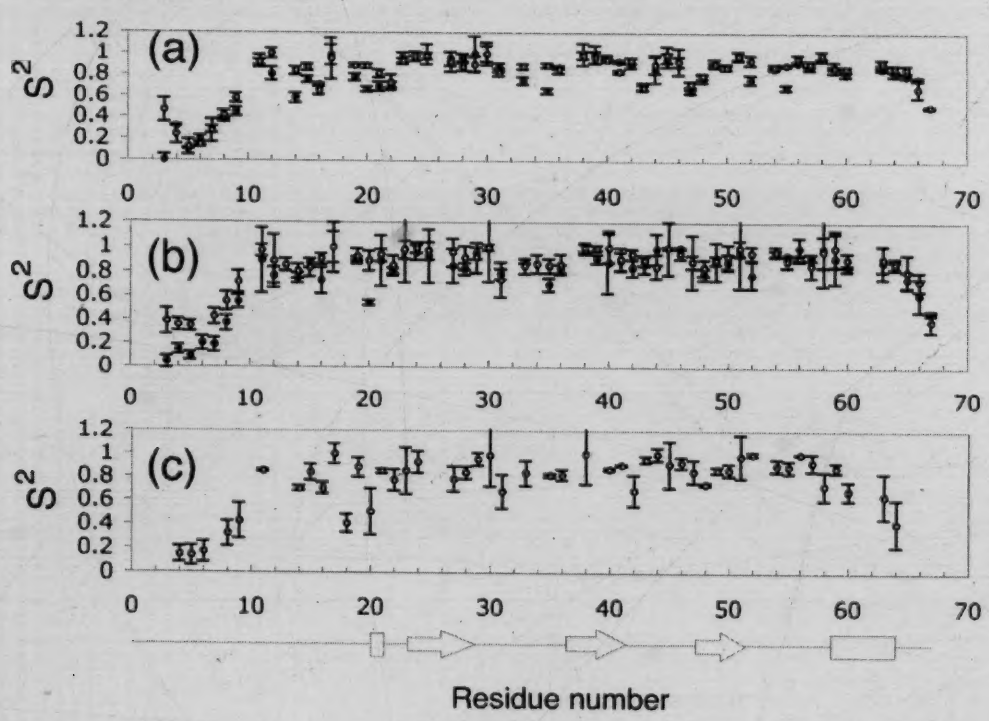

Figure D-8. R_{ex} parameters obtained for samples containing different concentrations of SDF-1α and for the case where relaxation parameters extrapolated to infinite dilution. R_{ex} parameters for 1.5 mM SDF-1α at 500 (●) and 600 (○) MHz (a). R_{ex} parameters for 0.3 mM SDF-1α at 500 (●) and 600 (○) MHz (b). R_{ex} parameters obtained using T_1^{500} and T_2^{500} values extrapolated to infinite dilution (c).

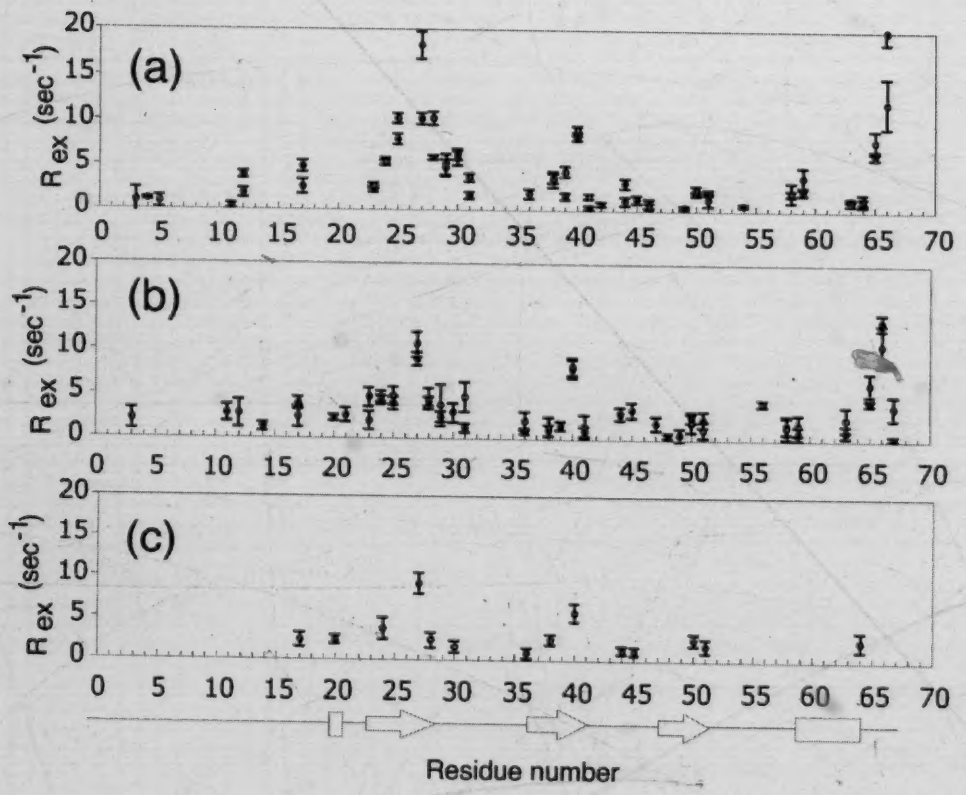

Figure D-9. Mapping of the residues requiring R_{ex} terms on the structure of SDF-1α dimer. The structure of dimeric SDF-1α is taken from Ohnishi *et al.* (*16*), (PDB code 1QG7). The two monomers are shown in grey and blue, with the residues suspected to undergo chemical exchange indicated with labels on the blue monomer. Regions colored in red are directly involved in the formation of dimer. Regions colored in pink may be indirectly affected by the formation of dimer. Residues in black are missing from the model free analysis due to line broadening or inadequate quality of the extrapolations.

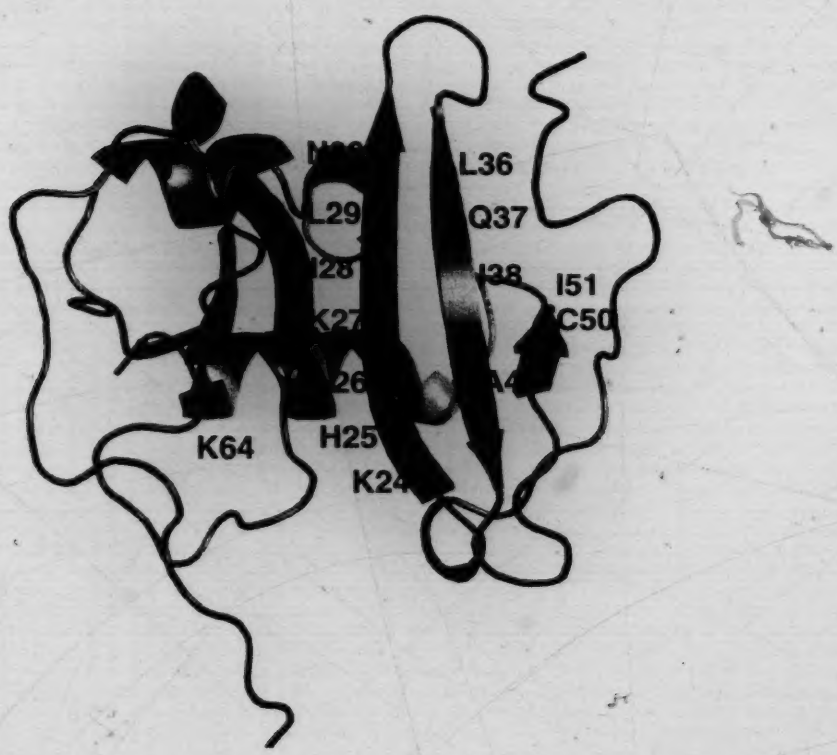

References

(1) Baggiolini, M. (1998) Chemokines and leukocyte traffic. *Nature 392(6676)*, 565.

(2) Kunkel, S. L., and Godessart, N. (2002) Chemokines in autoimmunity: from pathology to therapeutics. *Autoimmun Rev 1*, 313-20.

(3) Berson, J. F., Long, D., Doranz, B. J., Rucker, J., Jirik, F. R., and Doms, R. W. (1996) A seven-transmembrane domain receptor involved in fusion and entry of T-cell-tropic human immunodeficiency virus type 1 strains. *J Virol. 70(9)*, 6288.

(4) Murphy, P. M. (2001) Chemokines and the molecular basis of cancer metastasis. *N Engl J Med. 345(11)*, 833-5.

(5) Rubin, J. B., Kung, A. L., Klein, R. S., Chan, J. A., Sun, Y., Schmidt, K., Kieran, M. W., Luster, A. D., and Segal, R. A. (2003) A small-molecule antagonist of CXCR4 inhibits intracranial growth of primary brain tumors. *Proc Natl Acad Sci U S A 100*, 13513-8.

(6) Cooper, C. R., Chay, C. H., Gendernalik, J. D., Lee, H. L., Bhatia, J., Taichman, R. S., McCauley, L. K., Keller, E. T., and Pienta, K. J. (2003) Stromal factors involved in prostate carcinoma metastasis to bone. *Cancer. 97(3 Suppl)*, 739-47.

(7) Phillips, R. J., Burdick, M. D., Lutz, M., Belperio, J. A., Keane, M. P., and Strieter, R. M. (2003) The stromal derived factor-1/CXCL12-CXC chemokine receptor 4 biological axis in non-small cell lung cancer metastases. *Am J Respir Crit Care Med. 167(12)*, 1676-86.

(8) Muller, A., Homey, B., Soto, H., Ge, N., Catron, D., Buchanan, M. E., McClanahan, T., Murphy, E., Yuan, W., Wagner, S. N., Barrera, J. L., Mohar, A., Verastegui, E., and Zlotnik, A. (2001) Involvement of chemokine receptors in breast cancer metastasis. *Nature 410*, 50-6.

(9) Epstein, R. J. (2004) The CXCL12-CXCR4 chemotactic pathway as a target of adjuvant breast cancer therapies. *Nat Rev Cancer 4*, 901-9.

(10) Crump, M. P., Gong, J. H., Loetscher, P., Rajarathnam, K., Amara, A., Arenzana-Seisdedos, F., Virelizier, J. L., Baggiolini, M., Sykes, B. D., and Clark-Lewis, I. (1997) Solution structure and basis for functional activity of stromal cell-derived factor-1; dissociation of CXCR4 activation from binding and inhibition of HIV-1. *EMBO J. 16*, 6996-7007.

(11) Kuschert, G. S., Coulin, F., Power, C. A., Proudfoot, A. E., Hubbard, R. E., Hoogewerf, A. J., and Wells, T. N. (1999) Glycosaminoglycans interact selectively with chemokines and modulate receptor binding and cellular responses. *Biochemistry 38*, 12959-68.

(12) Mammen, M., Choi, S. K., and Whitesides, G. M. (1998) Polyvalent Interactions in Biological Systems: Implications for Design and Use of Multivalent Ligands and Inhibitors. *Angewandte Chemie International Edition 37*, 2754-2794.

(13) Fernandez, E. J., and Lolis, E. (2002) Structure, function, and inhibition of chemokines. *Annu Rev Pharmacol Toxicol. 42*, 469-99.

(14) Rajarathnam, K., Sykes, B. D., Kay, C. M., Dewald, B., Geiser, T., Baggiolini, M., and Clark-Lewis, I. (1994) Neutrophil activation by monomeric interleukin-8. *Science 264*, 90-2.

(15) Proudfoot, A. E., Handel, T. M., Johnson, Z., Lau, E. K., LiWang, P., Clark-Lewis, I., Borlat, F., Wells, T. N., and Kosco-Vilbois, M. H. (2003) Glycosaminoglycan binding and oligomerization are essential for the in vivo activity of certain chemokines. *Proc Natl Acad Sci U S A 100*, 1885-90.

(16) Ohnishi, Y., Senda, T., Nandhagopal, N., Sugimoto, K., Shioda, T., Nagal, Y., and Mitsui, Y. (2000) Crystal structure of recombinant native SDF-1alpha with additional mutagenesis studies:. *J Interferon Cytokine Res 20*, 691-700.

(17) Dealwis, C., Fernandez, E. J., Thompson, D. A., Simon, R. J., Siani, M. A., and Lolis, E. (1998) Crystal structure of chemically synthesized [N33A] stromal cell-derived factor 1alpha, a potent ligand for the HIV-1 "fusin" coreceptor. *Proc Natl Acad Sci U S A. 95*, 6941-6.

(18) Gozansky, E. K., Louis, J. M., Caffrey, M., and Clore, G. M. (2005) Mapping the binding of the N-terminal extracellular tail of the CXCR4 receptor to stromal cell-derived factor-1alpha. *J Mol Biol 345*, 651-8.

(19) Holmes, W. D., Consler, T. G., Dallas, W. S., Rocque, W. J., and Willard, D. H. (2001) Solution studies of recombinant human stromal-cell-derived factor-1. *Protein Expr Purif 21*, 367-77.

(20) Veldkamp, C. T., Peterson, F. C., Pelzek, A. J., and Volkman, B. F. (2005) The monomer-dimer equilibrium of stromal cell-derived factor-1 (CXCL 12) is altered by pH, phosphate, sulfate, and heparin. *Protein Sci 14*, 1071-81.

(21) Zhang, O., Kay, L. E., Olivier, J. P., and Forman-Kay, J. D. (1994) Backbone 1H and 15N resonance assignments of the N-terminal SH3 domain of drk in folded and unfolded states using enhanced-sensitivity pulsed field gradient NMR techniques. *J Biomol NMR 4*, 845-58.

(22) Goodman, J. L., Pagel, M. D., and Stone, M. J. (2000) Relationships between protein structure and dynamics from a database of NMR-derived backbone order parameters. *J Mol Biol 295*, 963-78.

(23) Lipari, G., and Szabo, a. (1982) Model-Free Approach to the Interpretation of Nuclear Magnetic-Resonance Relaxation in Macromolecules.1. Theory and Range of Validity. *J Am Chem Soc 104*, 4546-4559.

(24) Lipari, G., and Szabo, a. (1982) Model-Free Approach to the Interpretation of Nuclear Magnetic-Resonance Relaxation in Macromolecules.2. Analysis of Experimental Results. *Journal of the American Chemical Society 104*, 4559.

(25) Crump, M. P., Spyracopoulos, L., Lavigne, P., Kim, K. S., Clark-lewis, I., and Sykes, B. D. (1999) Backbone dynamics of the human CC chemokine eotaxin: fast motions, slow motions, and implications for receptor binding. *Protein Sci 8*, 2041-54.

(26) Mizoue, L. S., Bazan, J. F., Johnson, E. C., and Handel, T. M. (1999) Solution structure and dynamics of the CX3C chemokine domain of fractalkine and its interaction with an N-terminal fragment of CX3CR1. *Biochemistry 38*, 1402-14.

(27) Grasberger, B. L., Gronenborn, A. M., and Clore, G. M. (1993) Analysis of the backbone dynamics of interleukin-8 by 15N relaxation measurements. *J Mol Biol 230*, 364-72.

(28) Spyracopoulos, L., Lavigne, P., Crump, M. P., Gagne, S. M., Kay, C. M., and Sykes, B. D. (2001) Temperature dependence of dynamics and thermodynamics of the regulatory domain of human cTn C. *Biochemistry 40*, 12541-51.

(29) Schurr, J. M., Babcock, H. P., and Fujimoto, B. S. (1994) A test of the model-free formulas. Effects of anisotropic rotational diffusion and dimerization. *J Magn Reson B 105*, 211-24.

(30) Clore, G. M., Szabo, A., Bax, A., Kay, L. E., Driscoll, P. C., and Gronenborn, A. M. (1990) Deviations from the Simple 2-Parameter Model-Free Approach to the Interpretation of N-15 Nuclear Magnetic-Relaxation of Proteins. *J Am Chem Soc 112*, 4989-4991.

(31) Spyracopoulos, L., and Sykes, B. D. (2001) Thermodynamic insights into proteins from NMR spin relaxation studies. *Curr Opin Struct Biol 11*, 555-9.

(32) Korchuganov, D. S., Nolde, S. B., Reibarkh, M. Y., Orekhov, V. Y., Schulga, A. A., Ermolyuk, Y. S., Kirpichnikov, M. P., and Arseniev, A. S. (2001) NMR study of monomer-dimer equilibrium of barstar in solution. *J Am Chem Soc 123*, 2068.

(33) Fushman, D., Cahill, S., and Cowburn, D. (1997) The main-chain dynamics of the dynamin pleckstrin homology (PH) domain in solution: analysis of 15N relaxation with monomer/dimer equilibration. *J Mol Biol 266*, 173-94.

(34) Pfuhl, M., Chen, H. A., Kristensen, S. M., and Driscoll, P. C. (1999) NMR exchange broadening arising from specific low affinity protein self-association: analysis of N15 nuclear relaxation for rat CD2. *J Biomol NMR 14*, 307-20.

(35) Gryk, M. R., Abseher, R., Simon, B., Nilges, M., and Oschkinat, H. (1998) Heteronuclear relaxation study of the PH domain of beta-spectrin: restriction of loop motions upon binding inositol trisphosphate. *J Mol Biol 280*, 879-96.

(36) Grzesiek, S., Bax, A., Hu, J. S., Kaufman, J., Palmer, I., Stahl, S. J., Tjandra, N., and Wingfield, P. T. (1997) Refined solution structure and backbone dynamics of HIV-1 Nef. *Protein Sci 6*, 1248-63.

(37) Mercier, P., Spyracopoulos, L., and Sykes, B. D. (2001) Structure, dynamics, and thermodynamics of the structural domain of troponin C in complex with the regulatory peptide 1-40 of troponin I. *Biochemistry 40*, 10063-77.

(38) Baryshnikova, O. K., Rainey, J. K., and Sykes, B. D. (2005) Nuclear magnetic resonance studies of CXC chemokine receptor 4 allosteric peptide agonists in solution. *J Pept Res 66*, 12-21.

(39) Luz, Z., and Meiboom, S. (1963) NMR Study of Protolysis of Trimethylammonium Ion in Aqueous Solution - Order of Reaction with Respect to Solvent. *J Chem Phys 39*, 366-&.

(40) Baldo, J. H., Halford, S. E., Patt, S. L., and Sykes, B. D. (1975) The stepwise binding of small molecules to proteins. Nuclear magnetic resonance and temperature jump studies of the binding of 4-(N-acetylaminoglucosyl)-N-acetylglucosamine to lysozyme. *Biochemistry 14*, 1893-9.

(41) Luz, J. G., Yu, M., Su, Y., Wu, Z., Zhou, Z., Sun, R., and Wilson, I. A. (2005) Crystal Structure of Viral Macrophage Inflammatory Protein I Encoded by Kaposi's Sarcoma-associated Herpesvirus at 1.7A. *J Mol Biol 352*, 1019-28.

(42) Ye, J., Mayer, K. L., Mayer, M. R., and Stone, M. J. (2001) NMR solution structure and backbone dynamics of the CC chemokine eotaxin-3. *Biochemistry 40*, 7820-31.

(43) Mayer, K. L., and Stone, M. J. (2003) Backbone dynamics of the CC-chemokine eotaxin-2 and comparison among the eotaxin group chemokines. *Proteins 50*, 184-91.

(44) Liao, T. S., Yurgelun, M. B., Chang, S. S., Zhang, H. Z., Murakami, K., Blaine, T. A., Parisien, M. V., Kim, W., Winchester, R. J., and Lee, F. Y. (2005) Recruitment of osteoclast precursors by SDF-1 in giant cell tumor of bone. *J Orthop Res 23*, 203-9.

(45) Li, M. X., Corson, D. C., and Sykes, B. D. (2002) Structure determination by NMR. Isotope labeling. *Methods Mol Biol 173*, 255-65.

(46) Smith, B. J. (2003) Chemical cleavage of polypeptides. *Methods Mol Biol 211*, 63-82.

(47) Gagne, S. M., Tsuda, S., Spyracopoulos, L., Kay, L. E., and Sykes, B. D. (1998) Backbone and methyl dynamics of the regulatory domain of troponin C: anisotropic rotational diffusion and contribution of conformational entropy to calcium affinity. *J Mol Biol 278*, 667-86.